Investigation on High Performance Diagnosis Method of Induction Motor Fault using Machine Learning and Artificial Neural Network

機械学習および人工知能を用いた誘導電動機の故障診断法の高性能化に関する研究

By

Esakimuthu Pandarakone Shrinathan

A thesis submitted for the degree of Doctor of Engineering

Graduate School of Engineering

Department of Electrical and Mechanical Engineering

Nagoya Institute of Technology

Nagoya, Japan

March 2019

Investigation on High Performance Diagnosis Method of Induction Motor Fault using Machine Learning and Artificial Neural Network

A thesis submitted to Graduate School of Engineering,

Department of Electrical and Mechanical Engineering,

Nagoya Institute of Technology, for the degree of

Doctor of Engineering.

By

Esakimuthu Pandarakone Shrinathan

Supervisor

Professor Yukio Mizuno

Department of Electrical and Mechanical Engineering

March 2019

Declaration of Originality

I hereby declare that the research recorded in this thesis and was composed and originated entirely by myself in the Graduate School of Engineering, Department of Electrical and Mechanical Engineering at the Nagoya Institute of Technology.

Esakimuthu Pandarakone Shrinathan

To the spirit of my beloved father (Esaki),

To the spirit of my beloved mother (Saru),

To my beloved sister (Kitty),

To my Professor,

To all members of my family,

To all my friends,

Those people's love is always the source of power

Abstract

For the past few decades, three phase induction motor has been used for driving most of the industrial loads. In general, induction motor holds many useful advantages such as easy handling, high efficiency, low cost, robustness and high reliability which will be hardly found in other motors. The usage of the induction motor has increased worldwide. Even though the application of induction motor has been increased, the proper maintenance and condition monitoring have not been carried out. If this condition prevails, there is a consequence of high operating cost and maintenance cost. There is also a chance for the reduction in the reliability of the induction motor. When the faulty motor is not identified and replaced in the earlier stage, it would result in the shutdown of the entire plant. So, when we visualize from the economic point, the cost for replacing the faulty motor will be cheaper than the entire unit shutdown. Therefore, proper maintenance and condition monitoring are adequate to make the motor sustainable for a longer duration.

In recent years, many techniques have been developed for identifying the fault in the induction motor. The goal is to detect and diagnose both the electrical and mechanical failure of the induction motor at the early stage of fault. Hence the fault occurring with respect to both electrical and mechanical point of view must be paid more attention. With considering these facts about the induction motor failure, the present motor failure study is based on short circuit insulation failure, broken rotor bar failure, and bearing failure. The failure detection analysis is performed using Fast Fourier Transform (FFT). The analysis is carried out by characterizing the specified frequency components of the load current and this will be considered as the main feature. On further, to enhance the accuracy of the proposed systems,

the proper diagnosis is performed with the help of Distortion Ratio, Self-Organizing Map (SOM), and Support Vector Machine (SVM). Additionally, the Artificial Intelligence method like Deep Learning is also employed to perform the diagnosis of the induction motor failure. The common diagnosis method is established for detecting the short circuit insulation failure, broken rotor bar failure, and bearing failure using SVM and the results are compared with the other traditional machine learning algorithm for ratifying the effectiveness.

The proposed methodology for detecting the minor fault occurring in the induction motor gives a satisfactory result as follows. The one-turn in case of short circuit insulation failure; one broken rotor bar in case of broken rotor bar failure and 0.5 mm hole, 5 mm scratch to be the case of bearing failure. The minor fault detection and identifying the present state of the motor is made possible using the proposed method. The diagnosis between the faulty motor and healthy motor and among the faulty motors are also achieved. The method is opted for the industrial environment and variable speed applications.

Acknowledgements

First and foremost, I want to thank my supervisor Prof. Yukio Mizuno. It has been an honour to be his Doctor Student and to work with his laboratory. I appreciate all his contribution of time, ideas and funding towards my success. The joy and enthusiasm he has for the research was contagious and motivational for me, even during the tough time in the research. I am also thankful for the excellent example he has provided as a successful researcher and as a teacher. Also, for his continual support and enthusiasm for this project, for his ability to focus my work, for his help in preparing this thesis and on a more personal level moral support he provided.

For this thesis, I would like to thank my committee member Professor Takaharu Takeshita, Professor Takashi Kosaka of Nagoya Institute of Technology and Professor Naohiro Hozumi of Toyohashi University of Technology for their time, interest and helpful comments.

With great thanks, I want to acknowledge partial financial support for the research, TOENEC Corporation and the joint researcher Dr Hisahide Nakamura for his valuable guidance towards the success of many types of research. A special gratitude to my lab Technical staff; Information and Analysis Technologies Division Ms Mitsuki Shimada for her assistance in arranging many things in the years of my stay in Nagoya Institute of Technology. Particularly on computer related problems encountered during the study are also very much appreciated.

I also would like to thank all past and present members of Mizuno Laboratory for their kind help and for creating a stimulating working environment, as well as for their friendship. This

gratitude to Mr. Toshiki Matsumura, Mr. Keisuke Akahori, Mr. Makoto Masuko, and Mr. Keisuke Asano. This note would not be finished without thanking my friends Mr Takayuki Yokoyama, Mr. Fushimi Ueda and Mr. Kazuki Komatsu who were very supportive and helpful during my stays in Japan. In a similar vein, the author cannot forget to thank the Professor and Staff members of the Nagoya Institute of Technology of International Exchange centre. The heartful gratitude is expressed to Professor Izumi Yamamoto, Mrs. Chika Mizutani and Mrs. Kazumi Yamashita.

With distinguish thanks, I feel grateful to my uncle Mr. V. Ramakrishnan for his initial support and information regarding the scholarship and university. In this note, I would like to thank Mr. Shridhar Babu Muthu Babu for his support. I also appreciate my friends in Japan, who blessed me with their worm support and help during the stay in Japan. My special thanks go to Mr. K. Vinodh Babu and Mr. G. Santhosh.

I would like to thank my father Mr. P. Esaki Muthu, my mother Mrs. V. Saratha Devi and my sister Miss. G. Thilagavathi (Kitty) who deserves a special mention for all their love and encouragement. Most importantly, I would like to express my deep appreciation to my beloved sister for all her encouragement, understanding, support, patience, and love throughout the ups and downs. My sincere gratefulness to the Government of Japan, particularly the Japanese Ministry of Education, Culture, Sports, Science and Technology (MEXT) for the fellowship granted to pursue the study. Finally, I would like to thank everyone who was part of my success and as well as my apology that I could not mention personally one by one.

Esakimuthu Pandarakone Shrinathan

List of Contents

List of Figures

Chapter 1

Chapter 2

Chapter 3

Chapter 4

Chapter 5

Chapter 6

Chapter 7

Chapter 8

List of Tables

Chapter 2

Chapter 3

Chapter 4

Chapter 5

Chapter 6

Chapter 7

Chapter 8

Chapter 1
Introduction and Literature Review

1.1 Background

To the world of modern life including automobiles, electric motor plays a vital role and specifically, in the most recent decades, induction motors is widely used in both the industrial application and domestic. Specifically, water pump, vacuum cleaners, air conditioners, automatic car windows, refrigerators and multitudes of other domestic appliance use the motors to convert the electrical energy into mechanical energy. In the industrial environment, motor's role is getting increased in the manufacturing process and automotive production, which results in the production of every conceivable industrial product. Even the machine in the industry is made to run using the induction motors. Thus, they play a significant role in a range of industries and most of the industrial loads are driven by the three-phase induction motors. Having various advantages like easy handling, low cost, high reliability, high efficiency, robustness and the usage in the power converters make the induction motor as most suited for the industrial applications. The recent development in the field of power electronics, electric locomotive, machinery manufacturing and finally the assembly processes has additionally enhanced the reliability and ruggedness of the induction motor. The induction motor develops its own scale of meter in all the fields. Despite the high availability, the application of induction motor in new fields such as off-shore wind current turbines, aero engines, and high-speed trains justifies the demand for condition monitoring and operating state supervision.

The condition monitoring deals with the process of observing the physical quantities related to motor. The entire process continues during the operation and can identify the changes, which is the main basis of condition monitoring scheme. This process also helps to cut down the maintenance cost and unscheduled downtime. In other words, fault should be identified at the initial stage to make an appropriate control decision that often has an adverse effect on

quality of the product and adds the safety of the process. When the faulty motor is not identified and replaced in the earlier stage, it would result in the shutdown of the entire plant. Generally, the defect in an induction motor can be defined as the reduction in the capacity to perform a required function. If a defective motor is kept in operation for an extended period, it will exhibit symptoms including increases in temperature, variation in the current harmonics, changes to the electromagnetic field, or vibration [1].

But in most of the industries, the induction motor is being operated without proper maintenance and condition monitoring. This condition leads to the reduction in the reliability of the induction motor and increases the maintenance cost as well as the operating expenses. Due to usage of an induction motor in many applications, the need to improve the reliability and condition monitoring of the machinery in the industrial application has been increased. Also, when we visualize from the economical point of view, maintaining the induction motor properly and replacing the faulty motor are quite cheaper, rather than letting the faulty motor to shut down the entire company. Therefore, proper maintenance and condition monitoring are adequate to make the motor sustainable for a longer duration. The fault diagnosis of the induction motor has received an intense interest. Thus, to satisfy the above requirement, the fault diagnosis is made as hotspot and the research is carried out. During my present study, induction motor has been selected among the electrical machines because of its various advantages as illustrated above and the fault analysis and diagnosis are performed.

1.2 Overview

The three main paradigm progress of fault detection and diagnosis: model-based, data-driven and experience-based approaches [2]-[3]. These approaches have application in various fields such as aviation, aerospace, and navy space. It is mainly used to improve maintenance signals and decisions. The model-based approach uses and constructs a mathematical models to study the degradation phenomenon. However, the system is very complex and it takes time to construct the model for enabling the diagnosis process. The data-driven approach is the alternative method to model-based approach. It uses the statistical pattern recognition and machine learning method to identify the failure and also to detect the changes observed in

the measured data. Further, the experience-based approach uses the statistical reliability approach to predict the probability failure of the machines.

For the last couple of decades, numerous technique has been developed for identifying the fault in the electrical machinery and many types of researches are still undergoing. The main aim of these research is to detect the mechanical and electrical fault of the induction motor. Depending on their origin, failures in the induction motors [4]-[20] can be broadly divided into two categories; electrical and mechanical failures. Among the possible motor failure, bearing failure (44%) takes the highest percentage of fault occurring in the induction motors, which is followed by short-circuit stator insulation failure (26%), broken rotor bar (18%) and other kinds of fault (12%) [21] and fault may cause the industry to shut down, loss of production and even it may create an origin for catastrophic effect and human causalities [22]-[23]. The induction motor failure classification is shown in Figure 1.1 [21].

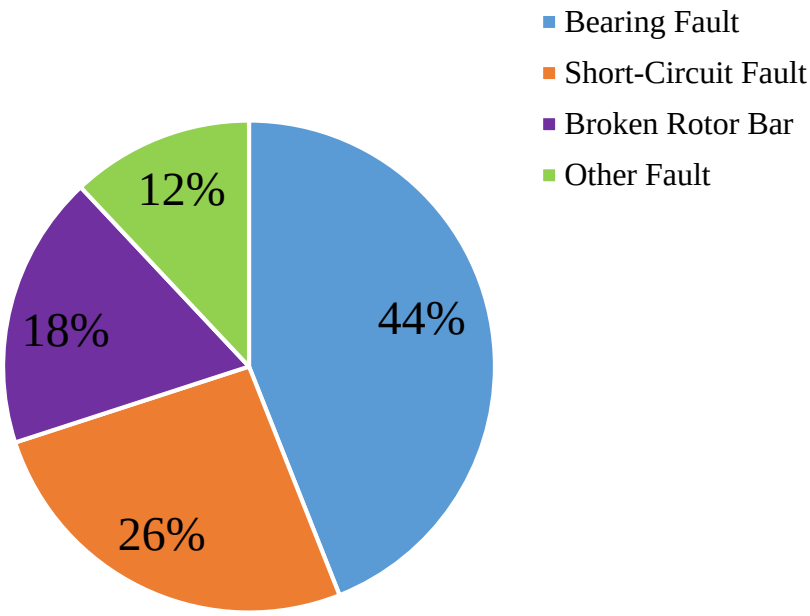

Figure 1.1 *Induction motor failure classification [21].*

Thus, the bearing failure, short-circuit insulation failure and broken rotor bar failure has been considered in the present study and the fault analysis is performed.

1.3 Technical Issues caused by Induction Motor

Many problems are a result of high or low voltage, unbalanced voltage, ungrounded power systems, or voltage spikes. The following are examples of the most common of these types of problems seen [24].

1.3.1 Low Voltage

Low voltage is normally not the direct cause of motor overheating since the overload relays will kick the motor off line when the current exceeds rated amps. As a result, the motor will not generate rated horsepower. The motor slip also increases proportionally to the square of the voltage drop. As a result, the motor will be running slower with a lower output and the process would not be producing as expected. Low voltage during start can create additional problems. When specifying the motor, it is important to understand what the true voltage at the motor terminals is during starting. This is not the power system voltage, or the tap on the autotransformer. To determine this voltage, one must consider the total line drop to the motor terminals during the high current draw, which is present while the motor is starting.

On designs which are subject to reduced voltage start and have an elevated risk of not properly starting, it is recommended that the voltage at the motor terminals be measured on the first couple of starts, after this motor or any other machinery is added to the power system, to eliminate concerns or problems in the future.

1.3.2 Over Voltage

It is normally true that motors tend to run cooler at rated horsepower at voltages exceeding rated voltage by up to 10%, but the current draw is only controlled by the load and at rated current and 10% overvoltage the motor will be overloaded by approximately 10%. The core loss is 20 to 30% greater than normal and could causes the machine to overheat. If it is verified that the motor will see an overvoltage, the overload current relay must be adjusted downward to compensate, or stator temperature detectors should be used to monitor the temperature.

1.3.3 Unbalanced Voltages

Unbalanced voltage will produce negative sequence currents that will produce excess heating in the stator winding and rotor bars but will not produce useful power output. Derating of the motor is necessary when unbalanced voltages exceed 1% as defined. This condition which produces increased heating, increased energy consumption and lower efficiency. Note, a 2% voltage unbalance can produce as much as 10% increased losses in the machine.

1.4 Reason and Technical Issues of Induction Motor Failure

In this section, the discussion is done regarding the most common faults occurring in the induction motor. It is illustrated as below [25]-[27].

1.4.1 Stator Coil Failure

The reason and some of the examples for the failure occurring in the stator coil of the induction motor is discussed.

1.4.1.1 *Removing of stator winding by frequent start/stop of the induction motor*

Thermal deterioration of electrical insulation occurs due to high magnitude transient current.

1.4.1.2 *Thermal deterioration of stator winding insulation due to high-temperature*

Thermal deterioration of winding insulation obeys Arrhenius's rule. In the case of E-type insulation, its lifetime reduces by half when temperature rises 10 degrees.

1.4.1.3 *Influence of dust in removing the stator winding*

Attachment of dust and/or oil to cooling fun and its cover lowers cooling efficiency, leading to temperature rise of motor.

1.4.1.4 *Role of moisture absorption in burning the stator winding*

Infiltration of water into motor or condensation reduces insulation characteristics of winding.

1.4.1.5 *Localized Removal of stator coil by eddy current*

Electrical breakdown caused by contact of rotor iron and stator winding results in localized eddy current flow in iron. Winding is heated by the current.

1.4.2 Cause of Broken Rotor Bar Failure

The reason and some of the examples for the broken rotor bar failure occurring in the induction motor is discussed.

1.4.2.1 *Motor Overheating*

The most common cause of overheating is improper ventilation or high ambient temperature. A typical compressor room or pump house will heat up quickly if the room is not properly ventilated. The temperature in the room will continue to rise until it reaches an equilibrium with the heat radiating out through the walls. This may seem a little ridiculous, and assume that it could avoid this condition, but rooms such as this have existed in various plants around the world, and motors were failing repeatedly until fans are installed in the walls to exchange the necessary amount of air.

1.4.2.2 *Industries Fault Study*

Apart from this, several case studies have been done regarding the fault occurring in the industries. Based on the result, the sample of the broken rotor fault is shown in Figure 1.2.

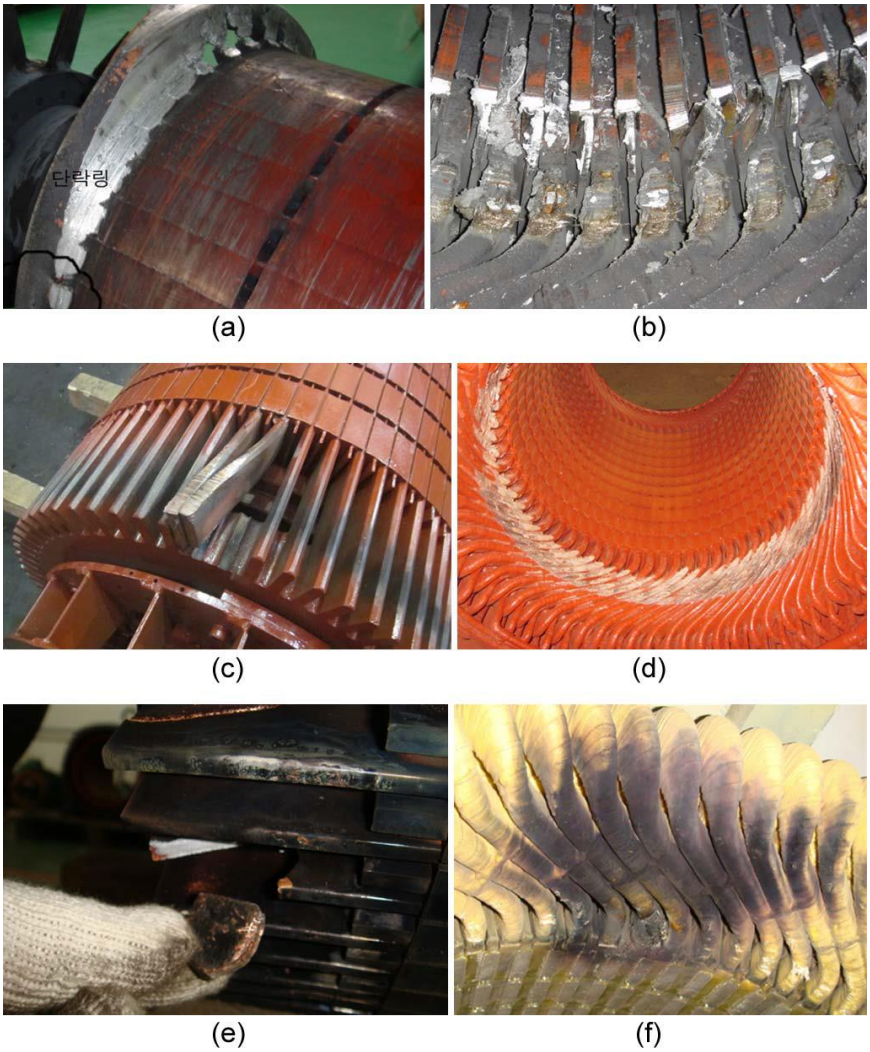

Figure 1.2 *Broken rotor bar damage for (a), (b) 2400-kW, (c), (d) 1400-kW, and (e), (f) 500-kW motors [25].*

1.4.3 Bearing Failure Causes

The reason and some of the examples for the bearing failure occurring in the induction motors discussed.

1.4.3.1 *Fluting, abnormal abrasion and scuffing*

This effect is mainly caused by overload, abnormal thrust load, bad assembly, bad lubrication, flection of shaft, and slip abrasion. The most commonly used detection methods are

monitoring vibration and degree of abrasion. The sample of bearing fluting is shown in Figure 1.3.

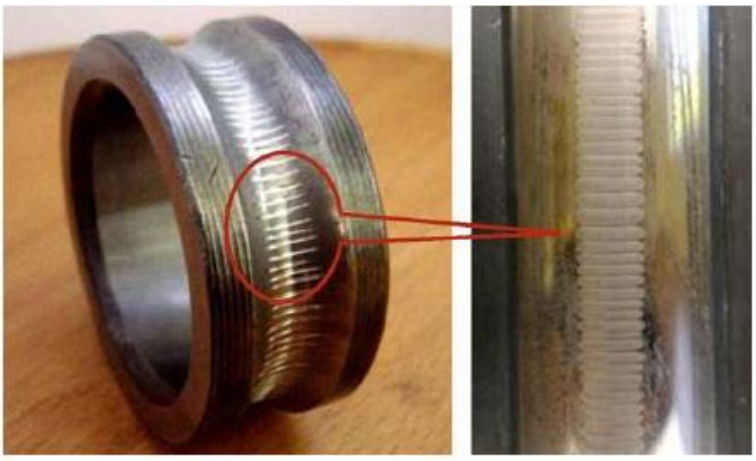

Figure 1.3 *Sample of Fluting [26].*

***1.4.3.2** Damaged Cases*

It is mainly caused by progression of flaking, excess impact load, bad assembly, and bad lubrication. The detection methods are monitoring the vibration and temperature.

***1.4.3.3** Electric corrosion*

The reason for the electric corrosion stands because of the spark that is caused due to current flow, condensation, and water infiltration. The detection methods are monitoring vibration and degree of abrasion.

***1.4.3.4** Practical Case of Bearing Fault*

Apart from this, several case studies have been done regarding the fault occurring in the industries. Based on the result, the sample of the bearing failure is shown in Figures 1.4.

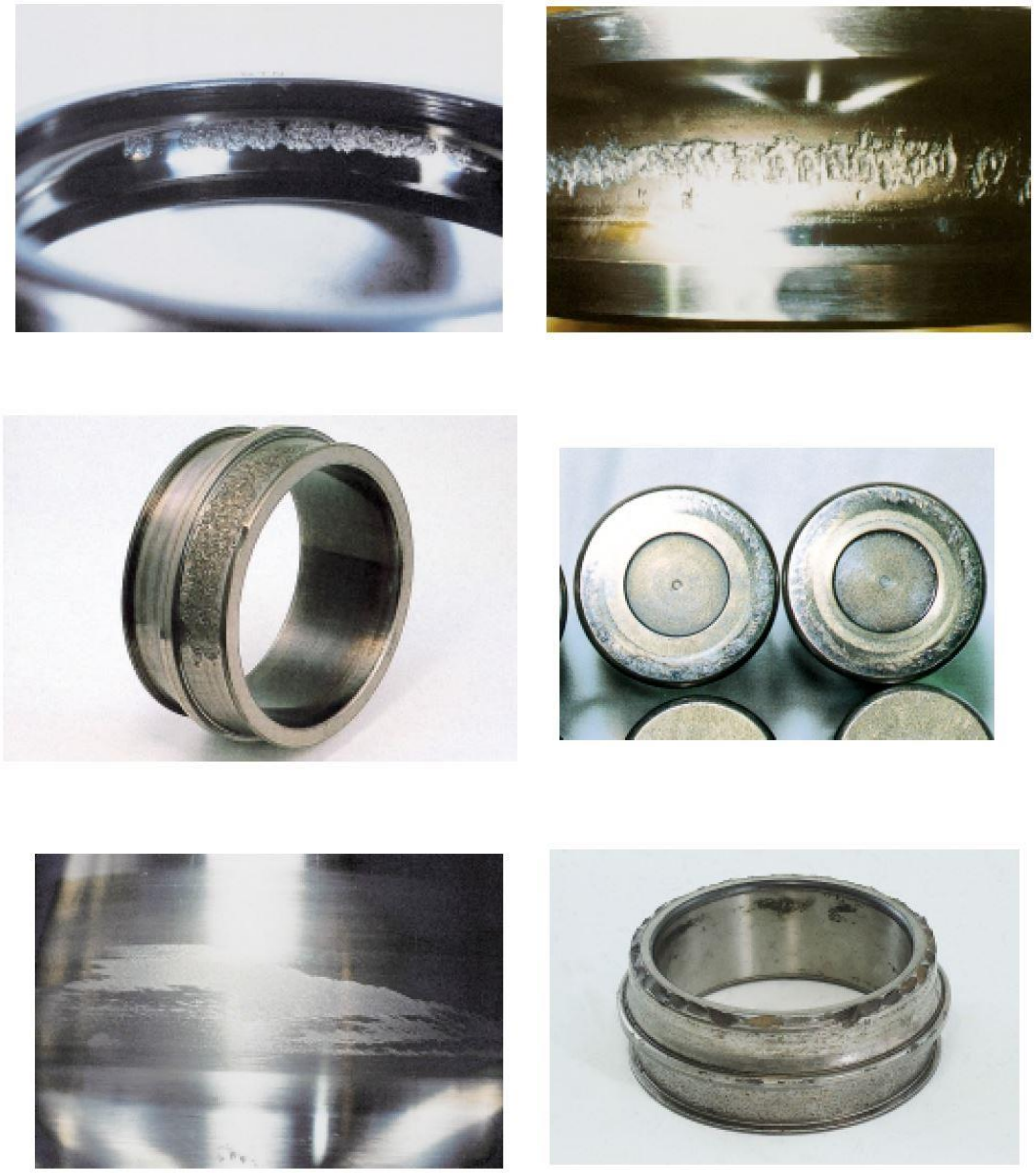

Figure 1.4 *Sample of bearing failure [27].*

1.5 Previous Works and Literature Survey

1.5.1 Short Circuit Insulation Failure

Similarly, in the case of short circuit insulation failure in the stator winding of the induction motor, several researches have been done. It is well known fact that short circuit failure of a

stator winding due to aging or damage of electrical insulation is one of the most probable electrical faults in motor drive systems, which accounts for about 35 % of all failures [28]. This short-circuit fault is recognized as a crucial failure. It is interesting to note that even the safety system used for detecting malfunctions in electrical motors cannot react to short-circuit failures because they only cause insignificant changes in the magnitude of the phase current. This problem can be addressed using digital diagnostic signal processing. This system looks after the motor condition and alerts the user at the initial stage of a fault.

The diagnostic methods based on the shape of Park vector, air-gap torque and so on have been proposed for detecting the short-circuit insulation failure [8], [29]-[31]. On further, partial discharge characteristics are an effective element in detecting the insulation failure in high voltage motor or generator winding [33]-[35]. Also, application of guided waves and probability imaging approach are discussed for detection of insulation damage of stator bar in large generator [36]. But in the case of low-voltage induction motors, impulse testing is available [4]-[5]. These high-frequency resonance is also applied to turn-turn insulation diagnosis of motors fed by adjustable speed drives [6]. The turn-to-turn capacitance is suggested as an aging indicator of stator winding insulation [7]. A load-immune diagnosis method was proposed to detect minor level short circuit fault in stator winding, which was based on suitable features from Park's vector modulus of motor line current [8].

In addition to this, a simple and reliable diagnosis method is also established to identify the turn-to-turn insulation failure based on the load current [9]-[10]. In this method, a novel diagnosis method was discussed to detect the short circuit insulation failure based on Support Vector Machine (SVM). The analysis is carried out by characterizing the magnitude of load current and to be treated as the main feature for diagnosis. This method has the advantage of simple, low cost and short data processing time. It was found that more than two turn-to-turn short-circuit could be easily diagnosed with practically acceptable accuracy. However, winding with one turn-to-turn short-circuit failure could not be distinguished from the healthy winding.

However, one turn-to-turn short circuit failure is still an existing fault and no proper diagnosis has been done till to date. The problem is discussed and overwhelmed during the present research work.

1.5.2 Broken Rotor Bar Fault

As rotor bar fault is one of the common fault in the induction motor, lots of researches have been carried out in detecting the breakage of rotor bars [12]-[17]. Failure in rotor cages of induction motors, such as breakage of rotor bars and end-rings, is one of the most probable mechanical faults in motor drive systems, which accounts for about 5-10 % of all failures [11]. To detect the geometrical asymmetry of a rotor caused by breakage of bar(s), the method using side-band components has been widely focused. The sideband components appear below and above the fundamental component in frequency spectrum of load current. It is since such a mechanical failure affects magnetic flux in the air gap between a stator and a rotor and causes changes in the load current through counter-electromotive force. This sideband components method has the following drawbacks. In the case of a slight failure, for example, one rotor bar is broken, it is rather difficult to detect the failure, because only slight changes are observed in the load current. Accuracy of diagnosis is not necessarily satisfactory when detection system has low frequency resolution. Load current is not constant, but it is affected by deviation of applied voltage as well as load condition [18]. The output signal of a sensor usually contains noise.

On the other hand, characteristic frequencies are also used in detecting the broken rotor bar fault, which uses the amplitude of the characteristic frequency components of load current spectrum as features [19]. However, with the employment of this method, it is very difficult to detect the slight failure in the rotor bar. For example, one rotor bar is difficult to be detected as we observe only slight changes in the load current. With this discussion, it is concluded that detecting the minor rotor bar fault is difficult and method identifying the number of broken rotor bars is still under research. The problem is discussed and overwhelmed during the present research work.

1.5.3 Bearing Failure

Among all the failures, bearing faults are the most common faults in an electric motor [21], [37]-[38], and may cause the industry to shut down, loss of production and even it may create an origin for catastrophic effect and human casualties [22]-[23]. The main factors behind the bearing faults are dust, corrosion and inadequate lubrication. The detection of the bearing fault at the incipient stage will avoid the unexpected breakdown and automatically increase the reliability of operation [24], [39]-[40].

Normally, most of the research for detecting the bearing failure is done based on the vibration analysis [41]-[43]. Although this method is quite effective in detecting the bearing fault, the choice and positioning of the sensor are difficult, and will vary based on the location of the equipment. The acquisition of vibration data requires transducers or accelerometers that makes the method expensive and difficult. To overcome the disadvantage of the vibration method, detection is done by means of the stator current [44]-[49]. This method uses the signal from the stator current so that choice and positioning of the sensor are not required. However, this method fails in identifying the present state of the bearing. Some of the other bearing fault detection methods are based on time domain analysis [50] and electric current analysis [51]. Both the analysis produces promising results and gained prominence.

The introduction of digital signal processing has extended its range of applications over detecting the bearing fault [52]. Digital systems mainly rely on the use of artificial intelligence tools such as artificial neural networks [53], fuzzy logic, or expert systems [54]. The widely used techniques include squared envelope analysis [55], spectral kurtosis analysis [56], and the wavelet kurtogram [57]. In most cases, however, the raw signal cannot be used to identify a failure, and features must be extracted from time domain or frequency domain analysis. Time domain analysis allows processing of both stationary and non-stationary signals. Techniques include the use of root mean square [58] analysis, high-order statistical methods [59], and the short impulse method [60]. Time domain analysis is one of the simplest methods available for identification of bearing faults. It uses features extracted from the raw signal. The value of such a feature will change if a defect appears on the bearing of an induction motor, providing diagnostic information. However, this approach is often incapable

of isolating the fault conditions. Frequency domain analysis has high process gain and is less sensitive to noise in the signal. It can detect faults only from a stationary signal and cannot be applied to non-stationary signals [61].

Over the past few years, the usage of acoustic emission sensors (AE) are reported in condition monitoring and fault diagnosis [62]. The comparison is made with the traditional methods like vibration analysis and AE signals have the advantage of capturing the bearing fault features and detecting the incipient faults [63]. The detection is made possible by using the frequency of selected components as primary features. Additionally, using Hilbert-Huang Transform (HHT) along with AE signals, the fault detection is performed on rotational machinery systems [64]. Nowadays, the digital signal processing has extended their application to identify the bearing failure of the induction machines [65]. Generally, raw signals will not be sufficient to identify the existence of the failure. Therefore, to identify the fault, features are extracted from time domain or frequency domain analysis. Time domain analysis can be used to process both stationary and non-stationary signals and it includes the analysis of such as root mean square [66], high-order statistical method [67], and short impulse method [68].

Intelligent diagnosis methods to identify the defects are rapidly increasing and in most of the cases Support Vector Machine (SVM), Artificial Neural Network (ANN), and Adaptive Neuro-Fuzzy Inference System (ANFIS) are applied [69]-[76]. In general, two steps are mostly involved in intelligent bearing fault diagnosis; feature extraction and their classification. Soualhi et al. [57] proposed an algorithm using ANN for fault diagnosis using six features. Again Prieto et al. [39] investigated the bearing conditions using the time-domain statistical parameter and then extracted the features followed by ANN. The ANN with time-frequency features are performed by Boukra et al. [77]. Lei et al. [78] performed the fault diagnosis using ANFIS algorithm and reveals the working bearing conditions. Ebrahimi et al. [79] performed the bearing fault diagnosis using the wavelet transform for feature extraction and Principle Compound Analysis (PCA) for feature fusion, then SVM is carried out. The hybrid optimized bearing fault diagnosis method is proposed [80] using optimized stationary wavelet packet transform (Op-SWPT). The LAMSTAR neural network

also extended its application to diagnose the bearing faults [81]. Although these many intelligence methods are used in bearing fault diagnosis, they still have some inherent disadvantages. Most of the intelligent systems are non-linear and belong to the shallow learning models. The accuracy also varies with the selection of features, largely depends on diagnosis model and requires the engineering experience.

Most of the fault categories belong to the single fault considering pitting (hole), in some cases compound fault is discussed [82]-[83]. As a case, Valeria et al. [65] carried out the experiment for the hole of diameter 2.3 mm and 2.8 mm and able to distinguish the healthy motor and faulty motor. The detection of bearing fault is achieved by spectral kurtosis and envelope analysis of stator current. However, no results were obtained regarding the smaller size of the hole. Also, Christelle and Kay Hameyer [82] carried out the diagnosis for two low level depths of the hole. The fault examination and diagnosis are carried out by means of the linear discriminant analysis of stator current features from the selected frequency components. Although the faulty motors are distinguished from the healthy motors, the difference between the two types of fault is not possible by this method.

In summary, many papers are available with the bearing failure concept and all those papers have explained the differences between the healthy and faulty motors by different analysis method. However, several studies and experiments are highly required to gain the adequate expertise about the physical location of fault. The challenging factors said to be continued. Also, in practical point of view, the faults in induction motor bearings often arise from scratches. The chance of faults with scratches is considerably high than that of holes. Hence it is also important to undergo many researches for the fault analysis using scratch. The problem is discussed and overwhelmed during the present research work.

1.6 Motivation and Objectives

To overcome the disadvantages of the previous methods and to detect the minor fault occurring in the induction motor, the following methods are proposed and the confirmed with the experimental results. The methodology used, and the main objectives of the thesis are shown in Figure 1.5.

- Proposing a simple method using the load current of the stator
- Detection of the minor faults using the spectral analysis and feature distribution
- Application of Machine Learning Algorithm (MLA) and Artificial Neural Network (ANN) to increase the diagnosis accuracy

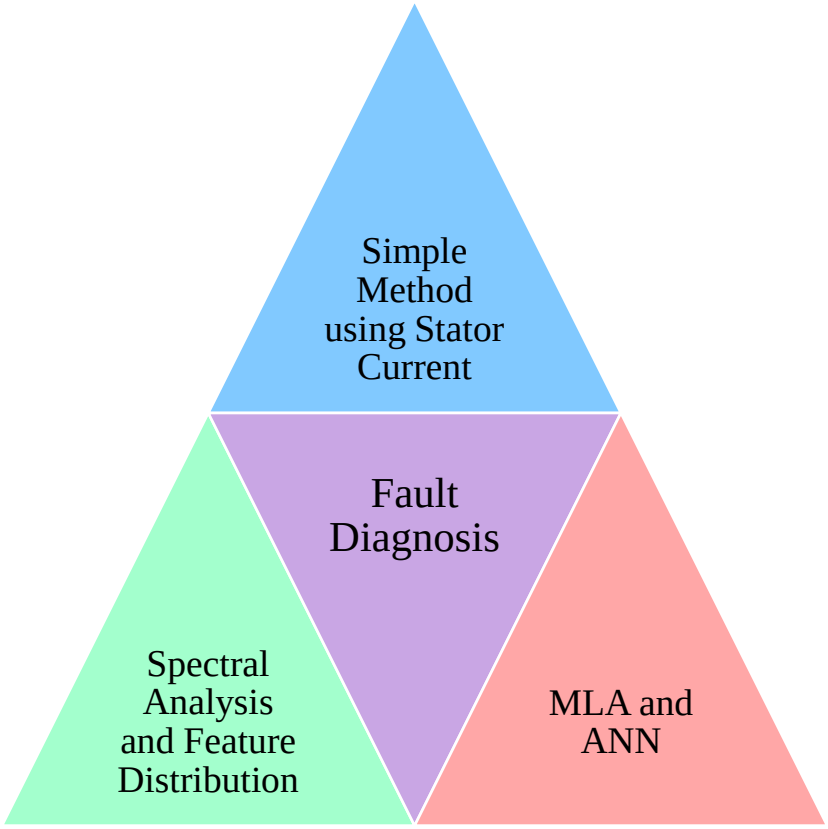

Figure 1.5 *Thesis objective.*

1.6.1 Short-Circuit Insulation Failure

The reason for the short-circuit insulation failure is discussed in the section 1.4.1. With these facts, the turn failure occurring in the stator winding of the induction motor is made possible. To match the condition, artificially faults are induced by removing the insulation by soldering and the short-circuit insulation failure detection analysis is performed. Though it is not possible to repeat the exact criteria, the reason for the early detection of the minor faults is discussed.

Generally, in the case of low voltage induction motor, if a minor short-circuit fault occurs, such as one-turn short-circuit insulation failure, the motor will not immediately result in a fatal electrical breakdown and continue to operate for a certain period even with the presence of a fault. However, the thermal deterioration of insulating material progresses gradually and certainly increases the number of short-circuit turns and finally the motor breakdown at some point of time. Thus, it is necessary and crucial to detect the slight insulation winding failure (one-turn) at the early stage to avoid the progression of insulation failure. The diagnostic method is proposed to identify the one turn-to-turn short circuit failure in the induction motor. The amplitude of the characteristics frequency components was extracted, and the proper diagnosis are performed with the help of the Support Vector Machine [84]. This method is also suitable for the on-line diagnosis at the industrial site.

This method suffers drawbacks such as a convoluted process of selecting the combinational frequency components for diagnosis, and an accuracy rate that varies depending on this selection [80]. Hence it does not provide a permanent solution for diagnosing one-turn short-circuit insulation failures. Thus, to overcome the disadvantages of previous work, the new clustering technique is applied to the diagnosis process of short-circuit fault [85]. The research work is broadly classified into three distinct categories. First, frequency-spectrum analysis of the load current is performed, and characteristic frequency components are extracted by a Fast Fourier Transform (FFT). Then, the frequency spectrum distortion ratio is derived using these components. Finally, a new diagnostic method is proposed using a support vector machine (SVM), and the proposed method is validated.

1.6.2 Broken Rotor Bar Fault

The cause for the broken rotor bar failure is discussed in the section 1.4.2. Since it is not possible to create the broken rotor bar fault as like occurring in the industries, in the present research work, the broken rotor bar failure is induced artificially by drilling the hole in the rotor bar. To match the condition to a certain point, the size of the hole is selected appropriately. Though it is not possible to match the exact criteria, the minor fault detection is achieved.

Still there is no solution and research result that show the defect of identifying the slight failure in the broken rotor bar. For this purpose, a probabilistic method is proposed to diagnose the broken rotor bar based on the feature distribution, where the amplitude of the two characteristics frequency components of load current spectrum is used as features [86]. This method will mainly focus on the characteristics frequency components of load current spectrum around the rated rotating speed. In this method, two important analysis is carried out. Firstly, by the help of the characteristic frequency components, it is possible to trace the existence or non-existence of the broken rotor bar. In addition to this, this method has a diagnosis result up to 4 broken bars. These results confirm that the proposed method has a property of even diagnosing the breakage of 1 broken rotor bar around the rated rotating speed. In both steps, clustering is carried out based on Self-Organizing Map (SOM). Although several diagnosis methods have been proposed, there is no proper report of applying clustering technique to the diagnosis of the rotor bar(s) failure. Hence this method has an advantage of using clustering to diagnosis the broken rotor bar.

1.6.3 Bearing Failure

The reason for the bearing failure is discussed in the section 1.4.3. From the case study, it is well-known that the fluting is the most common fault occurring in the bearing of the induction motor. Since it is not possible to create the exact fault occurring, the bearing failure analysis has been performed by creating the fault that almost matches the condition of fluting. The scratch and abrasion scratch are induced artificially on the outer raceway of the bearing and the failure analysis has been performed. The bearing failure analysis considering hole as the faulty is performed for reference. To match the condition to a certain point, the size and dimension of the faults are selected appropriately. Though it is not possible to match the exact criteria, the minor fault detection is achieved through the present study.

The signal from the load current is analyzed by means of Fast Fourier Transform (FFT). This analysis is carried out by characterizing the magnitude of the spectral analysis and to be considered as a main feature. To enhance the accuracy, a proper diagnosis is done with the help of the Support Vector Machine (SVM). Considering the industrial environments, hole, scratch and abrasion scratch have been considered as the faulty factor and the entire diagnosis

is performed without considering the rotating speed of the induction motor.

Initially, obtain the raw data from both the healthy and faulty motors under different rotating speed conditions. The collected raw data are preprocessed using fast Fourier transform analysis (FFT) and gain the frequency domain transformation. This transformation is necessary to study the difference in the constitutive frequency components and how they are distributed with respect to different bearing conditions. The amplitude of the selected frequency components is extracted and considered as features, and are used to train the SVM algorithm. The architecture gets varied depending on the application. Apply the proposed SVM model to diagnose the bearing fault considering industrial conditions. For validation, the SVM-based fault diagnosis method is tested for various fault analysis.

This method of scrutiny is employed for identifying the following bearing fault analysis. In case of hole, the following analysis is performed to study the fault difference in detail; identifying the distinct types of hole with respect to healthy motor [87]-[89], multiple hole analysis and localization of hole [90]. In practical point of view, scratch has the highest probability than hole, so the following bearing fault analysis is performed to identify the bearing fault in case of scratch; identification of scratches with respect to healthy motor [91]-[92], multiple scratches [90] and orientation of scratch [92]. Additionally, analysis has been performed considering both the hole and scratch, and identifications are done by differentiating both the faulty factor mutually and with the healthy motor [93]. Specially, abrasion scratch analysis is performed and found to have an impact on the bearing fault as like hole and scratch [94].

1.7 Thesis Outline

The organization of the thesis is as follows:

Chapter 2 explains about the diagnosis method proposed to detect the minor short-circuit fault using FFT analysis and SVM. Additionally, the frequency spectrum distortion ratio is derived to increase the accuracy rate of the proposed method.

Chapter 3 deals with the broken rotor bar fault. The analysis is performed using the FFT and the diagnosis is carried out using the clustering technique SOM. Based on the analyzes, the presence or absence of the broken rotor bar fault is detected and identifying the number of broken rotor bar is also made possible.

Chapter 4 is categorized to explain the bearing fault diagnosis that is performed considering hole as the faulty factor. The entire diagnosis is performed using SVM. The amplitude results from the spectral analysis is used to train the algorithm. The failure analysis is accomplished in relation to multiple hole analysis, localization of hole and identification of hole.

Chapter 5 is devoted to the analysis on the bearing fault diagnosis that is accomplished considering scratch as the faulty factor. Considering the fault that has the highest probability of occurrence, the failure analysis is performed in terms of identification of scratch, multiple scratch analysis and orientation of scratches. The entire diagnosis is performed using SVM and it is trained using the amplitude that results from the spectral analysis.

Chapter 6 deals with the compound analysis that has been performed inducing hole and scratch on the outer raceway of the bearing. A comparison is made between compound fault analysis and single fault analysis. The fault defects study is achieved using FFT and SVM.

Chapter 7 presents a detailed study regarding the common fault diagnosis method and multiple fault diagnosis system. A common diagnosis method is proposed to detect the short-circuit insulation failure, broken rotor bar fault and the bearing failure. Fault detection is achieved in a single method to any kind of failure occurring in the induction motor. The application of the proposed method is extended to identify the multiple faults occurring in the induction motor. The bearing fault and broken rotor bar failure is induced simultaneously, and the diagnosis is performed.

Chapter 8 presents the comparison results of diagnosis result among various machine learning algorithm and artificial neural network methods. The bearing fault has been selected for this case study. This chapter finds its usefulness in selecting the algorithm based on the objective and the application.

Chapter 9 concludes the remark of the thesis. These include the accomplished targets, limitation of the study as well as unaccomplished but interesting tasks that are related to this study and have been listed for consideration as future research works.

The thesis ends with a list of the publications made during the study.

Chapter 2
Diagnosis of Short-Circuit Insulation Failure in Stator Winding

2.1 Introduction

The short-circuit fault in stator winding is mainly due to the damage or deterioration of electrical insulation. Till now it was found that more than two-turn short-circuit fault could be diagnosed and still one-turn short-circuit fault could not be diagnosed properly. It is well known fact, at motor running condition once the fault begins with the one-turn and if it continues to proceed further if the fault is not identified. The one-turn short-circuit fault is initiating the stator winding insulation failure, which may lead to the breakdown of the entire system.

Thus, in the present study, the solution to identify the one-turn short-circuit fault is performed. The analysis is carried out using FFT and the diagnosis by Support Vector Machine (SVM).

2.2 One-Turn Fault Analysis

In this section, the details regarding the artificially induced short-circuit fault and the experimental setup is discussed.

2.2.1 Introduction of artificial fault

Three-phase induction motor (2.2 kW, 200 V, 8.9 A, 1680 min^{-1}, 4 poles) is used as a specimen. The stator winding of the motor is a double star connection as shown in Figure 2.1(a). The number of turns is 120 for each phase winding. The number of slots is 36. It is a time consuming and costly work to collect the motors with one turn-to-turn insulation failure in their windings, which occurred during operation at the site. Thus, in the present study, one turn-to-turn insulation failure was artificially introduced to a U-phase stator winding of a new

motor as shown in Figure 2.1(b).

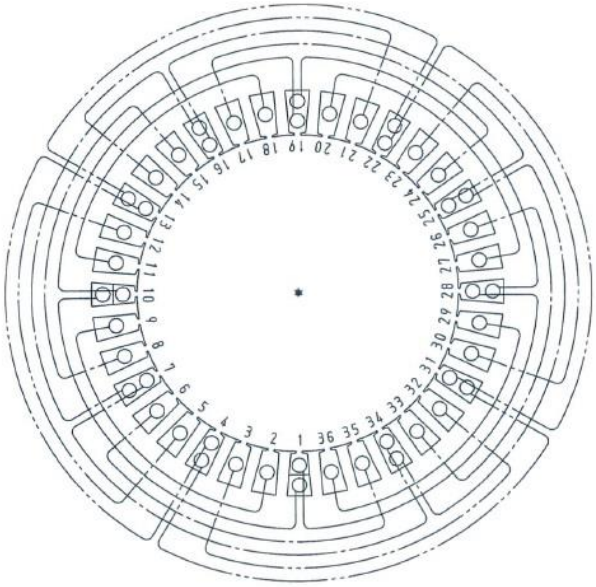

a) Construction of stator winding

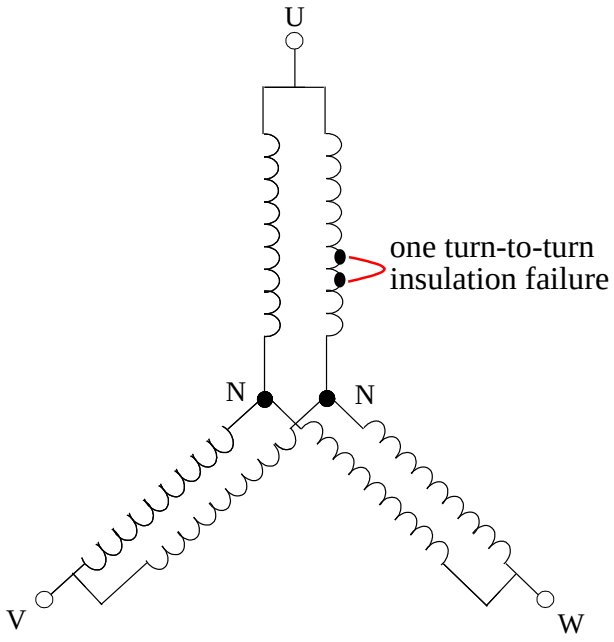

b) 1-Turn insulation failure

Figure 2.1 *Stator winding and fault configuration.*

2.2.2 Experimental Procedures

Figure 2.2 shows the experimental setup. Load currents of the stator windings and the voltages were measured with current probes (HIOKI 9695-02) and voltage probes (HIOKI 9666), respectively. The rotating speed was monitored with a speed indicator (Ono Sokki HT-5500). Outputs from the sensors were acquired simultaneously with a measurement system developed by the author. Also, the obtained output signals from the various sensors were transferred to a desktop computer via measurement equipment and recorded. The measurement equipment has seven input terminals and seven A/D converters. The sampling time was 10 μs and the data recording length was 2^{17} per channel. Thus, the frequency resolution was about 0.76 Hz. In the present study, 7 channels were used to record 3 phase currents, 3 line-to-line voltages and rotating speed. Data acquisition was triggered by a timer for every 30 s and the time required for data transfer of 7 channels was less than 20 s.

A healthy motor was also tested for reference before the artificial one turn-to-turn insulation failure was made. The rotating speed of the induction motor was varied by changing the load so that the value of instantaneous load current lay between 8 and 12 A. Experiments were also carried out under no load condition (1800 min^{-1}). During the experiment, maintaining the rotating speed of the induction motor as constant find difficult and always a variation about 2-3 min^{-1} in the rotating speed was observed. Presumably, 83 and 89 measurements were carried out for motors with healthy winding and one turn-to-turn insulation failure winding, respectively. The frequency of the power source was 60 Hz.

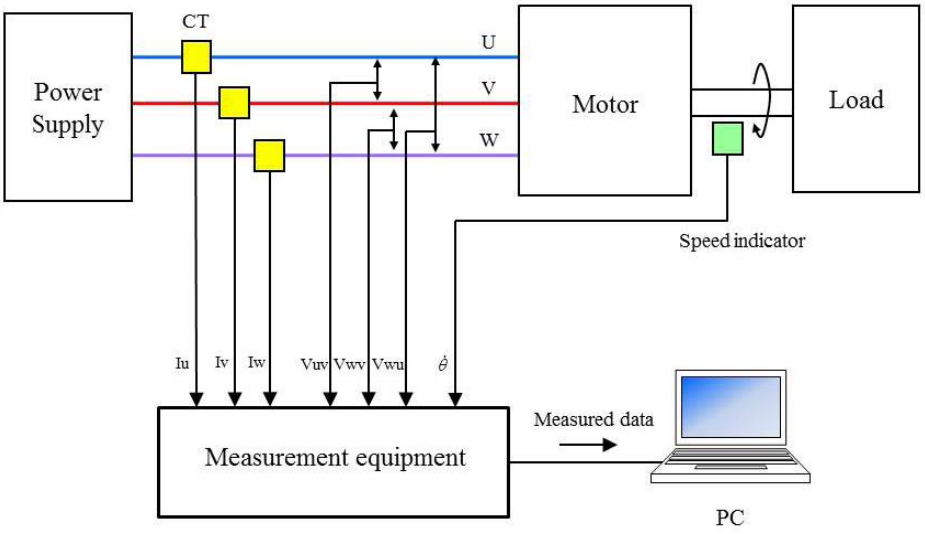

Figure 2.2 *Experimental setup of proposed system.*

2.3 Frequency Spectrum Analysis

In this section, the amplitudes of characteristic frequency components of load current are extracted and considered as features. These features are extracted by close analysis of frequency spectrum and its dependence on load current variation.

2.3.1 Frequency Spectrum of Load Current

Fast Fourier transform (FFT) Analysis was performed to the data of healthy and one-turn insulation failure windings.

Figures 2.3 and 2.4 show frequency spectrum of the load current flowing into healthy and one turn-to-turn insulation failure windings under no load condition, respectively. Amplitude in the vertical axis of these figures is normalized so that the maximum value is 0 dB. No remarkable difference is confirmed in frequency spectra between healthy and one turn-to-turn insulation failure conditions. Diagnosis of turn-to-turn insulation failure is impossible by the load current spectrum obtained under no load condition.

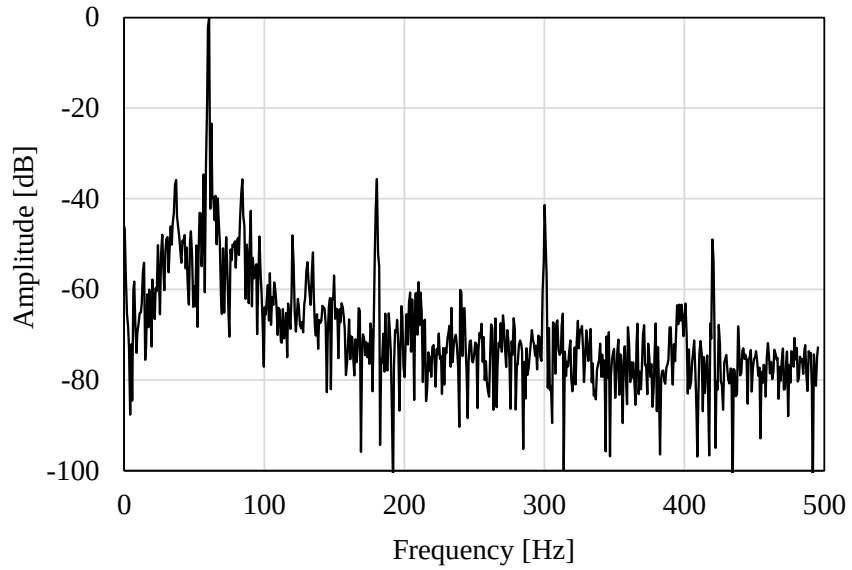

Figure 2.3 *Spectrum of load current for healthy stator winding under no load condition.*

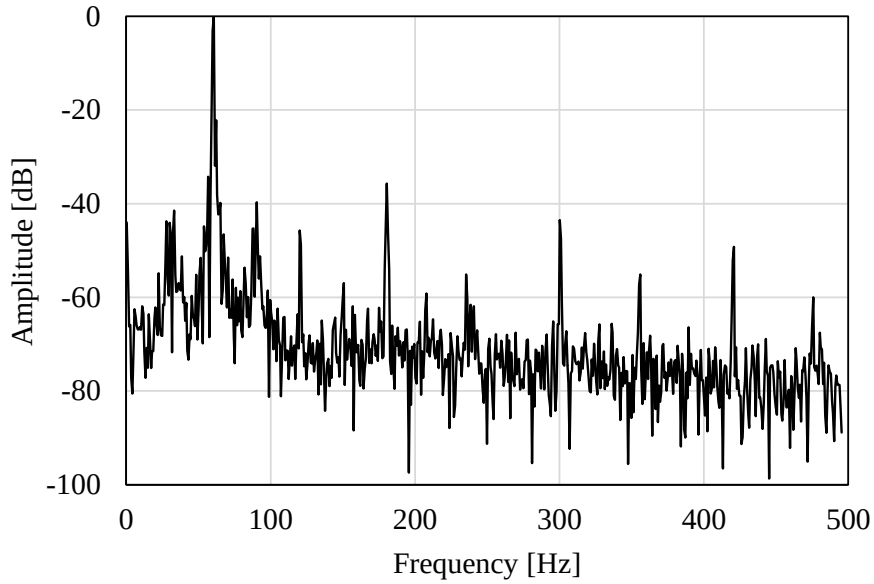

Figure 2.4 *Spectrum of load current for one-turn insulation failure stator winding under no load condition.*

Examples of frequency spectra of load currents under the load condition are shown in Figures 2.5 and 2.6 for healthy and one-turn insulation failure conditions, respectively.

The difference in magnitude is recognized between healthy and one turn-to-turn failure windings at some frequency components. The peak amplitudes are observed at the integral multiple of frequency 30 Hz, which corresponds to the ratio of power frequency (60 Hz) to the number of pole pairs (2).

$$\mathrm{A} = \frac{P_f}{P} \tag{2.1}$$

where P_f stands for the power frequency and P stands for the number of pole pairs. In the present study, the number of poles is 4.

2.3.2 Determination of Features

To quantify the difference in frequency spectra shown in Figures 2.5 and 2.6, absolute value for the difference in amplitude is calculated. Figure 2.7 shows the result, where the average of 80 frequency spectra was used for each winding condition considering a temporal variation of frequency spectrum under load condition. Amplitude difference larger than 15 dB is recognized between healthy and one-turn insulation failure windings at some of the frequencies of an integral multiple of 30 Hz; 30, 90, 120, 150, 240, 270, 330, 360, 390, 450 and 480 Hz. The amplitude of these frequencies is considered as features and the diagnosis is carried out.

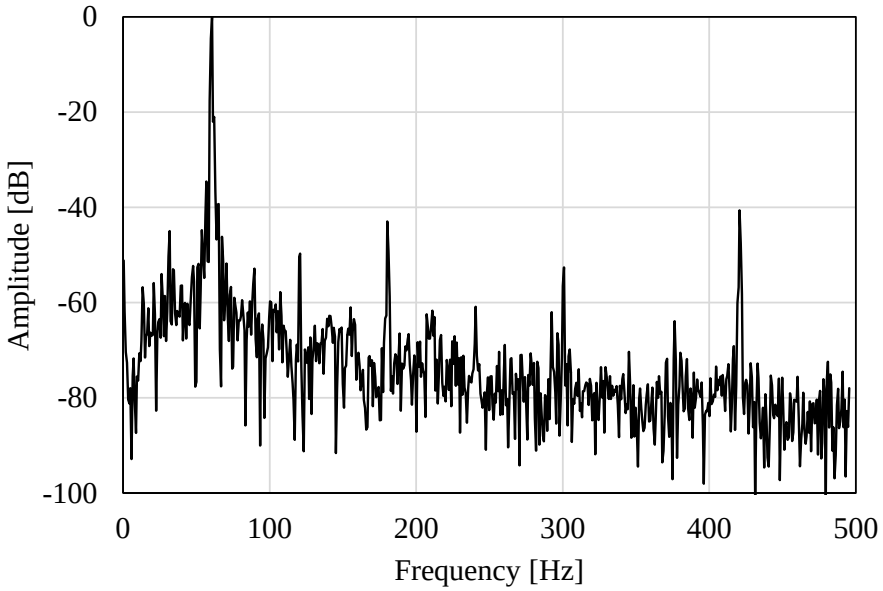

Figure 2.5 *Spectrum of load current for healthy stator winding under load condition.*

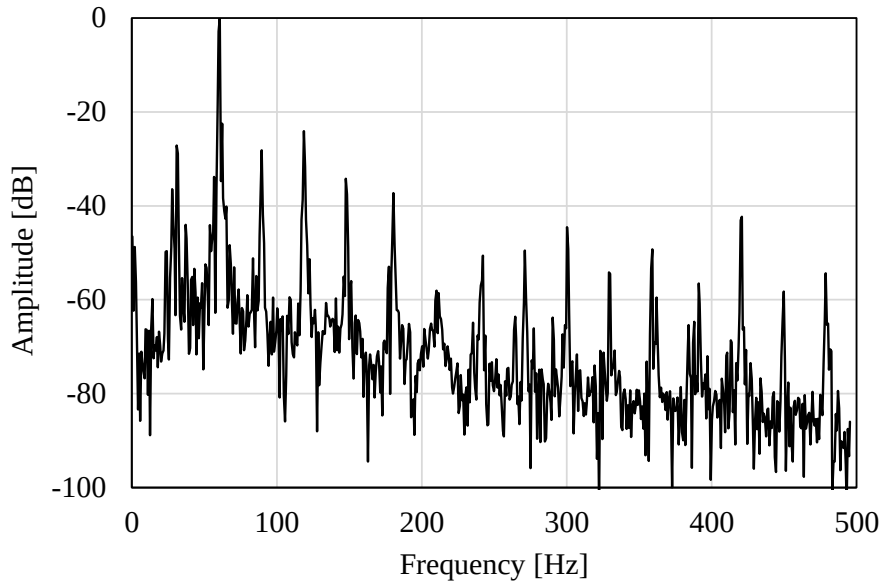

Figure 2.6 *Spectrum of load current for one-turn insulation failure stator winding under load condition.*

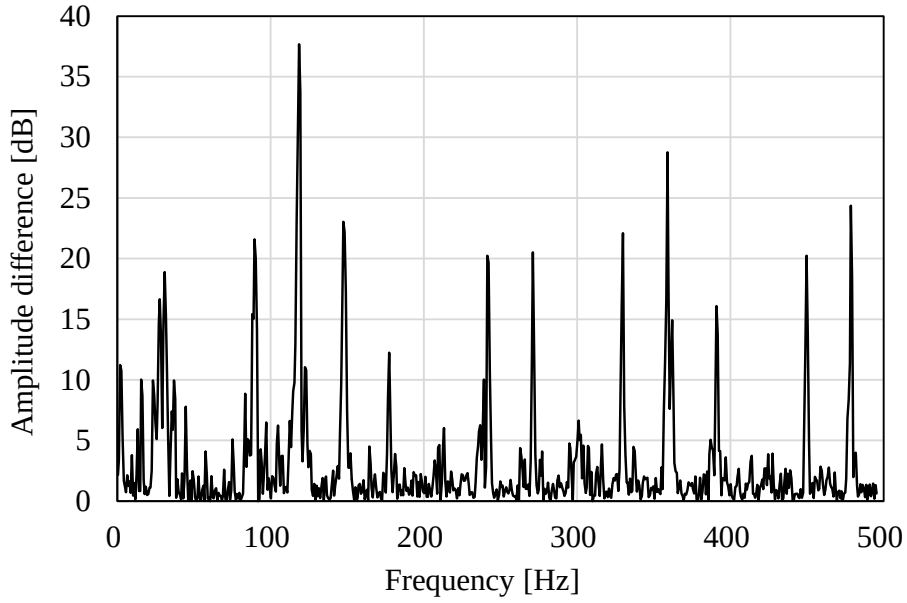

Figure 2.7 *Absolute amplitude difference between Figures 2.5 and 2.6.*

Load current dependence of the magnitude of these frequency components is shown in Figures 2.8 and 2.9 for healthy and one turn-to-turn insulation failure windings, respectively. In the case of healthy winding, the magnitude decreases with current. The relation between the magnitude of frequency components and the load current is complicated for one-turn insulation failure winding. Since load current is subjected to change at the site depending on load, it is necessary to select appropriate frequency components for diagnosis. These selected frequency components should have a larger difference when compared with two winding conditions regardless of the load current.

The amplitude distribution of the frequency components for a healthy winding obtained by 83 measurements is shown in Figure 2.10. Similarly, that of one-turn insulation failure winding acquired by 89 measurements is shown in Figure 2.11.

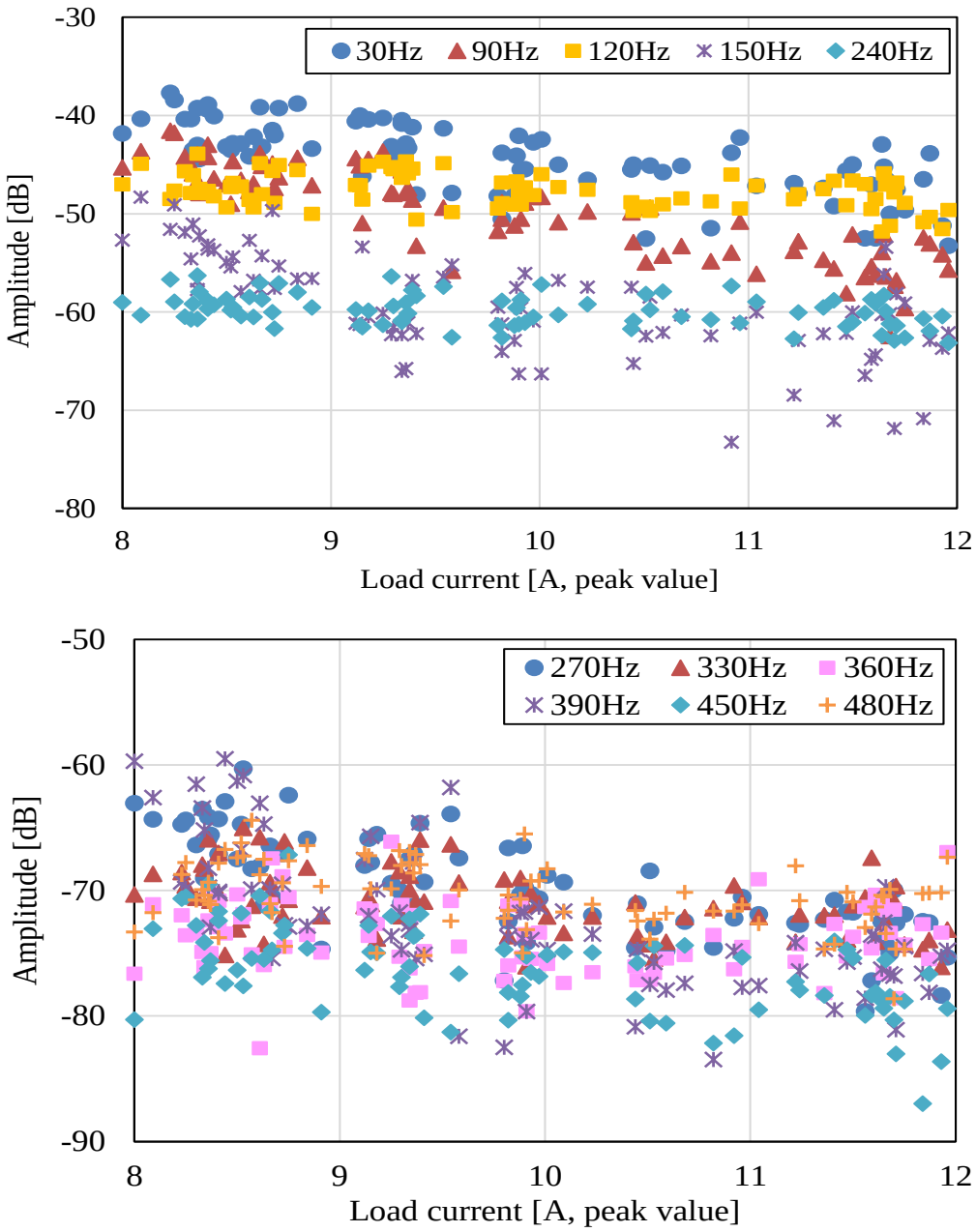

Figure 2.8 *Magnitude of frequency components in the case of healthy winding.*

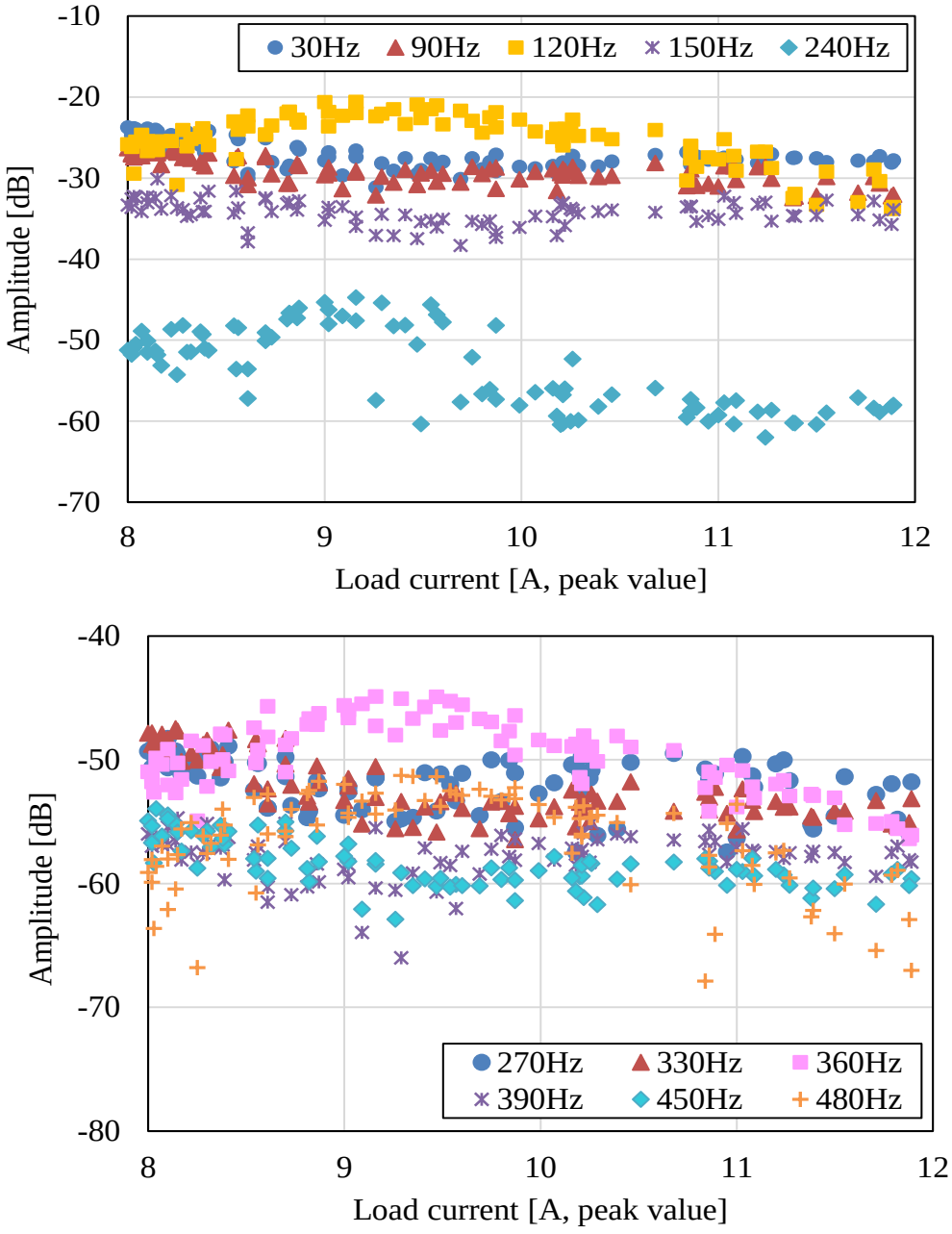

Figure 2.9 *Magnitude of frequency components in case of one turn-to-turn insulation failure winding.*

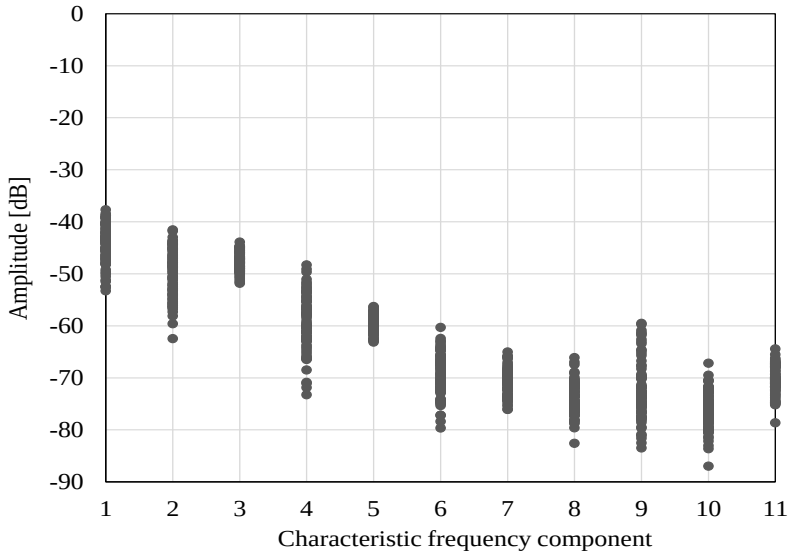

Figure 2.10 *Amplitude distribution of characteristic frequency component for healthy winding. Horizontal axis stands for 1:30Hz, 2:90Hz, 3:120Hz, 4:150Hz, 5:240Hz, 6:270Hz, 7:330Hz, 8:360Hz, 9:390Hz, 10:450Hz, and 11:480Hz.*

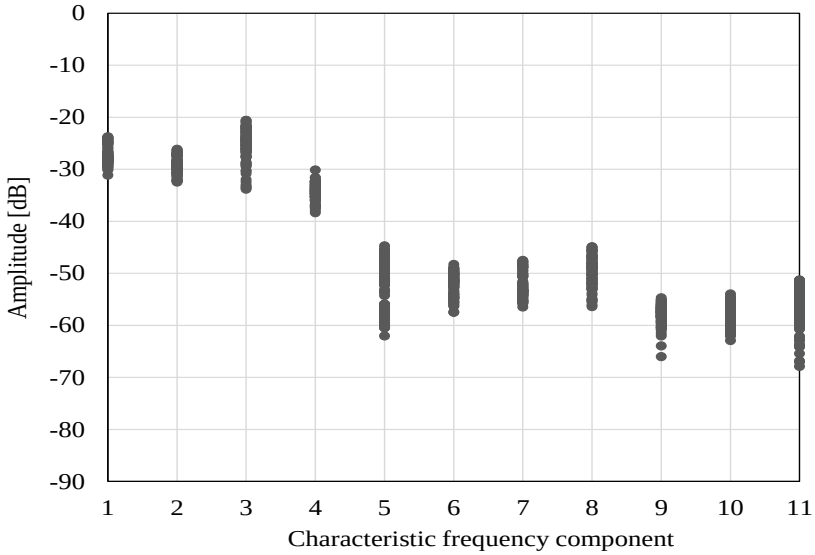

Figure 2.11 *Amplitude distribution of characteristic frequency component for one-turn insulation failure winding. Horizontal axis stands for 1:30Hz, 2:90Hz, 3:120Hz, 4:150Hz, 5:240Hz, 6:270Hz, 7:330Hz, 8:360Hz, 9:390Hz, 10:450Hz, and 11:480Hz.*

In the present study, 90, 120 and 150 Hz are selected as characteristic frequency components. The reasons are stated as follows:

- Amplitude is large when compared with those of higher frequency components.
- Amplitude distributions of healthy and one turn-to-turn insulation failure windings do not overlap each other.
- Amplitude difference between the two-winding condition is about 10 dB or larger.

2.4 Diagnosis using SVM

2.4.1 Brief Explanation of SVM

In this section, the use of SVM for detecting short-circuit failures is discussed. SVM is a pattern recognition method that has been used to classify objects into categories. SVM belongs to the group of linear classification methods but can also perform non-linear classification. This is done using a kernel function, mapping high input operators with high dimensional features. SVM uses soft margins and hard margins. The SVM type and its usage are determined by the linearity condition. This study applied non-linear classification so that the soft margin matched the prescribed condition.

In Soft Margin SVM, cost parameter C is introduced, which controls the trade-off between maximizing the margin and minimizing the training error. If the value of C is lower, it tends to emphasize the margin, ignoring the outliers in the training data. Contrarily, larger C value tends to overfit the training data. Besides, Radial Basis Function kernel is also used commonly as gamma parameter γ and the boundary decision is established. Smaller γ value leads to a simple decision boundary and vice-versa. Thus, both the cost parameter and gamma parameter play a significant role and their tuning are accomplished.

In the present work, initially data were divided into eight groups, the first seven of which provided training data. Data from group eight were used for evaluation. By alternating the groups, seven group diagnosis accuracy rates were obtained, and the average was calculated. The process was repeated for the different values of C and γ.

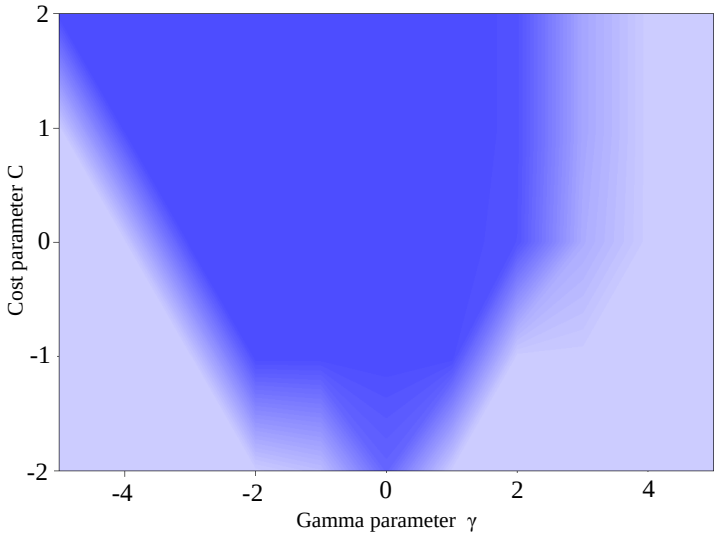

Figure 2.12 *Accuracy variation between cost parameter and gamma parameter.*

Figure 2.12 shows the two-dimensional map plotted against the accuracy rate variation involving cost parameter C and gamma parameter γ. The higher accuracy rate is obtained in the deep blue color portion by varying the values of C and γ. Table 2.1 summarizes the SVM specification handled for present study of short-circuit failure diagnosis. Programming was done using R language software and python. The accuracy rate was derived as follows:

$$\text{Accuracy rate } (\%) = \frac{Number\ of\ data\ diagnosed\ properly}{Total\ number\ of\ data\ used\ for\ diagnosis} \text{X100} \qquad (2.2)$$

Table 2.1 *SVM description*

Type of SVM	**Soft Margin SVM**
Kernel	Radial Basis Function Kernel
Gamma parameter	2^{-4}
Cost parameter	2^{-1}
Number of support Vectors	8
Number of classes	2
Threshold in training	0
Threshold in prediction	0.5

2.4.2 Diagnosis result

In the current study, both 83 and 89 sets of data were used as training data for healthy and one turn-to-turn insulation failure windings, respectively. Likewise, 60 and 110 sets of data were used as verification data for each winding condition, respectively. In this action, a datum set consists of 6 components; amplitude of the healthy and one-turn insulation failure winding conditions of 90, 120 and 150 Hz components. A verification datum was evaluated with a model constructed beforehand by using training data and then classified into one of the two specified categories of winding condition (healthy or one-turn insulation failure).

Results of diagnosis for 90, 120 and 150 Hz components are shown in Table 2.2. A yellow-colored cell means the case where the precise diagnosis is performed. The accuracy rate is 100 % (60/60) for the case of healthy winding and 91.8 % (101/110) for one-turn insulation failure windings. The overall accuracy rate is 94.7 % (161/170). This value is practically acceptable.

Table 2.2 *Results of diagnosis for 90, 120 and 150Hz components.*

		Winding condition of target motor	
		healthy	one-turn insulation failure
Diagnosis Result	healthy	60	9
	one-turn insulation failure	0	101
Accuracy rate (%)		100	91.8
Overall accuracy rate (%)		94.7	

The diagnosis was also performed by using amplitude of other combinational frequency components as features, resulting a little lower accuracy rate as shown in Table 2.3. Inherently it is clear that, usage of 90, 120 and 150Hz frequency components results in the best accuracy rate. This may be attributed to the reason described in 2.3.2.

This method suffers from the major drawbacks such as a convoluted process of selecting the combinational frequency components for diagnosis, and an accuracy rate that varies

depending on this selection. Hence it does not provide a permanent solution for diagnosing one-turn short-circuit insulation failures.

Table 2.3 *Diagnosis results for other frequency components.*

Characteristic frequency components (Hz)	Overall accuracy rate (%)
90, 120, 150, 330, 360	92.94
30, 90, 120, 150, 240, 270, 330, 360, 390, 450, 480	92.94
90, 120, 150, 270, 330, 360	92.35
90, 120, 270	90.59
30, 150, 270	90.00
330, 360	90.00
30, 90, 120, 150, 330, 360	89.09
30, 330, 360	88.82
270, 330, 360	88.82
330, 360, 480	88.24

2.5 Diagnosis using Distortion Ratio

To overcome the disadvantages of previous work, the new clustering technique is applied to the diagnosis process of short-circuit fault. The presently carried research is broadly classified into three distinct categories. First, frequency-spectrum analysis of the load current is performed, and characteristic frequency components are extracted. Then, the distortion ratio is derived using these components. Finally, diagnosis is carried out using a support vector machine (SVM).

2.5.1 Discussion of the Frequency Spectrum

The load tests are performed on both two healthy and one-turn short-circuit insulation failure windings. Initially, FFT analysis for the measured load current is carried out continuously for current waveforms and the results are recorded. The examples of frequency-spectrum

analysis on the U phase of a stator winding for healthy motor 1, healthy motor 2 and one-turn short-circuit failure motor are illustrated in Figures 2.13 to 2.15, respectively.

The amplitude of the vertical axis is normalized to take 0 dB as its maximum value. A remarkable difference in magnitude is observed between these windings (two healthy and faulty winding) at certain frequency components due to the occurrence of the short-circuit fault.

The phenomenon for the appearance of signals at the integral multiple of 30 Hz and their mechanism is discussed below. Generally, asymmetry is created when the short-circuit fault occurs and leads to the generation of two opposite direction MMF (±f) inside the stator winding. Because of magnetomotive force, the following current harmonics (k/p±1)*f is generated in the rotor [1], where k=1, 2, 3 takes the sequential value and p represents the number of pole pairs. Furthermore, due to the interaction caused between stator and rotor, the circulating current harmonics (k/p±1)*f of the rotor affect the stator of the induction motor just like the case of the broken rotor bar [2]-[3]. Therefore, it is considered that the current harmonics with an integer multiple frequencies f/p are generated in the stator current. In the case of low load that is a nearly no-load condition, the current harmonics flowing into the rotor part are very small and the stator is barely affected. In this condition, it is hard to measure the f/p signals in the load current. Indeed, the signals calculated at the low load condition is hardly measured during the experiment and this circumstance turns out to be the mechanism to support the appearance of the signals at the integral multiples of 30 Hz.

An amplitude difference larger than 15 dB is recognized for some frequency components, namely 30, 90, 120, 150, 210, 270, 330, 360, 390, 450, and 480 Hz. Since fluctuation often occurs in the frequency spectrum, it is better to choose multiple frequency components. Thus, attention should be paid to these eleven frequencies to identify the one-turn short-circuit insulation failure of the stator winding.

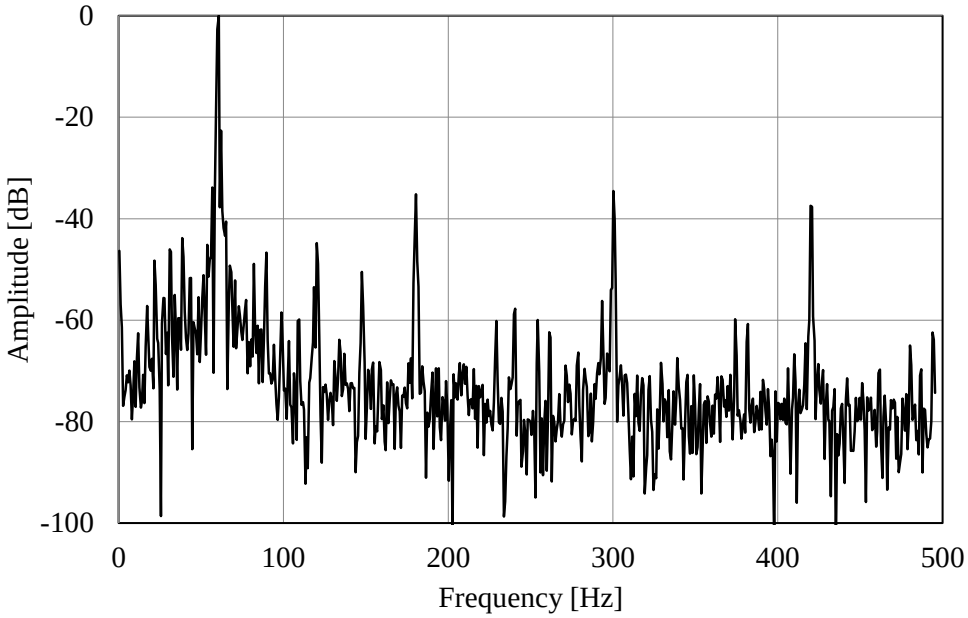

Figure 2.13 *Frequency-spectrum analysis of healthy winding 1.*

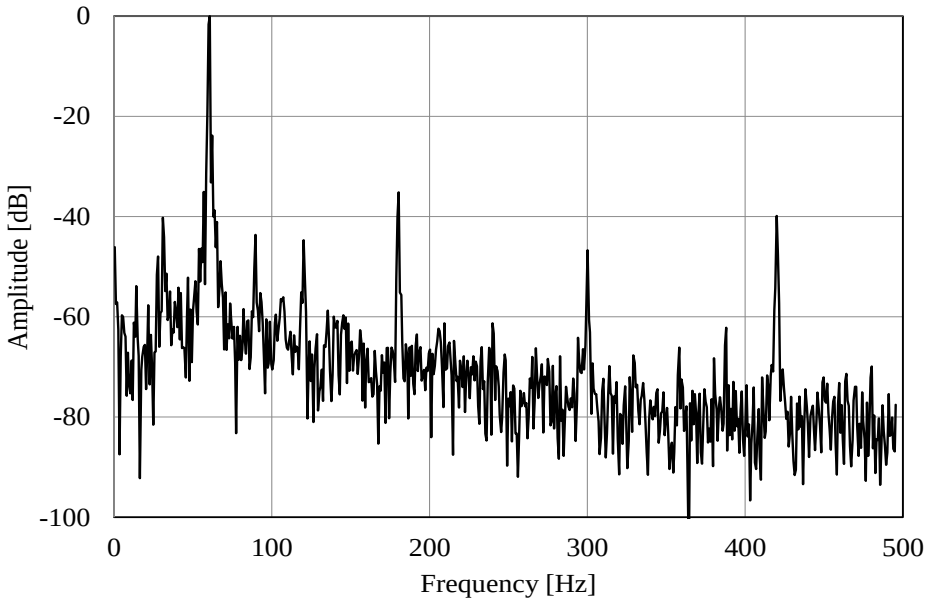

Figure 2.14 *Frequency-spectrum analysis of healthy winding 2.*

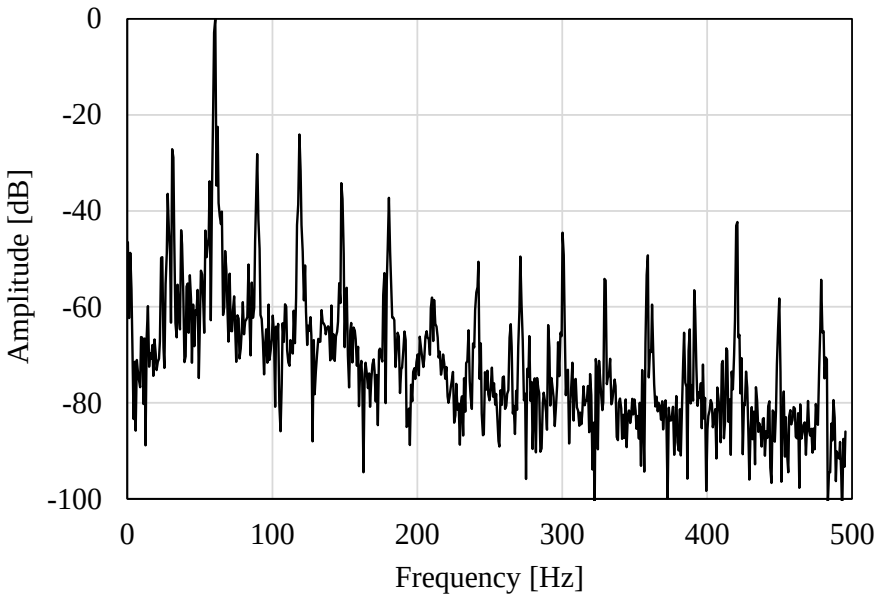

Figure 2.15 *Frequency-spectrum analysis of one-turn short-circuit insulation failure winding.*

2.5.2 Introduction of Distortion Ratio

Generally, the distortion ratio is defined as the ratio of the sum of the RMS amplitude of higher harmonic frequencies to the RMS amplitude of the fundamental frequency. It is defined as

$$\mathrm{D} = \frac{\sqrt{\Sigma_i A_i^2}}{A_f} \tag{2.3}$$

where A_i and A_f stand for the RMS amplitudes of the harmonic and fundamental frequencies, respectively. In the present study, the RMS amplitude of eleven characteristic-frequency components is used instead of harmonics. Thus, the distortion ratio is defined as the ratio of the sum of the RMS amplitudes at selected frequencies to the RMS amplitude of the fundamental frequency. The fundamental frequency is 60 Hz. Therefore, the distortion ratio

of the load current is defined as

$$D = \frac{\sqrt{A_{30}^2 + A_{90}^2 + \cdots + A_{480}^2}}{A_{60}} \tag{2.4}$$

The amplitude of frequency spectrum changes at all time. The result of distortion ratio shows less amount of variation between the amplitude. Adding further advantages, irrespective of each phase current, the features of 8^{th} order frequency can be reduced to one feature. Thus, the handling of the feature is made easy and the detection can be done flawlessly.

2.5.3 Results of Distortion Ratio

Figures 2.16 and 2.17 show the distortion ratios of three-phases (D_u, D_v, and D_w) and the amplitudes for load currents of the healthy stator winding, respectively. It clarifies the fact that the amplitude of the load current between each phase varies intensely, whereas the distortion ratio has fewer changes between each phase.

Similarly, Figures 2.18 and 2.19 show the distortion ratios of three-phases (D_u, D_v, and D_w) and amplitudes of load currents for the one-turn short-circuit insulation failure stator winding, respectively. The result obtained is like that of the healthy winding. That is, the amplitude of load current between each phase varies intensely, whereas the distortion ratio has fewer changes between each phase.

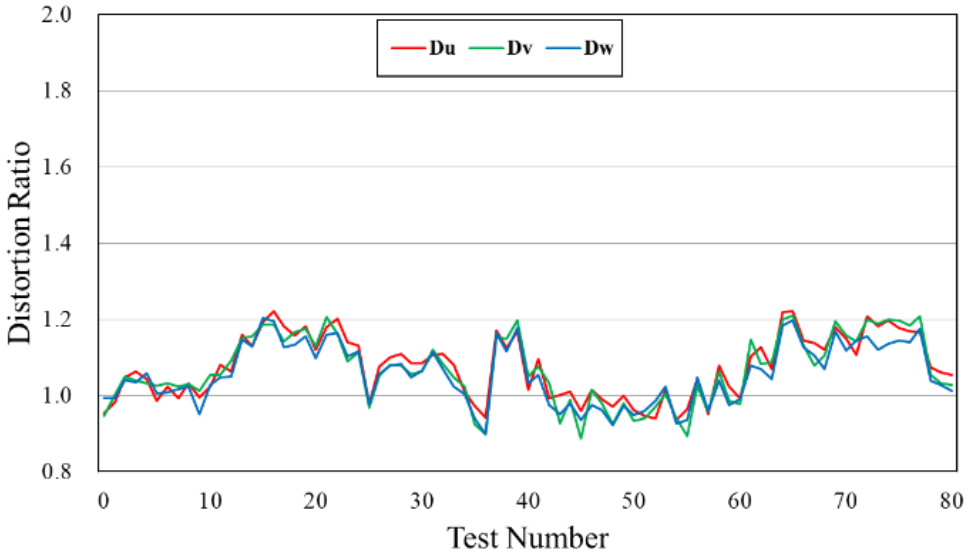

Figure 2.16 *Three phase-distortion ratios of load current (healthy).*

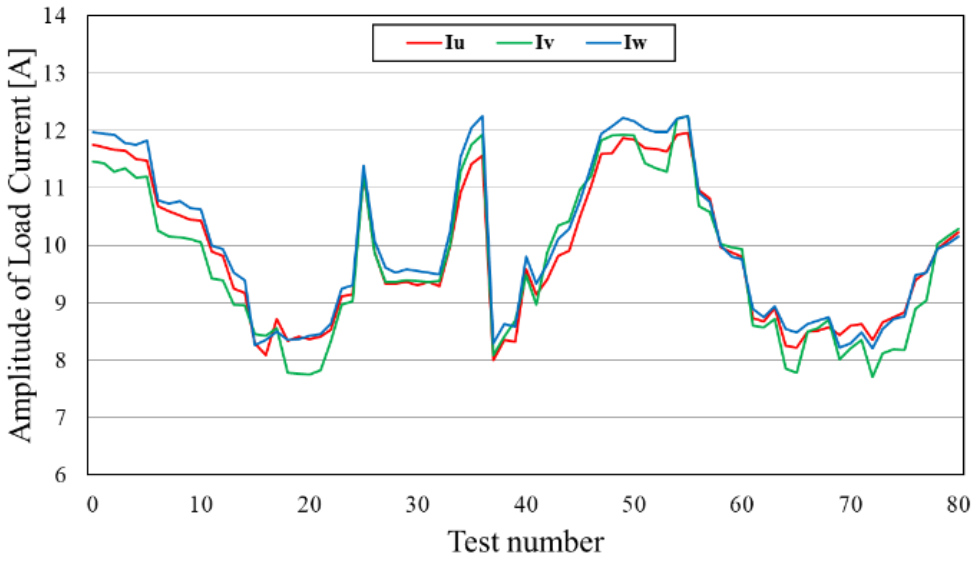

Figure 2.17 *Amplitude of the load current (healthy).*

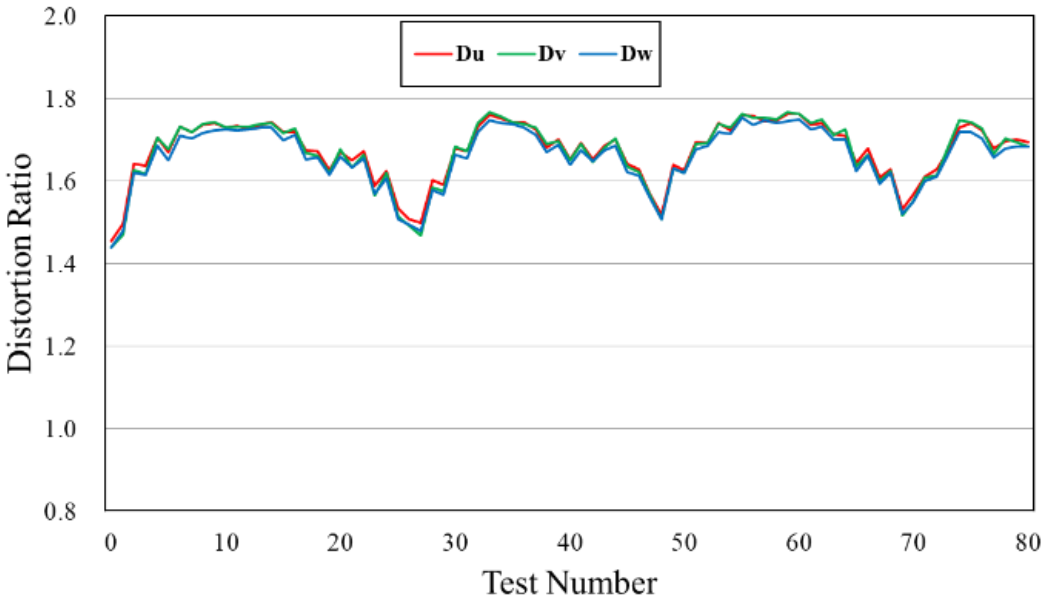

Figure 2.18 *Three phase-distortion ratios of the load current (one-turn short-circuit insulation failure winding).*

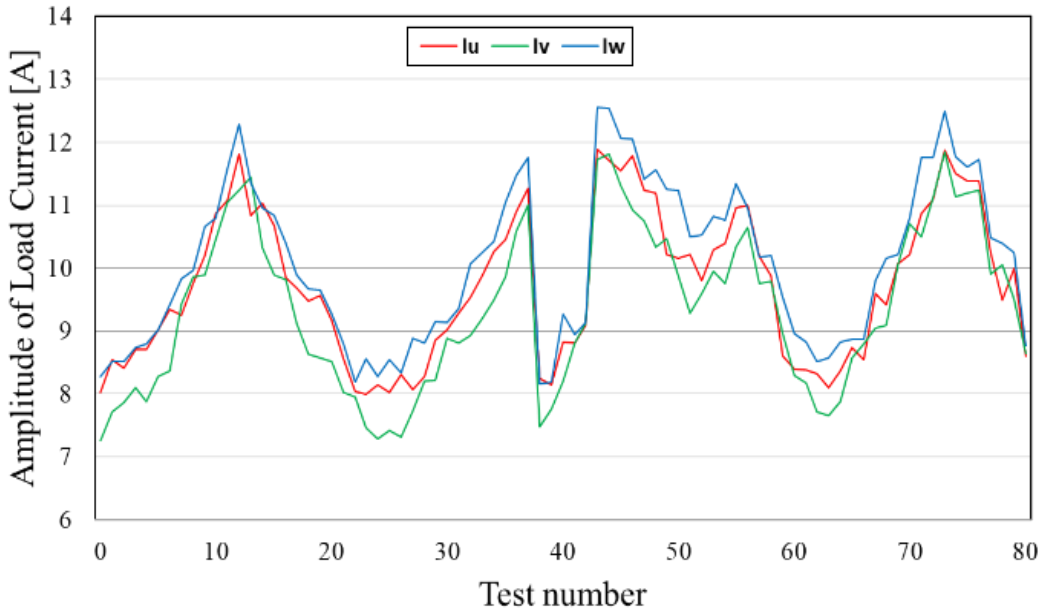

Figure 2.19 *Amplitude of the load current (one-turn short-circuit insulation failure winding).*

An interesting fact is that the distortion ratio of each phase takes nearly the same range. Moreover, a higher magnitude difference is observed between the distortion ratios of the healthy winding and the one-turn short-circuit insulation failure winding. These magnitude differences will enable the distortion ratio to discriminate healthy and one-turn short-circuit windings. The obtained distortion ratio is not influenced by the abrupt change of load current. The fault is introduced to the U-phase of the stator winding, but the distortion ratios of V and W-phase also similar changes as like U-phase. Thus, irrespective of the fault phase, the detection can be achieved by recording the data of any phase. In short, any one phase current is enough to detect the one-turn short-circuit insulation failure. This reduce the cost and processing time. Hence, this is a core feature of the present system and implies the advantages of using distortion ratio.

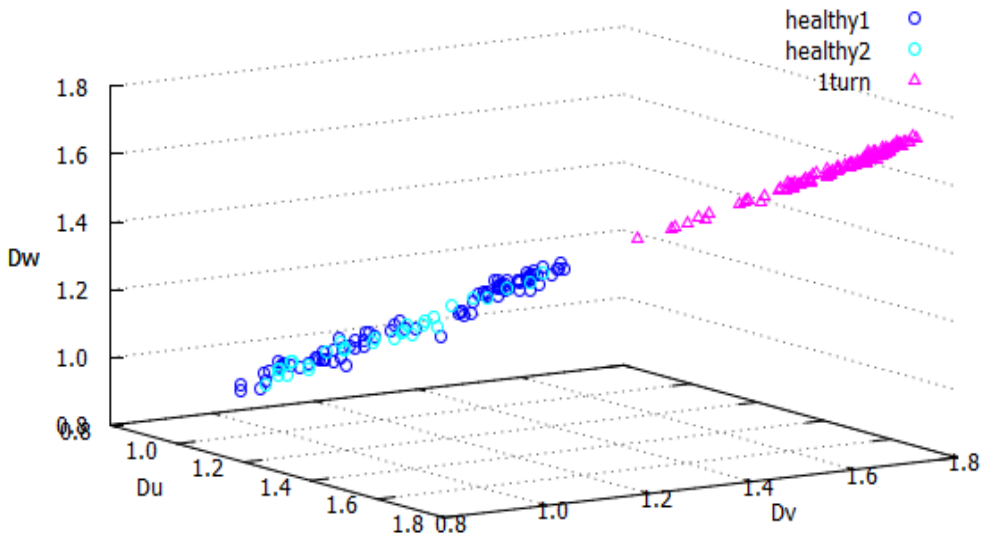

Figure 2.20 *Three-dimensional distortion-ratio analysis (D_u, D_v, D_w).*

For easy understanding, 2.20 is plotted, and it shows the three-dimensional distortion ratios of the three classes of motors (two healthy, and one turn failure motor). One of the interesting notes observed is that the condition of the motor is linearly distributed even when the load current changes discretely. The data of two healthy motors and one-turn short-circuit insulation failure motor are located according to their own classes. By representing the result

of distortion ratios three-dimensionally, the winding condition can be visualized and identified conveniently.

2.5.4 Diagnosis Result using SVM

Diagnosis based on SVM is performed using the distortion ratio of the load current, which is derived from the amplitudes at characteristic frequencies. This diagnosis is carried out by considering the distortion ratio of three-phases (D_u, D_v, D_w). For both the healthy and one-turn short-circuit winding, the datum consists of the amplitude of the distortion ratio.

In the present study, 90 (healthy 1: 60, healthy 2: 30), and 111 (1-turn short-circuit) datasets are used to train the SVM as healthy and faulty windings, respectively. Newly measured 107 (healthy 1: 24, healthy 2: 83), and 89 (1-turn short-circuit) datasets are used as diagnostic data to validate the method for each respective winding condition.

The yellow cells indicate where the proper diagnosis is performed. The accuracy rates for individual winding conditions, as well as the total accuracy rate, are 100%, as shown in Table 2.4. High accuracy rate can be obtained, even for one-turn short-circuit insulation failure in the stator winding of an induction motor. The diagnosis is performed using the distortion ratio without considering the frequency components. Hence, the reliability of the proposed diagnostic system is high. Thus, the drawbacks of selecting the frequency components are eliminated, and high accuracy rate is obtained.

Table 2.4 *Three-phase diagnosis results.*

		Data for evaluation	
		Healthy	one-turn insulation failure
Diagnosis Result	Healthy	107/107	0
	one-turn insulation failure	0	89/89
Accuracy rate (%)		100	100
Total accuracy rate (%)		100	

2.6 Summary

The method to diagnose the minor inter-turn short-circuit fault (one-turn) is proposed and the diagnosis results are discussed. The analysis is carried out using FFT of load current, distortion ratio and finally the diagnosis using SVM. Till now, the two-turn short-circuit insulation failure detection is made possible using the FFT analysis and SVM. In the present study, one-turn short-circuit insulation failure detection is made possible employing the distortion ratio of load current, which uses the feature of the selected specific characteristic frequency components. From the diagnostic result, the accuracy of different winding conditions is high (100%). Thus, the method is beneficial for diagnosing one-turn short-circuit insulation failure in the stator winding of induction motors and can be considered effective.

Chapter 3
Detection of Broken Rotor Bar Fault using Clustering Techniques

3.1 Introduction

Frequent starting and stopping of motors will cause thermal fatigue, which may cause breakage of rotor bars and/or end rings of cage induction motor. Mechanical vibration in passing rail junctures may result in rotor bar failure of motors installed in train. Failure in the rotor cages of induction motors such as end-rings and rotor bars are one of the main mechanical failure in the motor drive systems, which stands next to the bearing failure. Thus, identifying the broken rotor bar fault also must be considered and diagnosis should be carried out. Although several diagnosis methods have been proposed, there is no proper report of applying clustering technique to the diagnosis of the rotor bar(s) failure.

In the present study, the broken rotor bar fault diagnosis is carried out by focusing the several characteristic frequency components of load current spectrum around the rated rotating speed. In the first step, the existence or nonexistence of broken rotor bars is confirmed by using characteristic frequency components, whose amplitude changes greatly when rotor bars are broken. After diagnosing the rotor bar breakage, the next step is performed to identify the number of broken bars. Other characteristic frequency components are adopted, whose amplitude changes monotonically with the number of broken bar. In both steps, clustering is carried out based on Self-Organizing Map (SOM). The expediency of the proposed method is verified by some experiments.

3.2 Measurement of Load Current

Three-phase induction motors (2.2 kW, 200 V, 8.6 A, 1705 min^{-1}, 4 poles) were used as a specimen. Experimental setup is shown in Figure 3.1. The powder brake was connected to a motor and act as a load. Phase currents (load currents) and line-to-line voltages were measured at a given rotating speed. Current and voltage were measured with current probes (HIOKI 9695-02) and voltage probes (HIOKI 9666), respectively. Rotating speed was also monitored with a speed indicator (Ono Sokki HT-5500).

Output signals of the sensors were acquired simultaneously with a measurement system. It has eight BNC input terminals and A/D converters so that signals are transferred to a computer and recorded. The sampling time is set to 10 μs and the data recording length is 2^{17} per channel. Thus, the frequency resolution is about 0.76 Hz. In the present study, 7 channels (3 current, 3 voltage and rotating speed) were used. Data acquisition was trigged by a timer for every 30 s and time required for data transfer of 7 channels was less than 20s.

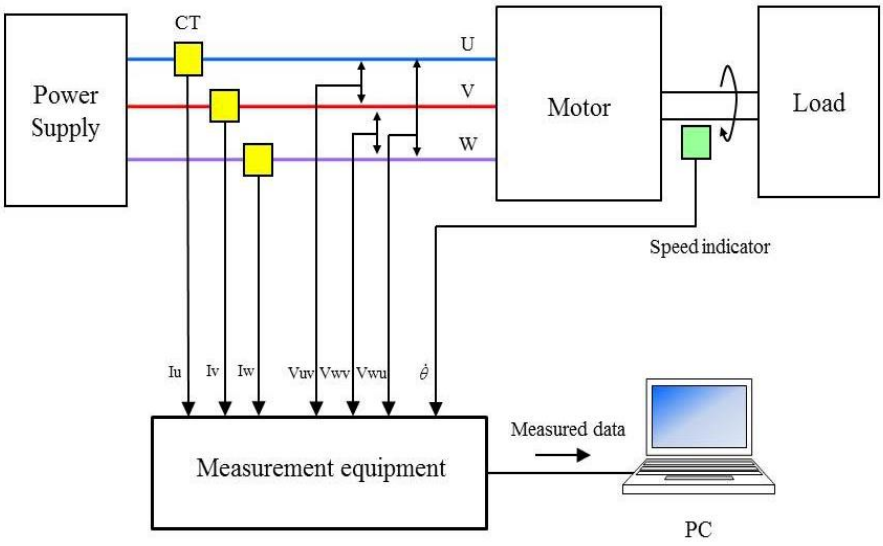

Figure 3.1 *Experimental setup.*

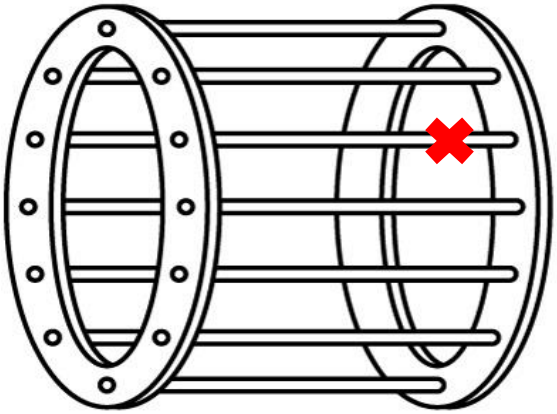

a) 1 broken bar

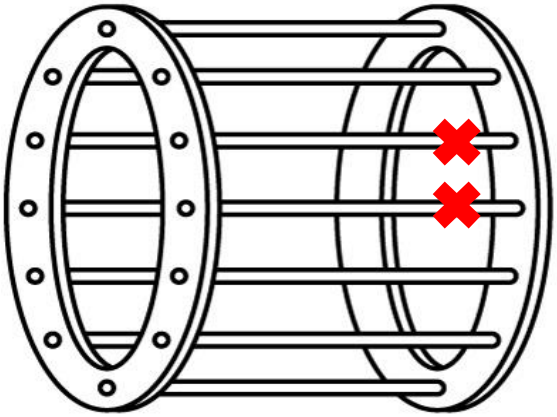

b) 2 broken bars

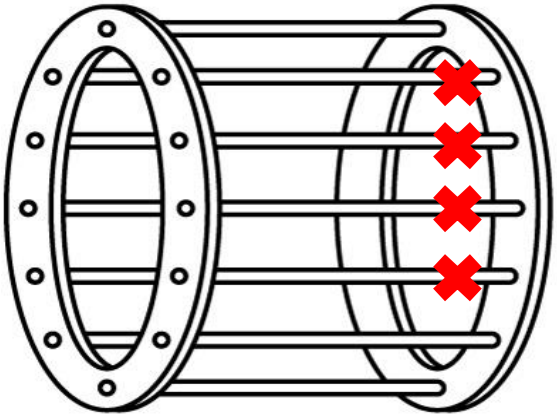

c) 4 broken bars

Figure 3.2 *Production of breakage in rotor bar.*

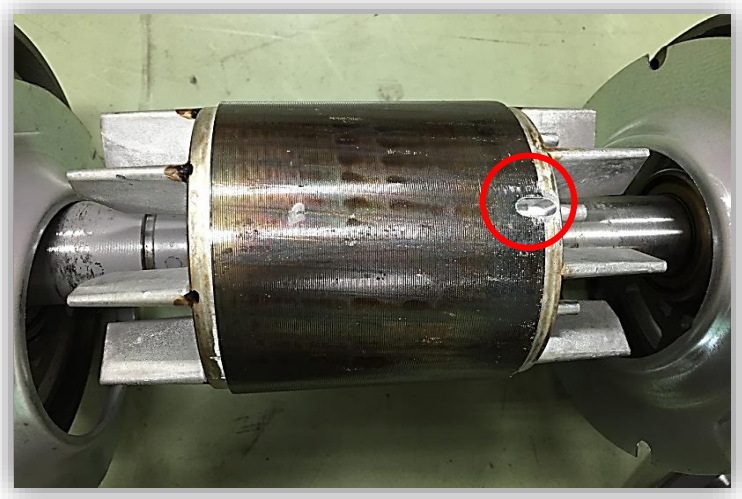

Figure 3.3 *Sample specimen.*

The 1, 2 or 4 rotor bar(s) of a healthy motor were broken by drilling holes in the bar(s). In the case of plural breakage bars, adjacent bars were broken. The artificially induced breakage in the rotor bar is shown in Figure 3.2. The sample image of 1 broken rotor bar is shown in Figure 3.3.

3.3 Frequency Analysis of Load Current

FFT analysis of U-phase load currents was performed for a healthy motor and motors with broken bars. As an example of the results, frequency spectrum of the healthy motor is shown in Figure 3.4 at the rotating speed of 1700 min^{-1}. At the same rotation speed, frequency spectrum of motors with 1, 2 and 4 broken bars are shown in Figures 3.5 to 3.7, respectively. The amplitude in the vertical axis of these figures is normalized so that the maximum value is unit. Arrows in Figures 3.5 to 3.7 show the characteristic frequencies extracted for diagnosis. The frequency of the power source is 60 Hz.

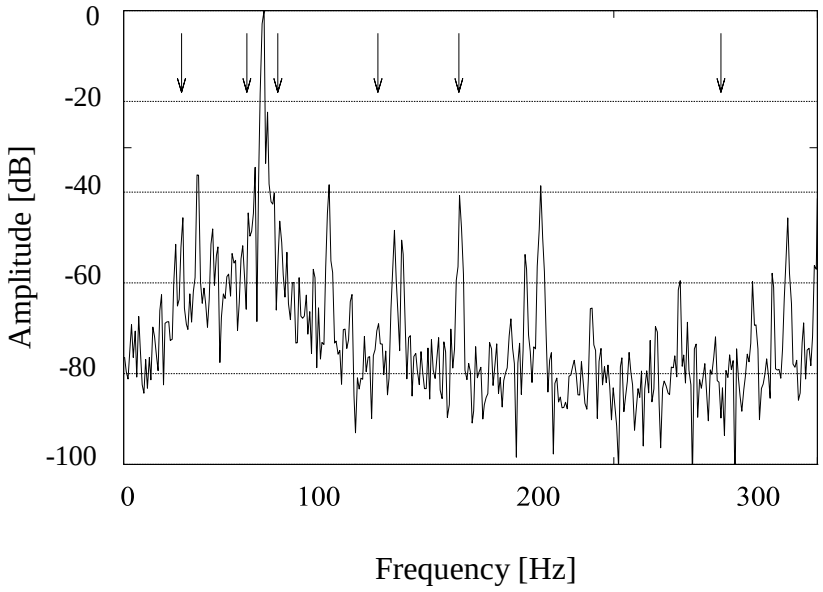

Figure 3.4 *Frequency spectrum of motor with healthy bar.*

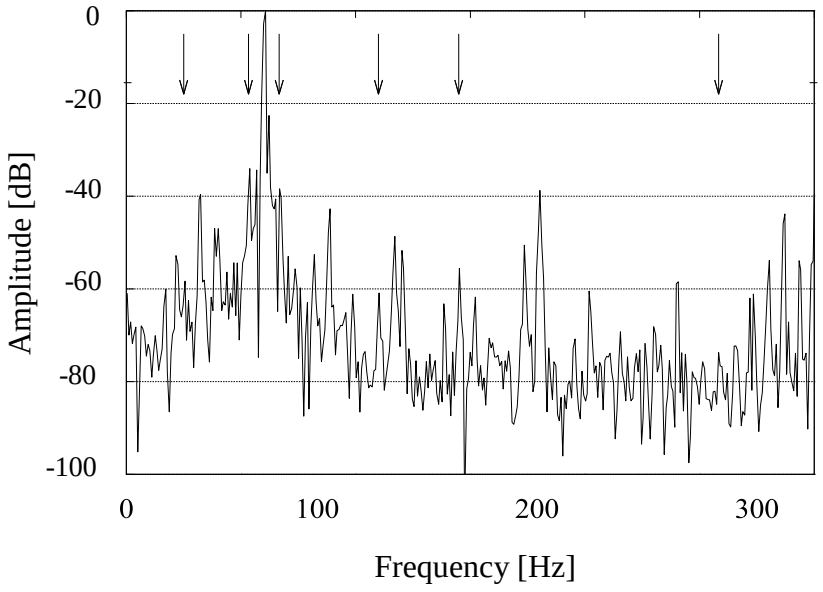

Figure 3.5 *Frequency spectrum of motor with 1 broken bar.*

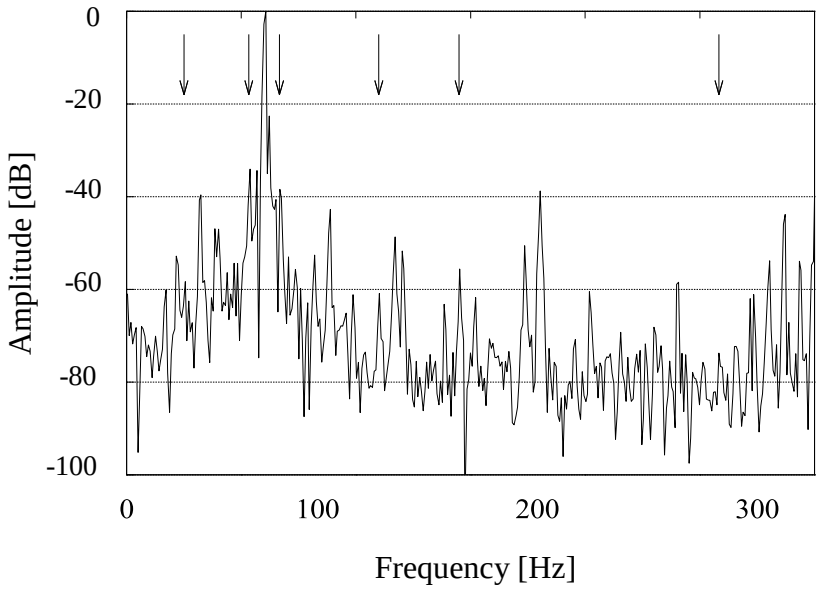

Figure 3.6 *Frequency spectrum of motor with 2 broken bars.*

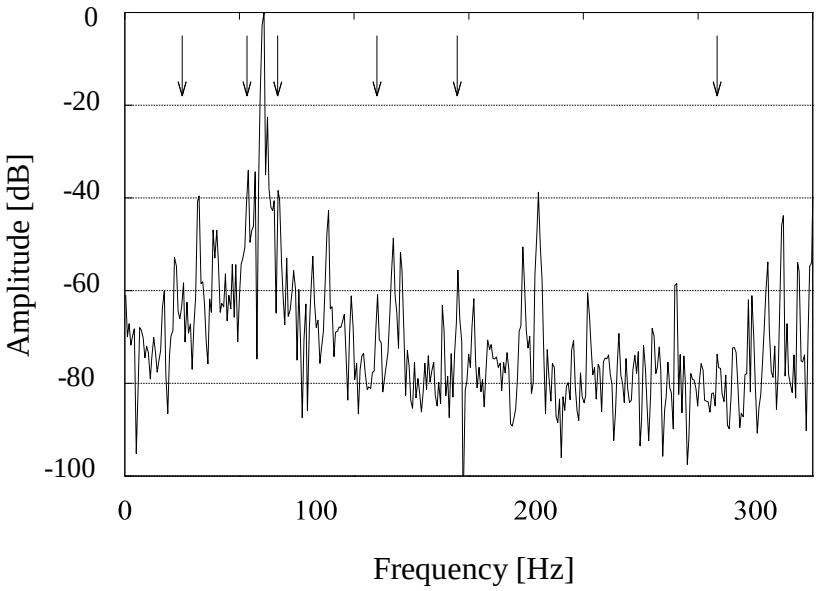

Figure 3.7 *Frequency spectrum of motor with 4 broken bars.*

The sidebands of a frequency modulated signal extend out either side of the main carrier and cause the bandwidth of the overall signal to increase well beyond that of the unmodulated carrier. As the modulation of the carrier varies, so do the sidebands and hence the bandwidth and overall spectrum of the signal. Whenever a carrier is modulated by an information signal, new signals at different frequencies are generated as part of the process. These new frequencies, which are called side frequencies, or sidebands, occur in the frequency spectrum directly above and below the carrier frequency. More specifically, the sidebands occur at frequencies that are the sum and difference of the carrier and modulating frequencies.

Thus, it is reported that two sideband components appear below and above the power frequency in frequency spectrum of load current. Frequencies of sideband components are given by Equation (3.1).

$$f_b = (1 \pm 2s)f \tag{3.1}$$

s and *f* denote the slip and frequency of power source, respectively [1]. The motor load inertia affects the magnitude of these side bands. Other spectral components that can be observed in the stator line current are given by Equation (3.2)

$$f_i = \left\{\frac{k}{p}(1 - s) \pm s\right\} f \tag{3.2}$$

where f_i is the detectable broken bar frequencies, *p* is the number of pole pairs and *k* is the harmonics index (*k* = 1, 2, 3, …….), respectively [2].

Frequencies of sideband components defined by Equation (3.1) are calculated as 53.3 Hz and 66.7 Hz for the rotating speed of 1700 min^{-1}. The amplitude of the sideband frequency components increases gradually with the increase in the number of broken bars. A little difference is recognized in the amplitude between the healthy motor and the motor with one broken bar.

Table 3.1 summarizes the frequencies calculated from Equation (3.2) for *k* values up to 10. The careful analysis of Figures 3.4 to 3.7 reveals that amplitude at some of the frequencies changes greatly depending on the rotor bar condition.

Table 3.1 *Analyzed Frequency Components.*

k	Frequency[Hz]	
	-	+
1	25.0	31.7
2	53.3	60.0
3	81.7	88.3
4	110.0	116.7
5	138.3	145.0
6	166.7	173.3
7	195.0	201.7
8	223.0	230.0
9	251.7	258.3
10	280.0	286.7

To visualize the change in the amplitude, Figure 3.8 is drawn. It shows the absolute amplitude of specified frequency components given in Table 3.1 under four broken rotor bar condition. Each mark is the mean value over 40 sets of measurement. The vertical axis is converted so that -20 dB and -100 dB in Figures 3.4 to 3.7 become 1.0 and 0.0 in Figure 3.8, respectively. The calculated lower frequency value is 60 Hz for *k* value of 2 in Equation (3.2), which is not suitable for evaluation because its amplitude for the frequency 60 Hz is unity regardless of the broken rotor bar condition. Thus, the frequency 66.7 Hz, higher frequency calculated by Equation (3.1) is used instead. Red marks and polygonal lines in Figure 3.8 are the characteristics of extracted frequency components for diagnosis.

The amplitude of the frequency components given by Equation (3.1) changes greatly with the number of broken rotor bars more than 2. These two frequency components are the features suitable to fix the number of broken rotor bar. But it is not appropriate to detect one broken rotor bar due to small difference observed in amplitude between healthy and one broken rotor bar conditions. On the contrary, some frequency components given by Equation

(3.2) show the momentous change in amplitude under one broken rotor bar condition compared with healthy state.

Additionally, to find the frequency components suitable to detect one broken bar failure, difference in amplitude of the frequency components between the healthy motor and the motor with one broken bar is analyzed and the results are shown in Figure 3.9. For example, in the case of k=5, 5- and 5+ stand for the lower and the higher frequencies according to Equation (3.2), respectively. The large amount of changes is recognized in the frequency components of 25.0 Hz (1-), 145.0 Hz (5+) and 258.3 Hz (9+). But their amplitude changes very slightly when the number of broken rotor bars increases from 2 to 4. On the contrary, amplitudes of 53.3 Hz (2-), 66.7 Hz (2+) and 110.0 Hz (4-) Hz components increases gradually with increase in the number of broken rotor bars more than two.

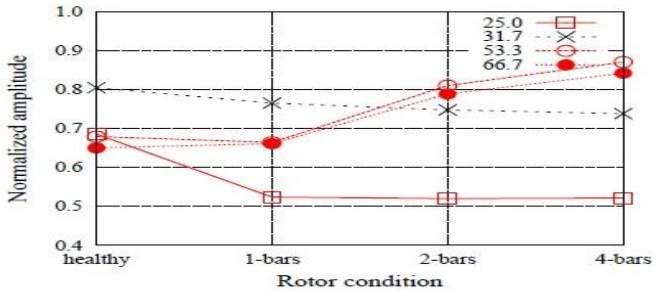

(a) k=1(25.0, 31.7Hz) and k=2(53.3, 66.7Hz)

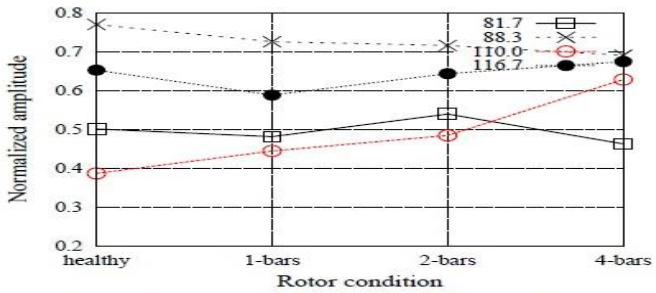

(b) k=3(81.7, 88.3Hz) and k=4(110.0, 116.7Hz)

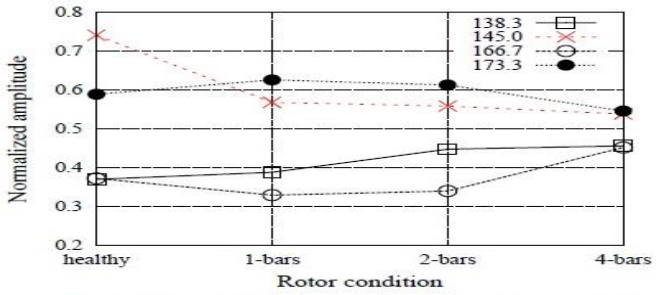

(c) k=5(138.3, 145.0Hz) and k=6(166.7, 173.3Hz)

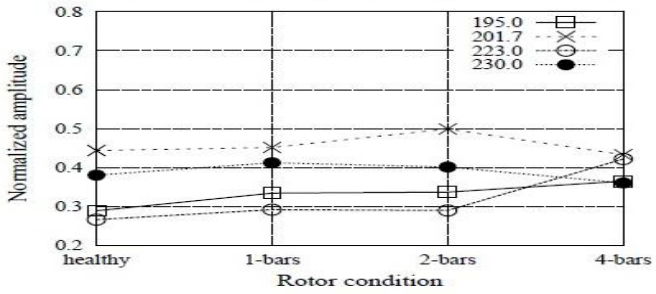

(d) k=7(195.0, 201.7Hz) and k=8(223.0, 230.0Hz)

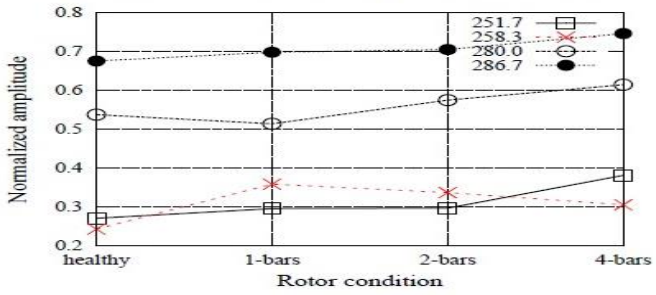

(e) k=9(251.7, 258.3Hz) and k=10(280.0, 286.7Hz)

Figure 3.8 *The changes of the amplitude of harmonic component.*

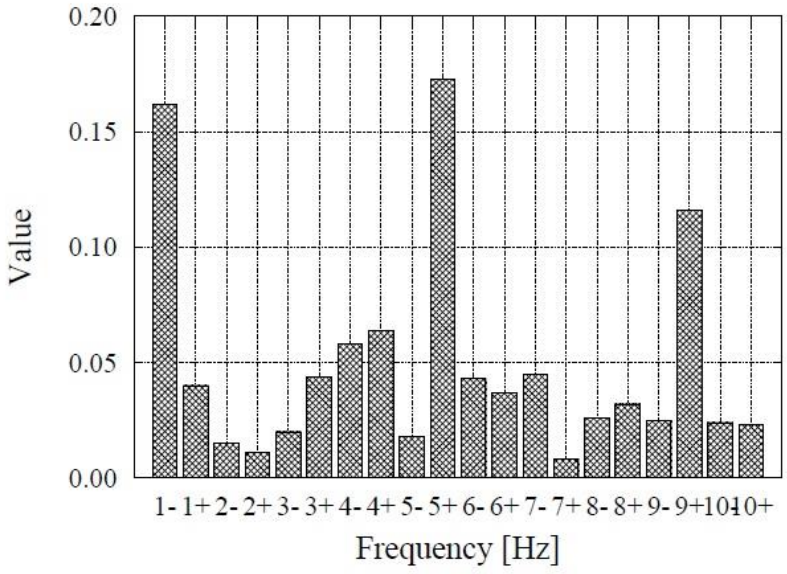

Figure 3.9 *Amount of change of harmonic component from healthy condition to 1 broken bar condition (1700 min^{-1}).*

3.4 Diagnosis using Clustering

The diagnosis is carried out using the clustering techniques employing the amplitude of the frequency components.

3.4.1 Method of Diagnosis

To proceed the diagnosis, initially two conditions are fixed. The two criteria necessary to diagnose the condition of rotor bar breakage are; to diagnose the existence or nonexistence of broken rotor bar, in other words to diagnose whether the target motor is healthy or not. The other criterion is applied to fix the number of broken bars.

In the present study, frequency components of 25.0, 145.0 and 258.3 Hz are suitable for the former criterion because their amplitude changes remarkably by introducing breakage in one rotor bar. As the latter criterion, frequency components of 53.3, 66.7 and 110.0 Hz are recommended because their amplitude increase gradually with increase in the number of broken rotor bars.

As a conclusion of analysis, two-step diagnosis method is constructed. Figure 3.10 shows the flowchart of diagnosis method. In the first step, diagnosis is carried out to confirm the presence or absence of broken rotor bar. As the second step of confirmation, the number of broken bar is fixed. Finally, clustering based on Self-Organizing Map (SOM) is used in both steps [3].

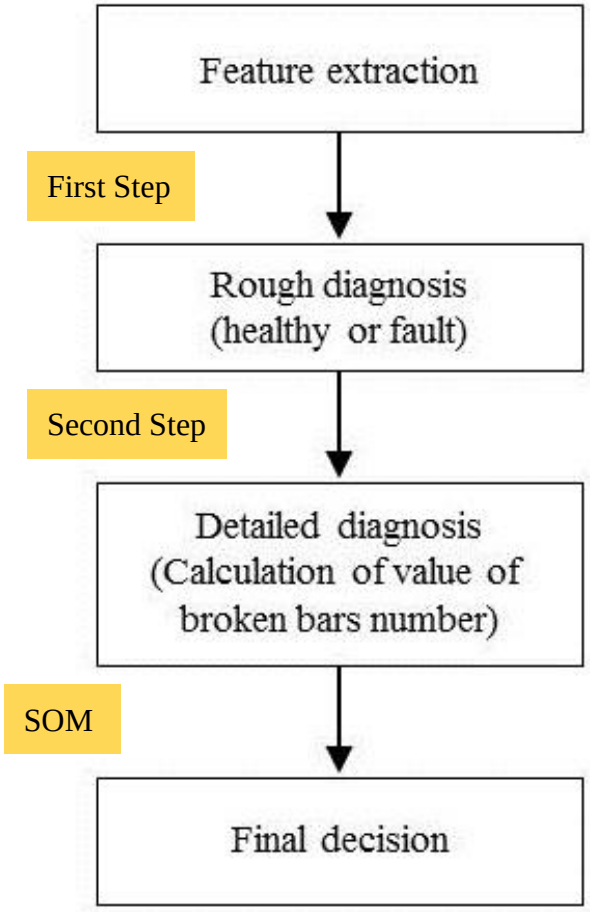

Figure 3.10 *Flow chart of diagnosis.*

3.4.2 Brief Explanation of SOM

SOM is one of neural network models based on unsupervised learning. Its algorithm provides a topology preserving mapping from the high dimensional space to map units. Map is easily visualized because it usually forms a two-dimensional hexagonal or rectangular lattice. The mapping preserves the relative distance between the points, wherein points close to each other

in the input space are mapped nearby units. SOM operates in two modes: training and mapping. Training mode builds the map using input data (vector quantization), while mapping mode automatically classifies a new input vector.

SOM has been used in various fields for intuitive understanding and/or exploratory analysis of classification of multi-dimensional data. For example, study on analytic technology to prevent clinical accidents in hospitals and nursing facilities, research of application to judgement technique of unique manipulations in operative procedure have been reported [3].

k-means method is also one of the clustering methods based on unsupervised learning. Compared with this method, SOM has an advantage of lower false recognition rate. Considering these merits, SOM is used for clustering. As described above, SOM transforms multi-dimensional features to a two-dimensional map. With the use of SOM, the change in amplitude for more than three characteristic frequency components can be recognized when rotor bars are broken and the relationship among the data can be visualized in a two-dimensional map. This process of using SOM results in easy diagnosis of failure in rotor bar.

3.5 Verification

Using the data obtained at two rotating speeds (1700 and 1710 min^{-1}), the ascendency of the proposal diagnosis method is verified. In addition to the above verification, the experiment is also done at the rotating speed of 1750 min^{-1}. This is to evaluate the ability and accuracy of the proposed method to other rotational speed far away from the rated one (1705 min^{-1}).

3.5.1 In case of 1700 min^{-1}

SOM is created with SOM PAK [4]-[5] obtained at the rotating speed of 1700 min^{-1}, respectively. Above mentioned data sets have three-dimensional data vectors which consist of amplitude of three frequency components: 25.0, 145.0 and 258.3 Hz. A map forms hexagonal lattice with vertical 12 nodes and horizontal 10 nodes. The iteration of learning is 10,000 and learning coefficient is 0.2.

At first, SOM was created to classify the presence or absence of broken rotor bar. The resulting map created from the three-dimensional vectors of 25.0, 145.0 and 258.3 Hz are shown in Figure 3.11. The gradation of colors in map denotes the distance between the adjacent nodes. The darker the color, the longer the distance. “H” and “F” in Figure 3.11 stand for healthy and broken bar failure, respectively. It is understood that “H” and “F” are clearly separated from each other in two regions depending on the existence or nonexistence of broken rotor bar. The 80 data in total are divided into two regions.

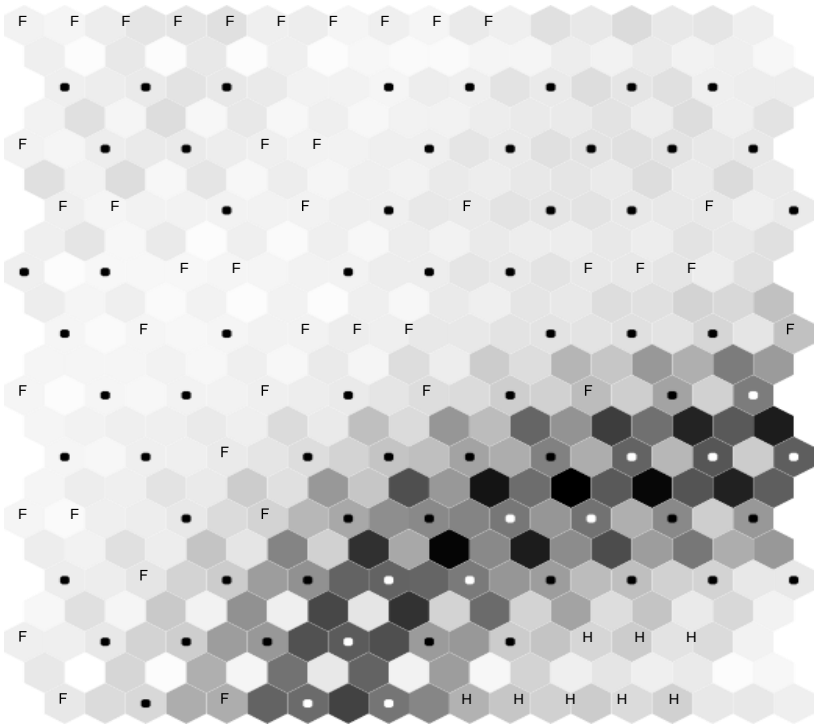

Figure 3.11 *Distribution of bar condition (healthy or bar broken condition, 1700 min^{-1}).*

Further, 60 data collected for the broken rotor bar failure in the first step were used. These data sets have three-dimensional data vectors which consist of amplitude of three frequency components: 53.3, 66.7 and 110.0 Hz. These data are used for SOM map to classify the number of broken rotor bar. Figure 3.12 shows a result of clustering using SOM. For example, “1b” in Figure 3.12 stands for datum with one broken bar. There are three regions separated

from each other and all data are allocated to one of these regions depending on the number of broken bars. By using both the amplitude of specific frequency component and SOM, training data are divided precisely according to the rotor bar's condition.

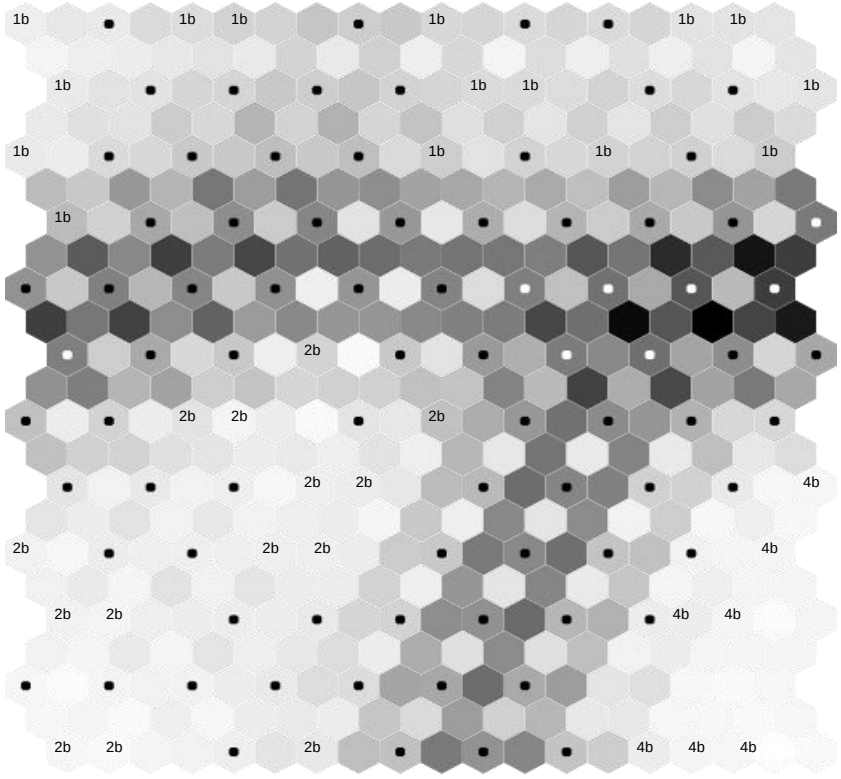

Figure 3.12 *Distribution of bar condition (1 bar to 4 bar broken condition, 1700 min^{-1}).*

Based on the above results, as the first step of diagnosis, the existence or nonexistence of broken rotor bar was diagnosed using a new 20 sets of data for each rotor bar conditions (healthy, 1, 2 and 4 broken bar(s)) as evaluation data obtained at the rotating speed of 1700 min^{-1}. The classification of these 80 data was also carried out. It was confirmed that data of a healthy motor were mapped in the healthy region "H" determined by the training process and that data of motors with broken rotor bars were assigned to the failure region "F". The results of classification were also perfect. In the second step of diagnosis, using 60 data collected during the diagnosis of breakage failure, broken rotor bars were classified. It was

confirmed that every datum was allocated to the correct region on the map shown in Figure 3.12.

3.5.2 In case of 1710 min^{-1}

The similar evaluation was also performed at the rotating speed of 1710 min^{-1}. Thus, to extract the frequency components suitable to detect broken bar failure or the number of broken rotor bars, the frequency analysis is carried out in the same way as 1700 min^{-1}. As the result of this analysis, concerning the amount of changes in frequency components, the same tendency is recognized as 1700 min^{-1}. Therefore, same frequency components are also used in this rotating speed. The training of SOM and the number of training data are also same as that of 1700 min^{-1}. Figures 3.13 and 3.14 show the classification results using SOM. As the result of evaluation, the two-step diagnosis method is also perfect as in the case of 1710 min^{-1}.

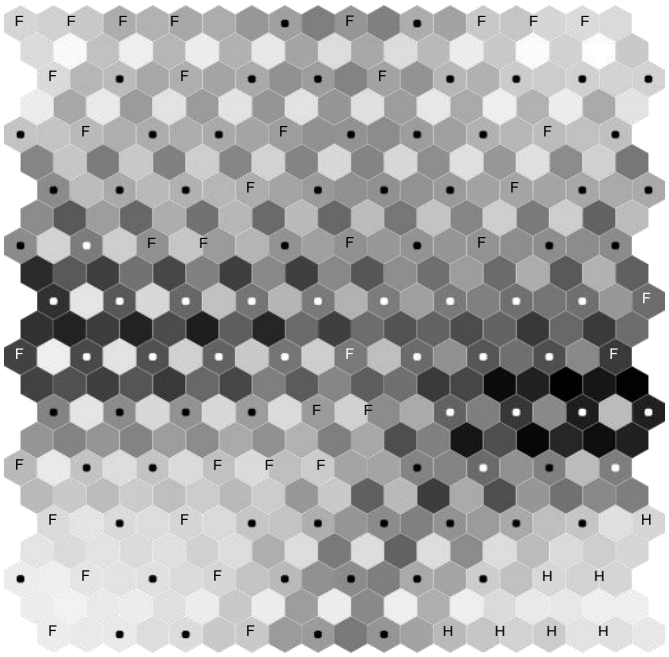

Figure 3.13 *Distribution of bar condition (healthy or bar broken condition, 1710 min^{-1}).*

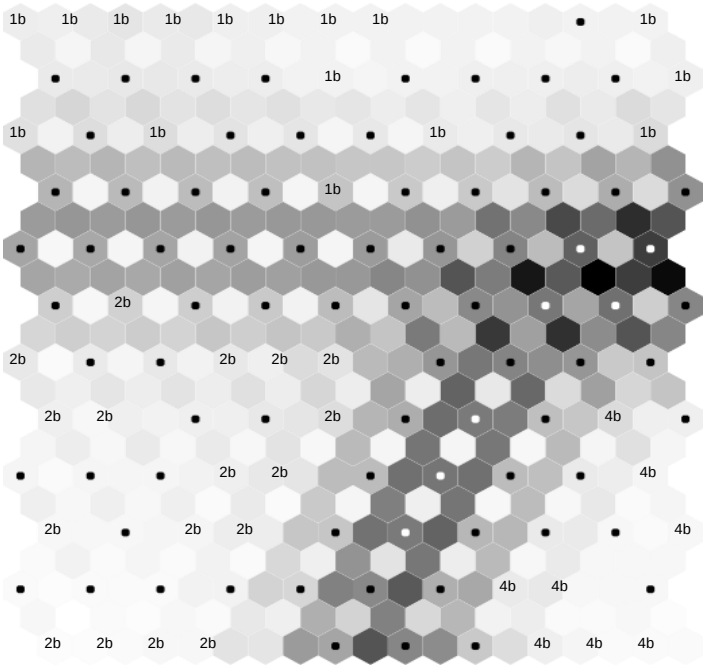

Figure 3.14 *Distribution of bar condition (1 to 4 broken bars, 1710 min^{-1}).*

3.5.3 In case of 1750 min^{-1}

To verify the ability of applying of this method to other rotating speed, additional analysis was carried out at 1750 min^{-1}. This is far from the rated rotating speed (1705 min^{-1}). In this case, new features for diagnosis must be extracted from load current spectrum. (20 sets of training data for each rotor bar condition (healthy, 1, 2 and 4 broken bar(s)) were used).

Amplitude of the characteristic frequency components (Table 3.1) is analyzed and the results are shown in Figure 3.15, which shows the difference in amplitude of the frequency components between the healthy motor and the motor with one broken bar.

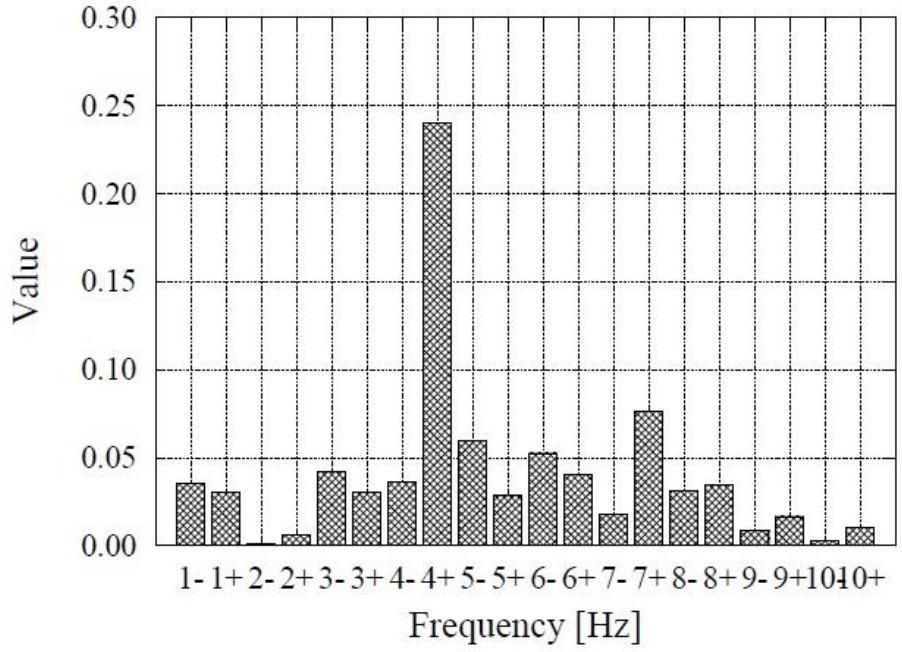

Figure 3.15 *The change of harmonic component from healthy condition to 1 bar broken condition (1750 min^{-1}).*

Unlike Figure 3.9 at the rotating speed of 1700 min^{-1}, only 118.3 Hz (4+) component is outstanding. It is adopted as a feature to diagnose the presence or absence of broken rotor bar. The threshold value was set to 0.15; considering an amplitude value in between 4+ and others in Figure 3.15. When the value of the frequency component 118.3 Hz exceeds 0.15, the existence of the broken rotor bars can be confirmed. In the case of 1750 min^{-1}, the accuracy of the first step diagnosis for 80 evaluation data is perfect without using SOM.

In the second step of diagnosis which identifies the number of broken rotor bars, amplitude of 63.3, 173.3 and 290 Hz components of load current spectrum was used, since the increase or decrease is monotonically with the number of broken bar. But the amount of change is very small, when compared with the change at the rotating speed of 1700 min^{-1} and 1710 min^{-1}. The classification of the number of broken rotor bar was carried out for 60 training data diagnosed as breakage failure in the previous step.

Figure 3.16 shows results of classification using SOM. Only data of 4 broken bar are clearly separated and located in the right lower region of the map, these can be identified easily. But it is difficult to identify the data of 1 broken bar from those of 2 broken bars. In other words, in the case of 1750 min^{-1}, even though SOM is applied, the detail diagnosis was not enough. This is attributed to small difference in features between the two cases due to smaller load current and less rotor current flowing into rotor bars at higher rotating speed of 1750 min^{-1}. Through verification, it was shown that the frequency components for classification depends on the rotating speed.

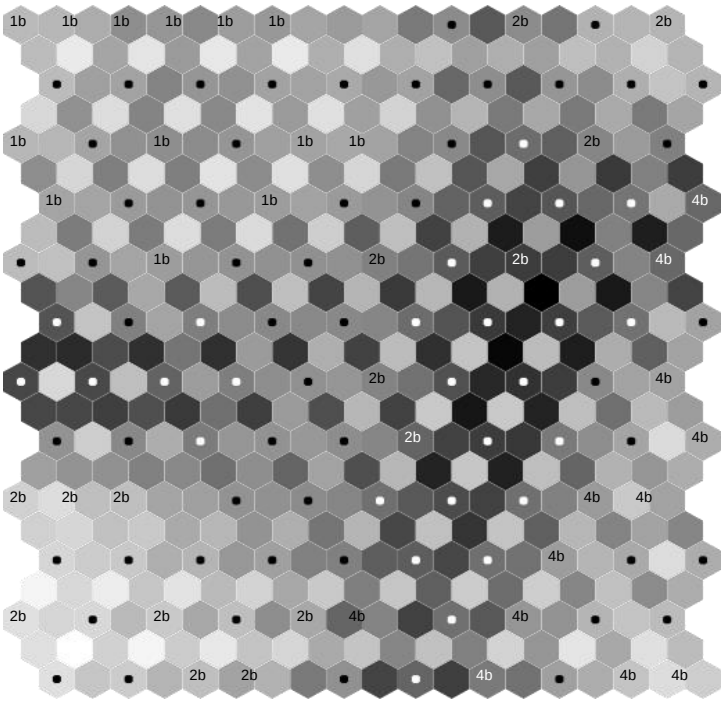

Figure 3.16 *Distribution of bar condition (1 bar to 4 bar broken condition, 1750min^{-1}).*

3.6 Summary

A two-step diagnosis method for broken rotor bars in a cage induction motor around rated rotating speed is proposed. The presence or absence of broken rotor bars is diagnosed in the first step, and the number of broken bars is identified in the second step. Based on the detailed

analysis of the frequency spectrum of load current, characteristic frequency components are extracted. The amplitude of characteristic frequency components was used in clustering using SOM.

Identifying the difference between the healthy and the faulty motor is made possible using the proposed method. The method confirms the possibilities of diagnosing one broken rotor bar failure around the rated rotating speed. Even detecting the multiple broken rotor bar is achieved up to 4 broken bars.

However, other rotating speeds rather than rated show partial significance result. Further examination will be done at other rotating speed and for other type of motors.

Chapter 4
Bearing Failure Diagnosis – Single Fault Analysis using Hole

In this chapter, bearing failure diagnosis of single fault is done considering hole as the faulty factor. The entire analysis is performed using Fast Fourier Transform (FFT) and the diagnosis by the Support Vector Machine (SVM).

4.1 Introduction - Faulty Factor as Hole

As in research point of view, most of the researches are done by considering hole as the faulty factor of bearing. However, there is no enough proof with respect to multiple hole analysis and explicit hole localization of bearing in the induction motor. Therefore, in the present study, considering hole as faulty factor, the following analysis is carried out; hole identification, multiple hole analysis and localization of hole analysis.

4.1.1 Localization of Bearing Fault

In general, bearing faults can be categorized as two types. They are distributed faults and localized faults [1]. Among the two types of faults, distributed faults can affect the whole current spectrum and it is highly difficult to characterize them based on the distinct frequencies. On the other hand, localized faults can be easily characterized. Normally, single-point defects are localized faults and that can be easily classified according to their affected element [2]. Single-point defects can be easily created offline. As a case, by drilling the hole or making a scratch in the bearing components. In fact, many research works have been focusing on the single-point defects, [3]-[10]. In contrast, single-point localized defect can be classified as the following:

- Outer raceway defect;
- Inner raceway defect;

- Ball defect;
- Cage defect.

In the present study, cylindrical roller bearing is used. Among the single-point localized defects, outer raceway defect is discussed. The characteristic fault frequency for the outer raceway defects is estimated based on the geometric specification of the bearing as illustrated in Table 4.1.

Table 4.1 *Bearing specification*

Bearing specification	Dimension
Inner diameter d	25 mm
Outer diameter D	52 mm
Roller diameter D_b	13.5 mm
Cage diameter D_c	38.5 mm
number of balls N_b	9

4.1.2 Experimental Setup

The experimental setup is shown in Figure 4.1. The present study was carried out considering powder brake as a mechanical load and it was coupled to the induction motor through coupling brushes. This powder brake allows the rotating speed of the induction motor to be varied. Speeds from 1780 to 1765 min^{-1} were used in the experiments. The load current was measured using current probes (HIOKI 9695-02), and the voltage of the stator winding was measured using voltage probes (HIOKI 9666). The rotating speed was monitored using a speed indicator (ONOSOKKI HT-5500). The output signal from the sensors were transferred to a desktop computer (PC) and recorded simultaneously using a system developed by the author with the tolerance error of ±2%. The full-scale measurement of current and voltages were 20 A and 300 V, respectively. The measurement system had seven input terminals and seven A/D converters. In the current study, the three-phase load currents, three line-to-line

voltages, and rotational speed were recorded through the seven channels. Frequency analysis resolution is determined by the sampling time, and it is preferable to achieve high frequency resolution. The sampling time was therefore set at approximately 10 μs, giving a frequency resolution of 0.76 Hz and a data recording length of 2^{17} per channel. Data were acquired at 30 s intervals, triggered by a timer. Data transfer across seven channels took less than 20 s.

Figure 4.1 *Experimental setup.*

4.1.3 Motor Specification

Three-phase induction motors were used as a specimen. The stator winding of the motor is a double star connection. The number of turns is 120 for each phase winding. The number of slots is 36. The motor specification for carrying out the bearing analysis is illustrated in Table 4.2. This section is dealing with the identification of hole, multiple hole analysis and localization of holes analysis. The holes are made artificially on the outer raceway of the bearing of the induction motor.

Table 4.2 *Motor specification*

Content	Rating
Rated Power	2.2 [kW]
Rated Voltage	200 [V]
Rated Current	8.5[A]
Rated Speed	1740 [min^{-1}]
Poles	4

4.2 Identification of Hole

The main work is to identify and differentiate the faulty motor with the healthy motor. In addition to this, it is found that, it is even possible to distinguish the two types of faulty motor (hole with diameter 0.5 mm and hole with diameter 2 mm). The depth of the hole to the both faulty motor is made common as 1 mm. The bearing with the hole 0.5 mm and the hole with 2 mm is shown in Figure 4.2.

Figure 4.2 *Bearing with a hole 0.5 mm (left) and hole 2 mm (right).*

Also, the procedure of analysis for diagnosing the bearing fault is shown in Figure 4.3. The experimental work begins with the observation made in the healthy motor. After that, the healthy bearing was replaced with the faulty bearing of hole 2 mm and performed the same analysis which has been carried out for the healthy bearing. Later, once again the experiment was carried out by changing the dimension of the hole in the bearing to 0.5 mm and the same analysis was performed.

The proposed method is evaluated by means of measuring the stator current. The current signals are collected from the healthy motor and two types of the faulty motors. The measurement was carried out under the load condition. The rotating speed was adjusted from 1765 min^{-1} to 1780 min^{-1}.

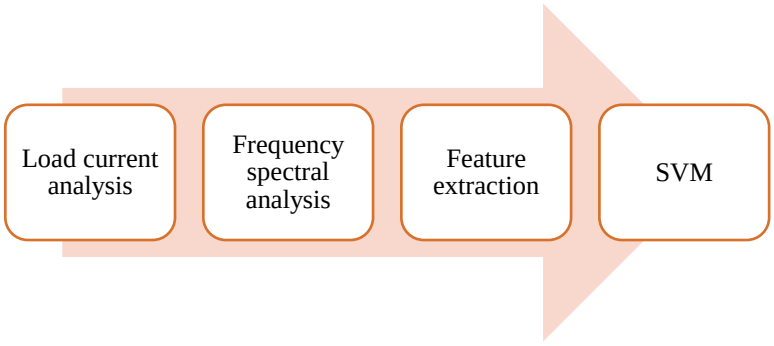

Figure 4.3 *Analysis Procedure.*

4.2.1 Frequency Spectrum Analysis

FFT analysis of the U-phase load currents was performed for all the three types of bearing conditions. Figures 4.4 to 4.7 show the frequency spectrum analysis carried out for all three-bearing condition at the rotating speed of 1780 min^{-1}. 283 fundamental wavelengths are used in FFT. The amplitude of the vertical axis is normalized so that the maximum level of frequency spectrum to be 0 dB. The frequency of the power source is 60 Hz. The difference in the amplitude of the frequency component is observed nearby frequencies of 30 Hz and 90 Hz. An additional comparison is made between two types of faulty motor and inherently considerable amplitude difference is observed at the same frequency 30 and 90 Hz. The other rotating speeds (1775, 1770 and 1765 min^{-1}) also show a similar difference. Thus, the

amplitude of the frequencies nearby 30 and 90 Hz play a predominant role in identifying the condition of the bearing.

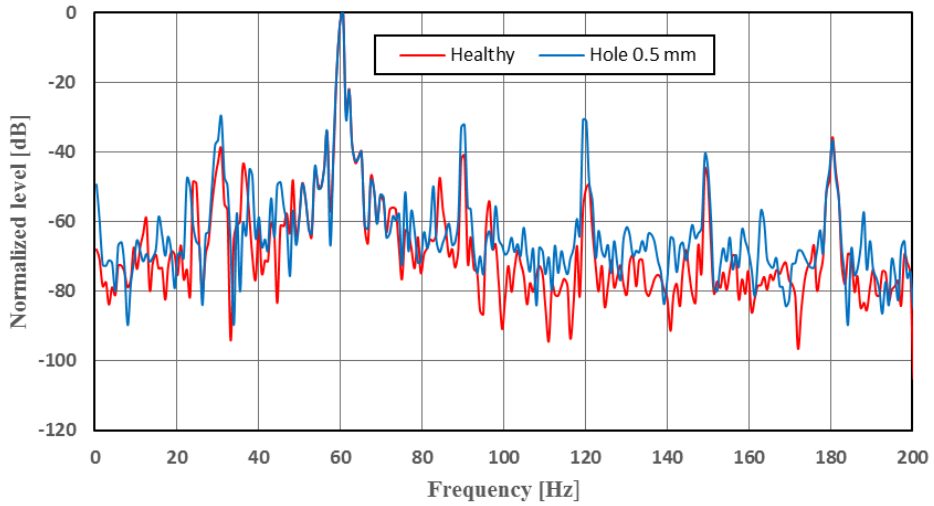

Figure 4.4 *Spectral analysis for Healthy and Hole 0.5 mm at 1780 min^{-1}.*

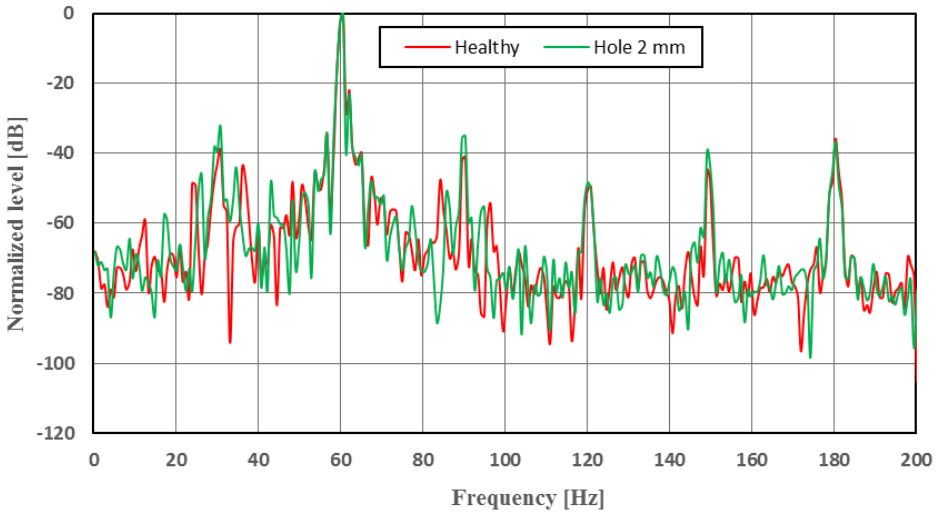

Figure 4.5 *Spectral analysis for Healthy and Hole 2 mm at 1780 min^{-1}.*

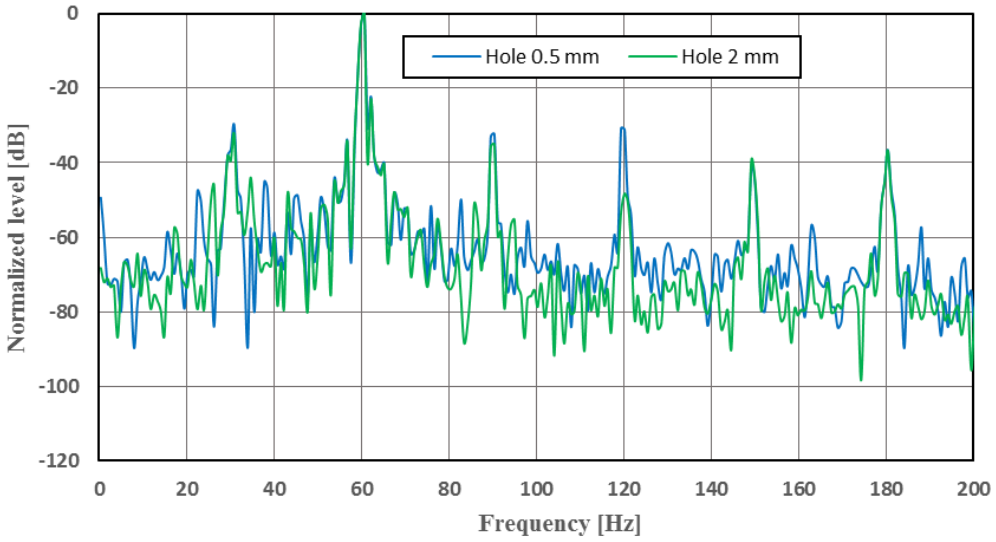

Figure 4.6 *Spectral analysis for Hole 0.5 mm and Hole 2 mm at 1780 min^{-1}.*

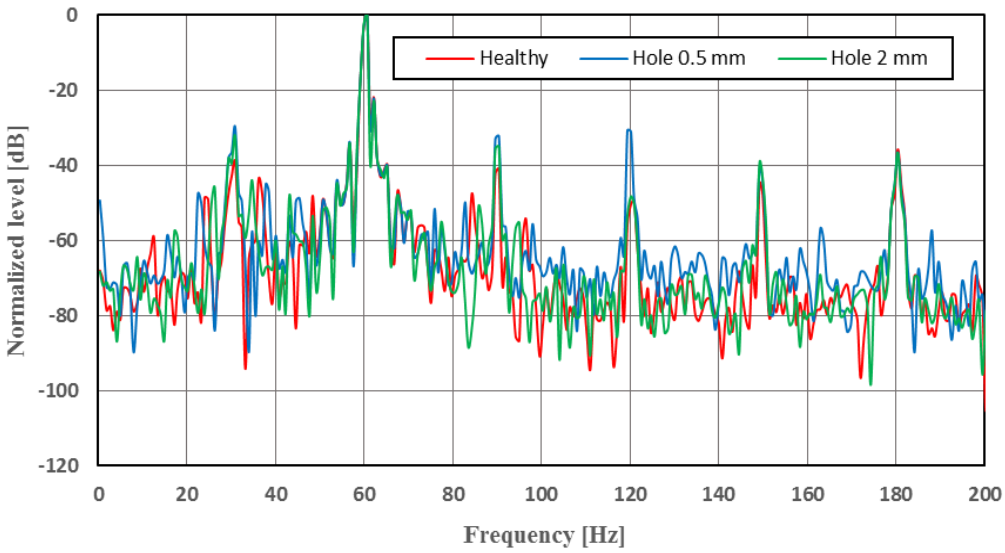

Figure 4.7 *Spectral analysis for Healthy, Hole 0.5 mm and Hole 2 mm at 1780 min^{-1}.*

4.2.2 Feature Distribution

The feature distribution analysis is carried out using the amplitude of the characteristics frequency 30 and 90 Hz. A two-dimensional graph is plotted, taking amplitude of 30 Hz component along the x-axis and 90 Hz component along the y-axis, respectively. The contribution of each feature is evaluated by considering the rotating speed of the induction motor. Figures 4.8 to 4.11 show the feature distribution for three types of bearing condition (healthy, hole 0.5 mm and hole 2 mm) at 1780, 1775, 1770 and 1765 min^{-1} rotating speeds. Each bearing condition sets its own class of location and hinge on the rotating speed of the induction motor.

While taking the individual rotating speed of the induction motor into consideration, the class of the faulty motor (Hole of 0.5 mm and 2 mm) are located far away from the healthy motor. Another interesting point to be considered is the class of the faulty motor with a hole of 0.5 mm is located apart from the faulty motor with the hole of 2 mm. Both these holes have the own class of location according to the bearing condition and rotating speed. Thus, this method is effective in diagnosing the three types of bearing conditions.

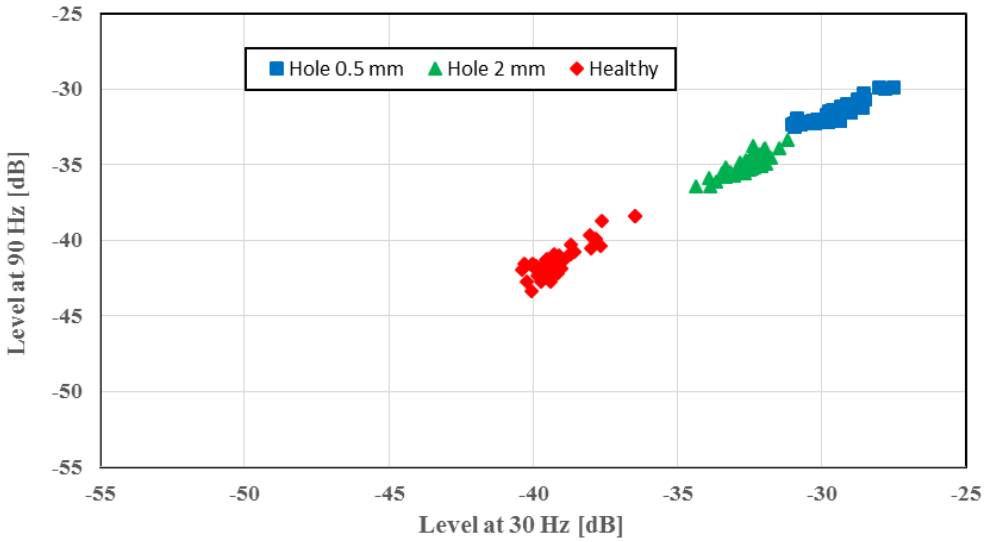

Figure 4.8 *Feature distribution at 1780 min^{-1}.*

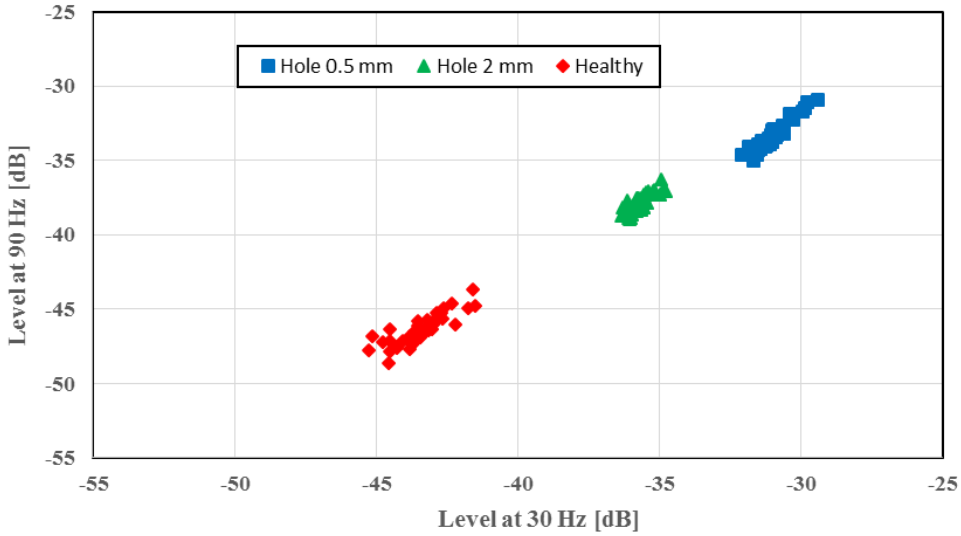

Figure 4.9 *Feature distribution at 1775 min^{-1}.*

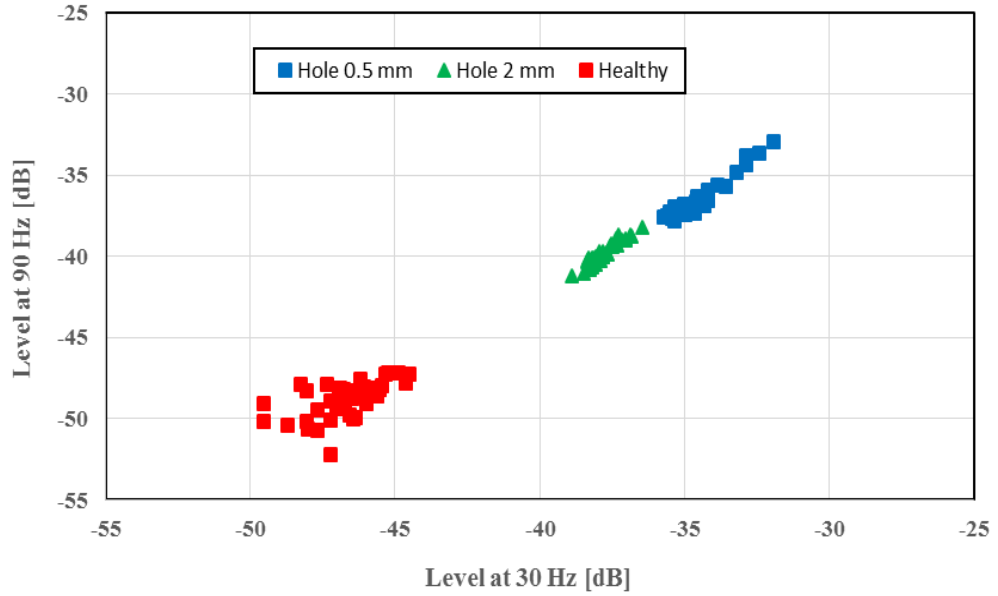

Figure 4.10 *Feature distribution at 1770 min^{-1}.*

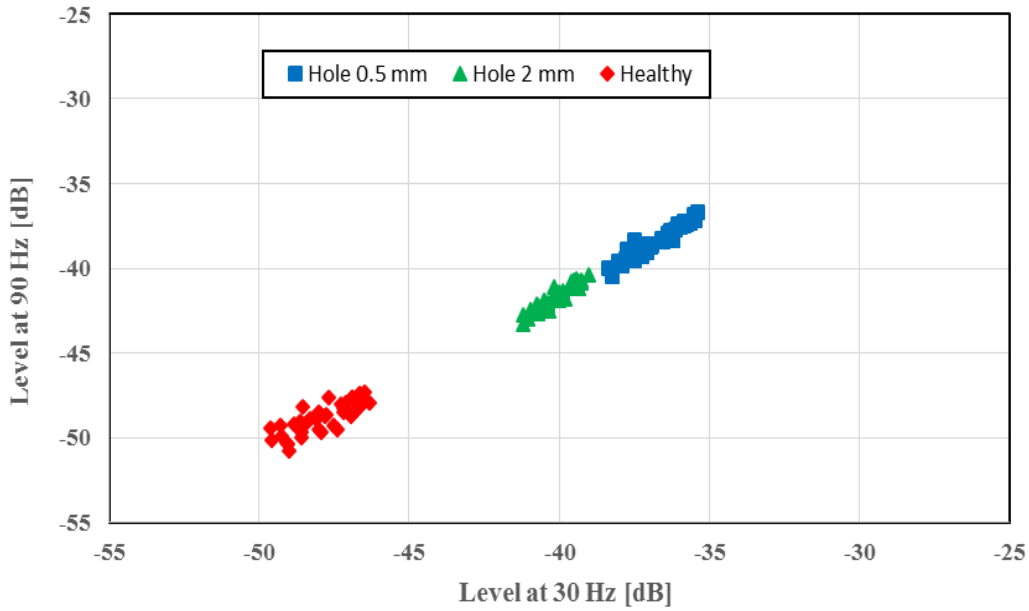

Figure 4.11 *Feature distribution at 1765 min^{-1}.*

In industries, the speed of the induction motor is not constant and said to be varied between the certain range. Considering the industrial environment, the analysis is also performed without considering the rotating speed of the induction motor and the result is shown in Figure 4.12. The overlapping of features is observed between the different bearing conditions of the induction motor, yet they are distributed linearly and segregated to their own classes. The faulty motors of hole 0.5 mm and hole 2 mm show large overlapping when comparing to the healthy motor. The average of the amplitude of three bearing conditions (healthy, hole 0.5 mm and hole 2 mm) at the frequency 30 and 90 Hz is shown in Figure 4.13. The amplitude of each class is in their own range and shows analogous characterization for both the frequencies.

For example, the amplitude of healthy motor lies between the range of -44 to -47 dB, similarly amplitude of faulty motors lies in the range of -33 to -35 dB for hole 0.5 mm and -37 to -39 dB for hole 2 mm, respectively. Additionally, the maximum difference observed between the healthy and faulty 1 (hole 0.5 mm) is 11 dB, and for healthy and faulty 2 (hole 2 mm) is 7 dB. Considerable difference has been observed between faulty 1 (hole 0.5 mm) and faulty 2 (hole 2 mm) and said to be 4 dB. Large amplitude is observed in the case of hole 0.5 mm and less in the case of hole 2 mm. However, even with the amplitude range analogous characterization, the diagnosis is still impossible.

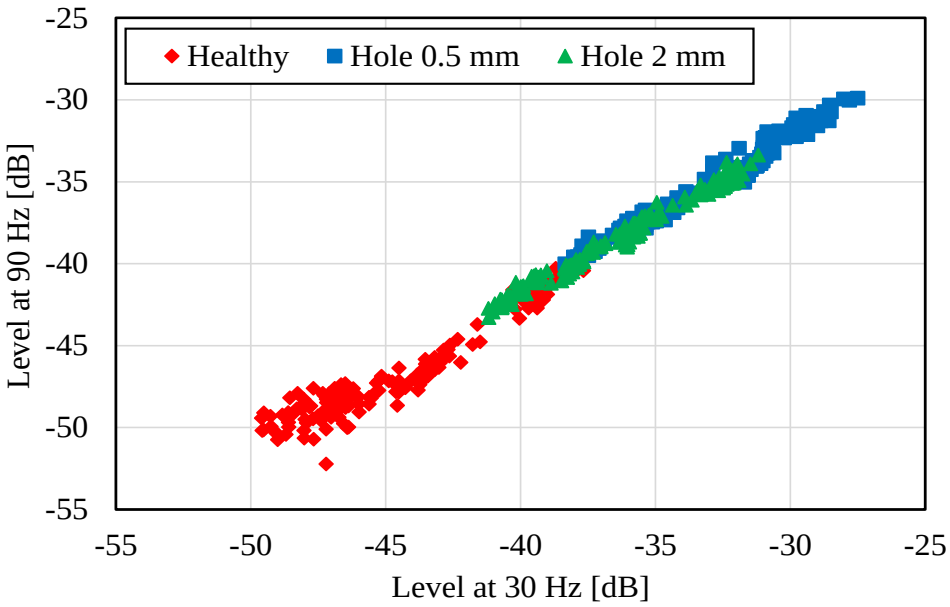

Figure 4.12 *Feature distribution at 1780 min^{-1}-1765 min^{-1}.*

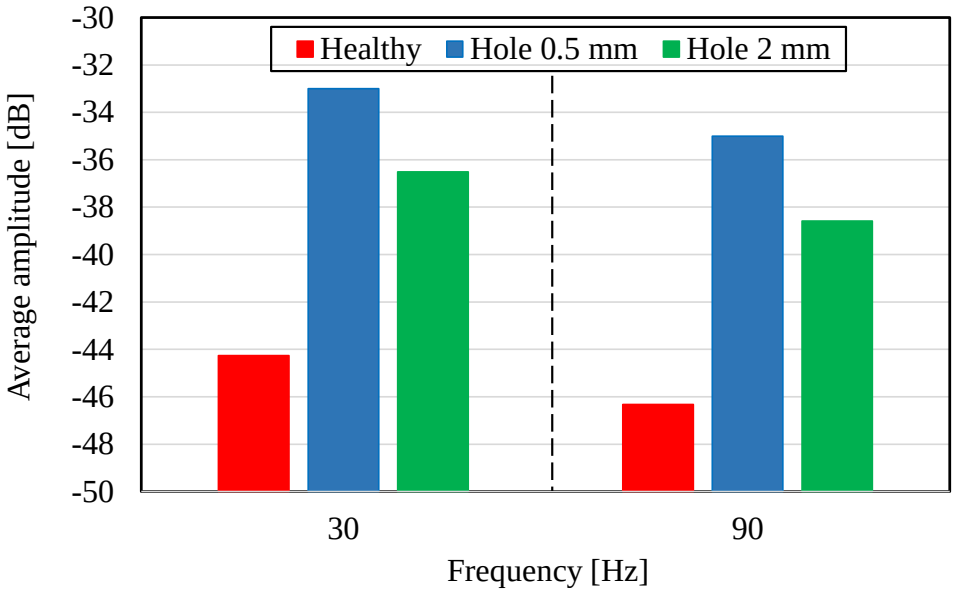

Figure 4.13 *Average amplitude of 30 and 90 Hz for three bearing conditions.*

4.2.3 Justification of 30 and 90 Hz

Normally, the bearing consists of outer and inner raceway, and both these raceways are separated by the rolling elements like balls or cylindrical rollers. Suppose, if a damage occurs in the bearing, then there is a possibility for shock pulses with characteristics frequencies to occur. This incident happens when the ball or rolling element passes through the damaged portion. Mainly, characteristic frequency components depend on the damaged part of the bearing and we can calculate them by means of the geometry of the rolling elements and the mechanical rotational frequency f_r. A detailed explanation of these analysis can be found in [11]. For the four types of considered faults, characteristic frequency takes the following expression.

- ✧ *Outer raceway defect:*

$$f_O = \frac{N_b}{2} f_r \left(1 - \frac{D_b}{D_c} \cos\beta\right) \tag{4.1}$$

- ✧ *Inner raceway defect:*

$$f_i = \frac{N_b}{2} f_r \left(1 + \frac{D_b}{D_c} \cos\beta\right) \tag{4.2}$$

- ✧ *Ball defect:*

$$f_b = \frac{D_c}{D_b} f_r \left(1 - \frac{D_b^2}{D_c^2} \cos^2\beta\right) \tag{4.3}$$

- ✧ *Cage defect:*

$$f_{cage} = \frac{1}{2} f_r \left(1 - \frac{D_b}{D_c} \cos^2\beta\right) \tag{4.4}$$

Also, it has been statically shown in [12], that the characteristic frequency can be approximated for the number of roller bearing between 6 and 12. It takes the following expression.

$$f_o = 0.4 N_b f_r \tag{4.5}$$

$$f_i = 0.6 N_b f_r \tag{4.6}$$

where N_b is the number of balls or bearing rollers, β is the contact angle between the ball and raceway, D_b is the diameter of the ball or bearing roller, D_c is the diameter of the cage.

The characteristic frequencies obtained from equations (4.1) and (4.5) are 87.5 and 108 Hz and it shows no similarity with the frequencies 30 and 90 Hz. Generally, when a pit is induced on a bearing, a shock wave with a characteristic frequency is generated [13]. The frequency mainly depends on the point at which the fault is induced and the level of damage. This characteristic frequency obtained from the equations (4.1) and (4.5) are constitutes the reason for the changes observed at the amplitude of the frequency 30 and 90 Hz. But the theoretical values obtained from the equations do not match with the observed frequency. The shock wave pulse stands as the reason for the frequency changes and the reason behind the amplitude change at the 30 and 90 Hz is explained as follows.

The power supply frequency (60Hz) is also independent of the selected frequency (30 and 90 Hz). The harmonics distortion is likely to appear in the voltage because the power supply is fed directly from the main system. The harmonic distortion analysis is performed to the faulty bearing and the result is shown in Figure 4.14. No harmonic signals are observed at the frequency 30 and 90 Hz and confirm the fact that changes are only due to the presence of a fault. Thus 30 and 90 Hz play a significant role in bearing fault diagnosis.

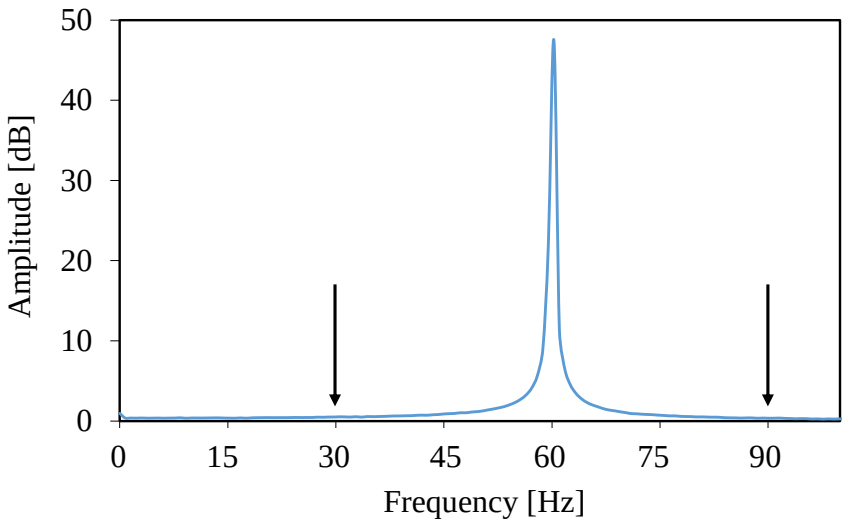

Figure 4.14 *Spectral analysis of voltage.*

Theoretically, the reason may be explained with two mechanisms. Generally, for a 4-pole induction motor, the synchronous speed Ns is given as 1800 min^{-1}. In the present study, for example, in the case of 1765 min^{-1}, the motor rotates at 1765/60 (revolutions/sec) and it takes a value of 29.41 Hz. When the motor rotates at 1765 min^{-1}, due to the sideband mechanism, two signals will be appeared in the spectrum of the load current. The frequencies of these signals F_B can be expressed as

$$F_B = F_L \pm F_R \tag{4.7}$$

where F_L stands for the frequency of the power supply (60 Hz) and F_R for the frequencies calculated based on the rotating speed. For the case of 1765 min^{-1}, the frequency F_B is found to be 30.59 Hz (60 Hz - 29.41 Hz) and 89.41 Hz (60 Hz + 29.41 Hz). Similarly, the side band frequency is calculated for other rotating speeds (1780 min^{-1}, 1775 min^{-1}, 1770 min^{-1}).

Also, the side band frequency of current spectrum will change according to their rotating speed. In current study, irrespective of the rotating speed, the changes in the amplitude of load current spectrum is observed at the same frequency 30 Hz and 90 Hz. This is due to frequency resolution (0.76 Hz) of the measuring equipment designed. Thus the frequency component 30 Hz and 90 Hz plays an important role in scrutiny the spectral analysis.

The second mechanism is explained as follows. Comparing the spectral analysis result of healthy and faulty bearing conditions, it is evident that harmonic components are amplified due to the fault occurrence. The amplified frequencies are given by [13],

$$F_B = (2k\text{-}1)\, f_r \tag{4.8}$$

where f_r stands for rotor synchronous speed in r/min and takes the value of 30 Hz, and k = 1, 2, 3 and so on. On substituting the value of k and f_r in equation (4.8), the value of F_B is found to be 30 and 90 Hz. It satisfies the results of spectral analysis.

The harmonic of frequency 30 and 90 Hz has higher amplitude at both the faulty condition when compared to the result of healthy motor. Because of a change in the amplitude of the frequency components, it is possible to distinguish both the healthy motor and faulty motor, irrespective of the bearing condition. The key point to be noted is that it is not only the healthy motor gets differentiated from the faulty motor, but also two types of faulty motor can be differentiated. The change in the amplitude of the frequency components between the two types of bearing condition (Hole of 0.5 mm and 2 mm) is observed. Therefore, these levels are considered as one of the crucial features in the present study.

The discussion confirms the reason for the amplitude changes observed at the frequencies 30 and 90 Hz. The shock wave pulse stands as the main reason for the occurrence of the amplitude changes and it is explained using the two mechanism. During the discussion, it is mentioned that the shock wave pulse crosses the center of the bearing outer raceway. Since the hole is inserted in the center, the changes are said to be obtained and detection is made possible. For the purpose of the confirmation, the offset analysis is carried out (hole is introduced 2.6 mm away from the center). The hole is artificially induced to the offset position and the feature distribution results is shown in Figure 4.15. The hole at the center shows more defect when compared to the analysis result of offset hole. The analysis result of offset hole is comparatively closer to the healthy bearing data. The existence of the shock wave pulse gets confirmed.

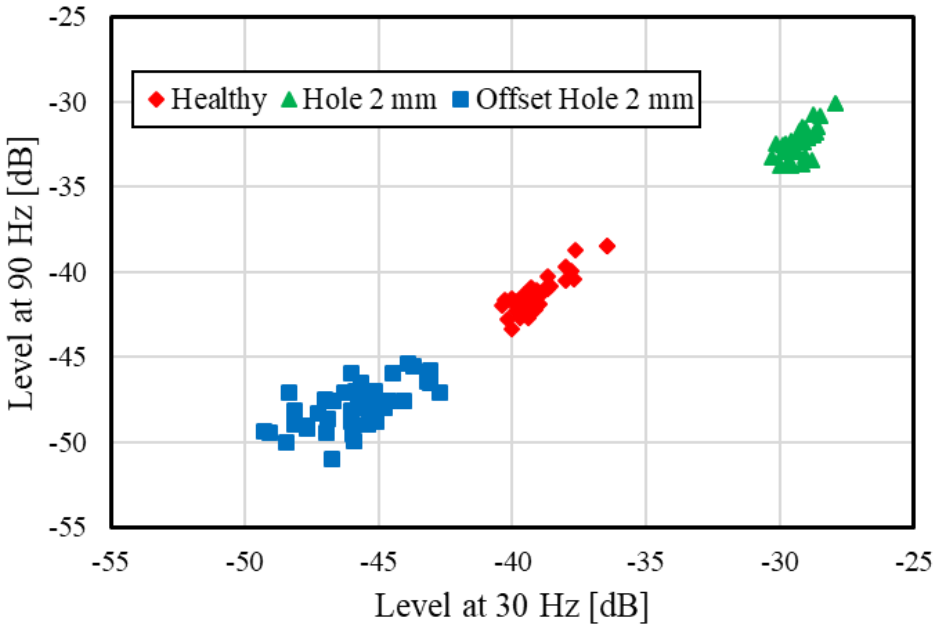

Figure 4.15 *Offset analysis - Hole.*

Additionally, the frequency changes at the 30 Hz and 90 Hz, are compared with the results of eccentricity fault. The frequencies monitored for detecting the eccentricity fault are 25 and 75 Hz (approximately) with the frequency of power source 50 Hz.

For the purpose of veracity, the purposed analytical concept is applied considering the frequency of power source to be 50 Hz. For the case of 1765 min^{-1}, the frequency F_B is found to be 14.7 Hz (50 Hz – 35.30 Hz) and 85.3 Hz (50 Hz + 35.30 Hz). Thus they do not duplicate with the result of eccentricity fault at the condition of supply frequency (50 Hz) as mentioned above. Hence it seems to be no longer in relation with eccentricity fault [14]. However, practical experimental analysis has to be done for verifying the results of analytical computation carried out at the frequency of 50 Hz.

4.2.4 Diagnosis using SVM

The main work is to identify the faulty motor with the healthy motor. In addition to this, it is found that it is even possible to distinguish the two types of faulty motor (hole with 0.5 mm and hole with 2 mm). For easy understanding, healthy bearing, bearing with hole of 0.5 mm and bearing with hole of 2 mm are illustrated as H, H0.5 and H2, respectively. The entire diagnosis analysis is performed in both the conditions of the rotating speed of induction motor. That is, considering and without considering the rotating speed of the induction motor. The results of the diagnosis are explained one by one as follows.

4.2.4.1 Diagnosis without Considering Rotating Speed

The diagnosis based on the SVM was performed to the hole identification analysis without considering the rotating speed of the induction motor. Around 320 sets of load current data were obtained for the condition H-H0.5, H-H2 and H0.5-H2. Each datum consists of two components that are the amplitude of frequency at 30 Hz and 90 Hz. Among the 320 sets of data, 240 data were used as a training data and the remaining 80 data were used as a verification data. In this proposed system, the accuracy rate of the diagnosis is defined as

$$\text{Accuracy rate } (\%) = \frac{number\ of\ data\ diagnosed\ accurately}{total\ number\ of\ data\ for\ diagnosis} \times 100 \qquad (4.9)$$

The combined data of all four-rotating speed has been analyzed for the three types of bearing condition. Table 4.3 shows the diagnosis accuracy rate of H-H0.5, H-H2, and H0.5-H2, respectively. It is very clear that, the accuracy rate for H-H0.5 and H-H2 is very high. This fact clearly shows that healthy motor is completely diagnosed from the two types of faulty motor. On comparing the H-H0.5 and H-H2, the accuracy level of H0.5-H2 is less, but it has a practically acceptable value. The average accuracy rate of all the three analysis is found to be 85 %. From the result, it is observed that this approach is possible to get used in the industrial applications.

Table 4.3 *Diagnosis result*

Bearing Failure Analysis	Accuracy Rate (%)
Healthy and Hole 0.5 mm (H-H0.5)	85.0
Healthy and Hole 2 mm (H-H2)	97.50
Hole 0.5 mm and Hole 2 mm (H0.5-H2)	72.50
Average	85.0

4.2.4.2 Diagnosis considering Rotating Speed

Diagnosis based on the SVM was performed for the hole identification analysis by considering the individual rotating speed of the induction motor for all the three types of bearing conditions. As an illustration, for the case of single rotating speed, around 80 sets of load current data were obtained for the condition H-H0.5, H-H2 and H0.5-H2. Each data consists of two components that are the amplitude of frequency components at 30 Hz and 90 Hz. Among the 80 sets of load current data, 60 data were used as training data and the remaining 20 data were used as verification data. In this proposed system, the accuracy rate of the diagnosis is defined as like the previous case without considering the rotating speed of the induction motor.

The bearing fault investigation was initially started with the 1780 min^{-1} rotating speed and then followed for other rotating speed (1775, 1770, and 1765 min^{-1}). The total diagnosis rate for H-H0.5, H-H2 and H0.5-H2 is 100 %. It is very clear from the diagnosis result that the high accuracy rate is achieved even for the slight mechanical failure in the bearing of the induction motor. Thus, the proposed system and the level of diagnosis rate is acceptable for constant speed operation of induction motor.

4.3 Multiple Hole Analysis

In this section, the multiple hole analysis is carried out. Five types of bearing conditions are discussed: healthy bearing, bearing with one hole and bearing with two holes (holes are made

180 degrees to each other), bearing with three holes (holes are made 120 degrees to each other), and bearing with four holes (holes are made 90 degrees to each other). The red color arrow in the Figure 4.16 shows the position of multiple hole on the bearing. The dimensions are made common. It is of diameter 2 mm and depth 0.5 mm. The experimental work begins with the observation made on the healthy motor, followed by the faulty motors. In the end, same analysis is performed for all bearing conditions. The rotating speed was adjusted from 1780 min^{-1} to 1765 min^{-1}.

Figure 4.16 *Multiple hole analysis.*

4.3.1 Frequency Spectrum Analysis for Multiple Hole

The FFT analysis of the U phase load current was carried out for all the five types of bearing condition. Figures 4.17 to 4.19 show the frequency spectrum analysis that is carried out for all the case of bearing conditions at the rotating speed 1780 min^{-1}, respectively. The vertical axis is normalized so that the maximum amplitude of the frequency spectrum to be 0 dB. The amplitude difference of the frequency components is clearly visible at the frequencies 30, 90, 120, 150 and 180 Hz. The frequencies 30 and 90 Hz show amplitude changes for all the rotating speed (1780, 1775, 1770 and 1765 min^{-1}). However, at the frequencies 120, 150 and 180 Hz no considerable amplitude changes have been observed for all the four-rotating speed. Hence, the frequency 30 and 90 Hz has been considered for the present study. Also, there is an explanation why the changes have been observed at the frequency of 30 Hz and 90 Hz in the section 4.2.2.

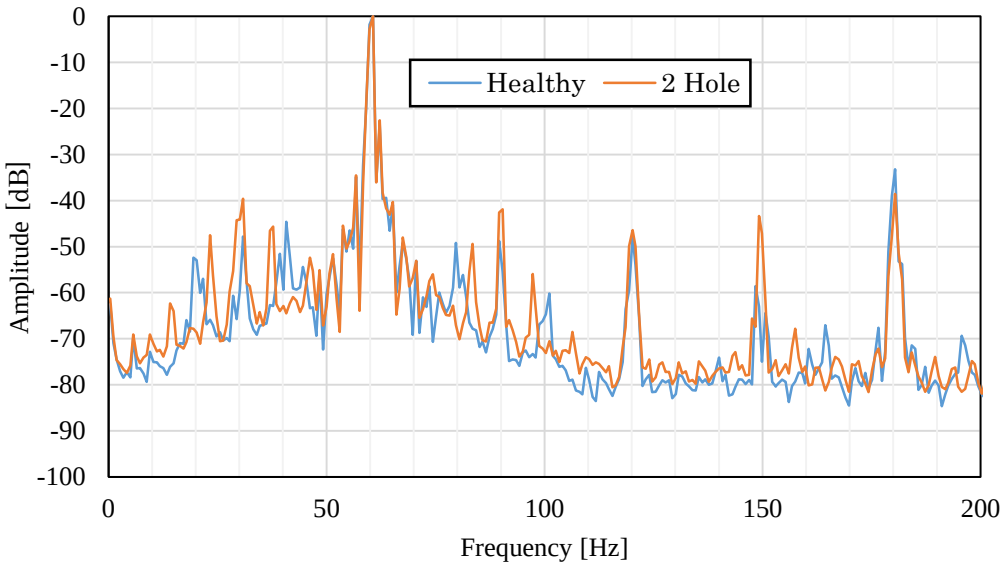

Figure 4.17 *Frequency spectrum analysis for 2 hole at 1780 min^{-1}.*

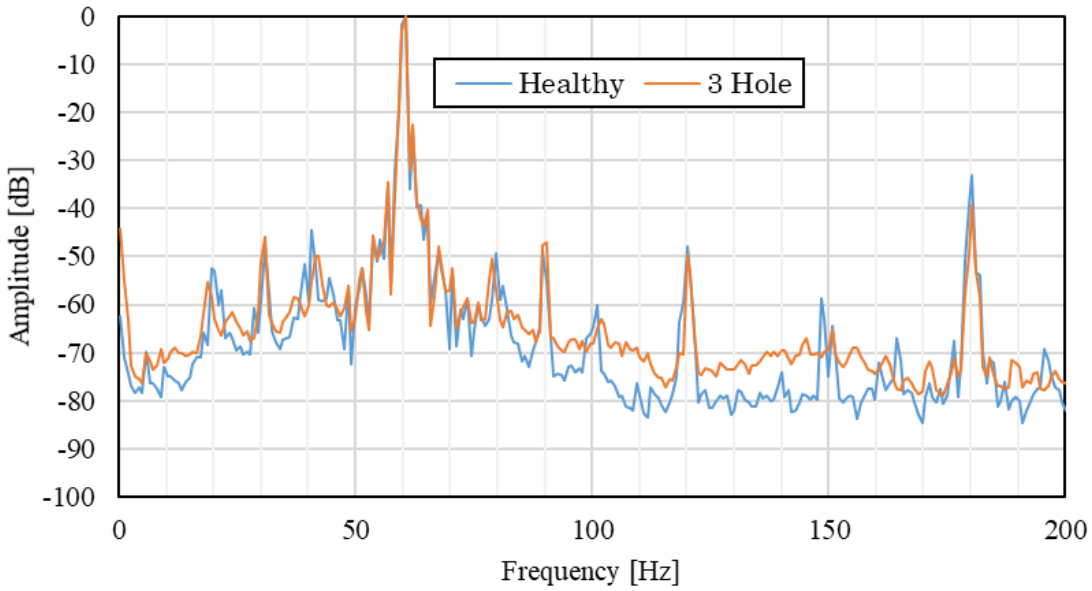

Figure 4.18 *Frequency spectrum analysis for 3 hole at 1780 min^{-1}.*

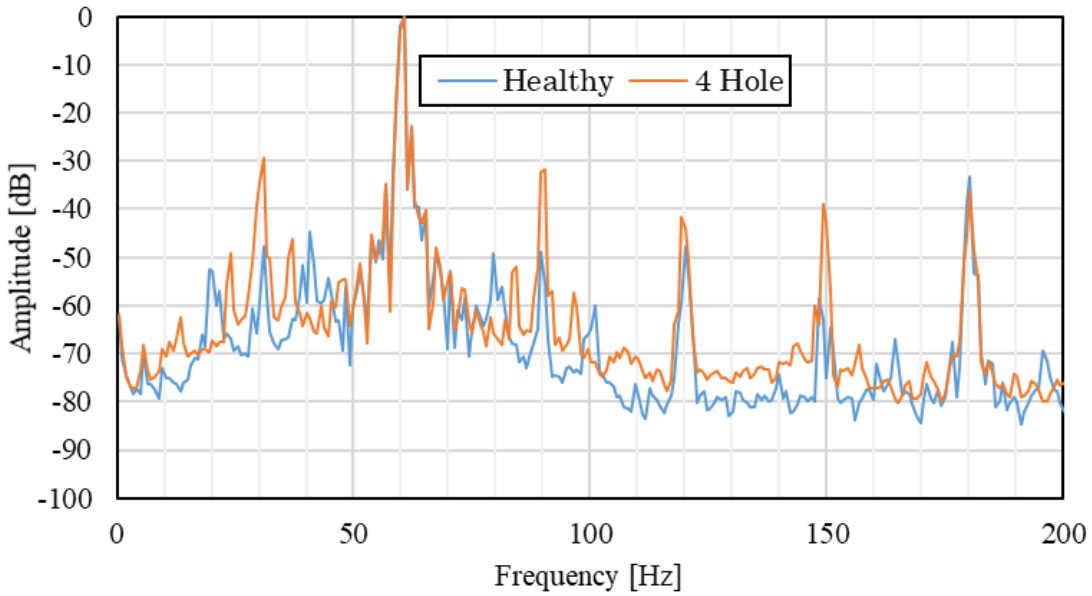

Figure 4.19 *Frequency spectrum analysis for 4 hole at 1780 min^{-1}.*

4.3.2 Feature Distribution for Multiple Hole Analysis

Figures 4.20 to 4.23 show the feature extracted at the frequency of 30 and 90 Hz for all the five types of bearing condition. For easy understanding, healthy bearing, bearing with one hole, bearing with two holes, bearing with three holes and bearing with four holes are illustrated as H, 1H and 2H, 3H and 4H, respectively.

The location of the classes mainly depends on the bearing condition and the rotating speed of the induction motor. It is very clear that, all the five types of bearing conditions (H, 1H and 2H, 3H and 4H) are located to their own classes and gets differentiated. Overlapping is observed between the different classes. However other than 3H, the proposed system manages to identify the multiple holes in the bearing of the induction motor. Therefore, these feature plays a key role in the prompt study.

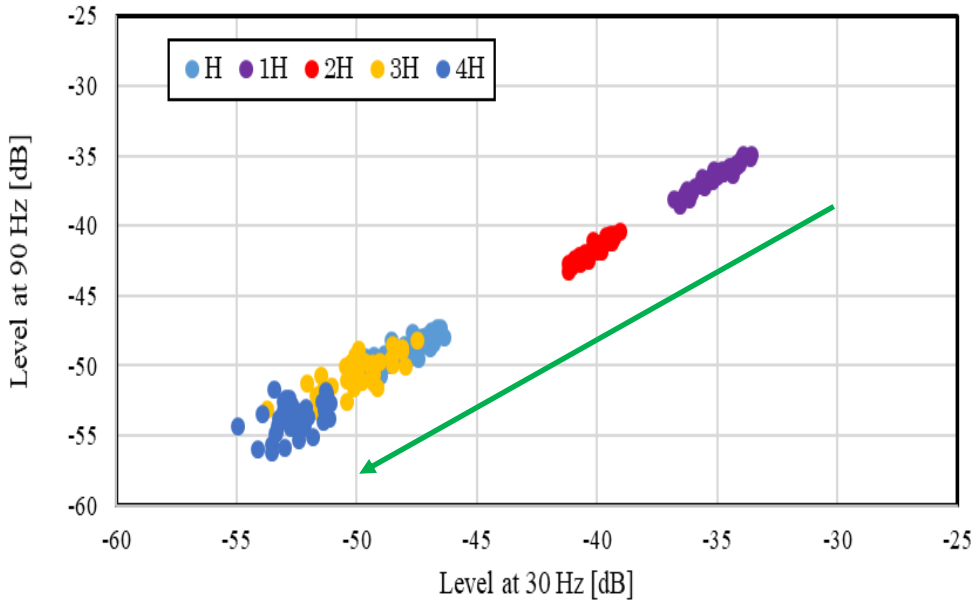

Figure 4.20 *Feature distribution for multiple hole analysis at 1765 min^{-1}.*

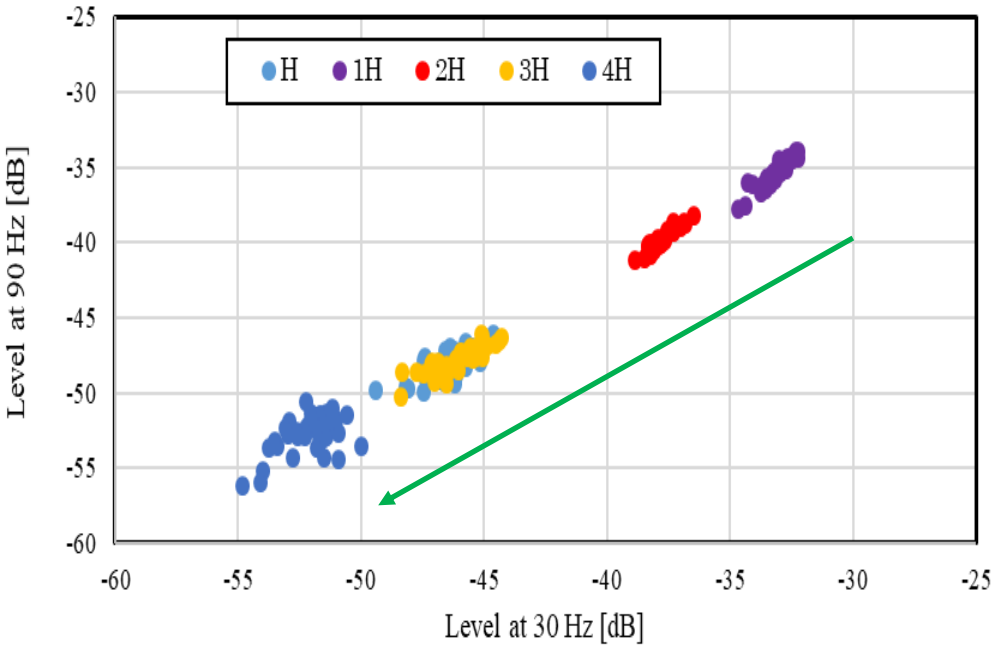

Figure 4.21 *Feature distribution for multiple hole analysis at 1770 min^{-1}.*

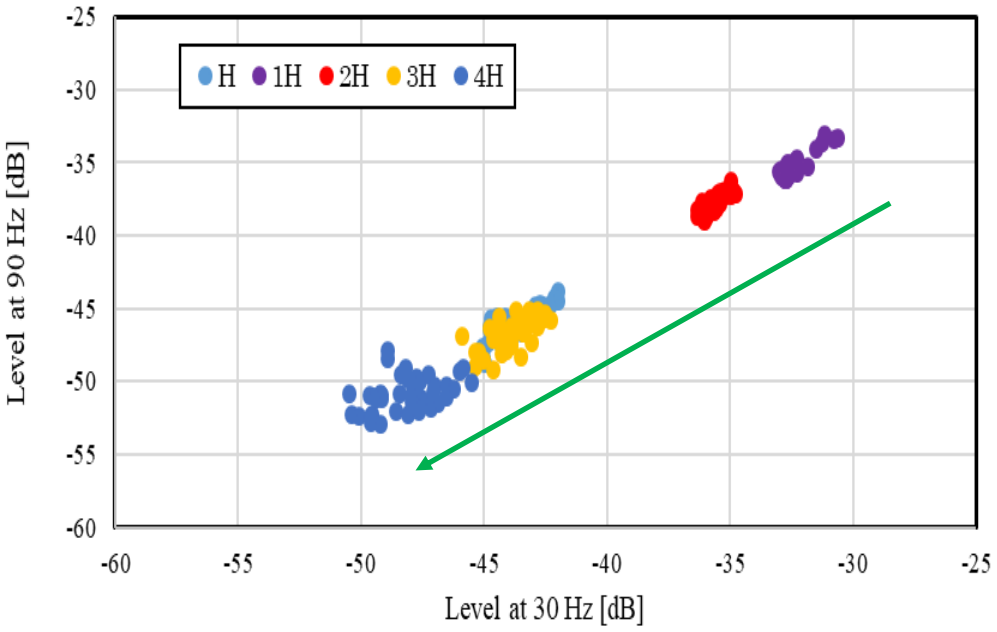

Figure 4.22 *Feature distribution for multiple hole analysis at 1775 min^{-1}.*

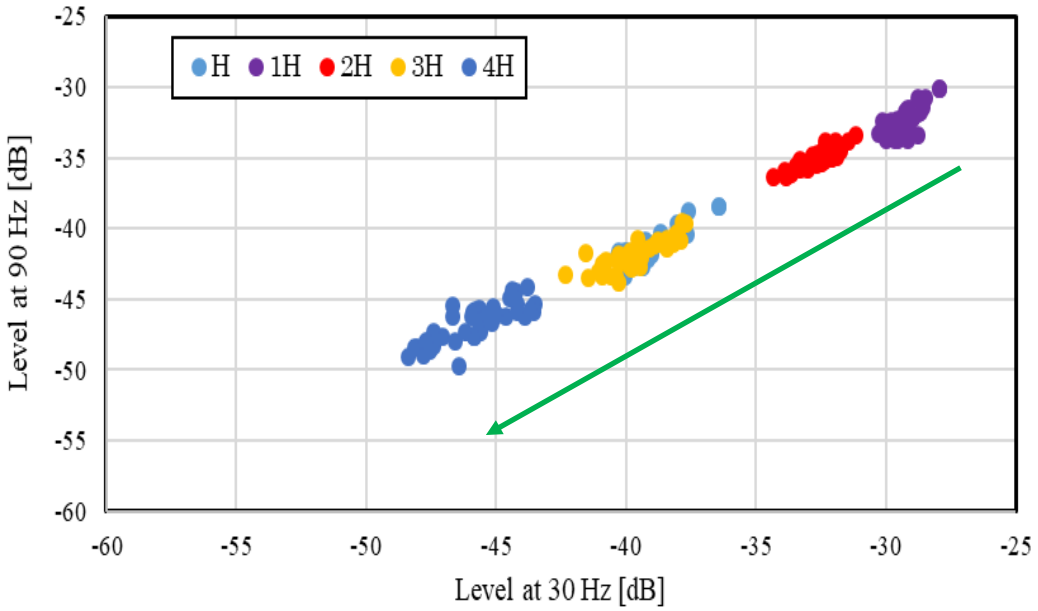

Figure 4.23 *Feature distribution for multiple hole analysis at 1780 min^{-1}.*

A special observation has been made from the feature distribution of multiple hole analysis. As the number of hole induced on the outer raceway of the bearing gets increased, the amplitude starts to decrease as shown in Figures 4.20 to 4.23. In the present study, the holes are induced in an asymmetrical manner and that may stand as the reason for the decrease in the amplitude. For the confirmation, multiple hole analysis of symmetrical pattern must be performed. In this case, the analysis results may be opposite to that of asymmetrical.

4.3.3 Diagnosis using SVM

The entire diagnosis analysis is performed in both the conditions of considering and without considering the rotating speed of the induction motor. The results of both the diagnosis are explained one by one as follows.

4.3.3.1 Diagnosis without Considering Rotating Speed

Around 320 sets of load current data were obtained for the condition H-1H, H-2H, H-3H and H-4H. Each datum consists of two components that is the amplitude of frequency at 30 Hz

and 90 Hz. Among the 320 sets of load current data, 240 data were used as training data and the remaining 80 data were used as verification data. But for the case of H-1H-2H-3H-4H, among the 800 sets of load current data, 600 data were used as training data and the remaining 200 data were used as diagnosis data.

The combined data of all four-rotating speed have been analyzed for the five types of bearing condition. Table 4.4 shows the diagnosis accuracy rate of H-1H, H-2H, H-3H and H-4H and H-1H-2H-3H-4H. It is very clear that, the accuracy rate for H-1H, H-2H and H-4H is very high. This fact clearly shows that healthy motor is completely diagnosed from one hole, two holes and four holes of the faulty motor. On comparing with the obtained result, the accuracy level of H-3H is very low. This result also affects the diagnosis result of H-1H-2H-3H-4H. This is because other than the rotating speed of 1780 min^{-1} of healthy bearing and 1765 min^{-1} of bearing with 3 holes, the entire data of other rotating speed is getting overlapped.

When looking the diagnosis result in a probabilistic manner, the rate of accuracy is good. This is because, among the 80 verifications data, almost 60 data get overlapped. In this condition, getting an accuracy rate and total accuracy rate above 50 % is practically acceptable. The average accuracy rate of all the five analysis is found to be 78.65 %. The obtained accuracy rate is practically acceptable. In the future, a method to improve the accuracy level of H-3H will be investigated.

4.3.3.2 Diagnosis Considering Rotating Speed

As an illustration, for the case of single rotating speed, 80 sets of load current data were obtained for the condition H-1H, H-2H, H-3H and H-4H. Each data consists of two components that are the amplitude of frequency components at 30 Hz and 90 Hz. Among the 80 sets of load current data, 60 data were used as training data and the remaining 20 data were used as verification data. Similarly, for the case of H-1H-2H-3H-4H, among the 200 sets of load current data, 150 data were used as training data and the remaining 50 data were used as diagnosis data.

Because of diagnosis, total accuracy rate for H-1H, H-2H and H-4H is above 90 %. But for the case of H-3H and H-1H-2H-3H-4H, the total accuracy rate is less than 85 %. It is very clear from the diagnosis result that the high accuracy rate is achieved even for the slight mechanical failure in the bearing of the induction motor. Thus, the proposed system and the level of diagnosis rate is practically acceptable by considering the rotating speed of the induction motor. Therefore, the multiple hole analysis is much suited with the condition of rotating speed consideration.

Table 4.4 *Diagnosis result*

Bearing Failure Analysis	Accuracy Rate (%)
H-1H	96.25
H-2H	87.5
H-3H	57.5
H-4H	80
H-1H-2H-3H-4H	72
Average	78.65

4.4 Localization of Holes

For localization of hole analysis, three types of bearing conditions were discussed: healthy bearing, bearing with two holes (holes are made 90 degrees to each other), bearing with two holes (holes are made 180 degrees to each other) as shown in 4.24. The red color arrow in the Figure 4.24 shows the localization of hole. For easy understanding they are illustrated as 2H90 and 2H180, respectively. The dimensions are made common. It is of diameter 2 mm and depth 1 mm. The experimental work begins with the observation made on the healthy motor, followed by the faulty motors. In the end, the same analysis is performed for all bearing conditions. The rotating speed was adjusted from 1780 min^{-1} to 1765 min^{-1}.

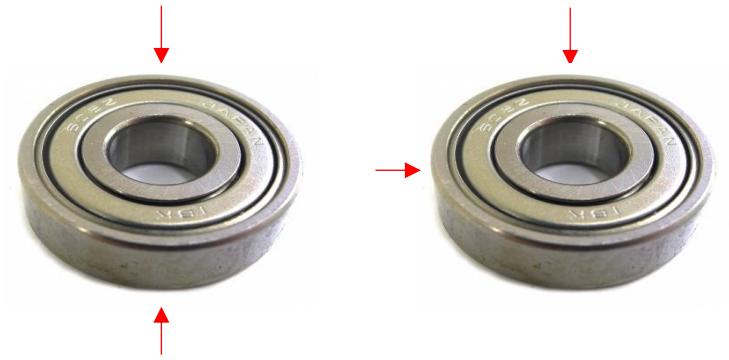

Figure 4.24 *Localization of hole analysis.*

4.4.1 Frequency Spectrum Analysis for Localization of holes

The FFT analysis of the U phase load current was carried out in the analogous way as like identification of holes and multiple hole analysis. Figures 4.25 to 4.27 show the frequency spectrum analysis that is carried out for all three bearing conditions at the rotating speed of 1780 min^{-1}. At the frequency of 30 Hz and 90 Hz, the difference in the magnitude of the frequency components was observed. The magnitude of characteristic frequency components gets differentiated with the faulty bearing condition also. Thus, it is likely to identify the difference between the localization of holes on the bearing.

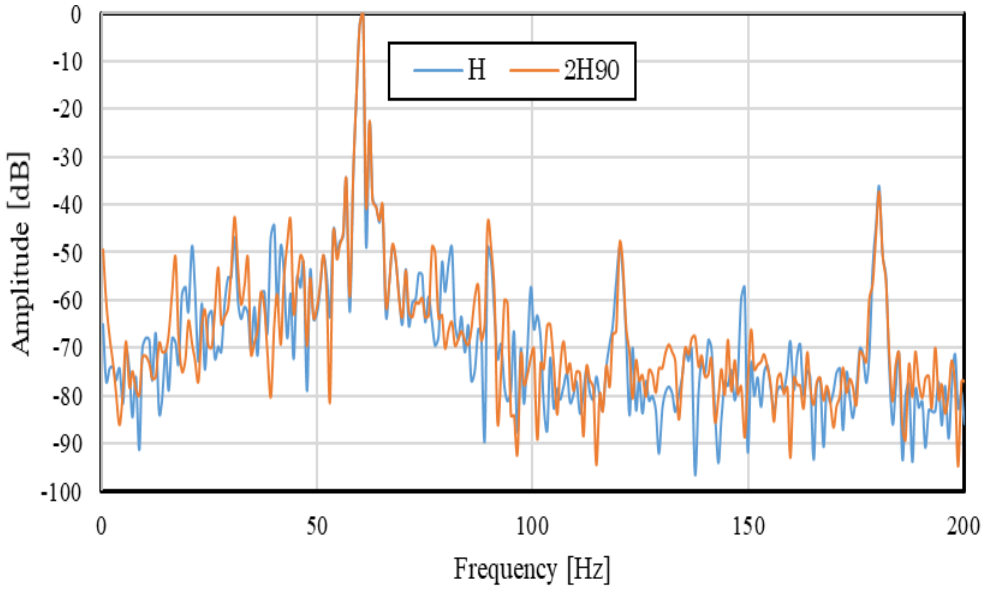

Figure 4.25 *Spectrum analysis for 2 holes with 180 degrees at 1780 min^{-1}.*

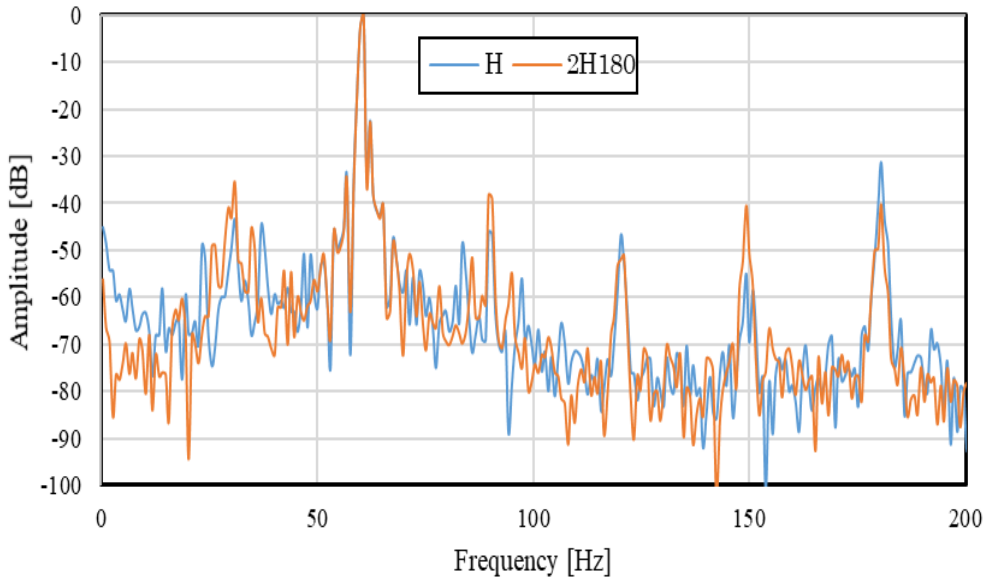

Figure 4.26 *Spectrum analysis for 2 holes with 90 degrees at 1780 min^{-1}.*

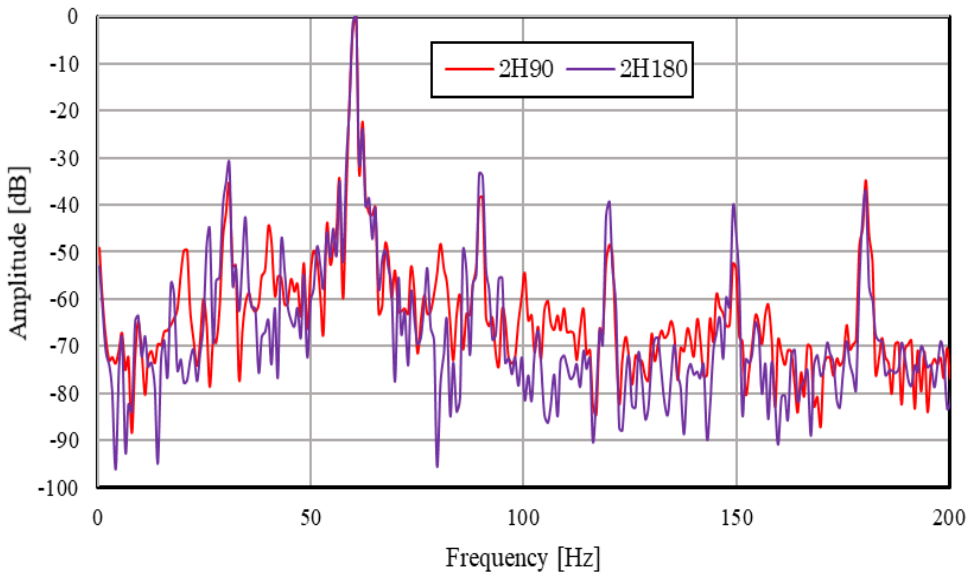

Figure 4.27 *Spectrum analysis between 2H90 and 2H180 at 1780 min^{-1}.*

4.4.2 Feature Distribution for Localization of Hole Analysis

Figures 4.28 to 4.31 show the feature distribution of the three types of bearing condition (H, 2H90 and 2H180) extracted at the frequency of 30 Hz and 90 Hz at the all the rotating speed. While taking the rotating speed into consideration, all the three types of bearing conditions get located to their own classes. Thus, it is possible to distinguish the three types of bearing conditions. Therefore, these levels of feature play a key role in the prompt study.

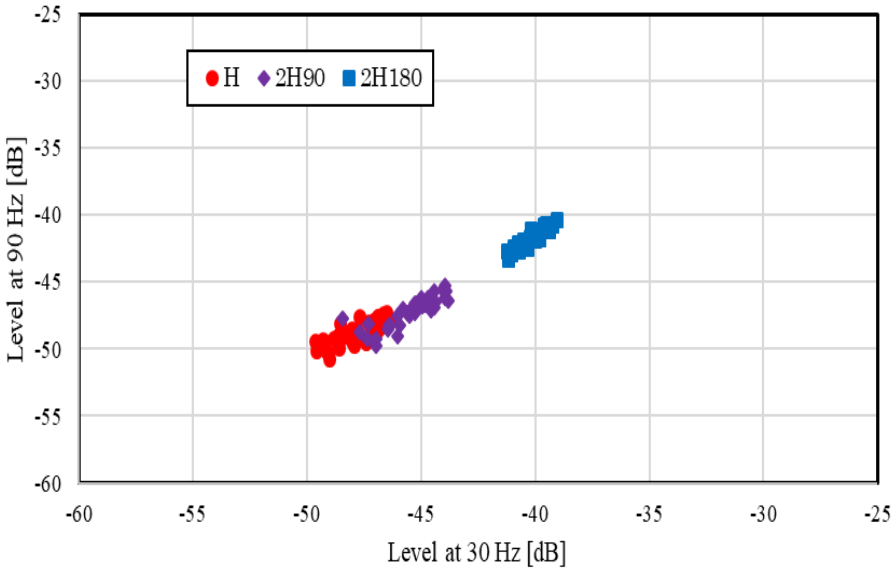

Figure 4.28 *Feature distribution for localization of hole analysis at 1765 min^{-1}.*

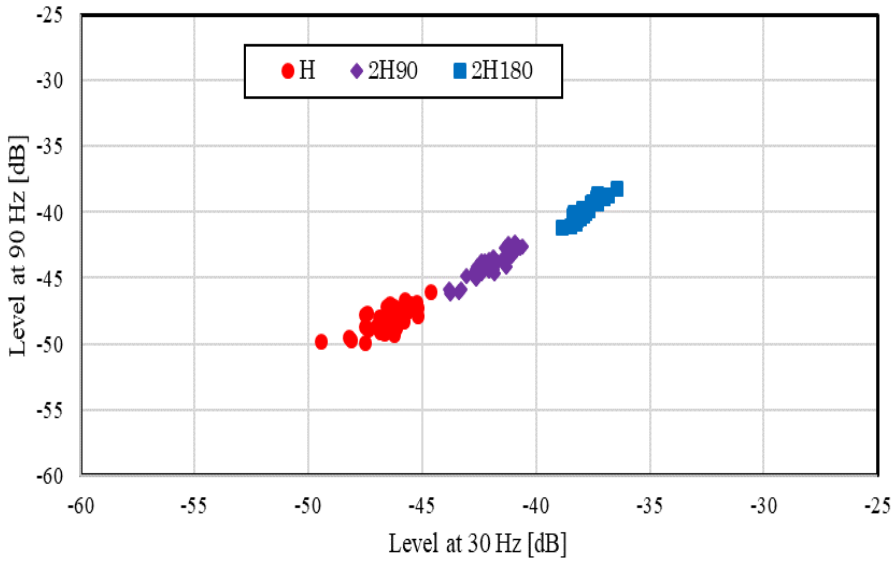

Figure 4.29 *Feature distribution for localization of hole analysis at 1770 min^{-1}.*

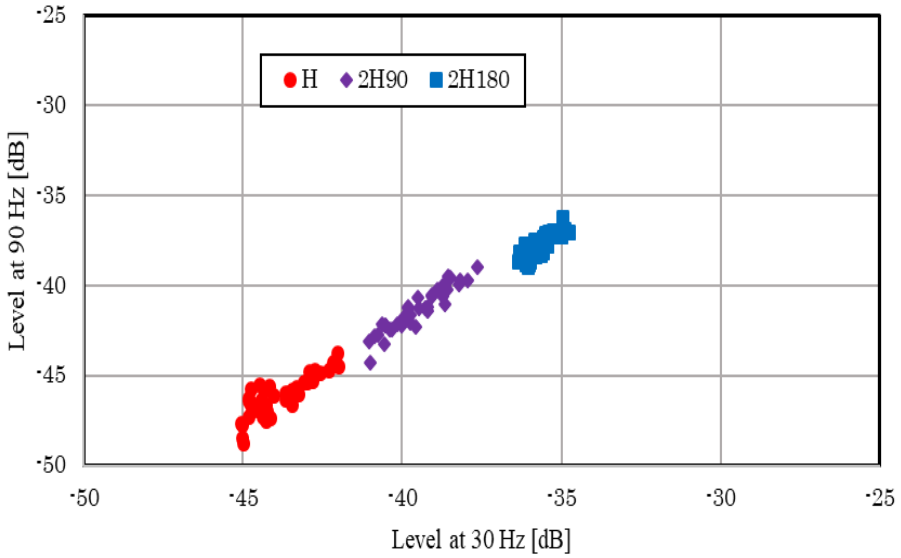

Figure 4.30 *Feature distribution for localization of hole analysis at 1775 min^{-1}.*

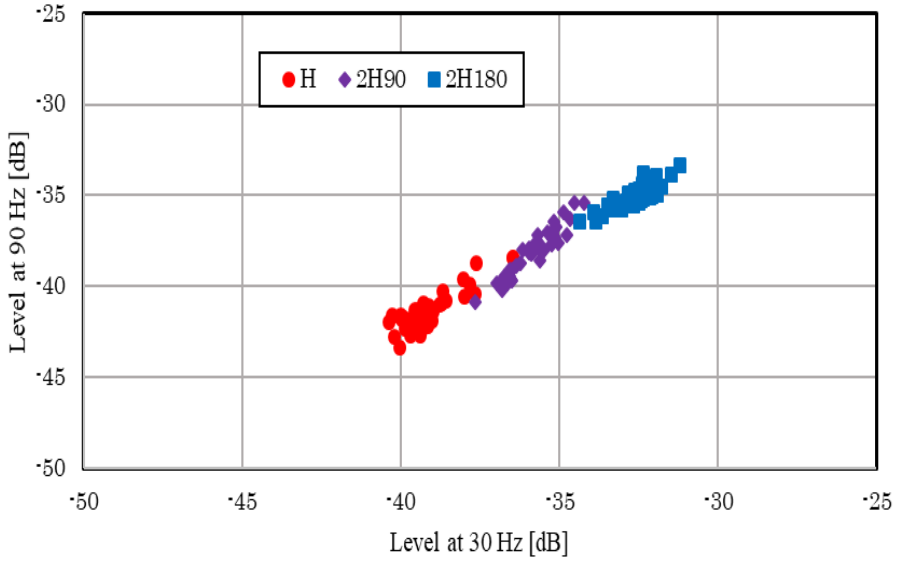

Figure 4.31 *Feature distribution for localization of hole analysis at 1780 min^{-1}.*

4.4.3 Diagnosis using SVM

The entire diagnosis analysis is performed in both the conditions of the rotating speed of induction motor. That is, considering and without considering the rotating speed of the induction motor. The results of both the diagnosis are explained one by one as follows.

4.4.3.1 Diagnosis without Considering Rotating Speed

320 sets of load current data were obtained for the condition H-2H90, H-2H180 and 2H90-2H180. Each datum consists of two components; the amplitude of frequency at 30 Hz and 90 Hz. Among the 320 sets of load current data, 240 data were used as training data and the remaining 80 data were used as verification data.

The combined data of all four-rotating speed have been analyzed for the three types of bearing condition. Table 4.5 shows the diagnosis accuracy rate of H-2H90, H-2H180 and 2H90-2H180. The yellow color cell reveals where the proper diagnosis has been performed. The average accuracy rate of all the three analysis is found to be 85.0 %. The obtained accuracy rate is practically acceptable.

From the result, it is observed that this approach is possible to get used in the industrial applications. Also, from the diagnosis result, it is evident that the physical location of holes on the bearing of the induction motor plays a key role. The accuracy rate for H-2H90, H-2H180 and 2H90-2H180 is very high. This fact clearly shows that healthy motor is completely diagnosed from the faulty motor. Thus, the proposed system managed to identify the localization of hole in the bearing of the induction motor. This discovery will be considered as a core point of the proposed system.

Table 4.5 *Diagnosis result*

Bearing Failure Analysis	Accuracy Rate (%)
H-2H90	82.5
H-2H180	87.5
2H90-2H180	85
Average	85

4.4.3.2 Diagnosis Considering Rotating Speed

As an illustration, for the case of single rotating speed, 80 sets of load current data were obtained for the condition H-2H90, H-2H180 and 2H90-2H180. Each datum consists of two components that are the amplitude of frequency components at 30 Hz and 90 Hz. Among the 80 sets of load current data, 60 data were used as training data and the remaining 20 data were used as verification data. In this proposed system, the accuracy rate of the diagnosis is defined as like the previous case without considering the rotating speed of the induction motor.

The diagnosis accuracy rate for H-2H90, H-2H180 and 2H90-2H180 is above 90 %. It is very clear from the diagnosis result that the high accuracy rate is achieved even for the localization of hole bearing failure. Thus, the proposed system and the level of diagnosis rate are practically acceptable by considering the rotating speed of the induction motor. Therefore, the localization of hole analysis is also much suited with the condition of rotating speed consideration.

4.5 Summary

Using the load current, the FFT analysis has been performed and the features are extracted. The amplitude of the frequency 30 and 90 Hz is considered as the main feature and the bearing failure detection using hole is carried out. The following analysis has been investigated; hole identification, multiple hole analysis and localization of hole. In most of the cases, the overlapping of features is observed between different bearing conditions and

the problem is overwhelmed using SVM. Based on the result of SVM, it is possible to detect the bearing fault and the diagnosis accuracy rate is improved. The proposed method has the following advantages:

- The healthy motor is completely diagnosed from the faulty motor
- The minor fault detection (hole 0.5 mm) is made possible
- The difference between the faulty motor is also observed (hole 0.5 mm and hole 2 mm)
- In case of multiple hole analysis, the number of hole identification is achieved
- The results of localization of hole analysis gives a clear idea about the role of physical location and difference between 2H90 and 2H180 is observed
- The total time to perform the diagnosis is short (approximately 80 seconds)

Chapter 5
Bearing Failure Diagnosis – Single Fault Analysis using Scratch

5.1 Introduction

Till now most of the researches have been carried out using hole as a faulty factor of bearing, but in practical point the chance of scratch has the highest probability when compared to the holes. Hence it is important to perform many researches for the fault analysis using scratch. Therefore, in the present research work, scratch has been made as a crucial factor for fault analysis. The bearing failure analysis is carried for identifying and study about the scratch progression with respect to healthy motor, multiple scratches and orientation of scratches on the bearing of the induction motor.

The analysis is carried out by characterizing the specified frequency components of the load current and to be considered as a main feature. Also, the signal from the stator load current is analyzed with the help of Fast Fourier Transform (FFT) and further investigation was performed. The experimental setup, induction motor and the analysis method are same as chapter 4.

5.2 Progression of a Scratch

If a scratch appearing on a bearing is not detected at an early stage, it may increase in size as the motor runs. To simulate this and to allow the progression of a fault on the outer raceway of the bearing to be analyzed, scratches with lengths of 5, 10, and 15 mm were induced. The depth and width of the scratches were held constant at 0.5 mm. Stimulated fault progression in one sample is shown in Figure 5.1. Generally, it is tedious and costly to collect the damaged motor from the industry. For this reason, the faults are made artificially on the bearing of the induction motor. The experimental work begins with the observation made on the healthy

motor. After that, the faulty motor gets replaced in the position of the healthy motor. The rotating speed was adjusted from 1780 min^{-1} to 1765 min^{-1}.

The following terminology is used, H, and HS denote the healthy motor, and horizontal scratch, respectively. The code is followed by the scratch length in mm. Thus, for example, a 10 mm horizontal scratch is denoted HS10.

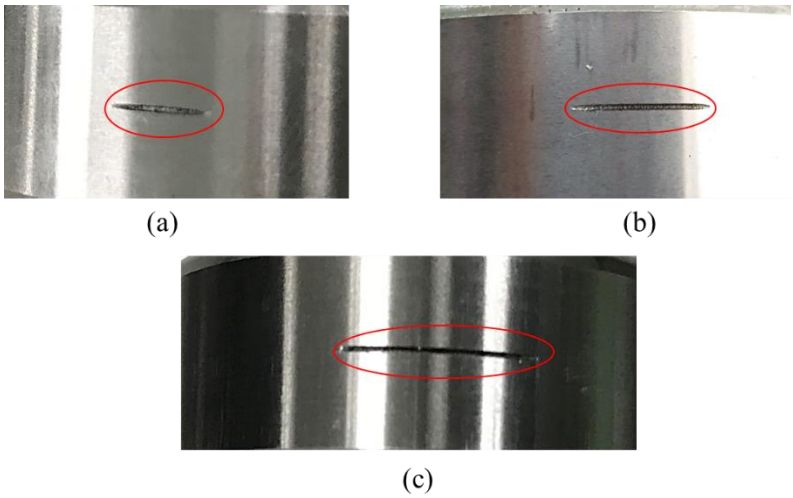

Figure 5.1 *Progressive bearing failure (a) horizontal scratch 5 mm (HS5) (b) horizontal scratch 10 mm (HS10) (c) horizontal scratch 15 mm (HS15).*

5.2.1 Frequency Spectrum Analysis

FFT analysis of the U-phase load current was performed under all four bearing conditions. Figures 5.2 and 5.3 compare the frequency spectra plotted for H–HS10 and HS5–HS10–HS15, respectively, at a rotating speed of 1765 min^{-1}. The amplitude on the vertical axis is normalized to a maximum of 0 dB.

A large amplitude difference can be observed between the healthy motor and all the three fault conditions (H–HS5, H–HS10, and H–HS15). When the faults on the bearings are compared (HS5–HS10–HS15), the amplitude difference observed is sufficient to differentiate the cases. Amplitude differences in the frequency components are clearly visible at

frequencies of 30, 90, 150, and 180 Hz. At 30 and 90 Hz, amplitude changes are observed at all rotating speeds (1780, 1775, 1770, and 1765 min^{-1}). At 150 and 180 Hz, in contrast, no significant amplitude change is observed when the speed was varied, under any of the four bearing conditions. Frequencies of 30 and 90 Hz are therefore used in the study.

When a hole is induced on a bearing, a shock wave with a characteristic frequency is generated. The frequency mainly depends on the point at which the fault is induced and the level of damage. The analysis performed in the present study assumed a scratch to be like a hole. Amplitude of the characteristic frequencies of 30 and 90 Hz were used to detect the bearing condition and were used to plot the feature distribution for more detailed study.

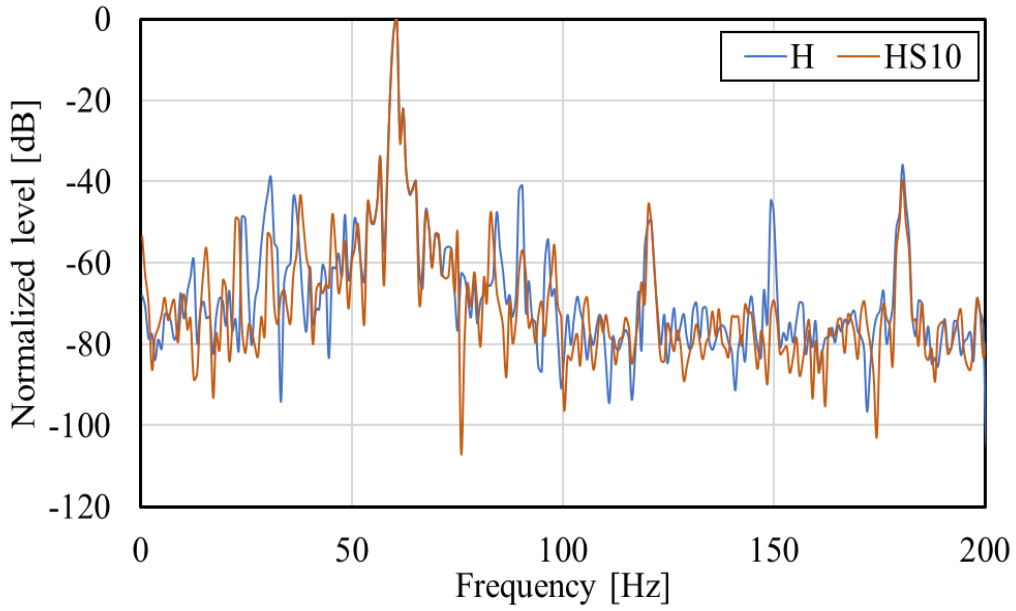

Figure 5.2 *Spectral analysis of H-HS10 at 1765 min^{-1}.*

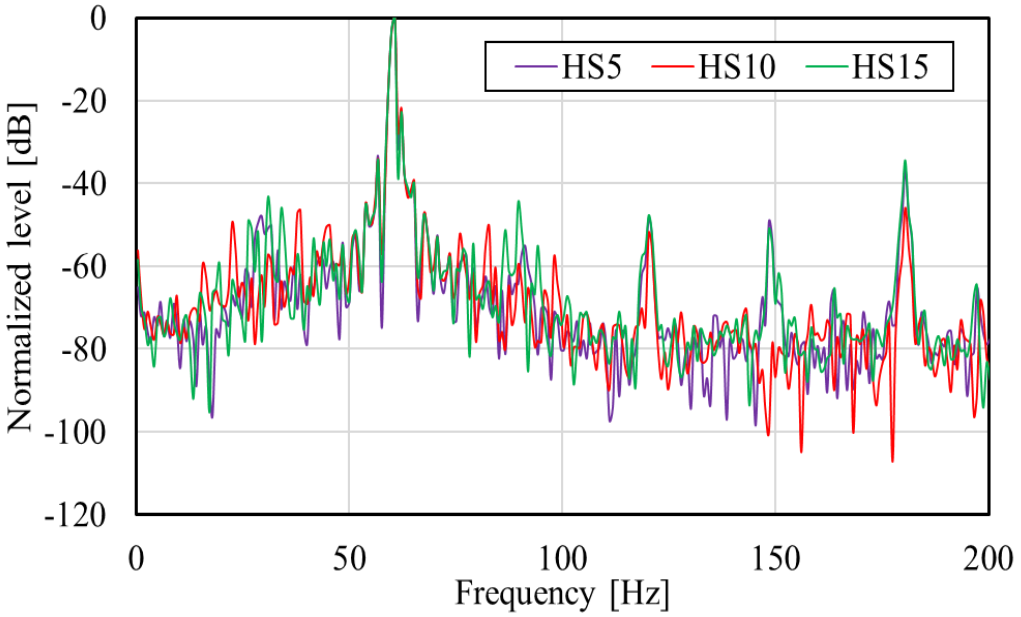

Figure 5.3 *Spectral analysis of HS5-HS10-HS15 at 1765 min^{-1}.*

5.2.2 Feature Distribution

The feature distribution analysis is carried out using the amplitude of the characteristics frequency 30 and 90 Hz. A two-dimensional graph is plotted, taking amplitude of 30 Hz along the x-axis and 90 Hz along the y-axis, respectively.

In both healthy and faulty motors, the contribution of each feature was evaluated from the load condition. In this section, we discuss four bearing conditions (H, HS5, HS10, and HS15). Figures 5.4 and 5.5 show the feature distribution at rotating speeds of 1770 and 1765 min^{-1} for all bearing conditions, respectively. The location distinguishing behavior depends on the rotating speed of the motor and the bearing conditions. The conditions HS10 and HS15 could be clearly distinguished from the healthy motor. In contrast, an overlap between HS5 and the healthy motor (H) made it possible to derive only a partial evaluation of the condition.

While taking the individual rotating speed of the induction motor into consideration, the class of the faulty motor is located far away from the healthy motor. These scratches have their

own class of location according to the bearing condition and rotating speed. Thus, this method is effective in diagnosing the four types of bearing condition. The proposed method could identify the bearing failure while the motor is in running condition and demonstrates the significant role that feature distribution plays in the analysis of progressive bearing failure.

In industries, the speed of the induction motor is not constant and said to be varied between the certain range. Considering the industrial environment, the analysis is also performed without considering the rotating speed and the result is shown in Figure 5.6. The overlapping of features is observed between the different bearing conditions of the induction motor, yet they are distributed linearly and segregated to their own classes. The faulty motors horizontal scratch 5 mm (HS5) and horizontal scratch 15 mm (HS15) show large overlapping when comparing to the healthy motor (H). In this case, SVM is employed and the diagnosis is performed.

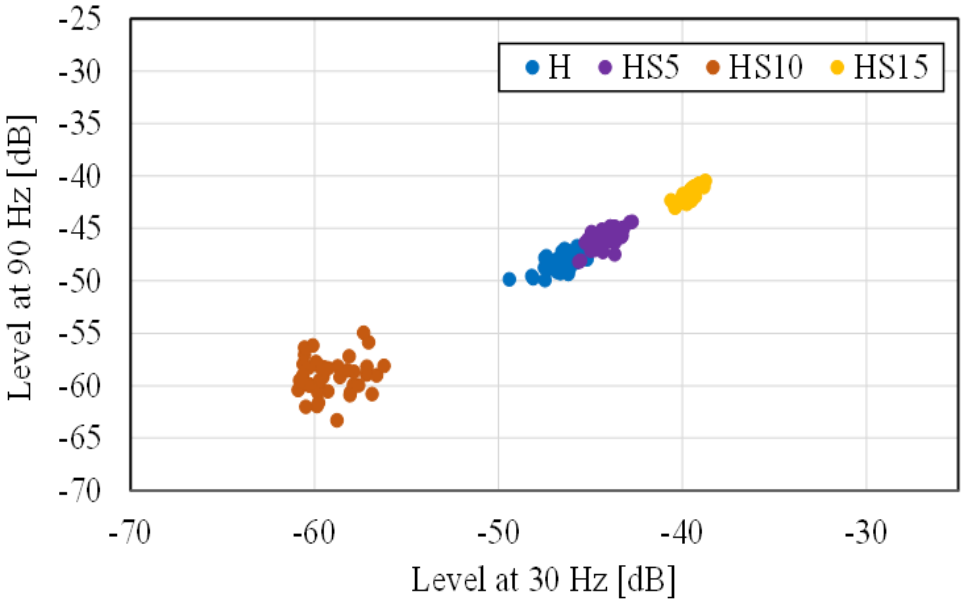

Figure 5.4 *Feature distribution of progressive failure analysis at 1770 min^{-1}.*

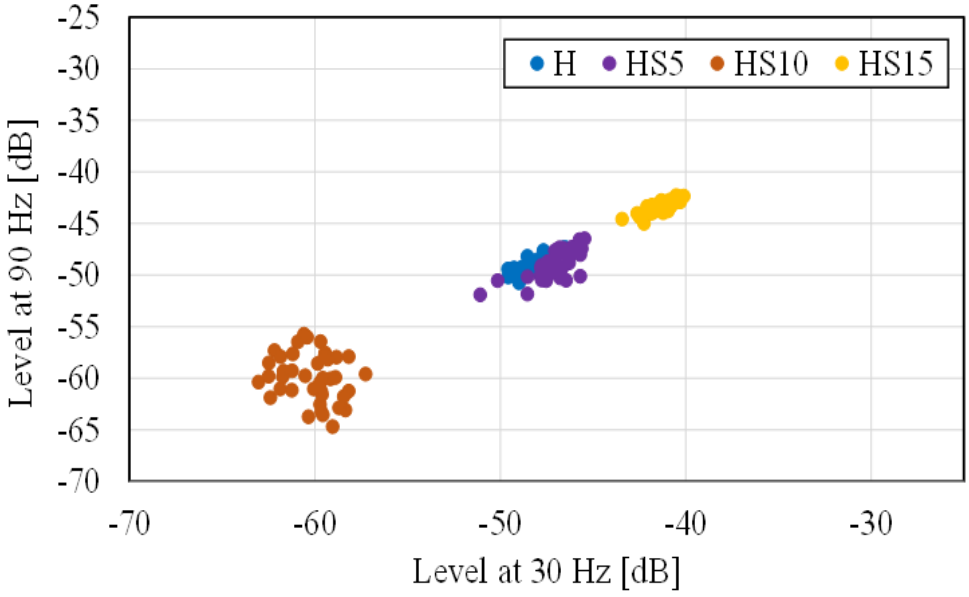

Figure 5.5 *Feature distribution of progressive failure analysis at 1765 min^{-1}.*

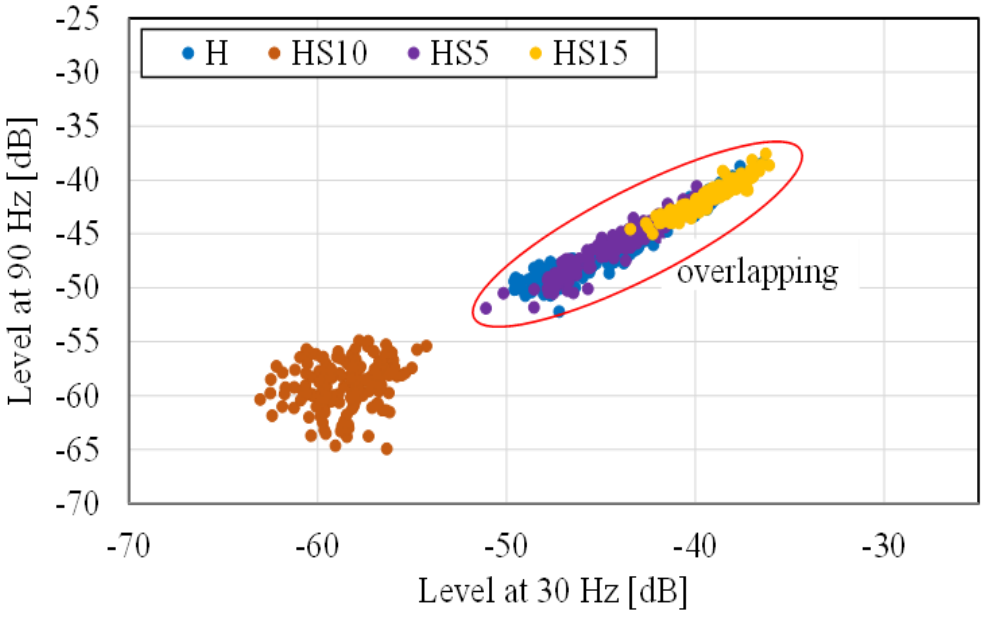

Figure 5.6 *Integrated progressive analysis.*

From the result of spectral analysis and the feature distribution, even in the case of scratch, the amplitude changes have been observed at the frequencies 30 and 90 Hz. The details regarding the amplitude changes are discussed in the section 4.2.3. The discussion confirms the reason for the amplitude changes observed at the frequencies 30 and 90 Hz. The shock wave pulse stands as the reason for the occurrence of the amplitude changes at the respective frequency and it is said to cross the center of the outer raceway of bearing. Similar to hole, scratch also induced in the center, as a result, the changes are said to be obtained and detection is made possible. For the purpose of the confirmation, once again the offset analysis is carried out. The scratch of same dimension is artificially induced to the offset position 2.6 mm away from the center of the bearing and the feature distribution results is shown in Figure 5.7. The scratch at the center shows more deviation when compared to the scratch result of offset. This confirms the occurrence of shock wave pulse and its impact in detecting the outer raceway bearing failure. The analysis result of offset scratch is comparatively closer to the healthy bearing data. The change in the level of defects is observed.

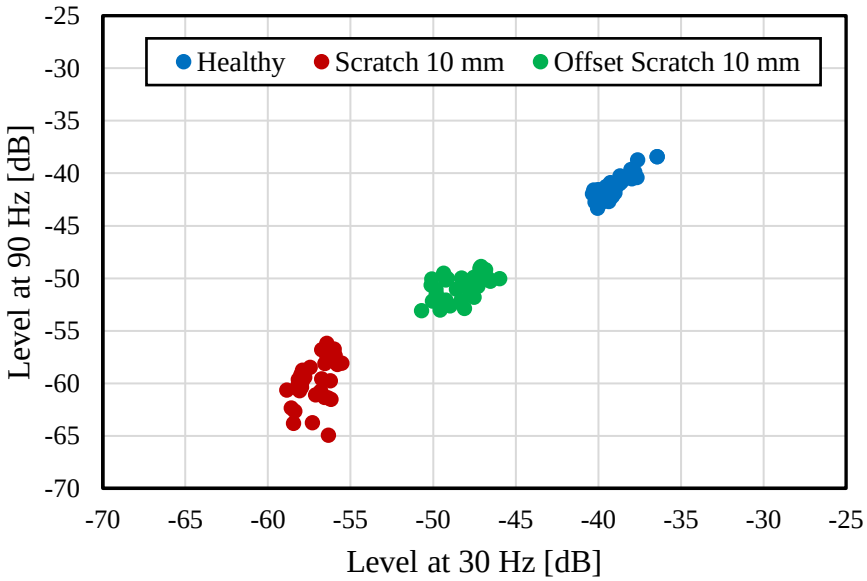

Figure 5.7 *Offset analysis – Scratch.*

5.2.3 Diagnosis using SVM

The main work is to identify and differentiate the faulty motor with the healthy motor. The entire diagnosis analysis is performed in both the condition of the rotating speed of induction motor. That is, considering and without considering the rotating speed of the induction motor. The results of both the diagnosis are explained one by one as follows.

5.2.3.1 Diagnosis without Considering Rotating Speed

The diagnosis based on the SVM was performed. For conditions H–HS5, H–HS10, and H–HS15, 320 sets of load current data were used. Each dataset had both 30 and 90 Hz frequency components. From the 320 sets, 240 were used as training data, and the remaining 80 were used as evaluation data. For H–HS5–HS10–HS15, 640 sets of loads current data were used, with 480 used as training data and the remaining 160 used as evaluation data. Four rotating speeds (1780, 1775, 1770, and 1765 min^{-1}) are combined and the diagnosis are performed.

Table 5.1 shows the accuracy rate when diagnosing progressive bearing failure. The accuracy rates for H–HS10 and H–HS15 are sufficiently high to be considered acceptable in practical applications. In the case of H–HS5, the accuracy rate is lower because of a significant overlapping between the healthy and faulty conditions (Figure 5.6).

In the analysis of H–HS5–HS10–HS15, significant overlaps are found between the different bearing conditions, making the diagnosis process tedious. However, the bearing condition is identified with an accuracy rate of 83.13% and the proposed method is effective in localizing the difference between four conditions, demonstrating its ability to produce a diagnosis, even when overlapping is encountered. The average accuracy rate of all the four analysis is found to be 87.35 %. This is a significant advantage of the proposed method, making it suitable for speed varying applications and in industrial environments.

Table 5.1 *Diagnosis result*

Bearing Condition	Accuracy Rate (%)	
H-HS5	73.75	
H-HS10	100	
H-HS15	92.5	
H-HS5-HS10-HS15	83.13	
	Average	87.35

5.2.3.2 Diagnosis Considering Rotating Speed

Diagnosis based on the SVM was performed for the scratch progression analysis by considering the individual rotating speed of the induction motor for all the four types of bearing conditions. In this proposed system, the accuracy rate of the diagnosis is defined as same as the case discussed in the previous section.

The diagnosis accuracy rate is 95 %. It is very clear from the diagnosis result that the high accuracy rate is achieved even for the slight mechanical failure in the bearing of the induction motor. Thus, the proposed system and the level of diagnosis rate are practically acceptable by considering the rotating speed of the induction motor and suitable for detecting the progression of fault.

5.3 Orientation of Scratch

As the direction that a scratch will take on the bearing is inherently unpredictable, the orientation of scratch analysis is carried out. For orientation of scratch analysis, five types of bearing conditions were discussed: healthy bearing, bearing with scratch made horizontally, bearing with scratch made vertically, bearing with scratch made left crosswise (left orientation scratch) and bearing with scratch made right crosswise (right orientation scratch). For easy understanding they are illustrated as H, HS, VS, LS and RS, respectively. The dimensions are made common and it is of length 10 mm, width 0.5 mm and depth 0.5 mm. The samples used for the orientation of scratch analysis are shown in Figure 5.8.

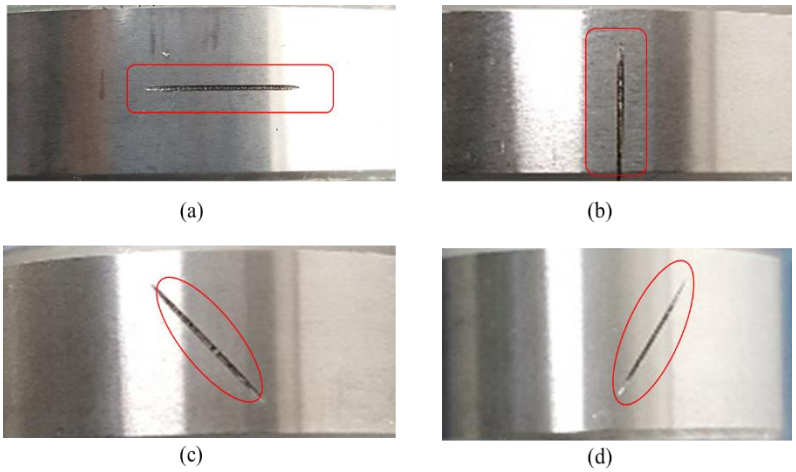

Figure 5.8 *Distinct orientation of 10 mm scratches (a) horizontal scratch (HS10) (b)vertical scratch (VS10) (c) left orientation scratch (LS10) and (d) right orientation scratch (RS10).*

5.3.1 Frequency Spectrum Analysis for Scratch Orientation

FFT analysis of the U-phase load current was performed for all bearing conditions (H, HS10, VS10, LS10, and RS10). Frequency spectra were plotted for H–VS10, LS10–RS10, and HS10–VS10 at a rotating speed of 1765 min^{-1}, and they are shown in Figures 5.9 to 5.11, respectively.

If it is possible to differentiate the healthy motor from the four faulty motors, it should also be possible to localize the differences among the faulty motors. As with the progression analysis, amplitude differences were observed at 30 and 90 Hz at all rotating speeds. This confirms the generation of the characteristic frequency, suggesting a relationship between scratching, load current, characteristic frequency, and shock wave pulse generation.

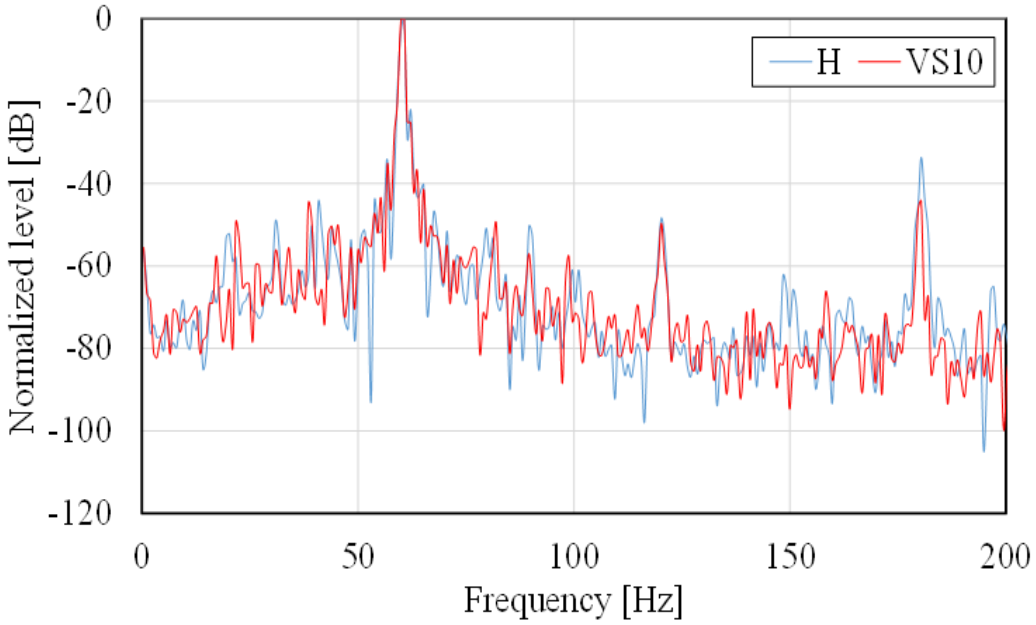

Figure 5.9 *Spectral analysis of H-VS10 at 1765 min^{-1}.*

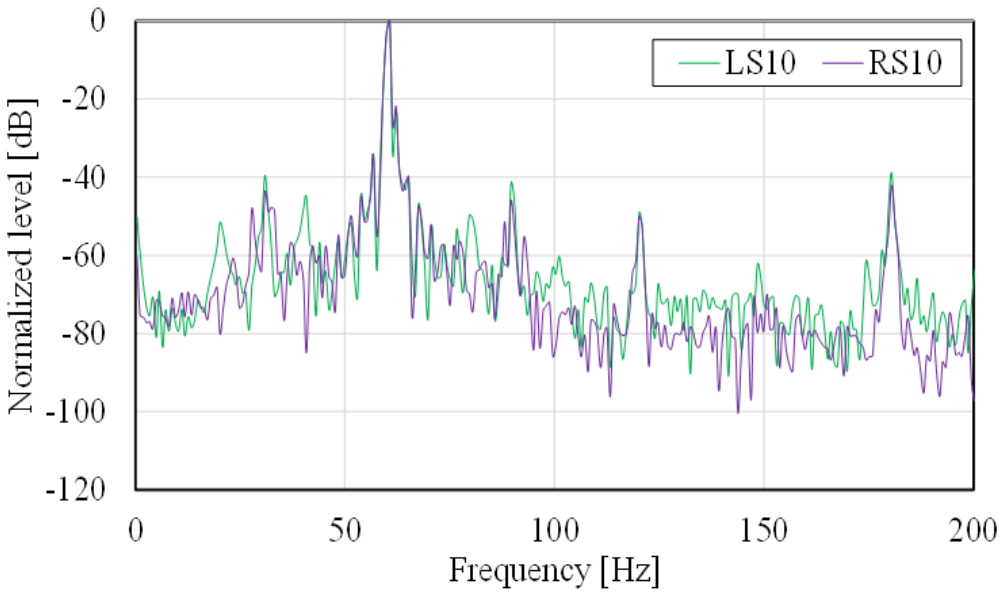

Figure 5.10 *Spectral analysis of LS10-RS10 at 1765 min^{-1}.*

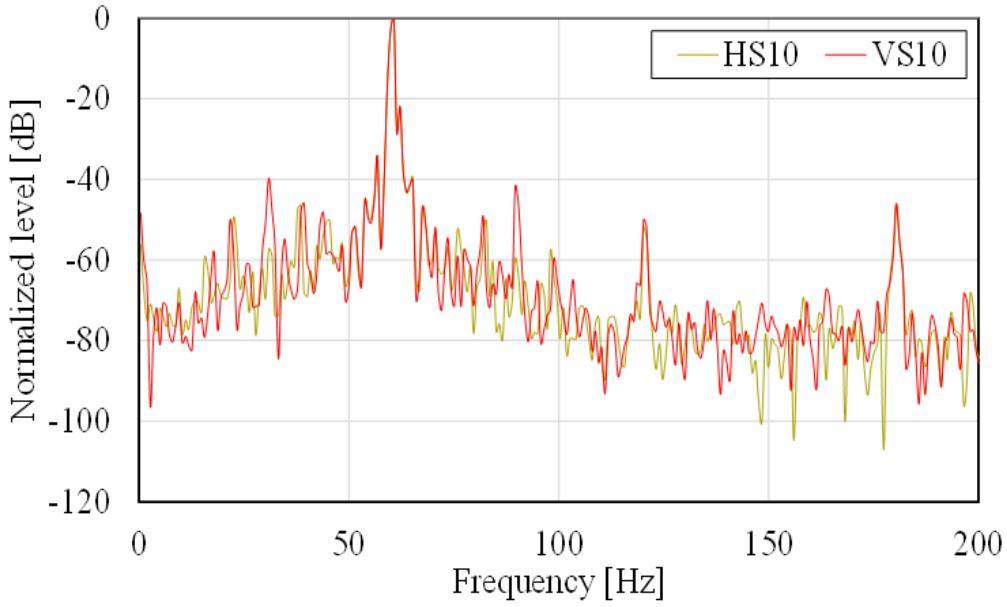

Figure 5.11 *Spectral analysis of HS10-VS10 at 1765 min^{-1}.*

5.3.2 Feature Distribution for Scratch Orientation

The feature distribution analysis is carried out using the amplitude of the characteristics frequency 30 and 90 Hz. The contribution of each feature is evaluated by considering the rotating speed of the induction motor.

In this section, the five bearing conditions (H, HS10, VS10, LS10, and RS10) are performed. Figures 5.12 and 5.13 show the feature distribution for all conditions at rotating speeds of 1770 and 1765 min^{-1}, respectively. These are classified according to their class of location and distinguishing behavior with respect to rotating speed. Apart from HS10, the classes are located adjacently. Even when overlaps occur, it is possible to differentiate the scratches. Scratches of the same size but with different orientations show a distinctive behavior. The orientation is shown to play a significant role, allowing the orientation to be identified. To fully understand the relationship between factors, a more detailed research will be necessary. However, the study confirmed that feature distribution plays a key role in identifying the orientation of scratches. Therefore, these feature distributions play a significant role.

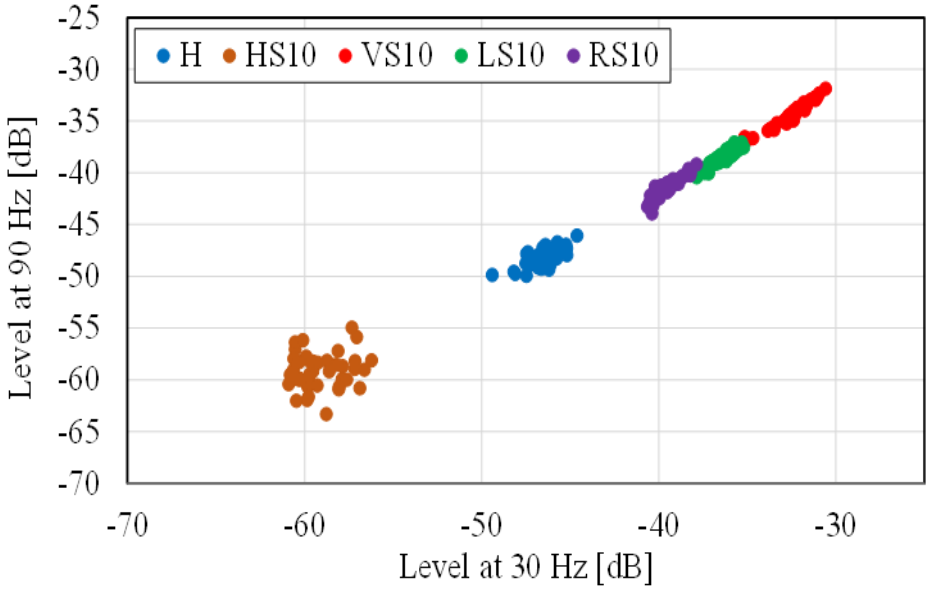

Figure 5.12 *Feature distribution of distinct orientation analysis at 1770 min^{-1}.*

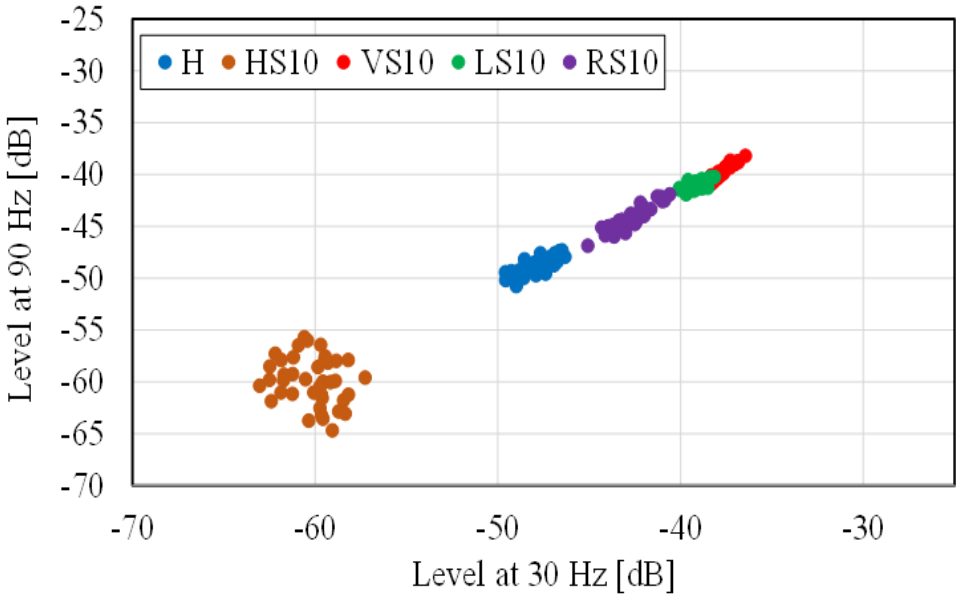

Figure 5.13 *Feature distribution of distinct orientation analysis at 1765 min^{-1}.*

Considering the industrial environment, the analysis is also performed without considering the rotating speed of the induction motor and the result is shown in Figure 5.14. The overlapping of features is observed between the different bearing conditions of the induction motor, yet they are distributed linearly and segregated to their own classes. The faulty motors VS10, LS10 and RS10 show large overlapping when comparing to the HS10.

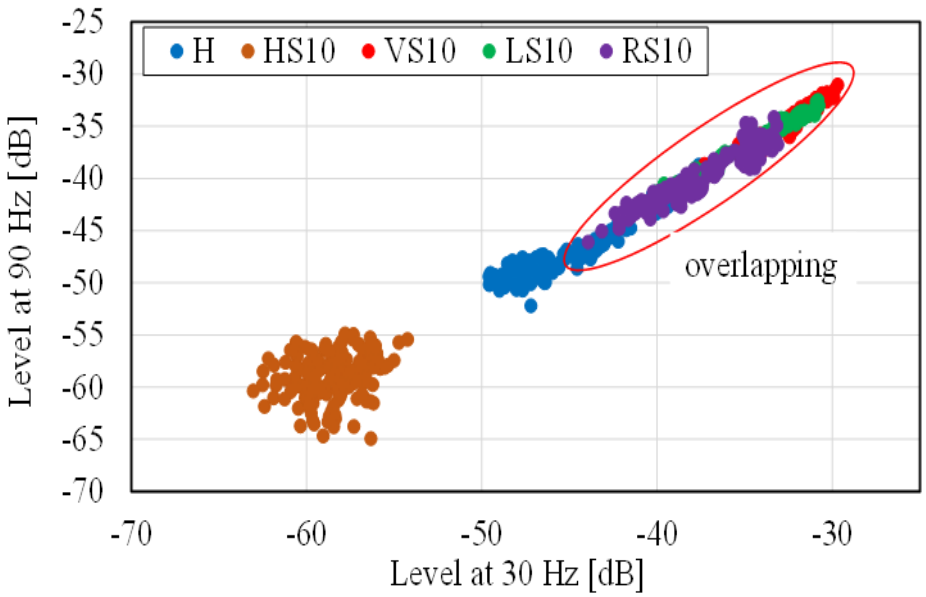

Figure 5.14 *Unified distinct orientation analysis.*

5.3.3 Diagnosis using SVM

The main work is to identify and differentiate the orientation of scratch. The results of both the diagnosis are explained one by one as follows.

5.3.3.1 Diagnosis without Considering Rotating Speed

Table 5.2 shows the diagnosis accuracy rate of H-HS10, H-VS10, H-LS10 and H-RS10 and H-HS10-VS10-LS10-RS10.

It is very clear that, the accuracy rate for H-HS10, H-VS10, H-LS10 and H-RS10 is very high. This fact clearly shows that healthy motor is completely diagnosed from horizontal scratch, vertical scratch, left orientation scratch and right orientation scratch of the faulty motor. On comparing with the obtained result, the accuracy level of H-HS10-VS10-LS10-RS10 is quite less. The main reason stands for the overlapping observed between the faulty motors. The average accuracy rate of all the five analysis is found to be 89.7 %. The obtained accuracy rate is practically acceptable.

Table 5.2 *Diagnosis result of scratch orientation*

Bearing Condition	Accuracy Rate (%)	
H-HS10	100	
H-VS10	96.25	
H-LS10	90	
H-RS10	87.5	
H-HS10-VS10-LS10-RS10	74.75	
	Average	89.7

5.3.3.2 Diagnosis Considering Rotating Speed

The analysis is done on the five types of bearing condition with respect to rotating speed. As an illustration, for the case of single rotating speed, 80 sets of load current data are obtained for the condition H-HS10, H-VS10, H-LS10 and H-RS10. Each datum consists of two components that are the amplitude of frequency components at 30 Hz and 90 Hz. Among the 80 sets of load current data, 60 data are used as training data and the remaining 20 data were used as verification data. Similarly, for the case of H-HS10-VS10-LS10-RS10, among the 200 sets of load current data, 150 data are used as training data and the remaining 50 data are used as diagnosis data. In this proposed system, the accuracy rate of the diagnosis is defined as like the previous case without considering the rotating speed of the induction motor.

The diagnosis rate is above 95 %. But for the case of H-HS-VS-LS-RS, the accuracy rate lies between the 93 % range. It is very clear from the diagnosis result that the high accuracy rate is obtained. Thus, the proposed system and the level of diagnosis rate are practically acceptable by considering the rotating speed of the induction motor. Therefore, the orientation of scratch analysis is much suited with the condition of rotating speed consideration.

5.4 Multiple Scratch Analysis

In this section, the multiple scratch analysis is carried out. For multiple scratch analysis, five types of bearing conditions were discussed: healthy bearing, bearing with one scratch and bearing with two scratches, bearing with three scratches and bearing with four scratches. The dimensions of each scratch are made common. It is of length 10 mm, width 0.5 mm and depth 0.5 mm. The samples used are shown in Figure 5.15.

The proposed method is evaluated by means of measuring the stator current. The current signals are collected from the healthy motor and four types of the faulty motors. The measurement was carried out under the load condition. The rotating speed was adjusted from 1780 min^{-1} to 1765 min^{-1}.

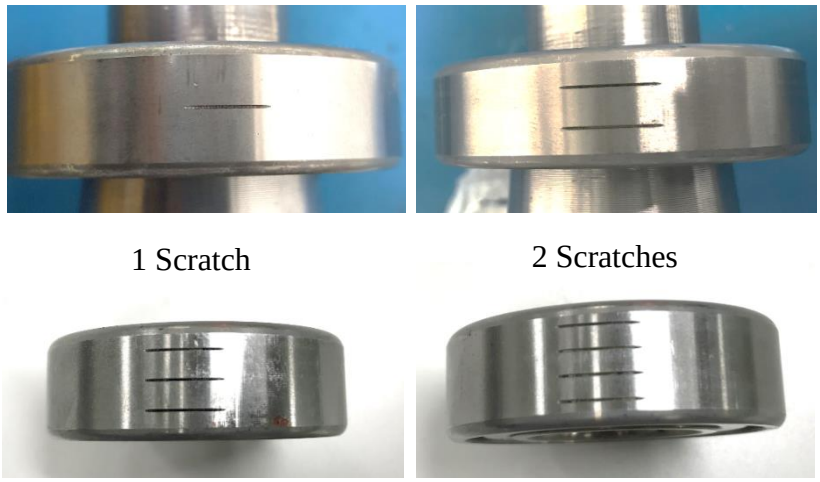

Figure 5.15 *Multiple Scratch Analysis.*

5.4.1 Frequency Spectrum Analysis for Multiple Scratch

The FFT analysis of the U phase load current was carried out for all the five types of bearing conditions. Figures 5.16 to 5.18 show the frequency spectrum analysis that is carried out at the rotating speed of 1780 min^{-1}. The vertical axis is normalized so that the maximum amplitude of the frequency spectrum to be 0 dB. From the figures at the frequency of 30 Hz and 90 Hz, the difference in the amplitude was observed. This change was observed in all four rotating speeds. As a result, these changes, it is possible to distinguish all the five types of bearing conditions.

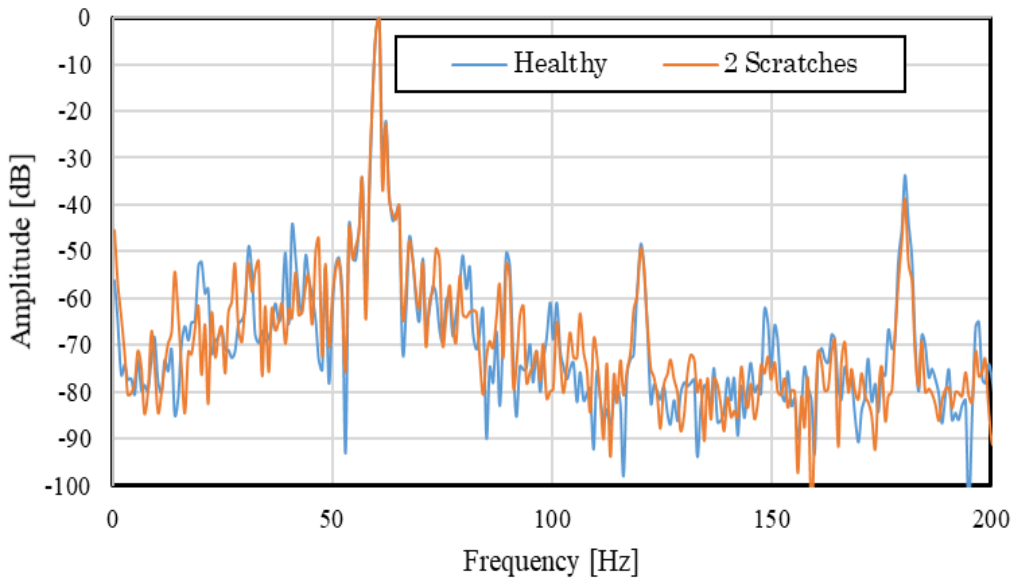

Figure 5.16 *Spectrum analysis for healthy and 2 scratches at 1780 min^{-1}.*

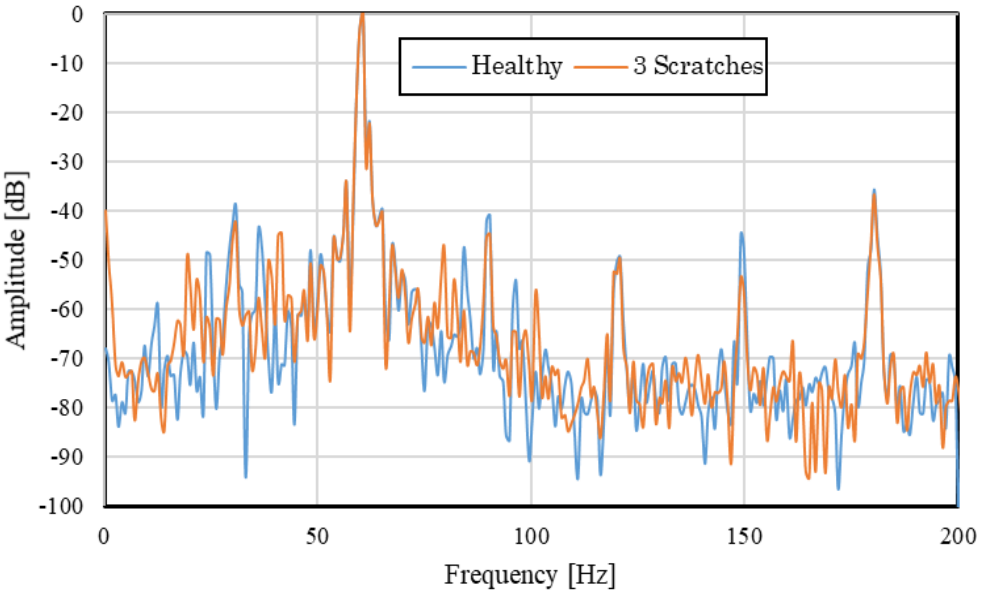

Figure 5.17 *Spectrum analysis for healthy and 3 scratches at 1780 min^{-1}.*

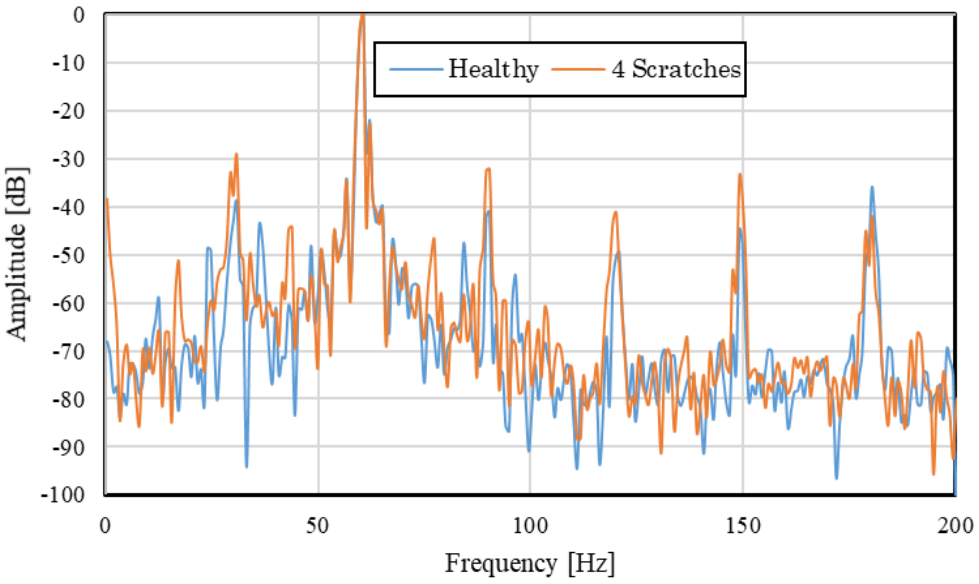

Figure 5.18 *Spectrum analysis for healthy and 4 scratches at 1780 min^{-1}.*

5.4.2 Feature Distribution for Multiple Scratch Analysis

Figures 5.19 to 5.22 show the feature extracted at the frequency of 30 Hz and 90 Hz for all the five types of bearing conditions at the rotating speed 1780, 1775, 1770 and 1765 min^{-1}, respectively. For easy understanding, healthy bearing, bearing with one scratch and bearing with two scratches, bearing with three scratches and bearing with four scratches are illustrated as H, 1S, 2S, 3S and 4S, respectively. These features will be generally obtained at the given condition and classified according to the rotating speeds. The location of the classes mainly depends on the bearing condition and the rotating speed of the induction motor.

It is very clear that, features of all the five types of bearing conditions are located to their own classes and overlapping are observed between them. Also, it is evident that, it is also possible to distinguish all the five types of bearing conditions.

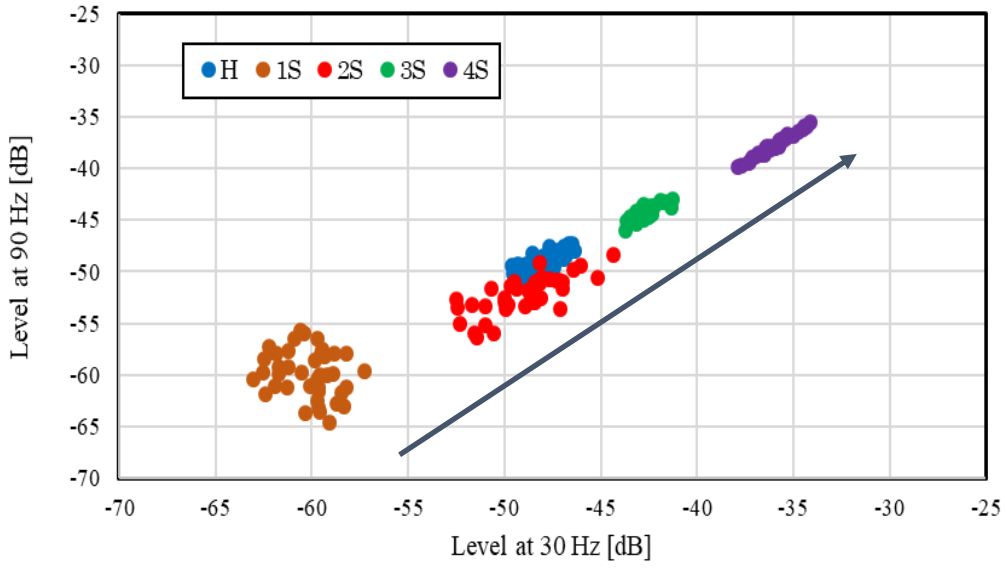

Figure 5.19 *Feature distribution for multiple scratch analysis at 1765 min^{-1}.*

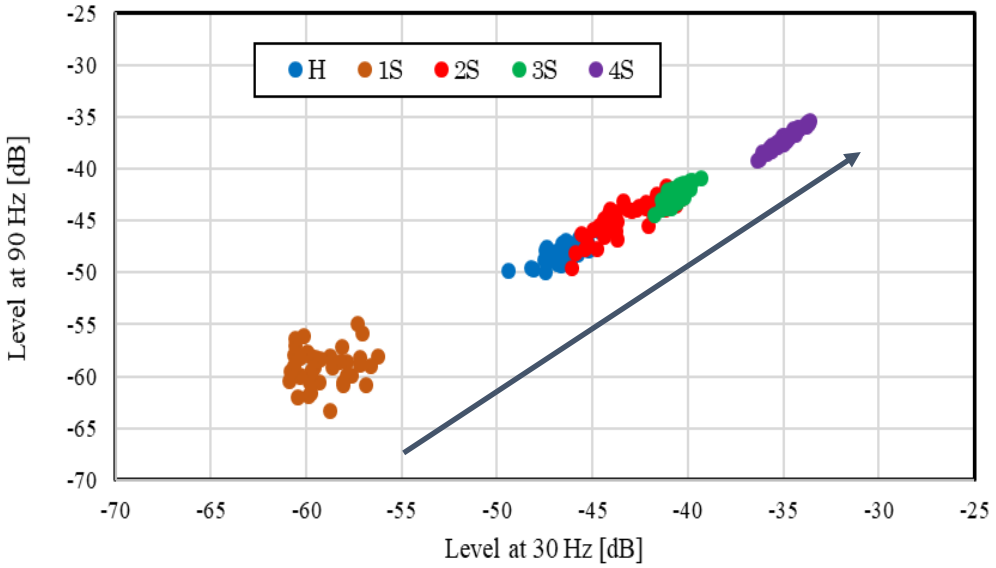

Figure 5.20 *Feature distribution for multiple scratch analysis at 1770 min^{-1}.*

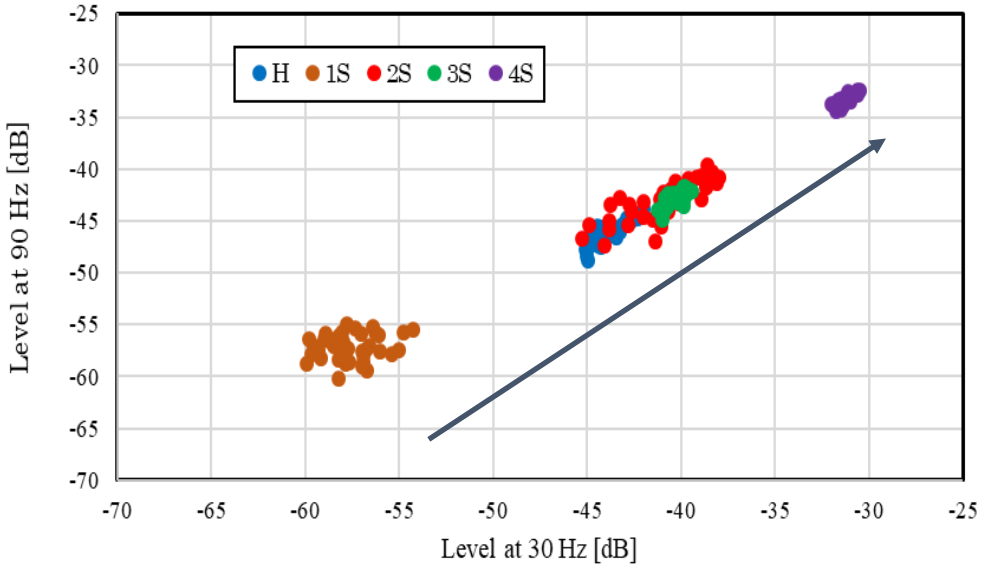

Figure 5.21 *Feature distribution for multiple scratch analysis at 1775 min^{-1}.*

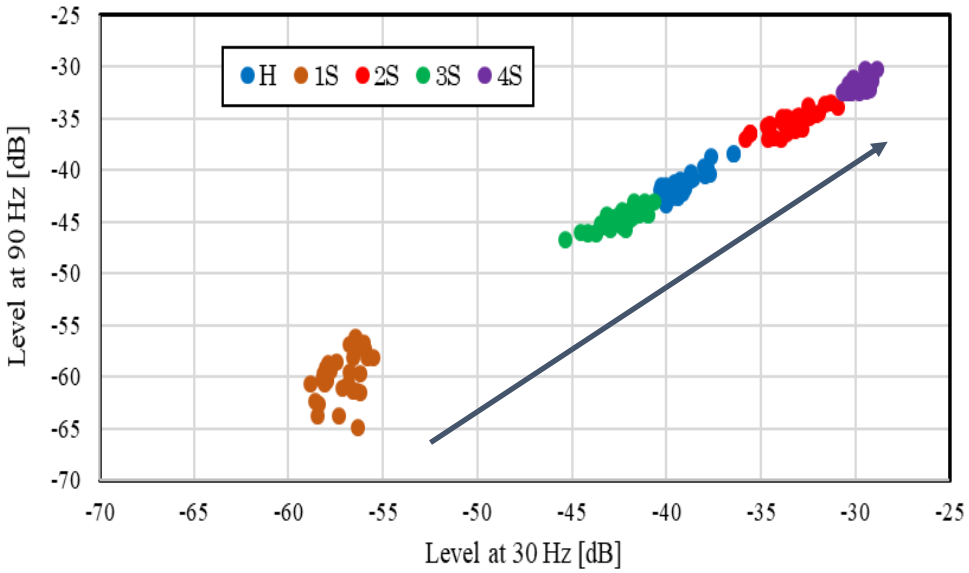

Figure 5.22 *Feature distribution for multiple scratch analysis at 1780 min^{-1}.*

A special observation has been made from the feature distribution of multiple scratch analysis. As the number of scratch induced on the outer raceway of the bearing gets increased, the amplitude starts to increase as shown in Figures 5.19 to 5.22. In the present study, the scratches are induced in a symmetrical manner and that may stand as the reason for the increase in the amplitude. The multiple hole analysis shows decrease in amplitude results because of the asymmetrical way of introducing the holes. Thus, it may be concluded that the symmetrical arrangement shows increase in amplitude result and asymmetrical shows decrease in amplitude result.

For the confirmation, multiple scratch analysis of symmetrical pattern is performed, and the results are shown in Figure 5.23. The analysis results are opposite to that of expected result. The amplitude is increasing instead to be decreased with number of scratch. From the result, it is concluded that the proposed mechanism of symmetrical and asymmetrical pattern needs more study and further investigation.

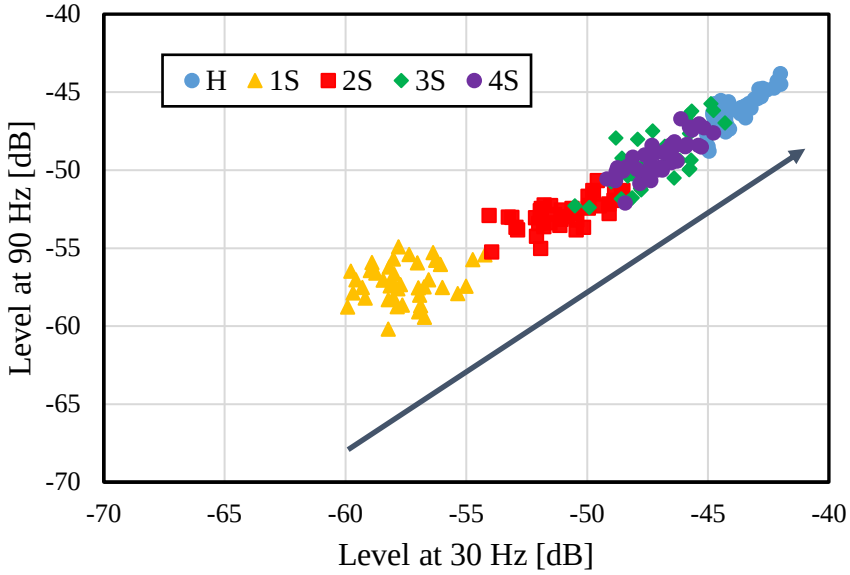

Figure 5.23 *Feature distribution for multiple scratch symmetrical analysis.*

5.4.3 Diagnosis using SVM

The main work is to carry out the diagnosis for the multiple scratch bearing fault. The diagnosis results are discussed below.

5.4.3.1 Diagnosis without Considering Rotating Speed

320 sets of load current data were obtained for the condition H-1S, H-2S, H-3S and H-4S. Each datum consists of two components that is the amplitude of frequency at 30 Hz and 90 Hz. Among the 320 sets of load current data, 240 data were used as training data and the remaining 80 data were used as verification data. But for the case of H-1S-2S-3S-4S, among the 800 sets of load current data, 600 data were used as training data and the remaining 200 data were used as diagnosis data. Each datum set consists of the amplitude of the frequency components.

Table 5.3 shows the diagnosis accuracy rate of H-1S, H-2S, H-3S, H-4S and H-1S-2S-3S-4S. It is very clear that, the accuracy rate for H-1S, H-3S and H-4S is very high. This fact clearly shows that healthy motor is completely diagnosed from one scratch, three scratches and four scratches of the faulty motor. On comparing with the obtained result, the accuracy level of H-2S is low. This result also affects the diagnosis result of H-1S-2S-3S-4S. The main reason is that, the data of faulty motor with two scratches on the bearing gets overlapped with the data of healthy motor bearing condition. The average accuracy rate of all the five analysis is found to be 88.55 %. The obtained accuracy rate is practically acceptable.

Table 5.3 *Diagnosis result of multiple fault analysis*

Bearing Condition	Accuracy Rate (%)	
H-1S	100	
H-2S	77.5	
H-3S	88.75	
H-4S	100	
H-1S-2S-3S-4S	76.5	
	Average	88.55

5.4.3.2 Diagnosis Considering Rotating Speed

As an illustration, for the case of single rotating speed, 80 sets of load current data were obtained for the condition H-1S, H-2S, H-3S and H-4S. Each datum consists of two components that are the amplitude of frequency components at 30 Hz and 90 Hz. Among the 80 sets of load current data, 60 data were used as training data and the remaining 20 data were used as verification data. Similarly, for the case of H-1S-2S-3S-4S, among the 200 sets of load current data, 150 data were used as training data and the remaining 50 data were used as diagnosis data.

Because of diagnosis, the accuracy rate for H-1S, H-3S and H-4S is above 95 %. But for the case of H-2S and H-1S-2S-3S-4S, the accuracy rate is around 85 %. It is very clear from the diagnosis result that the high accuracy rate is achieved. Thus, the proposed system and the

level of diagnosis rate are practically acceptable by considering the rotating speed of the induction motor. Therefore, the multiple scratch analysis is much suited with the condition of rotating speed consideration.

5.5 Summary

As like chapter 4, the diagnostic method using amplitude of the frequency 30 and 90 Hz components as the main feature was applied to diagnose the scratch on the outer raceway of the bearing. The analysis is performed in three ways; the progression, orientation and multiple fault scratch analysis. Further diagnosis was performed using an SVM. The problem of overlapping of features is overwhelmed with this proposed method. To extend the application, the diagnosis was performed without considering the rotating speed of the motor.

The result gives the satisfactory outcome for progression of scratch, orientation of scratches, and multiple scratch analysis. Thus, it is possible to identify all the types of bearing conditions involved in the present study. Thus, the proposed method is effective in diagnosing the types of bearing conditions. As a result, the proposed method has the following advantages:

- The healthy motor is completely diagnosed from the faulty motor.
- It is possible to distinguish the bearing fault of horizontal scratch 5 mm, horizontal scratch 10 mm and horizontal scratch 15 mm with respect to healthy motor, which suggests the possibility of tracking the progress of the scratch.
- Even the orientation of scratch plays a significant role and its distinguishing behavior is studied.
- This method has a property to identify the number of scratches interpolated on the bearings.

In a future work, application of this method can be intended to test the converter fed electrical machines and on the other types of industrial motor.

Chapter 6
Bearing Failure Diagnosis – Compound Fault Analysis

In this chapter, bearing failure analysis with the compound fault is done inducing both the hole and scratch simultaneously on the outer race-way of the bearing. The entire analysis is performed using Fast Fourier Transform (FFT) and the diagnosis by the Support Vector Machine (SVM).

6.1 Introduction

From the literature survey, most of the bearing failure analysis have been performed considering hole and scratch as the faulty factor but as the separate component. Only less research results are available regarding compound fault analysis. During the present research work, combination of hole and scratch i.e. compound fault bearing failure analysis is performed. Various combination of hole and scratch is performed, and the results are discussed.

6.2 Compound Faults

Both the hole and the scratch are induced simultaneously to the outer raceway of the bearing. Two different combination of hole and scratch are analyzed in the present study. The dimension of the hole is diameter of 2 mm and depth of 0.5 mm. Likewise the dimension of the scratch is length of 10 mm, width and depth of 0.5 mm. For clear understanding, the depth of the hole and scratch is made constant. The main objective behind the compound fault analysis, to investigate the effect of hole and scratch in detail and the change in the motor characteristics is also studied.

The two combinations of the compound fault analysis are illustrated as follows:

- Hole and Scratch – Induced 90 and 180 degrees to each other on the outer race-way

For reference, the following combination of fault analysis is carried out:

- Hole – Induced 90 and 180 degrees to each other on the outer race-way
- Scratch – Induced 90 and 180 degrees to each other on the outer race-way

The samples of the faults are shown in Figures 6.1 to 6.3. The following terminology is used, H, HS, H, S denote the healthy motor, hole and scratch, holes, scratches, respectively.

The code is followed by the degree of fault inducing. Thus, for example, hole and scratch fault induced 90 degrees to each other is denoted by HS90.

Figure 6.1 *Compound Fault Hole and Scratch.*

Figure 6.2 *Hole combination analysis.*

Figure 6.3 *Scratch combination analysis.*

6.3 Frequency Spectrum Analysis

FFT analysis of the U-phase load current was performed under all seven bearing conditions. 283 fundamental wavelengths were used in FFT. Figures 6.4 and 6.5 compare the frequency spectra plotted for H–HS90 and H–HS180, respectively, at a rotating speed of 1780 min^{-1}. The amplitude on the vertical axis is normalized to a 0 dB.

An amplitude difference can be observed between the healthy motor and all the six fault conditions (H–HS90, H–HS180, H-S90, H-S180, H-H90 and H–H180). Amplitude differences in the frequency components were clearly visible at frequencies of 30, 90, 150, and 180 Hz. At 30 and 90 Hz, amplitude changes were observed at all rotating speeds (1780, 1775, 1770, and 1765 min^{-1}). At 150 and 180 Hz, in contrast, no significant amplitude change was observed when the speed was varied, under any of the six bearing conditions. Frequencies of 30 and 90 Hz were therefore used in the study. Because of a change in the amplitude of the frequency component, it is possible to distinguish both the healthy motor and faulty motor, irrespective of the bearing condition. The characteristic frequencies of 30 and 90 Hz were used to plot the feature distribution for more detailed study.

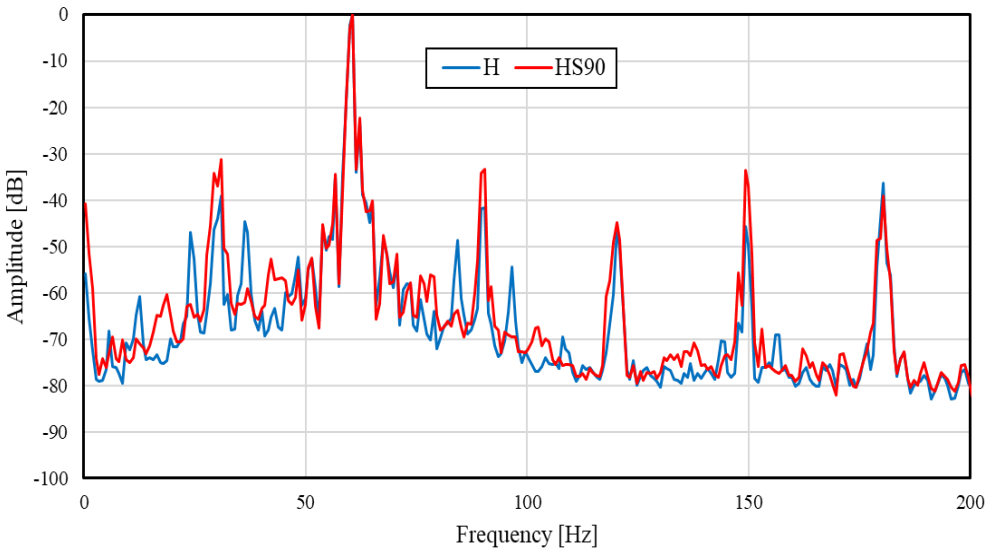

Figure 6.4 *Frequency spectrum analysis for H-HS90 at 1780 min^{-1}.*

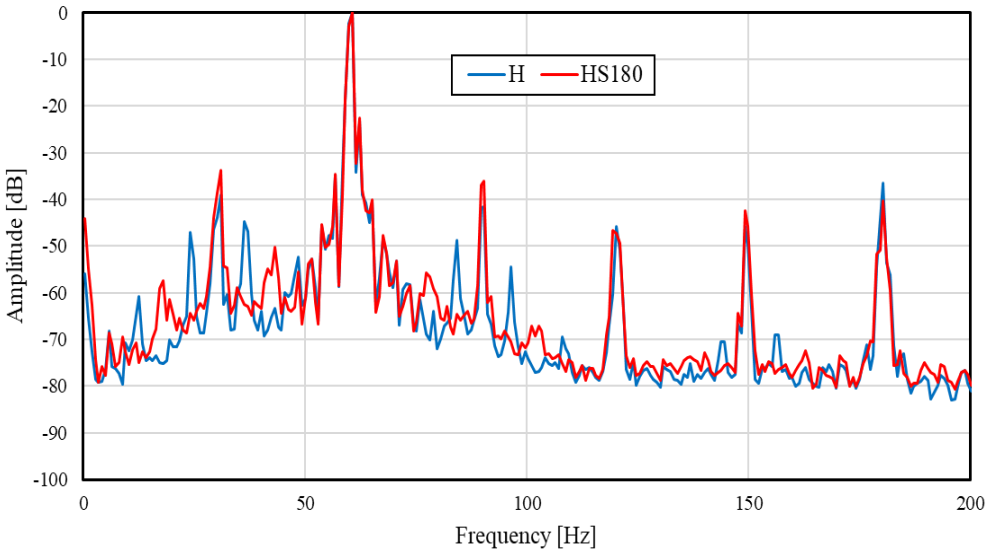

Figure 6.5 *Frequency spectrum analysis for H-H180 at 1780 min^{-1}.*

6.4 Feature Distribution

The feature distribution analysis is carried out using the amplitude of the characteristics frequency 30 and 90 Hz. A two-dimensional graph is plotted, taking amplitude of 30 Hz along the x-axis and 90 Hz along the y-axis, respectively. The contribution of each feature is evaluated by considering the rotating speed of the induction motor.

In both healthy and faulty motors, the contribution of each feature (30 and 90 Hz) is evaluated from the load condition. In this section, we discuss seven bearing conditions (H, HS90, HS180, H90, H180, S90, and S180). Figures 6.6 to 6.13 show the feature distribution at rotating speeds of 1780 and 1775 min^{-1} for all bearing conditions, respectively. Under each condition, the location of each class depends on the rotating speed of the motor and the bearing conditions. Even when overlaps occur, the bearing conditions fall into distinctive classes. Including HS90 and HS180 the remaining bearing conditions (H90, H180, S90, and S180) are significantly diffracted with respect to healthy motor and among the faulty motor. This proves that orientation of fault plays a significant role and the feature distribution analysis can identify the present state of the bearing. The proposed method could identify the bearing failure while the motor was running and demonstrates the significant role that feature distribution plays in the analysis of compound bearing failure analysis.

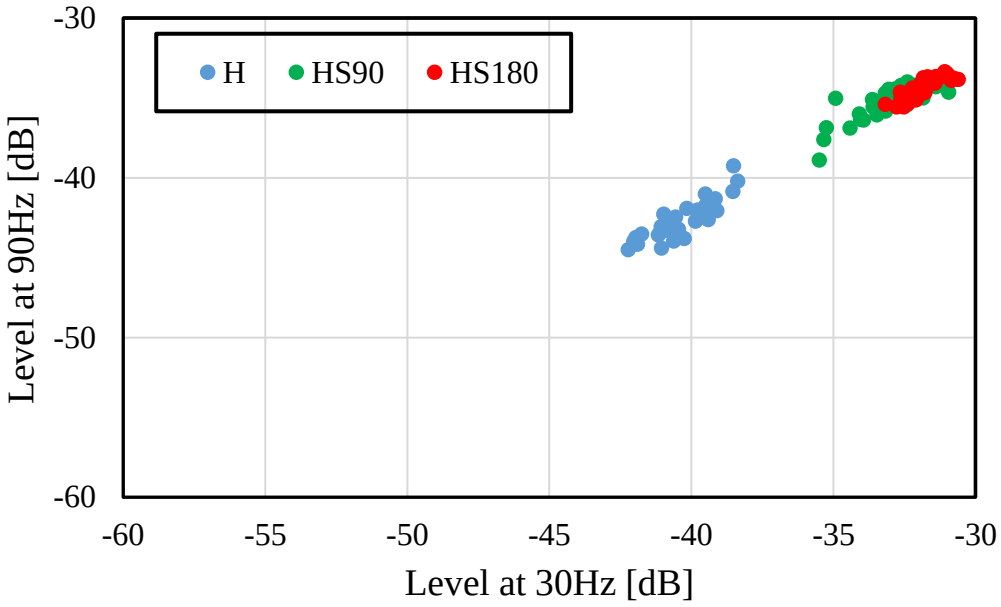

Figure 6.6 *Feature distribution for H-HS90-HS180 at 1780 min^{-1}.*

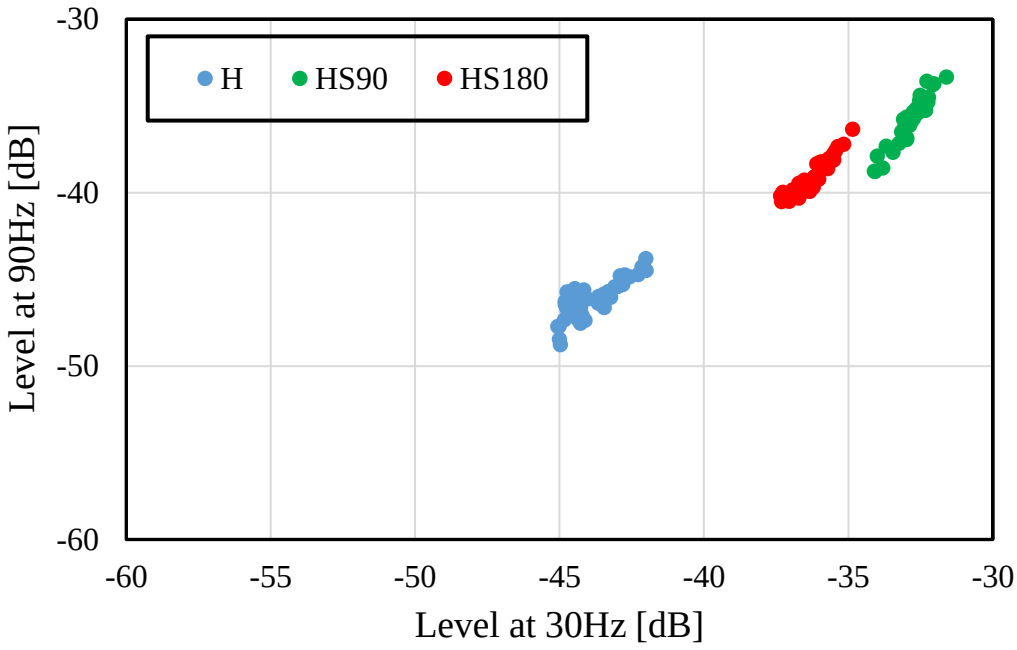

Figure 6.7 *Feature distribution for H-HS90-HS180 at 1775 min^{-1}.*

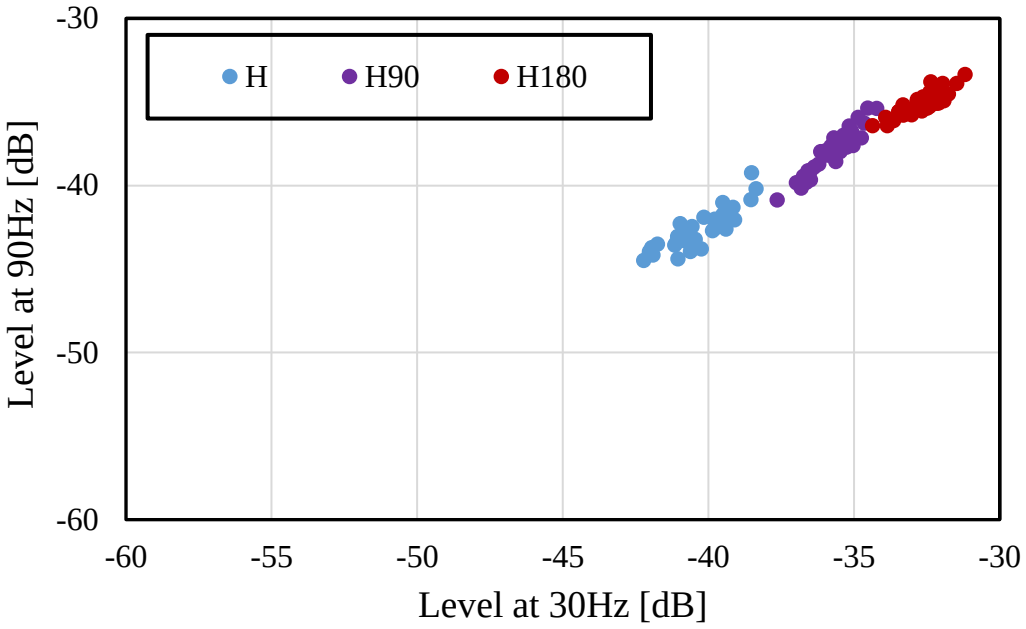

Figure 6.8 *Feature distribution for H-H90-H180 at 1780 min^{-1}.*

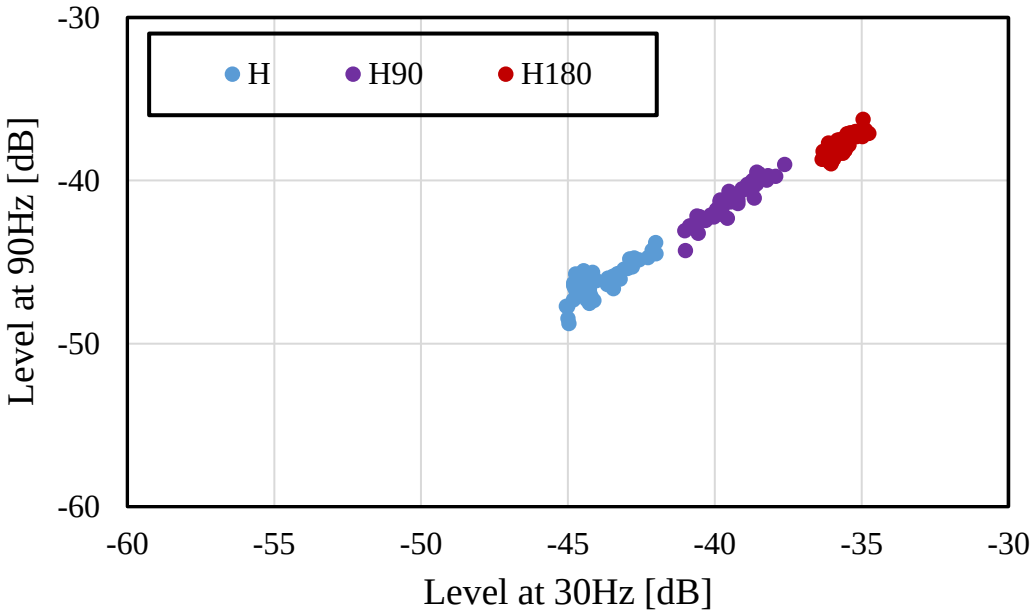

Figure 6.9 *Feature distribution for H-H90-H180 at 1775 min^{-1}.*

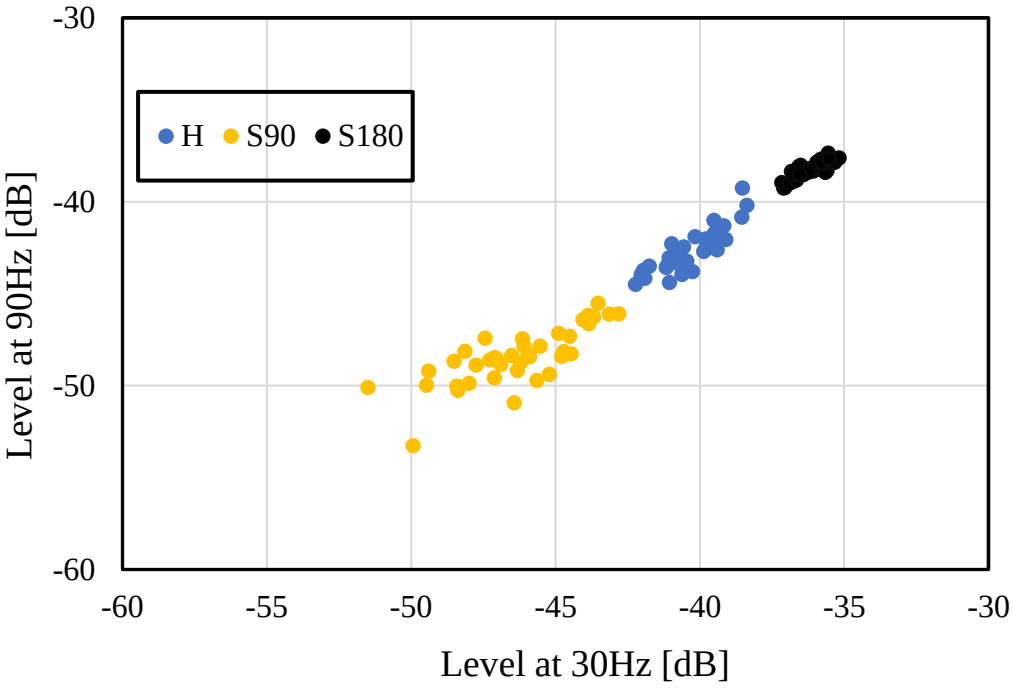

Figure 6.10 *Feature distribution for H-S90-S180 at 1780 min^{-1}.*

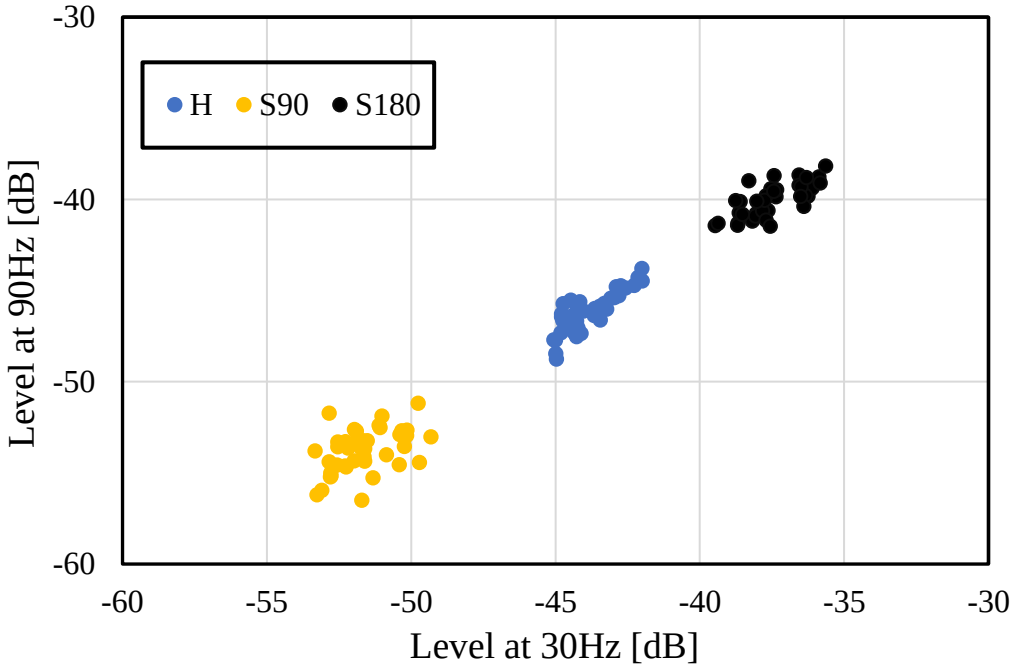

Figure 6.11 *Feature distribution for H-S90-S180 at 1775 min^{-1}.*

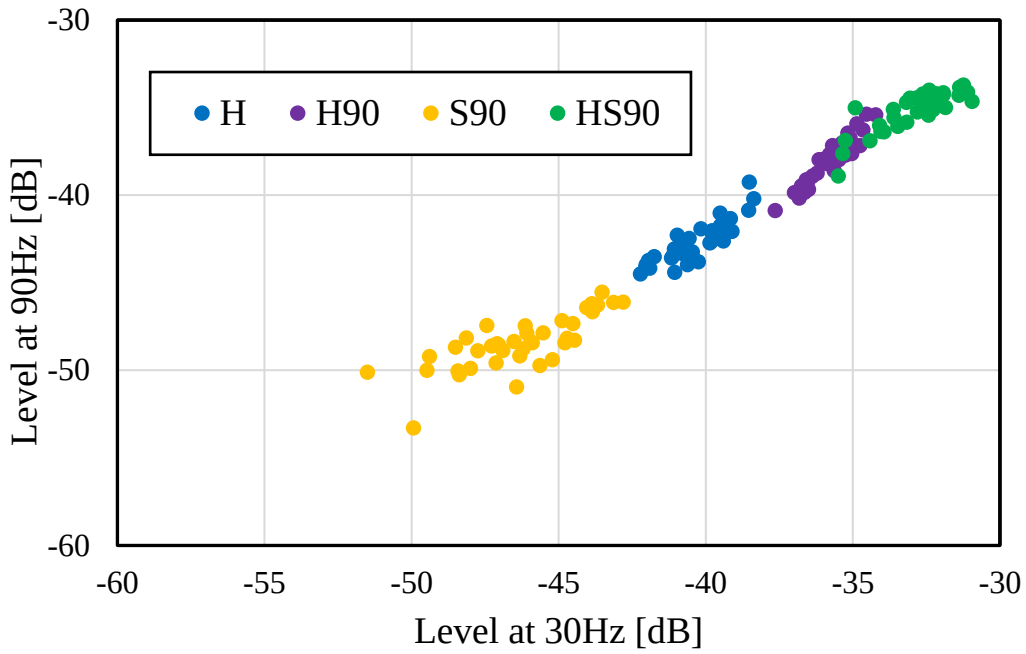

Figure 6.12 *Feature distribution for 90 degrees at 1780 min^{-1}.*

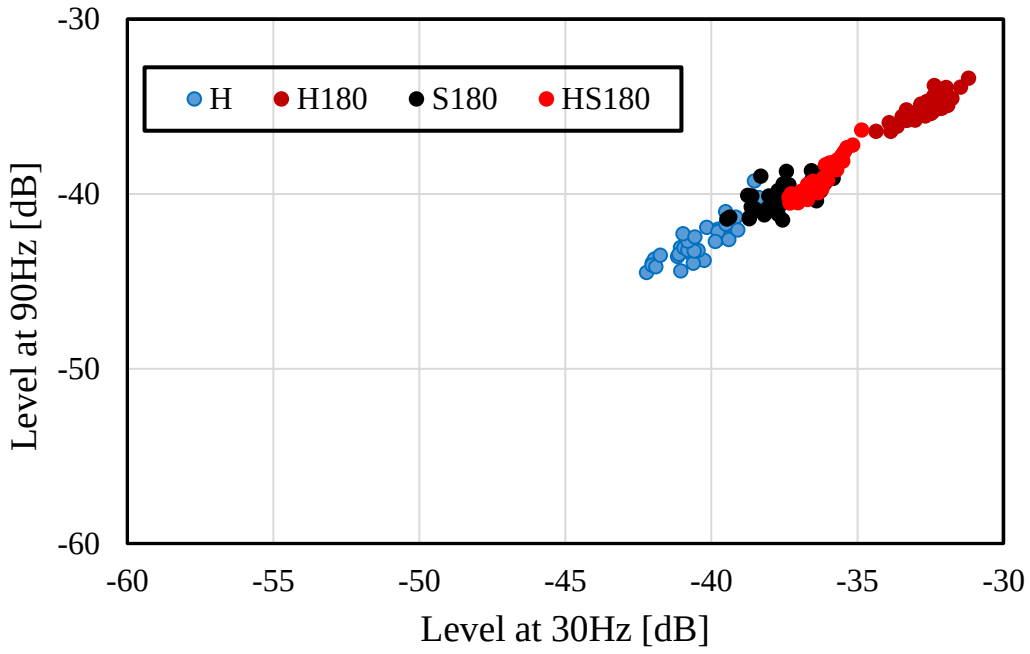

Figure 6.13 *Feature distribution for 180 degrees at 1780 min^{-1}.*

In industries, the speed of the induction motor is not constant and said to be varied between the certain range. Considering the industrial environment, the analysis is also performed without considering the rotating speed of the induction motor and the result is shown in Figures 6.14 to 6.16. The overlapping of features is observed between the different bearing conditions of the induction motor, and differentiation is not possible using feature distribution analysis. Thus, SVM is employed in carrying out the diagnosis for the compound bearing fault analysis.

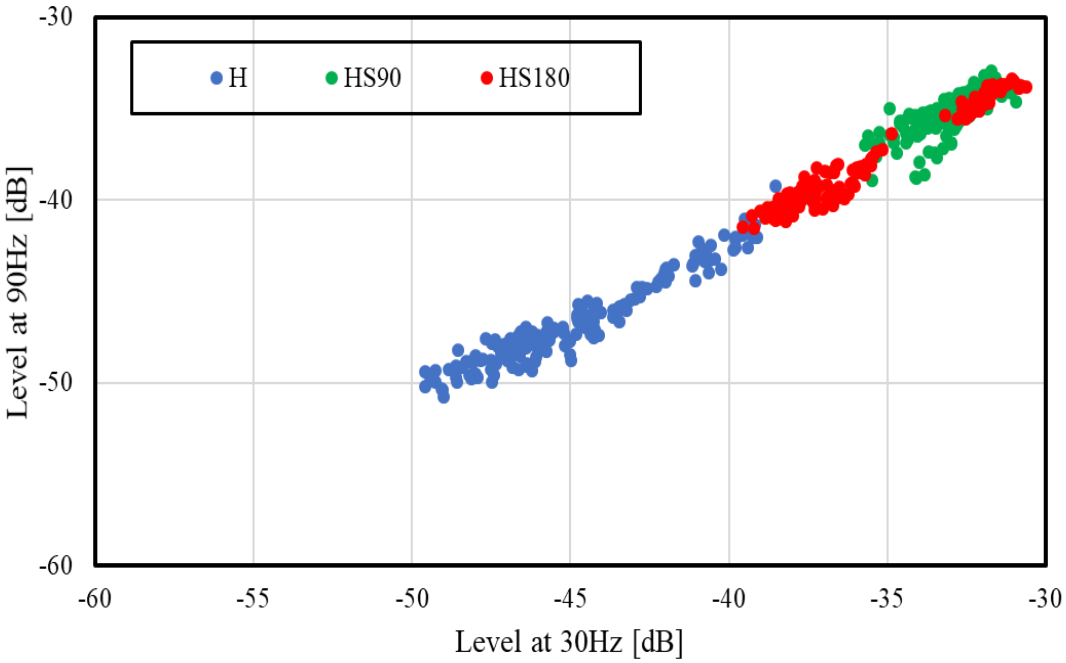

Figure 6.14 *Industrial analysis of hole and scratch.*

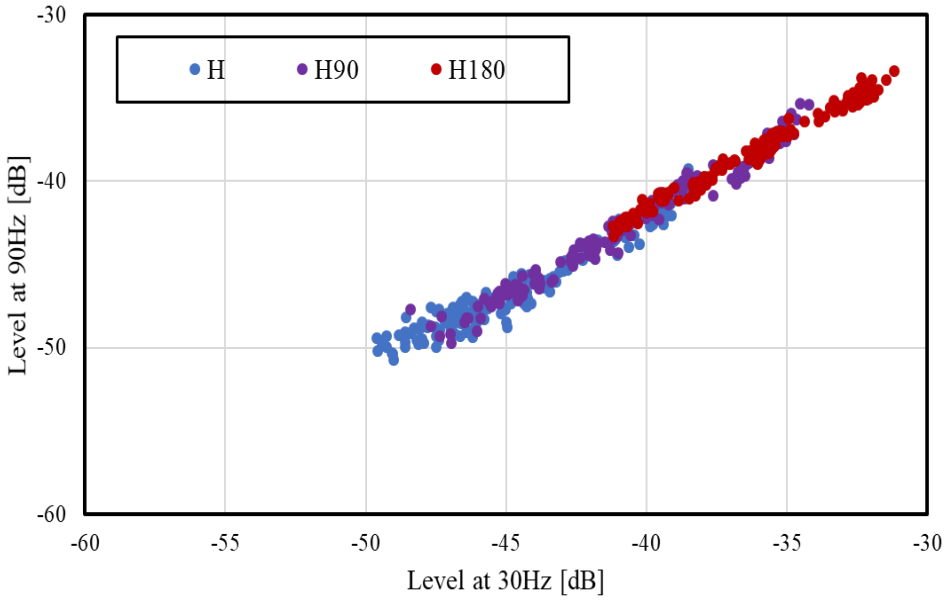

Figure 6.15 *Industrial analysis of hole.*

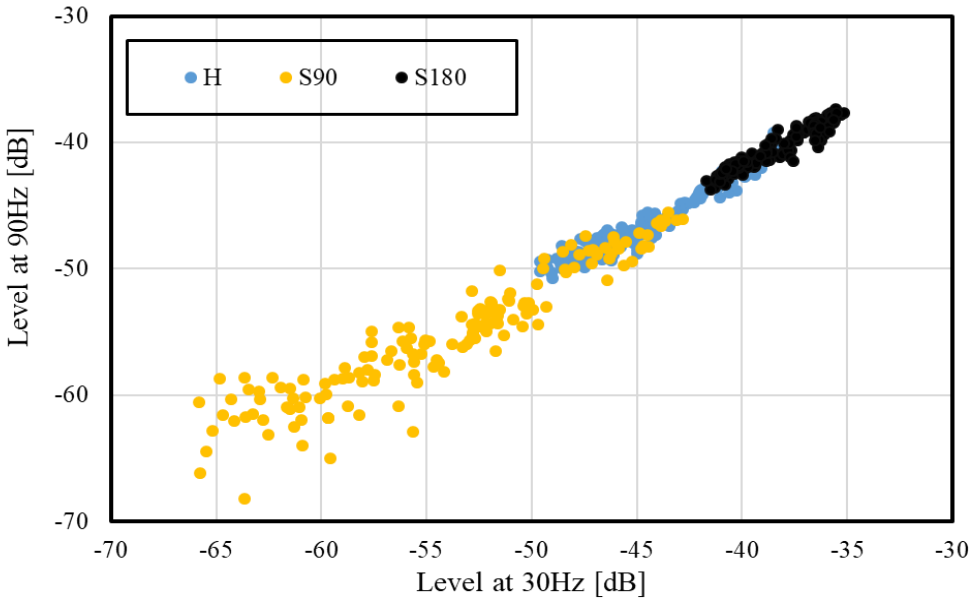

Figure 6.16 *Industrial analysis of scratch.*

6.5 Diagnosis using SVM

The main work is to identify and differentiate the faulty motor with the healthy motor. The entire diagnosis analysis is performed in both the conditions of the rotating speed of induction motor. That is, considering and without considering the rotating speed of the induction motor. The results of both the diagnosis are explained one by one as follows.

6.5.1 Diagnosis without Considering Rotating Speed

The diagnosis based on SVM was performed to the compound bearing failure analysis without considering the rotating speed of the induction motor. For conditions H–HS90, H–HS180, H-S90, H-S180, H-H90 and H–H180, 480 sets of load current data were used. Each dataset had both 30 and 90 Hz amplitude frequency components. From the 480 sets, 360 were used as training data, and the remaining 120 were used as evaluation data. Four rotating speeds (1780, 1775, 1770, and 1765 min^{-1}) were considered. In this proposed system, the accuracy rate of the diagnosis is defined as

$$\text{Accuracy rate (\%)} = \frac{number\ of\ data\ diagnosed\ accurately}{total\ number\ of\ data\ for\ diagnosis} \times 100 \qquad (6.1)$$

Table 6.1 *Diagnosis result*

Bearing Condition	Accuracy Rate (%)	
H-HS90	97.5	
H-HS180	100	
H-S90	90.35	
H-S180	88.75	
H-H90	82.5	
H-H180	87.5	
	Average	91.12

Table 6.1 shows the accuracy rate and found to be practically acceptable. The S90, HS90 and HS180 shows the maximum accuracy rate. While H90, H180 and S180 show accuracy rate in the range 80-90 %. However, it is sufficiently enough and suitable for practical applications. The average accuracy rate is 91.12 %. The proposed method is effective in overcoming the problem of overlapping. This is a significant advantage of the proposed method, making it suitable for speed varying application and in industrial environments.

6.5.2 Diagnosis Considering Rotating Speed

As an illustration, for the case of single rotating speed, 120 sets of load current data were obtained for the condition H–HS90, H–HS180, H-S90, H-S180, H-H90 and H–H180. Each datum consists of two components that are the amplitude of frequency components at 30 Hz and 90 Hz. Among the 120 sets of load current data, 90 data were used as training data and the remaining 30 data were used as verification data. In this proposed system, the accuracy rate of the diagnosis is defined as like the previous case without considering the rotating speed of the induction motor.

The diagnosis rate for all the bearing condition is found to be 100 %. Thus, the proposed system and the level of diagnosis rate are practically acceptable by considering the rotating speed of the induction motor and suitable for detecting the compound fault.

6.6 Summary

The diagnostic method proposed in the chapter 4 is applied to the compound fault analysis and the examination is performed using FFT. Further diagnosis was performed using an SVM. To mimic the use of motors in industrial environments, the diagnosis was performed without considering the rotating speed of the motor.

The hole and scratch fault combination shows more defects. Higher amplitude range is observed in the case of hole and scratch, and accordingly less overlapping is observed. The distinct fault combination stands as the reason, while identical fault combination (hole, scratch) shows less amplitude and at the same time overlapping is also observed. Apart from

the fault localization, the variable type plays a key role in estimating the defect caused. The distinct type shows higher defects when compared to identical type fault.

As a result, the proposed method has the following advantages:

- The method can distinguish the healthy and faulty motor.
- The conventional method (proposed in chapter 4) has an ability identify the compound bearing fault and the identification of the present state of bearing is made possible.

Chapter 7
Common Diagnosis Method of Electrical and Mechanical Fault

7.1 Common Diagnosis Method

Till the previous chapters, the diagnosis method is different for three-induction motor failure (short-circuit insulation failure, broken rotor bar failure and bearing failure). For example, distortion ratio of load curents in case of short-circuit insulation failure and SOM in case of broken rotor bar and SVM in case of bearing failure. However, spectral analysis is common before carrying out the clustering and the machine learning diagnosis process.

In respect of different diagnosis method, it is always preferable to have a common diagnosis method to all kind of faults occurring in the induction motor. Short-circuit insulation failure, broken rotor bar and bearing failure has been selected and the common fault diagnosis method proposed in chapter 4 is applied. The FFT analysis of the load current is performed and the diagnosis by SVM using the amplitude of 30 and 90 Hz as features. The entire analysis is performed without considering the rotating speed of the induction motor.

7.1.1 Faulty Factor

The experimental setup and the motor are same as explained in the chapter 4. In case of bearing failure, a hole or a scratch is made on the outer race-way of the bearing as shown in Figures 7.1 and 7.2, respectively. The dimension of the hole is diameter of 0.5 mm and depth of 0.5 mm. Likewise, the dimension of the scratch; length of 5 mm, width and depth of 0.5 mm. The depth is made constant for both the hole and scratch. Likewise, for broken rotor bar failure, a single hole is drilled on the rotor bar and for short-circuit insulation failure, one-turn fault is created in the stator winding as shown in Figures 7.3 and 7.4, respectively. The rotating speed was adjusted from 1780 min^{-1} to 1765 min^{-1}.

Figure 7.1 *Bearing with a hole 0.5 mm.*

Figure 7.2 *Bearing with a scratch 5 mm.*

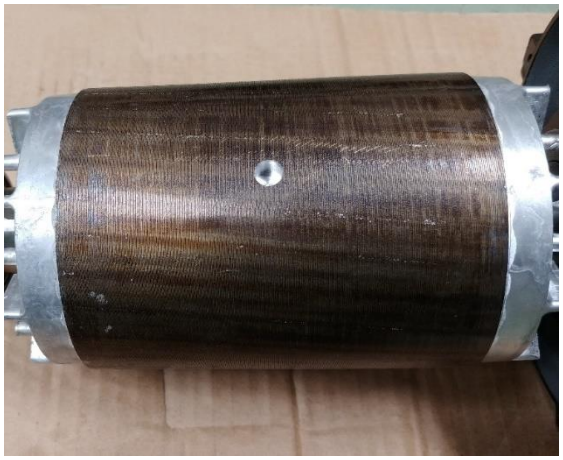

Figure 7.3 *Broken rotor bar failure.*

Figure 7.4 *Short-circuit insulation failure.*

Two motors of same rating are selected, and the faults are induced artificially. The broken rotor bar fault and the bearing failure experiment is performed to one motor and short-circuit insulation failure experiment to the other motor, respectively. For the reliability, the experiment is repeated for three times. The proposed method is evaluated by means of measuring the stator current. The current signals are collected from the healthy motor and from the faulty motors. The measurement was carried out under the load condition. Both the frequency spectrum analysis and the feature extraction are based on the value of the stator current under four types of bearing conditions. The diagnosis procedure is shown in Figure 7.5.

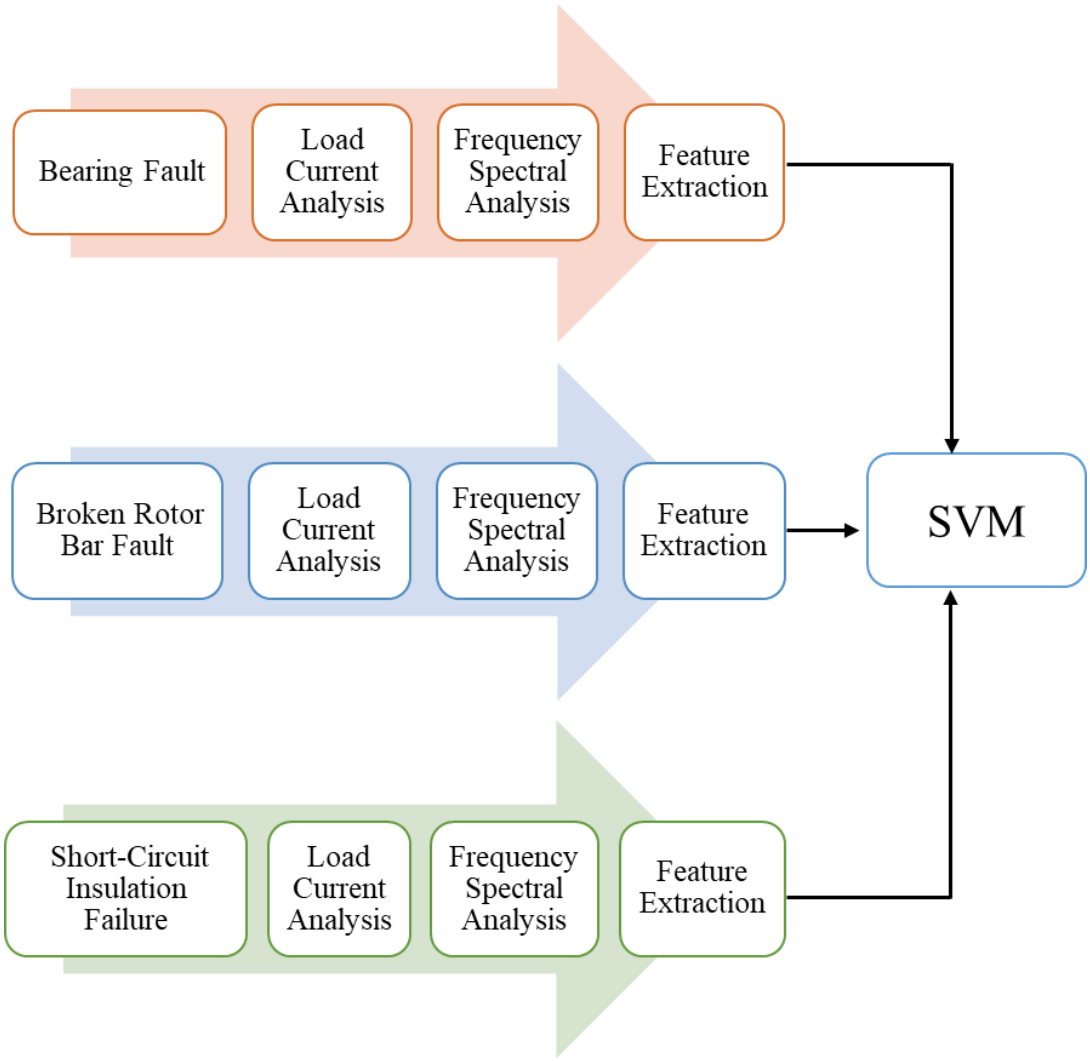

Figure 7.5 *Common diagnosis procedure.*

7.1.2 Frequency Spectrum Analysis

Initially, the FFT analysis is performed to the healthy motors 1 and 2. From the obtained frequency spectrum, feature distribution is plotted to check the data range of both the healthy motors. The amplitude of both the healthy motors lies within the same range. After the confirmation, the bearing failure, broken rotor bar fault and the short-circuit insulation fault are induced to the healthy motors. Figures 7.6 to 7.10 compare the frequency spectra plotted for healthy-hole, healthy-scratch and healthy-hole-scratch, and healthy-broken rotor bar,

healthy- short-circuit insulation failure, respectively, at a rotating speed of 1780 min^{-1}. The amplitude on the vertical axis is normalized to a maximum of 0 dB.

Initially, bearing failure analysis is discussed. A large amplitude difference can be observed between the healthy motor and all the two fault conditions (hole and scratch). When the faults on the bearings are compared (hole and scratch), the amplitude difference observed is sufficient to differentiate the cases. At 30 and 90 Hz, amplitude changes were observed at all rotating speeds (1780, 1775, 1770, and 1765 min^{-1}). Like the bearing failure, broken rotor bar and short-circuit insulation failure also show similar changes at the frequencies 30 and 90 Hz. Thus, for establishing the common diagnosis method, the frequencies 30 and 90 Hz have been selected and proceeded with the feature distribution.

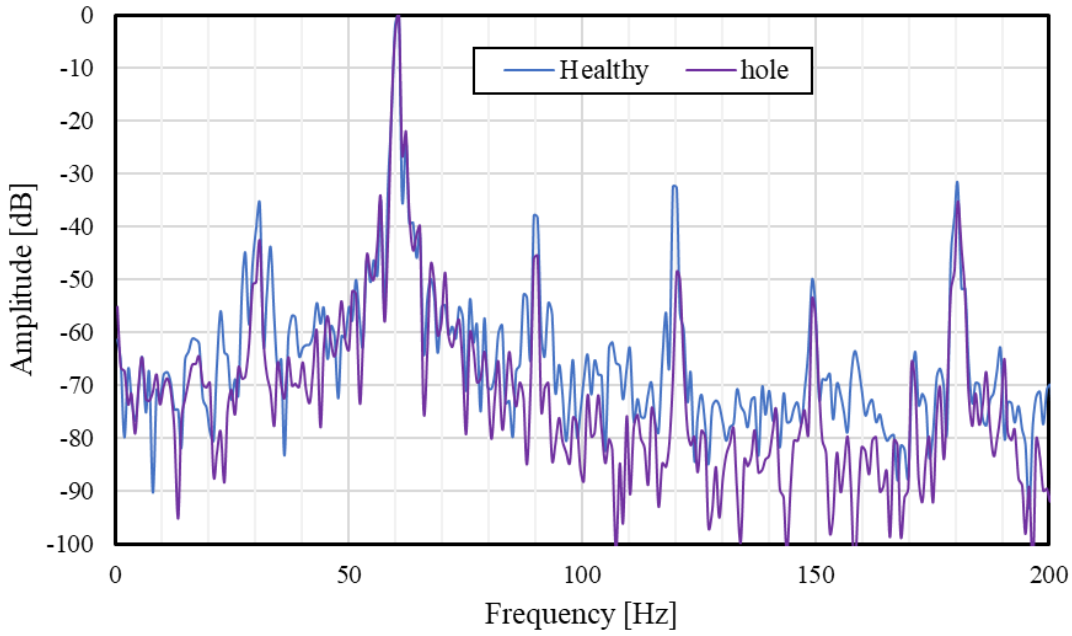

Figure 7.6 *Spectral analysis of healthy and hole at 1780 min^{-1}.*

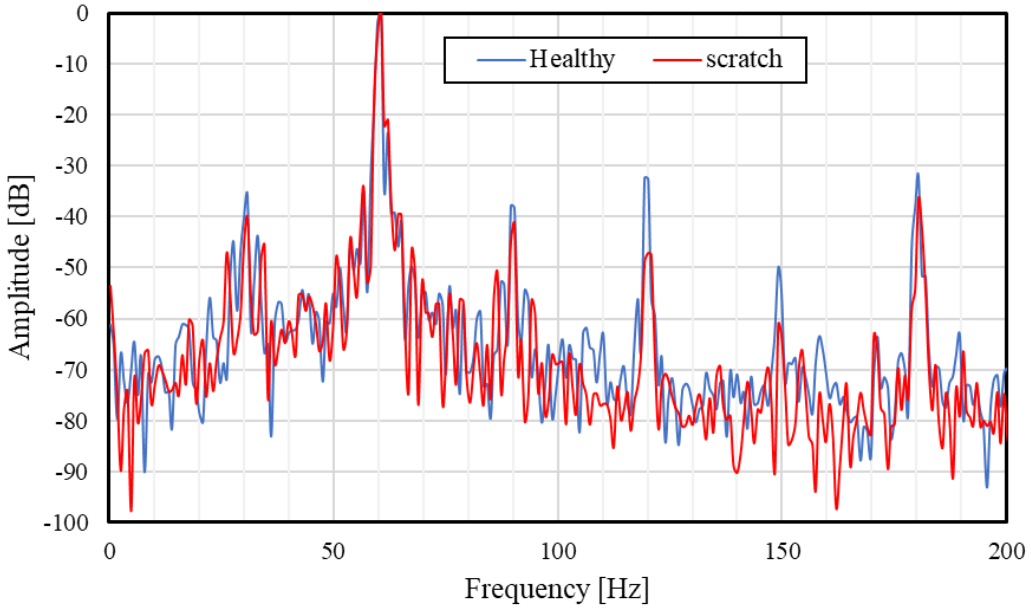

Figure 7.7 *Spectral analysis of healthy and scratch at 1780 min^{-1}.*

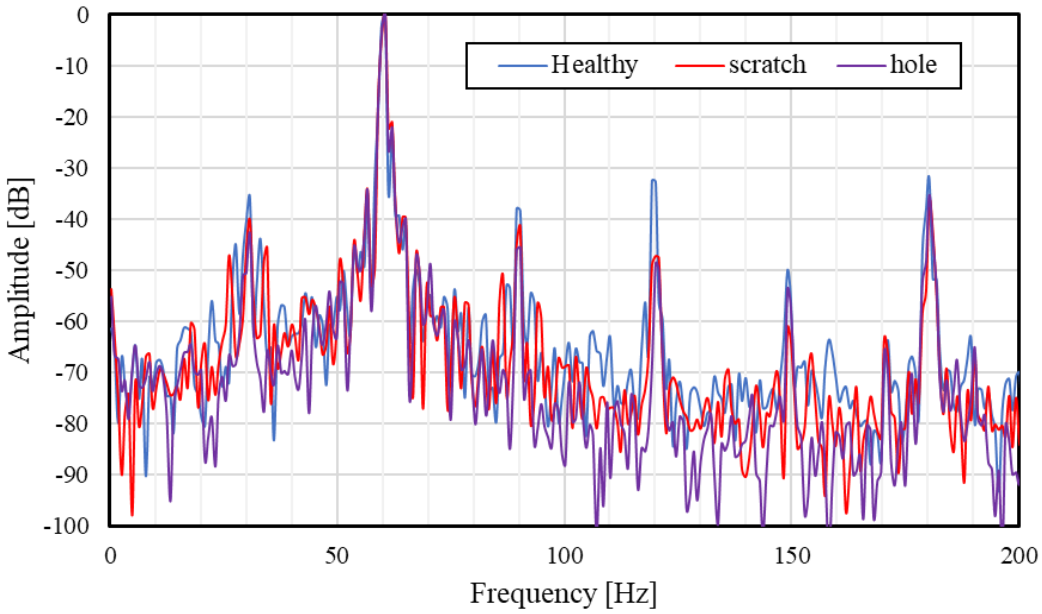

Figure 7.8 *Spectral analysis of healthy, hole and scratch at 1780 min^{-1}.*

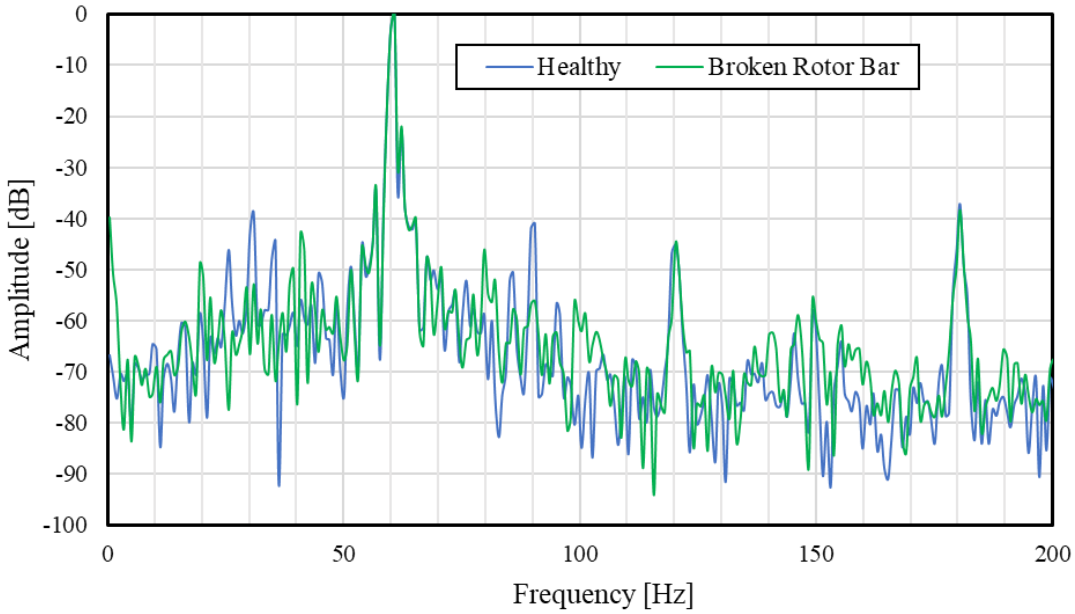

Figure 7.9 *Spectral analysis of healthy and broken roto bar at 1780 min^{-1}.*

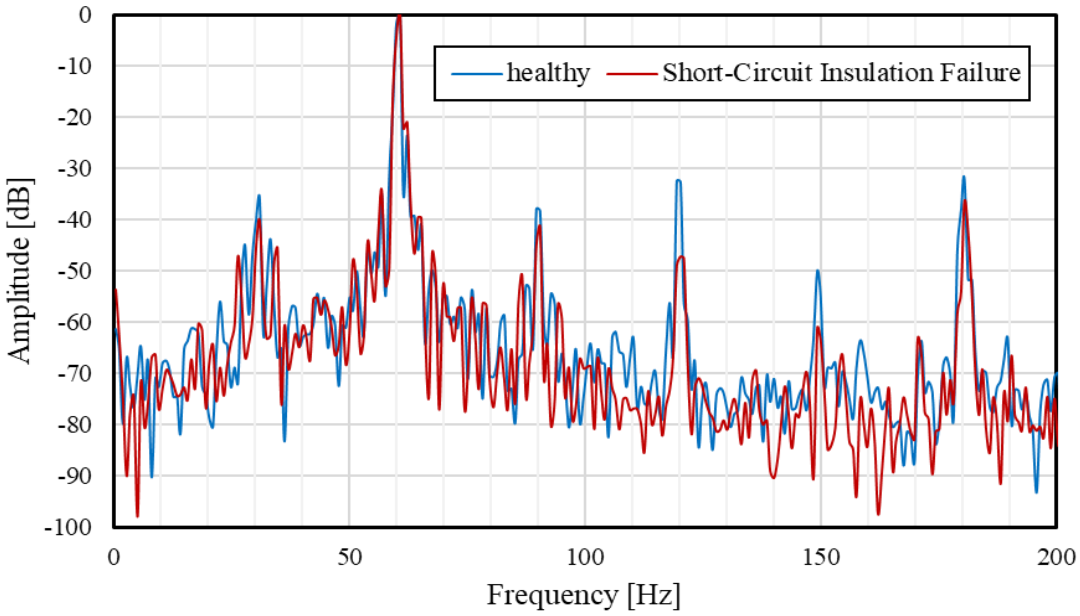

Figure 7.10 *Spectral analysis of healthy and short-circuit insulation failure at 1780 min^{-1}.*

7.1.3 Feature Distribution

The feature distribution analysis is carried out using the amplitude of the characteristics frequency 30 and 90 Hz. Under each condition, the location of the class depends on the rotating speed of the motor and the bearing conditions. Figures 7.11 to 7.14 show the feature distribution at rotating speeds of 1780 to 1765 min^{-1} for healthy (1 and 2), bearing failure (hole and scratch), and broken rotor bar failure. While taking the individual rotating speed of the induction motor into consideration, the classes of the faulty motor (hole, scratch, and broken rotor bar) are located far away from the healthy motor. No overlapping of features has been occurred, the bearing conditions fell into distinctive classes, allowing them to be differentiated. It is made possible to predict the current state of the motor and the proposed method could identify the failure while the motor is running. This allows a fault to be identified and demonstrates the significant role that feature distribution plays in the analysis the motor failure.

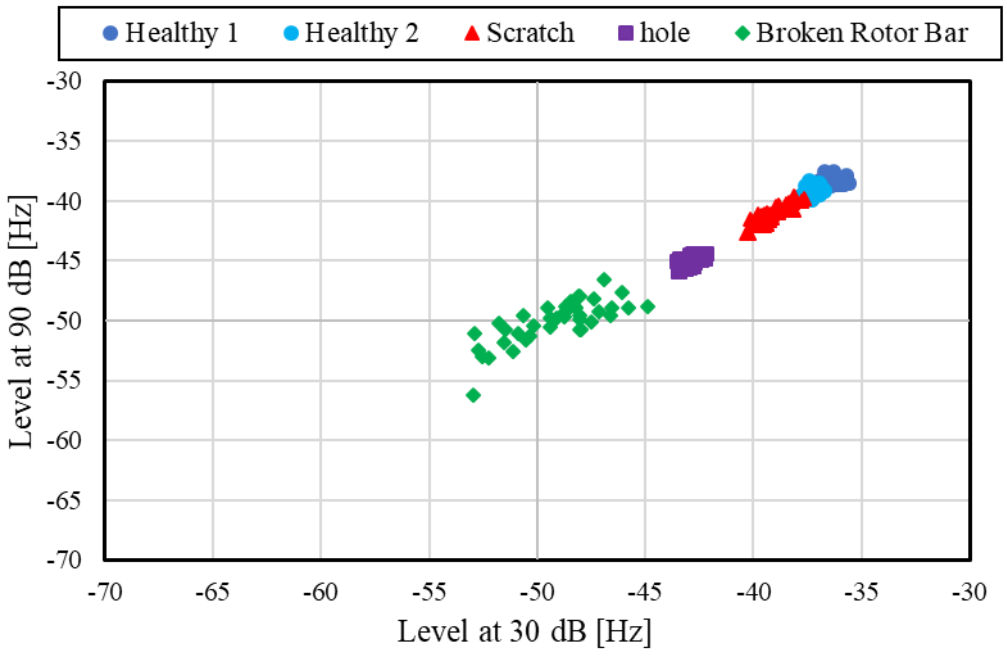

Figure 7.11 *Feature distribution analysis at 1780 min^{-1}.*

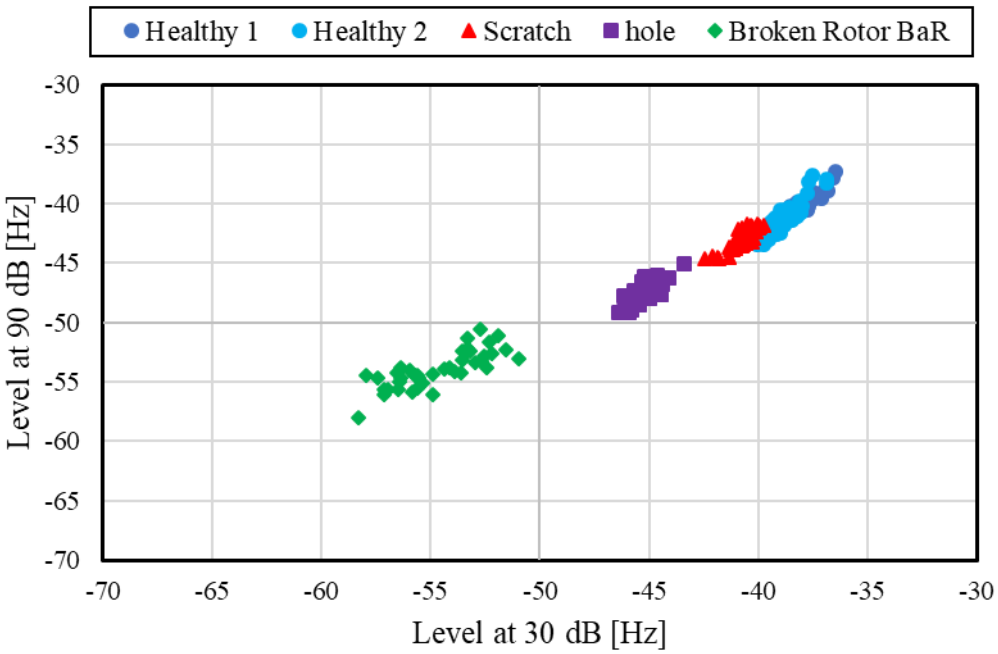

Figure 7.12 *Feature distribution analysis at 1775 min^{-1}.*

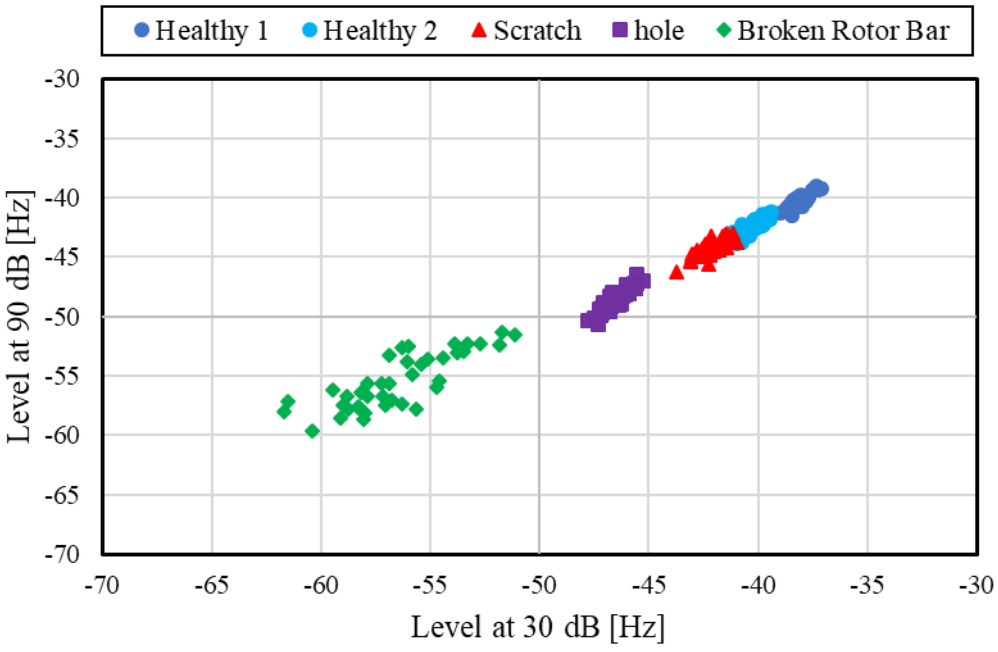

Figure 7.13 *Feature distribution analysis at 1770 min^{-1}.*

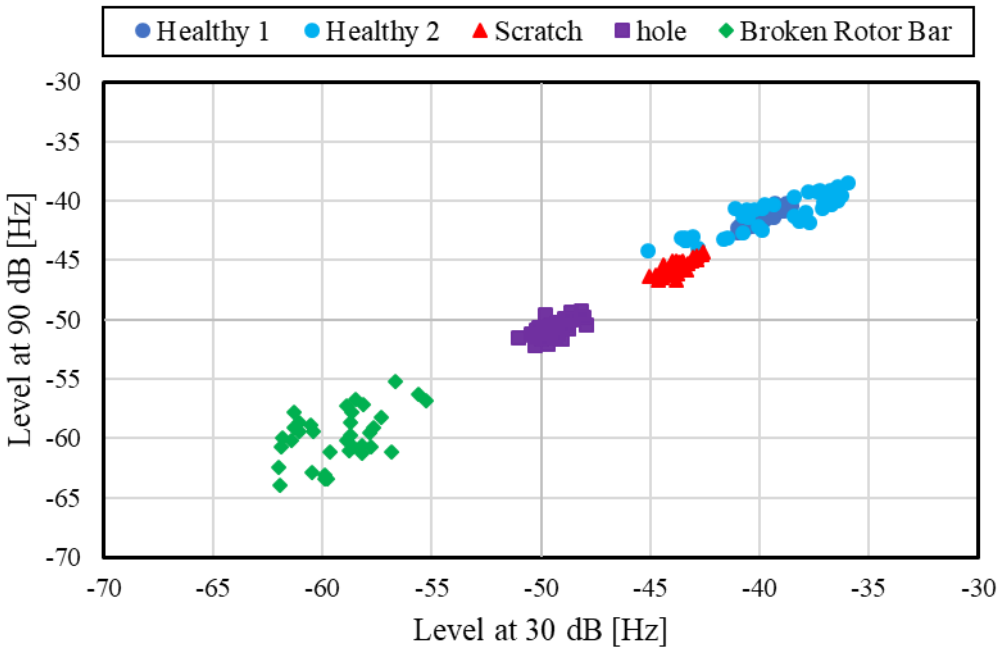

Figure 7.14 *Feature distribution analysis at 1765 min^{-1}.*

The analysis is also performed without considering the rotating speed of the induction motor and the result is shown in Figure 7.15. In this case, short-circuit insulation failure is included. The overlapping of features is observed between the healthy motors and faulty motors. Thus, it becomes impossible to diagnose using the feature distribution and the SVM is employed to identify the present state of the motor even in the case of without considering the rotating speed of the induction motor.

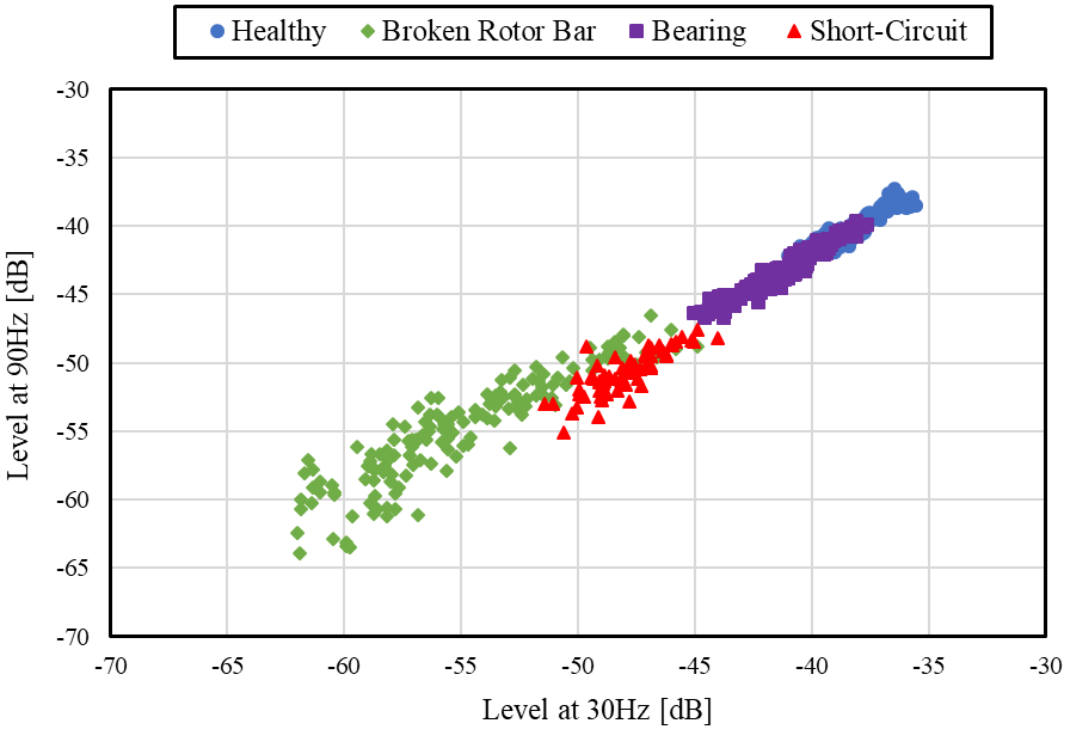

Figure 7.15 *Combined feature distribution analysis.*

7.1.4 Diagnosis using SVM

The main work is to identify and differentiate the faulty motor with the healthy motor. The entire diagnosis analysis is performed in both the conditions of the rotating speed of induction motor. That is, considering and without considering the rotating speed of the induction motor. The results of both the diagnosis are explained one by one as follows.

7.1.4.1 Diagnosis without Considering Rotating Speed

The diagnosis based on the SVM was performed without considering the rotating speed of the induction motor. The data of healthy motors are represented as H for easy understanding. Similarly, hole as HO, scratch as S, and broken rotor bar failure as BRB, short-circuit insulation failure as SC, respectively. The training data and the diagnosis data are spitted randomly in the ratio 70:30. Data obtained at four rotating speeds (1780, 1775, 1770, and 1765 min^{-1}) are combined and the diagnosis is being performed. In this proposed system, the

accuracy rate of the diagnosis is defined as

$$\text{Accuracy rate } (\%) = \frac{number\ of\ data\ diagnosed\ accurately}{total\ number\ of\ data\ for\ diagnosis} \times 100 \qquad (7.1)$$

Table 7.1 shows the accuracy rate and found to be practically acceptable. The HO, BRB and SC are completely diagnosed from the healthy motor and show the maximum accuracy rate. The difference between the faults induced on the outer raceway of the bearing also shows high accuracy rate of 91.25 %. With this accuracy rate, it is possible to identify the present state of the bearing as well as possible to distinguish the failure occurred on the bearing. The accuracy percentage of the S is 82.96 % and considered to be practically acceptable. This is a significant advantage of the proposed method, making it suitable for use at different speeds and in industrial environments. The diagnosis rate of three mechanical faults is 84.73 %, which is comparatively high than any other diagnosis method. It is possible to identify whether the motor is healthy or faulty motors and possible to identify the present state of the motor.

However, the results are better when compared to feature distribution analysis result and the future work lies in improving the diagnosis rate and method to identify the current state of the motor will be discussed.

Table 7.1 *SVM diagnosis result*

Bearing Conditions	Accuracy Rate (%)
H-HO	100
H-S	82.96
H-BRB	100
H-SC	100
HO-S	91.25
HO-S-BRB	84.73
Average	93.16

7.1.4.2 Diagnosis Considering Rotating Speed

Diagnosis based on the SVM was performed by considering the individual rotating speed of the induction motor. The training data and the diagnosis data are spitted randomly in the ratio 70:30. In this proposed system, the accuracy rate of the diagnosis is defined as like the previous case without considering the rotating speed of the induction motor.

The diagnosis rate is found to be 100 %. Thus, the identification of the current state of the motor is possible when the diagnosis is done considering the rotating speed of the induction motor. It is also possible to identify whether the motor is healthy or faulty and it can be distinguished using the proposed method. Predicting the current state of the motor is achieved in this diagnosis condition.

7.1.5 Discussion of Common Diagnosis Method

The common diagnosis method detecting the outer raceway bearing fault and broken rotor bar failure was applied using the FFT analysis. Further diagnosis was performed using an SVM. To satisfy the use of motors in industrial environments, the diagnosis was performed without considering the rotating speed of the motor.

From the result, it is understood that the proposed method can identify the two-different mechanical faults occurring in the induction motor and the differentiation between the broken rotor bar and the bearing was also achieved. Since the experiment is carried out for three time and at different days, the reliability of the data and the results are high. Identifying the present state of the motor in case of mechanical fault is made possible.

7.2 Multiple Fault Diagnosis Method

The application of the common diagnosis method is applied to detect the multiple fault occurred in the induction motor. Both the broken rotor bar fault and the bearing fault are induced simultaneously to induction motor and the analysis is performed using FFT. The diagnosis is performed using SVM. The entire analysis is performed without considering the

rotating speed of the induction motor.

7.2.1 Faulty Factor

The experimental setup and the motor are same as explained in the chapter 4. Two kinds of bearing fault are selected; hole and scratch. The dimension of the hole is diameter of 2 mm and depth of 0.5 mm. The dimension of the scratch; length of 10 mm, width and depth of 0.5 mm. The depth is made constant for both hole and scratch. Likewise, for broken rotor bar failure, a single hole is drilled on the rotor bar.

The broken rotor bar fault and the bearing failure are induced simultaneously to the motor. The combinational multiple fault of broken rotor bar and bearing fault is shown in Figures 7.16 and 7.17. The rotating speed is adjusted from 1780 min^{-1} to 1765 min^{-1}. For the reliability, the experiment is repeated for three times. The proposed method is evaluated by means of measuring the stator current. The current signals are collected from the healthy motor and from the faulty motors. The measurement is carried out under the load condition. Both the frequency spectrum analysis and the feature extraction are based on the value of the stator current.

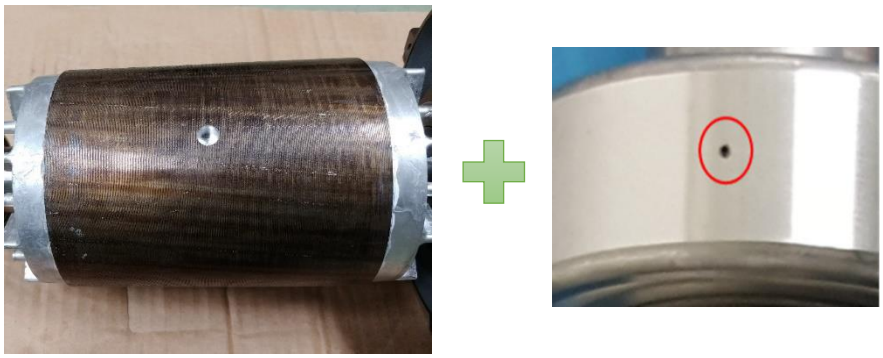

Figure 7.16 *Multiple fault broken rotor bar and bearing (hole).*

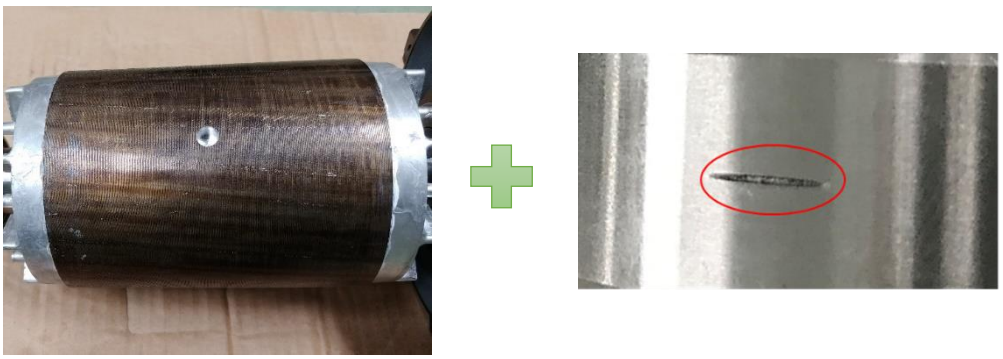

Figure 7.17 *Multiple fault broken rotor bar and bearing (scratch).*

7.2.2 Frequency Spectrum Analysis

Initially, the FFT analysis is performed to the healthy motor. After the confirmation, the broken rotor bar fault and bearing failure are induced to the healthy motors. For easy understanding, the healthy, bearing fault with scratch and broken rotor bar, bearing fault with hole and broken rotor bar, are indicated as H, BRB+BS, and BRB+BH, respectively. Figures 7.18 to 7.21 compare the frequency spectra plotted for the combination H, BRB+BS, BRB+BH at all rotating speeds. The amplitude on the vertical axis is normalized to a maximum of 0 dB.

A large amplitude difference can be observed between the healthy motor and the two fault combinations (BRB+BS, BRB+BH). When the faults are compared, the amplitude difference observed is sufficient to differentiate the cases. At 30 and 90 Hz, amplitude changes are observed at all rotating speeds (1780, 1775, 1770, and 1765 min^{-1}). For establishing the multiple fault diagnosis method, the frequencies 30 and 90 Hz have been selected and proceeded with the feature distribution.

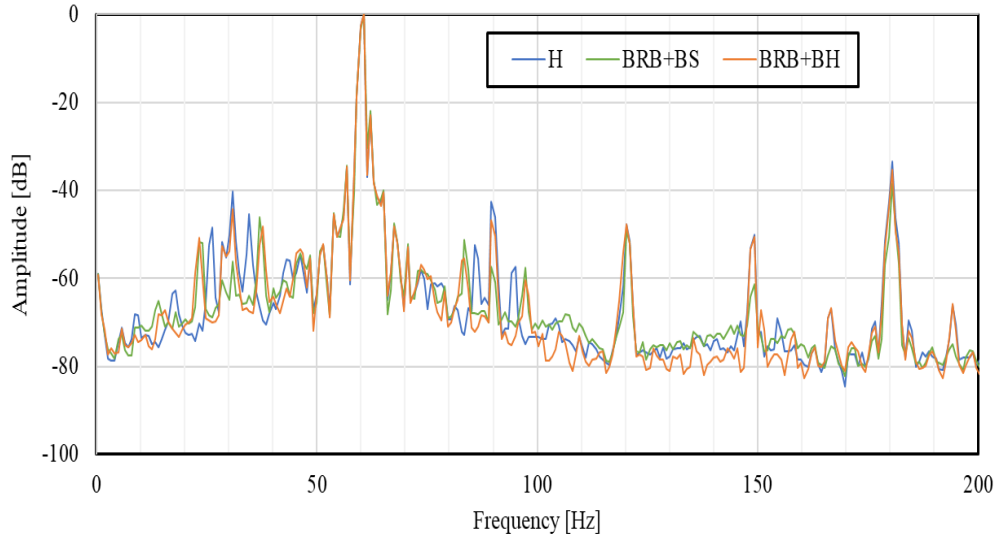

Figure 7.18 *Spectral analysis of multiple fault analysis at 1765 min^{-1}.*

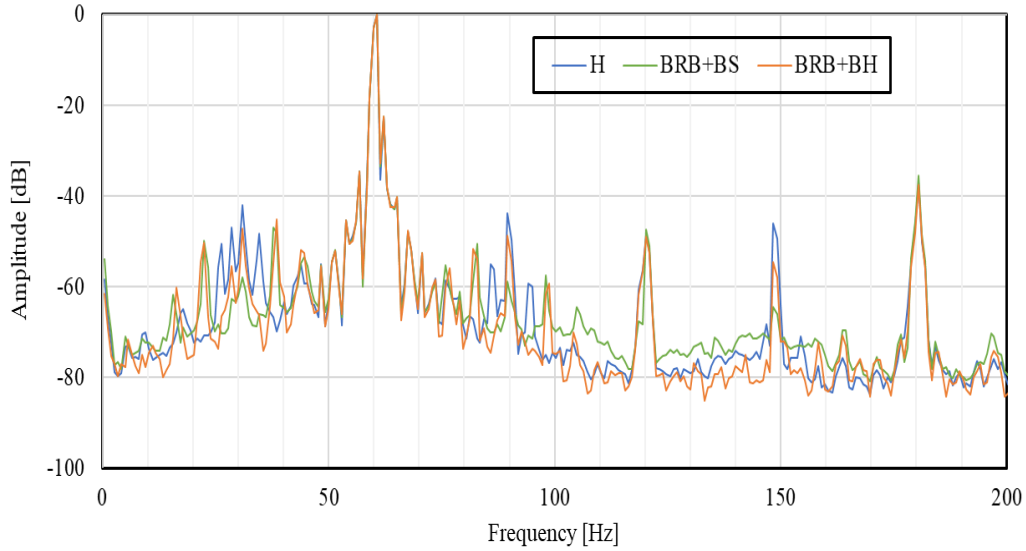

Figure 7.19 *Spectral analysis of multiple fault analysis at 1770 min^{-1}.*

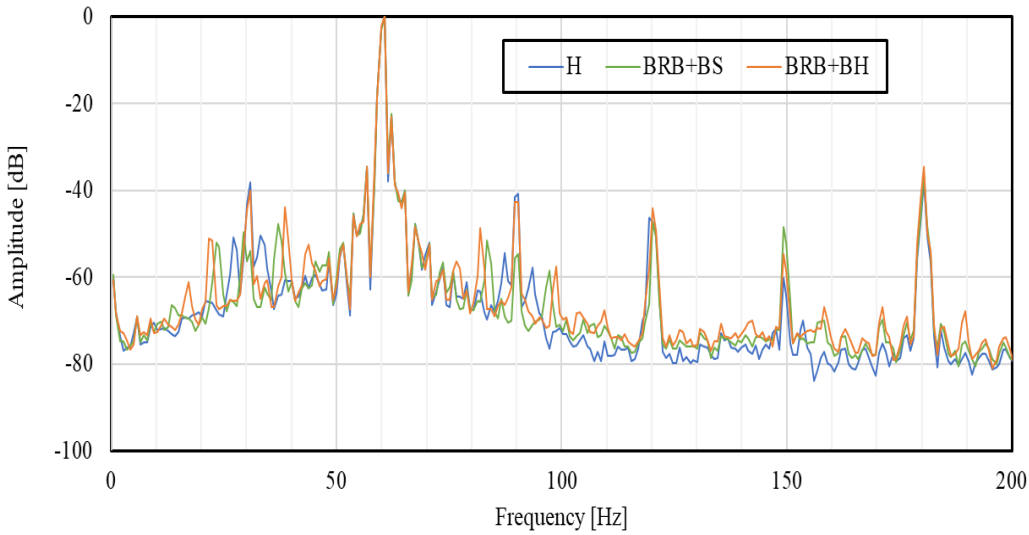

Figure 7.20 *Spectral analysis of multiple fault analysis at 1775 min^{-1}.*

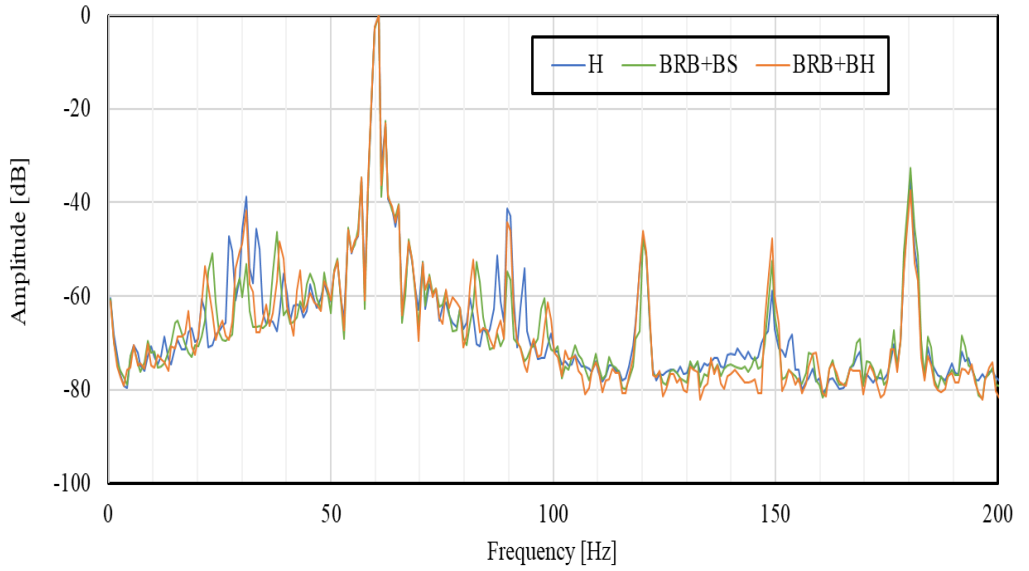

Figure 7.21 *Spectral analysis of multiple fault analysis at 1780 min^{-1}.*

7.2.3 Feature Distribution

The feature distribution analysis is carried out using the amplitude of the characteristics frequency 30 and 90 Hz. The location distinguishing behavior depends on the rotating speed of the motor and the motor conditions. Figures 7.20 to 7.23 show the feature distribution at rotating speeds of 1780 to 1765 min^{-1} for healthy, BRB+BH, BRB+BS. While taking the individual rotating speed of the induction motor into consideration, the classes of the faulty motors (BRB+BH, and BRB+BS) are located far away from the healthy motor. No overlapping of features has been occurred, the motor conditions fell into distinctive classes, allowing them to be differentiated. It is made possible to predict the current state of the motor and the proposed method could identify the failure while the motor is running. This allows a fault to be identified and demonstrates the significant role that feature distribution plays in the analysis the motor failure.

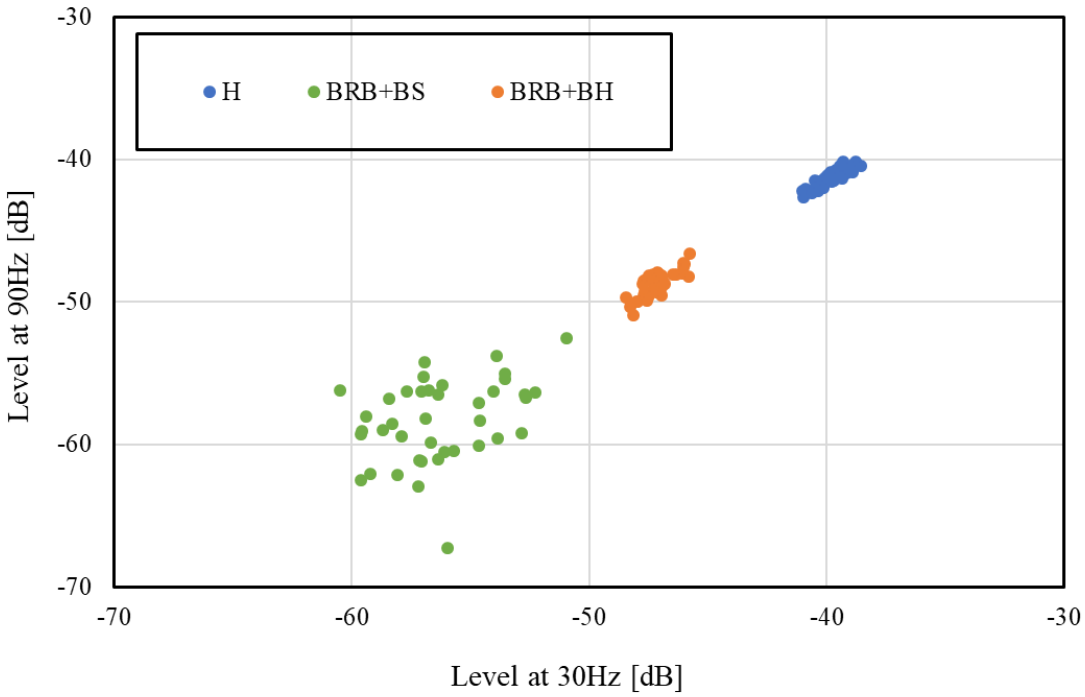

Figure 7.22 *Feature distribution analysis at 1765 min^{-1}.*

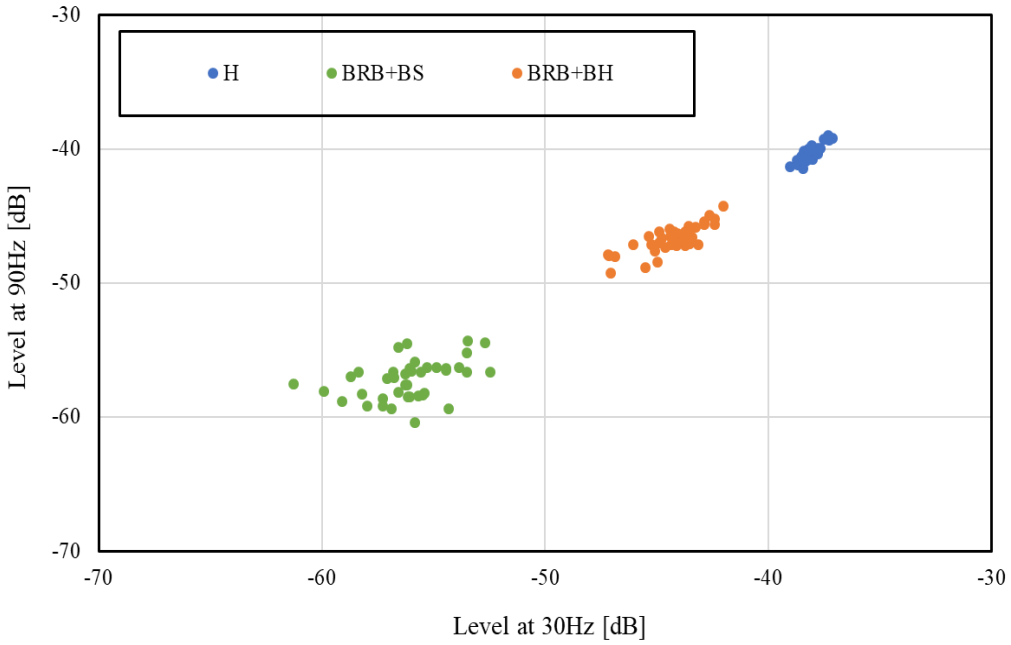

Figure 7.23 *Feature distribution analysis at 1770 min^{-1}.*

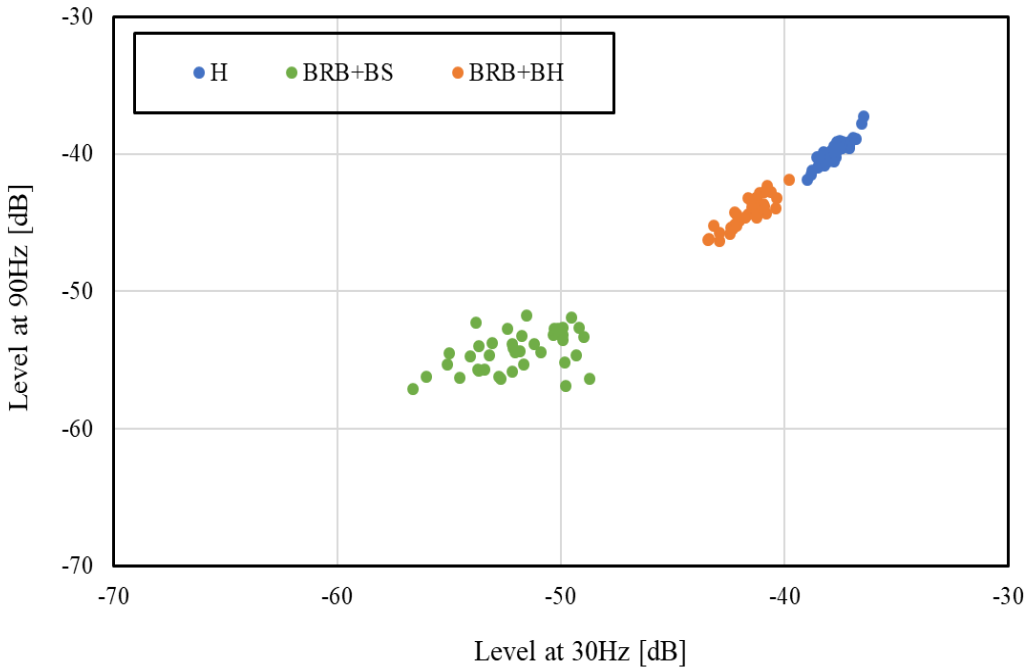

Figure 7.24 *Feature distribution analysis at 1775 min^{-1}.*

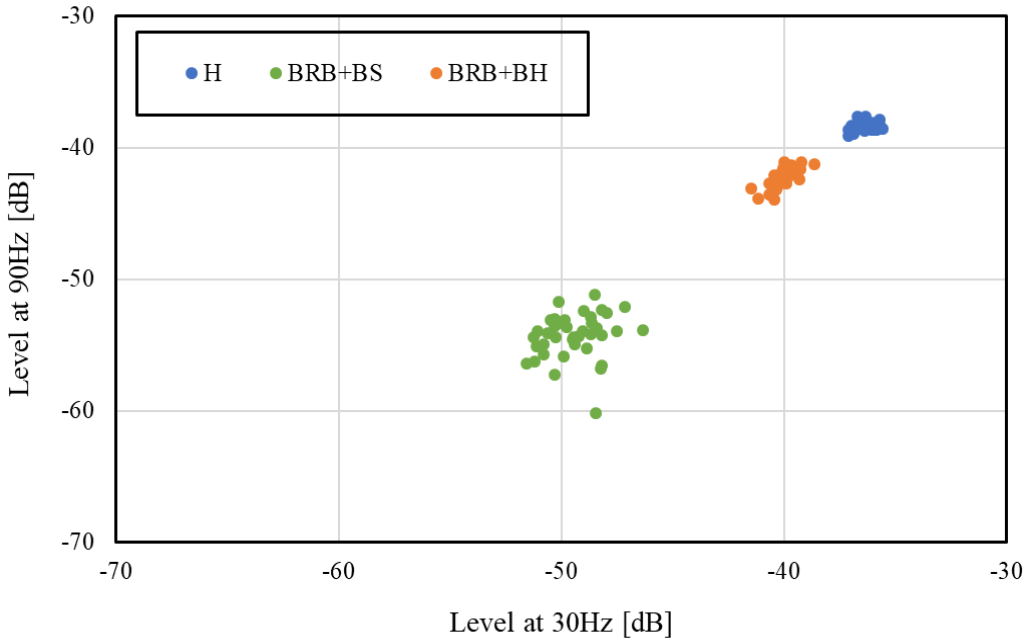

Figure 7.25 *Feature distribution analysis at 1780 min^{-1}.*

The analysis is also performed without considering the rotating speed of the induction motor and the result is shown in Figure 7.26. The overlapping of features is observed partially between H and BRB+BH. The hole has more effect when compared to the scratch. The partial diagnosis is possible using the feature distribution and to increase the accuracy rate, SVM is employed.

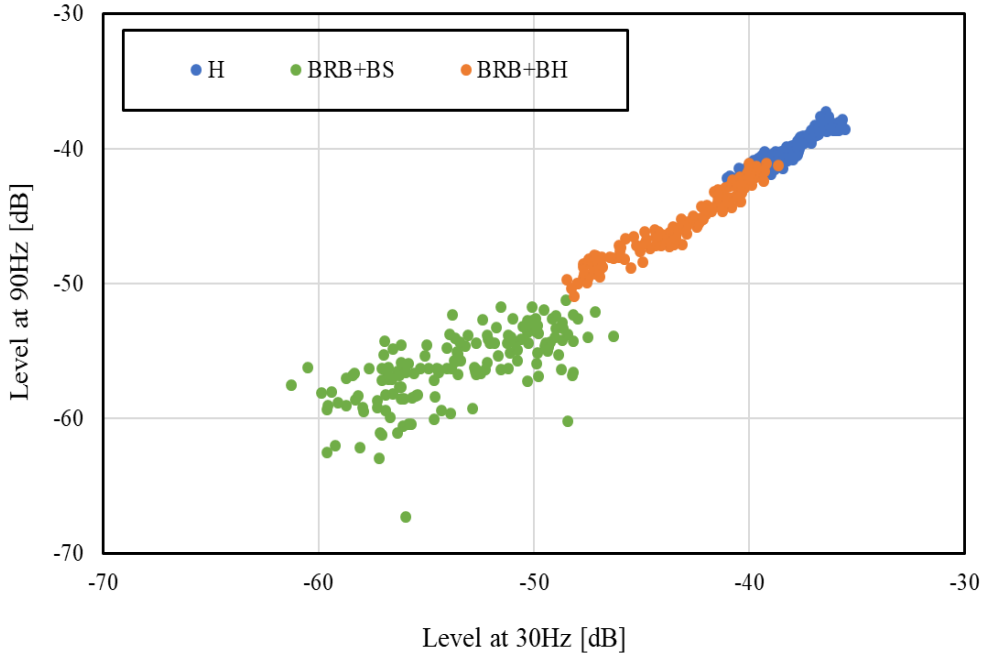

Figure 7.26 *Combined feature distribution analysis.*

7.2.4 Diagnosis using SVM

The main work is to identify the faulty motor with the healthy motor. The diagnosis analysis is performed in both the condition of the rotating speed of induction motor. That is, considering and without considering the rotating speed of the induction motor. The results of both the diagnosis are explained one by one as follows.

7.2.4.1 Diagnosis without Considering Rotating Speed

The diagnosis based on the SVM was performed without considering the rotating speed of the induction motor. The training data and the diagnosis data are divided randomly in the ratio 70:30. Data obtained at the four rotating speeds (1780, 1775, 1770, and 1765 min^{-1}) are combined and the diagnosis is being performed.

Table 7.2 shows the accuracy rate and found to be practically acceptable. The diagnosis is carried out for the combination (H-BRB+BH), (H-BRB+BS), (BRB+BH-BRB+BS), and (H-BRB+BH-BRB+BS). The complete diagnosis is observed, and the proposed method can find the present state of the motor. This is a significant advantage of the proposed method, making it suitable for use at different speeds and in industrial environments. The average diagnosis rate is 98.61 %, which is comparatively high than feature distribution result.

Table 7.2 *SVM diagnosis result*

Bearing Conditions	Accuracy Rate (%)
H-BRB+BH	97.28
H-BRB+BS	100
BRB+BH-BRB+BS	100
H- BRB+BH-BRB+BS	97.28
Average	98.61

7.2.4.2 Diagnosis Considering Rotating Speed

Diagnosis based on the SVM was performed by considering the individual rotating speed of the induction motor. The training data and the diagnosis data are divided randomly in the ratio 70:30. In this proposed system, the accuracy rate of the diagnosis is defined as like the previous case without considering the rotating speed of the induction motor.

The diagnosis rate is found to be 100 %. Thus, the identification of the current state of the motor is possible when the diagnosis is done considering the rotating speed of the induction motor.

7.2.5 Discussion of Multiple Fault Diagnosis

The multiple fault diagnosis method detecting the outer raceway bearing fault and broken rotor bar failure was proposed using the FFT analysis and SVM diagnosis. To satisfy the use of motors in industrial environments, the diagnosis was performed without considering the rotating speed of the motor.

From the result, it is understood that the proposed method can identify the two mechanical faults occurring in the induction motor and the differentiation between was also achieved. Since the experiment is carried out for three time and at different days, the reliability of the data and the results are high. Identifying the present state of the motor in case of mechanical fault is made possible.

7.3 Summary

Till now, different methods have been employed in detecting the short-circuit insulation failure (chapter 2), broken rotor bar failure (chapter 3), and bearing failure (chapters 4 and 5). In the study, using the proposed method of chapter 4, the common diagnosis method is applied to detect three kinds of fault (short-circuit insulation failure, broken rotor bar failure, and bearing failure). The application of the common diagnosis method is also applied to detect the multiple fault occurred in the induction motor. Both the broken rotor bar fault and the bearing fault are induced simultaneously to induction motor and the analysis is performed. The entire analysis is performed without considering the rotating speed of the induction motor.

The results are concluded as follows:

- The one-turn short-circuit insulation failure detection is made possible
- The method confirms the possibilities of diagnosing one broken rotor bar failure
- Detection of the multiple fault i.e. both the broken rotor bar and the bearing fault are induced simultaneously to induction motor is achieved

- From the result of the common diagnosis and the multiple fault diagnosis, the versatility of the present study is confirmed and found to be high.
- From this, it is possible to examine the applicability of the proposed method to other electric motors.

Chapter 8

Comparison of Machine Learning Algorithm and Artificial Intelligence Method to Fault Diagnosis

Most of the induction motor failure diagnosis including bearing fault, broken rotor bar and short-circuit fault has been carried out using Support Vector Machine (SVM). In this section, some of the other machine learning algorithm and the latest technology artificial intelligence have been selected and the diagnosis result is discussed. Though SVM has a superiority function among the machine learning algorithm, a case study is done by selecting the widely used diagnosis methods which are adopted in other application.

Three types of bearing fault have been selected; hole, scratch and a special one which abrasion type of scratch. The abrasion type of scratch is selected because it almost matches the industrial environment fault. Bearing failure analysis and diagnosis are carried out using various machine learning algorithm (MLA). Additionally, among the artificial intelligence method, deep learning (DL) is getting attention in various fields like medical, safety driving system, biological research etc. An attempt is made by testing the level of deep learning to the field of bearing failure analysis. The entire diagnosis results are compared and discussed.

8.1 Faulty Factor

The experimental setup is same as explained in the chapter 4. Two different type motors are used. A hole, scratch is induced in motor 1 and abrasion scratch on motor 2 as shown in Figures 8.1 to 8.3, respectively.

The dimension of the hole is diameter of 0.5 mm and depth of 0.5 mm. Likewise, the dimension of the scratch; length of 5 mm, width and depth of 0.5 mm. The dimension of

abrasion scratch is length of 12 mm, width of 8 mm and depth of 0.5 mm. The depth (0.5 mm) is made constant for a better understanding of fault analysis. The rotating speed was adjusted from 1780 min^{-1} to 1765 min^{-1}.

Figure 8.1 *Bearing with a hole 0.5 mm.*

Figure 8.2 *Bearing with a scratch 5 mm.*

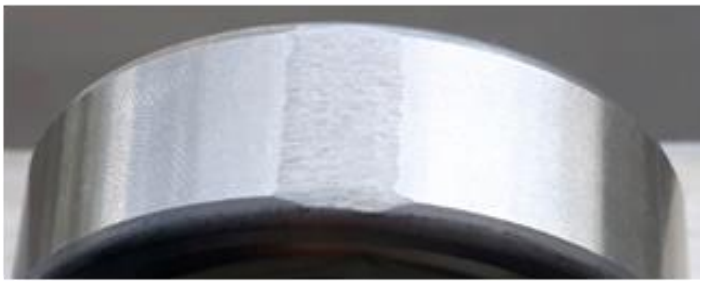

Figure 8.3 *Abrasion bearing sample.*

The proposed method is evaluated by means of measuring the stator current. The current signals are collected from the healthy motor and three types of the faulty motors. The measurement was carried out under the load condition. Both the frequency spectrum analysis and the feature extraction are based on the value of the stator current under four types of bearing conditions. The procedure of the case study is shown in Figure 8.4.

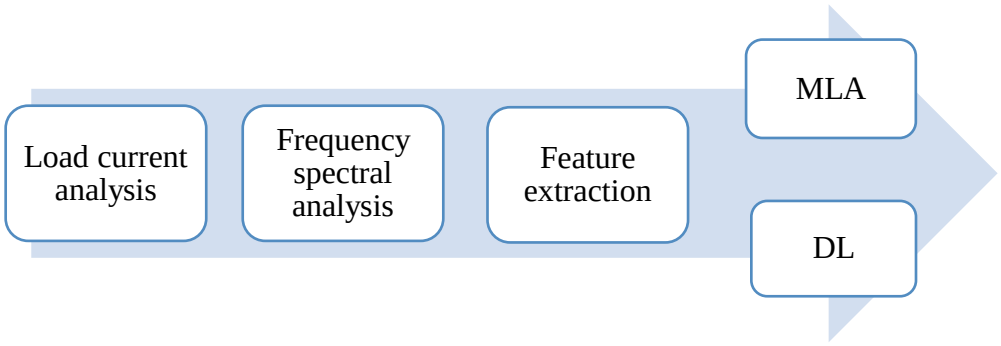

Figure 8.4 *Case study procedure.*

8.2 Frequency Spectrum Analysis

FFT analysis of the U-phase load current was performed under all four bearing conditions. Figures 8.5 to 8.8 compare the frequency spectra plotted for healthy-hole, healthy-scratch, hole-scratch, healthy-abrasion scratch respectively, at a rotating speed of 1765 min^{-1}. The amplitude on the vertical axis is normalized to 0 dB.

A large amplitude difference can be observed between the healthy motor and all the two fault conditions (hole and scratch). When the faults on the bearings are compared (hole and scratch), the amplitude difference observed is sufficient to differentiate the cases. Amplitude differences in the frequency components were clearly visible at frequencies of 30, 90, 150, and 180 Hz. At 30 and 90 Hz, amplitude changes were observed at all rotating speeds (1780, 1775, 1770, and 1765 min^{-1}). At 150 and 180 Hz, in contrast, no significant amplitude change was observed when the speed was varied, under any of the four bearing conditions. Frequencies of 30 and 90 Hz were therefore used in the study.

This allowed differences between the healthy and faulty conditions and between different fault conditions to be localized.

In the case of a hole and scratch, shockwave impulse gets generated and the characteristic frequency is set to occur, which is confirmed by various case study explained in the other chapter (4). An interesting fact, it is suggested even the abrasion type fault causes and creates some shock wave pulse which induces the characteristic frequency to occur. This characteristic frequency mainly depends on the faulty part and damage level of the bearing. Thus, the characteristic frequency 30 and 90 Hz plays a major role in detecting the bearing conditions of the induction motor and these frequencies are used to plot the feature distribution for further study.

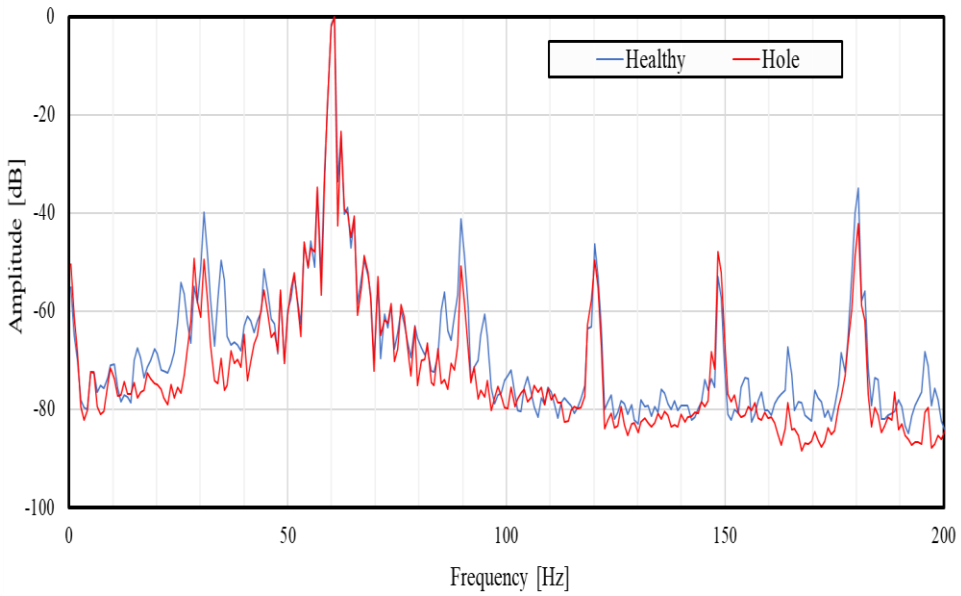

Figure 8.5 *Spectral analysis of healthy and hole at 1765 min^{-1}.*

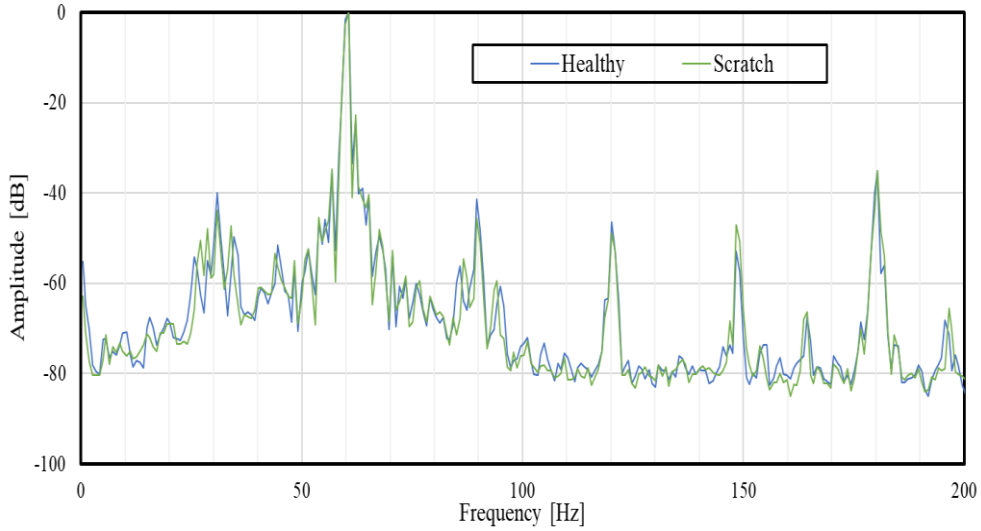

Figure 8.6 *Spectral analysis of healthy and scratch at 1765 min^{-1}.*

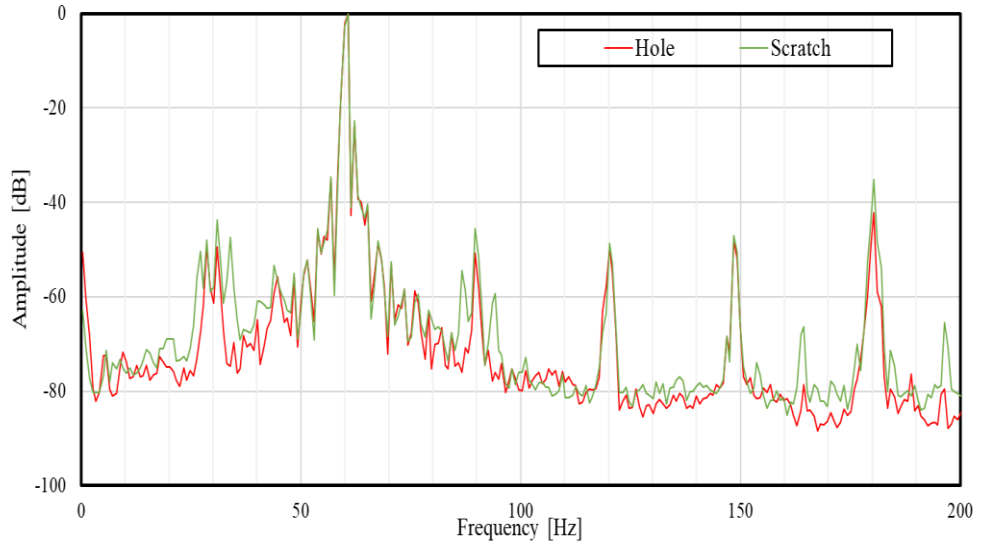

Figure 8.7 *Spectral analysis of hole and scratch at 1765 min^{-1}.*

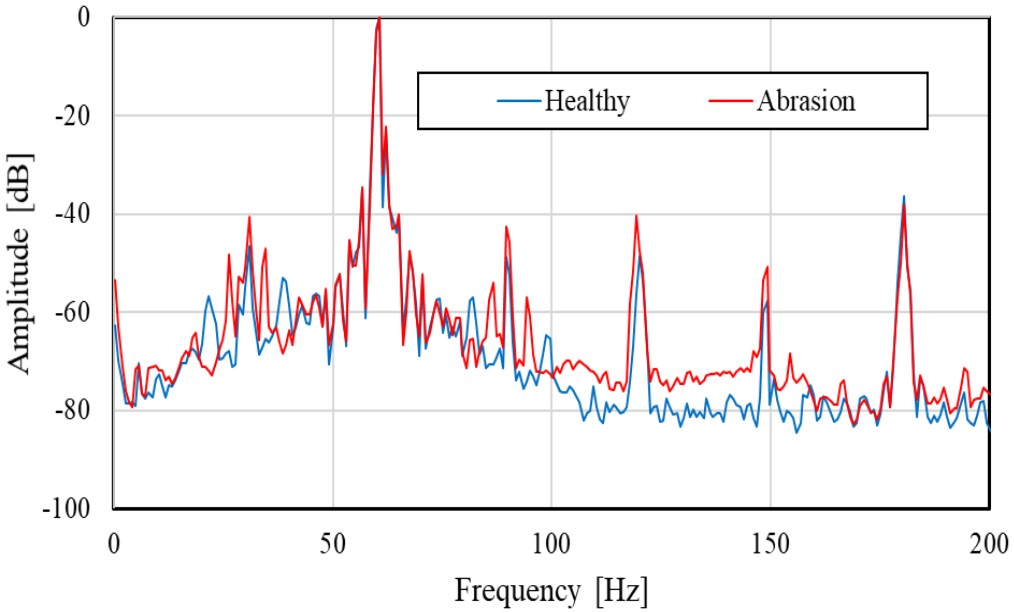

Figure 8.8 *Spectral analysis of healthy and abrasion scratch at 1775 min^{-1}.*

8.3 Feature Distribution

The amplitude of the fault frequency of 30 and 90 Hz is extracted as features and its effectiveness is discussed. The amplitude of frequency 30 Hz is plotted along X-axis and 90 Hz along Y-axis, respectively. The contribution of each bearing conditions at different rotating speed is evaluated in the study. The results of all rotating speed are shown from Figures 8.9 to 8.16. The location of the features mainly depends on the rotating speed of induction motor and the bearing conditions used in the present study. It is clear that the features are located according to their own classes of bearing condition. No overlapping exists when the analysis is performed considering the rotating speed of the induction motor and confirms the fact of identifying the fault.

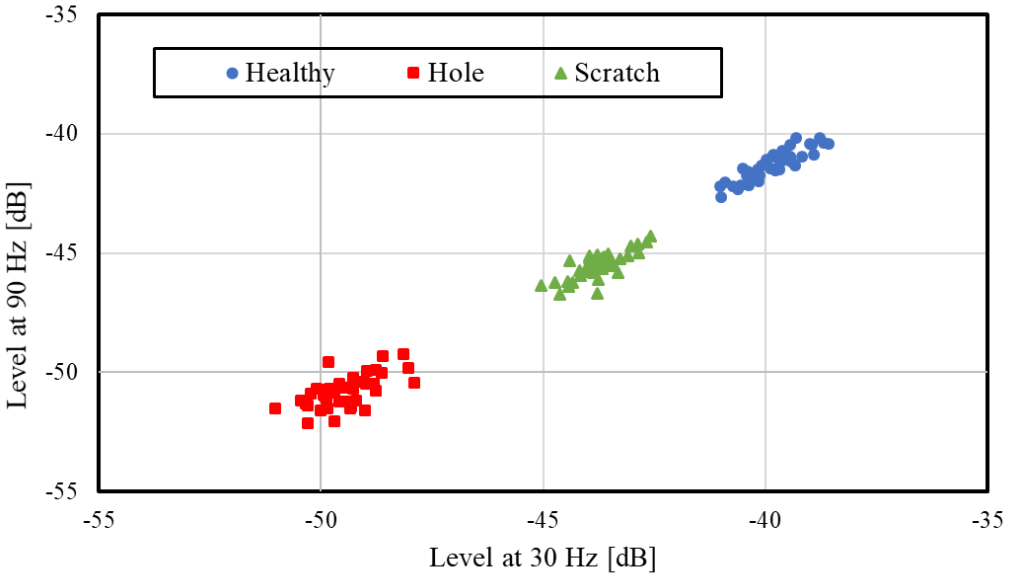

Figure 8.9 *Feature distribution of bearing failure analysis at 1765 min^{-1}.*

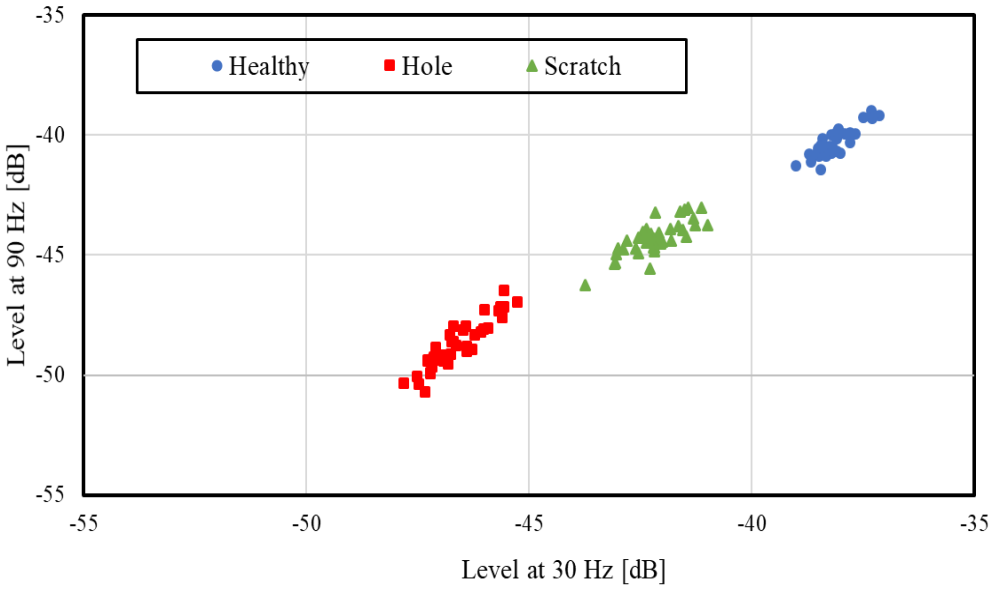

Figure 8.10 *Feature distribution of bearing failure analysis at 1770 min^{-1}.*

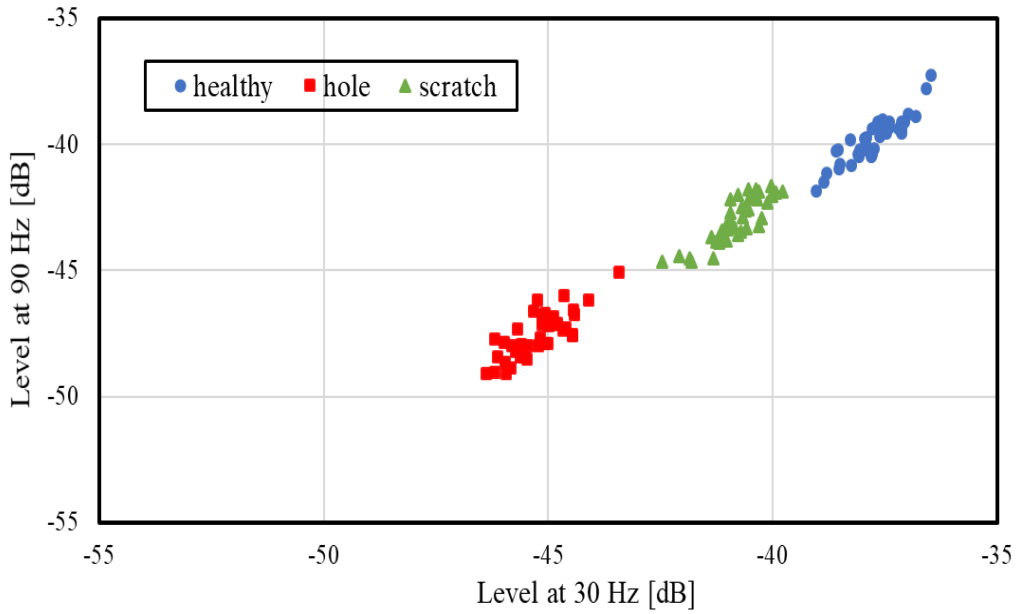

Figure 8.11 *Feature distribution of bearing failure analysis at 1775 min^{-1}.*

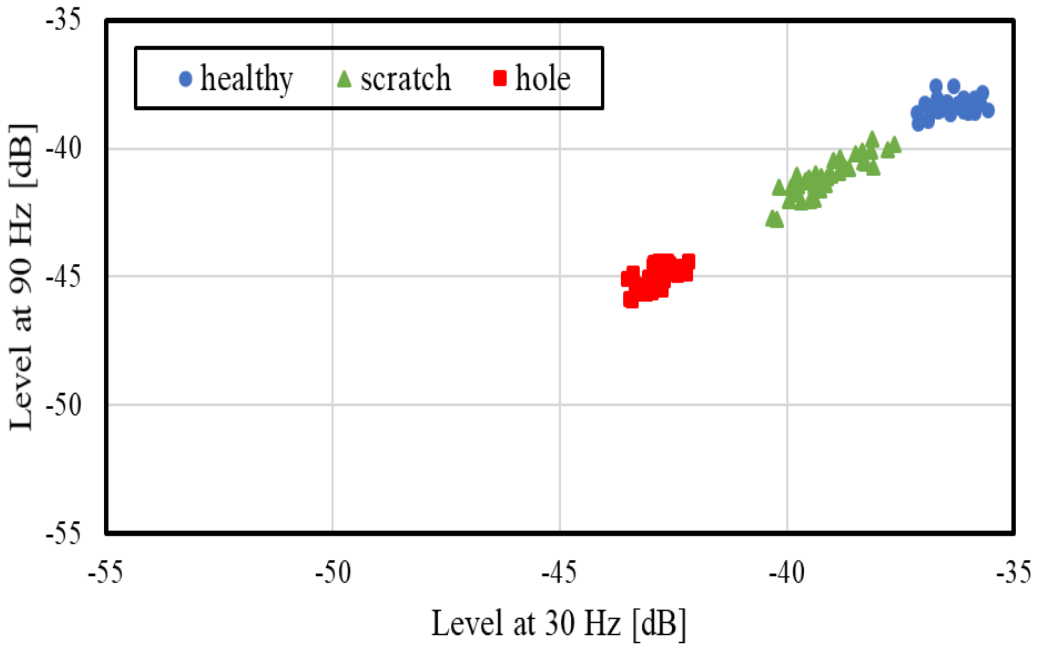

Figure 8.12 *Feature distribution of bearing failure analysis at 1780 min^{-1}.*

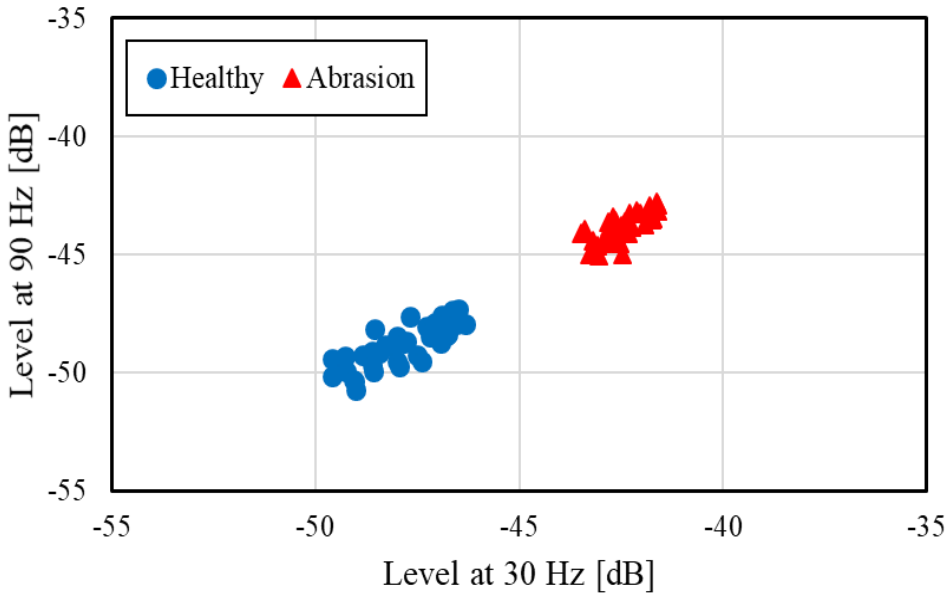

Figure 8.13 *Feature distribution analysis at 1765 min^{-1}.*

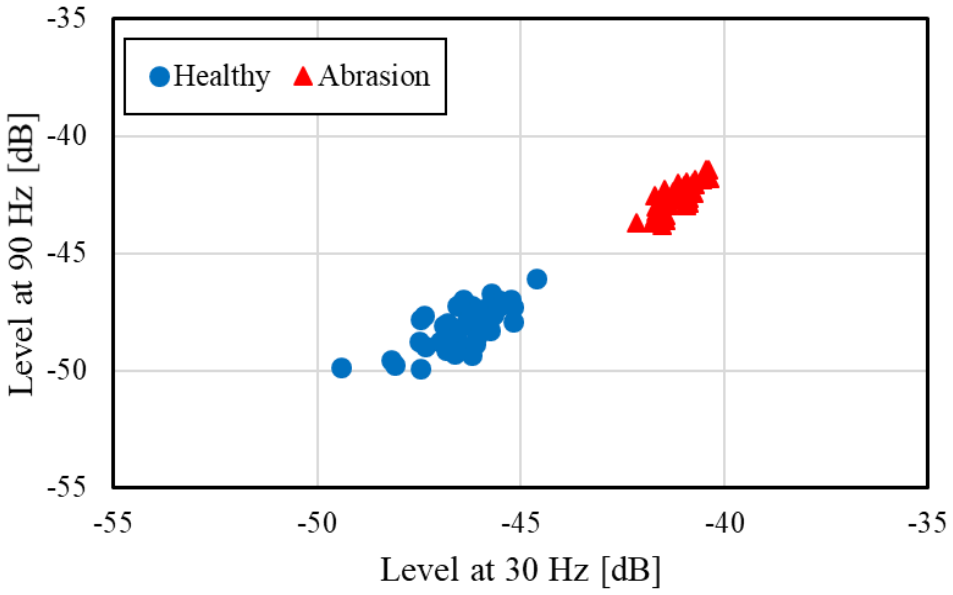

Figure 8.14 *Feature distribution analysis at 1770 min^{-1}.*

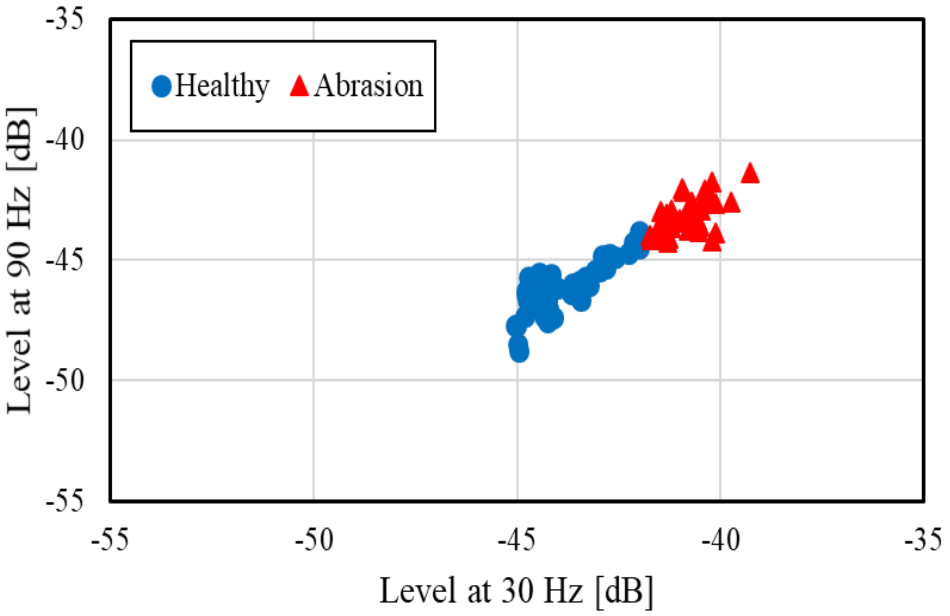

Figure 8.15 *Feature distribution analysis at 1775 min^{-1}.*

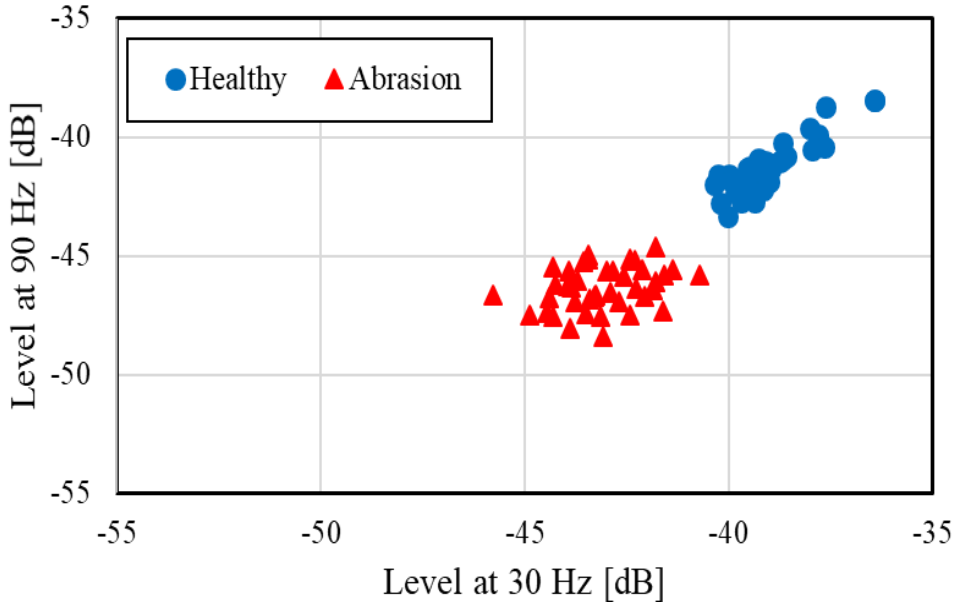

Figure 8.16 *Feature distribution analysis at 1780 min^{-1}.*

In factories, the rotating speed of the motor is not constant and feature extraction analysis is also performed in satisfying the industrial environment and the result is shown in Figures 8.17 and 8.18.

The overlapping of features is observed between the healthy and scratch, and some minute overlapping is observed between hole and scratch. The faulty motor hole and healthy motor show no overlapping and it is completely distributed to their own class of location. The slight fault of hole 0.5 mm is diagnosed and identified completely. But overlapping is observed between the healthy and abrasion scratch. In this situation, it is hard to differentiate the existing status of the motor. However, it is crucial to achieving the diagnosis even while considering the industry environment. To improve the diagnosis, the machine learning algorithm and artificial intelligence method is introduced.

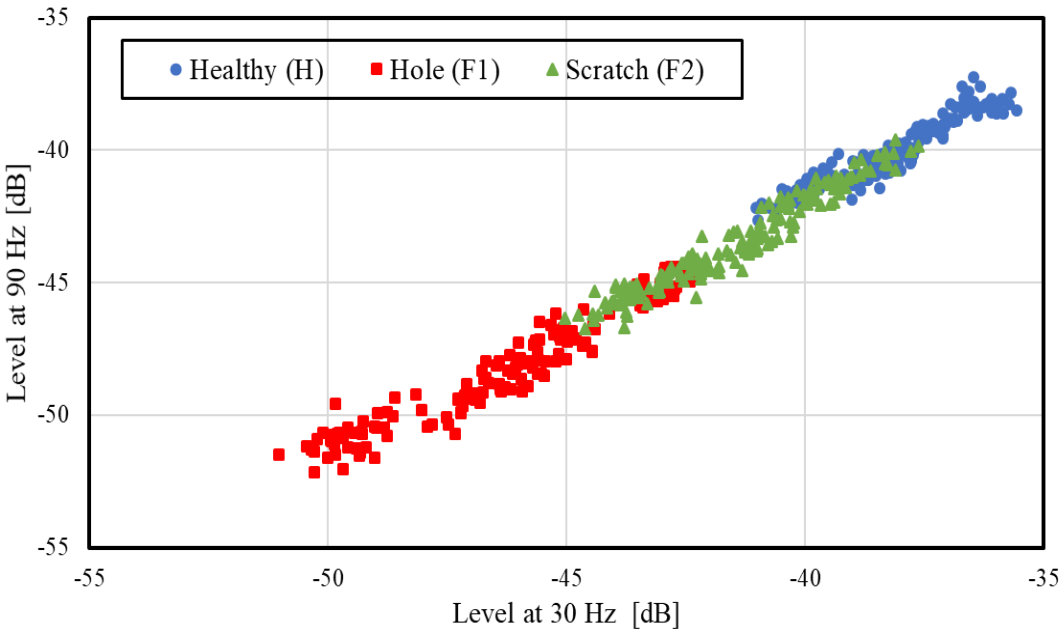

Figure 8.17 *Combined feature distribution of bearing failure analysis.*

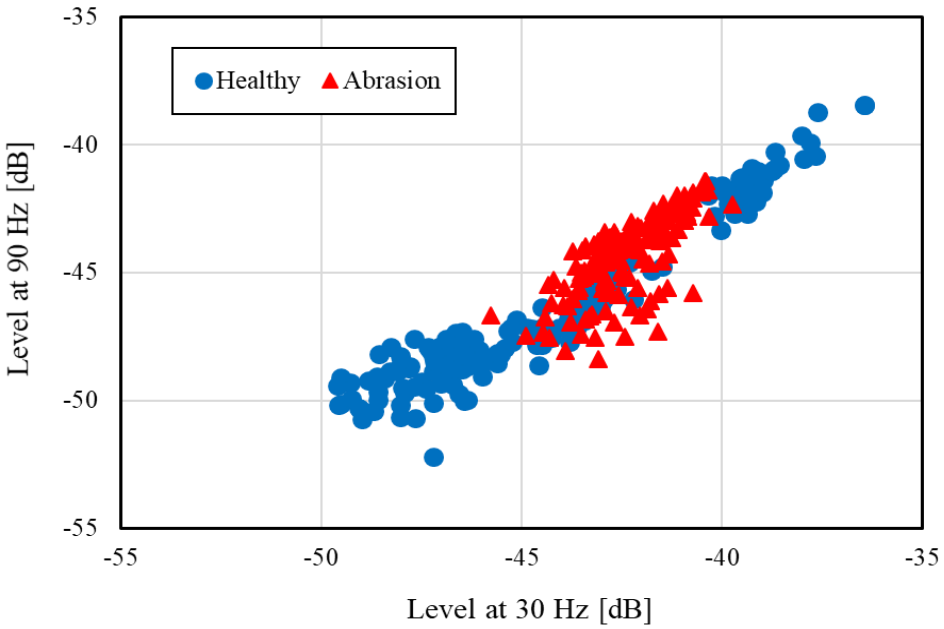

Figure 8.18 *Combined feature distribution analysis.*

8.4 Machine Learning Algorithm

The machine learning is a field of computer science that uses the statistical techniques to give the system the ability to perform the task or improvise the task, without being explicitly programmed. The machine learning is closely related to statistical analysis, which focuses on predicting the result that ties with the mathematical optimization. Sometimes it conflated with the data mining, data preprocessing can also be achieved through the machine learning.

Generally, the machine learning algorithm is classified as supervised and unsupervised algorithm. The supervised algorithm consists of a target variable which is to be predicted from a given set of independent variables. These variables are used to generate the function and maps of the input to get the desired output and the target is achieved. The datum is trained to achieve the better accuracy rate. The training process is continued until the model achieves the desired level of accuracy. But in case of unsupervised algorithm, there is no target variable and the clustering technique is adopted. These techniques may segment the group and certain

level of diagnosis can be achieved.

The role is to identify the current state of bearing and from the case study it is known that the supervised machine learning algorithm is the suited one to carry out the bearing failure analysis. The algorithms used in the present study are Support Vector Machine, Naives Bayes, K-nearest Neighbor Algorithm, Decision tree, and Random forest. It is organized as follows; the description, procedure and result, and finally characteristics difference between the approaches.

8.4.1 Support Vector Machine (SVM) [1]-[3]

SVM used for the diagnosis in the ongoing study is described shortly. SVM is one of pattern recognition methods, which determines a recognition result by categories after evaluating similarities of an input pattern with respect to categories, based on previous recognition results of training data. SVM was originally introduced to the classification of linearly separable classes of object. For example, when data of two classes are distributed as shown in Figure 8.19, they are separated by the line drawn between the two classes so that the margin d becomes maximum. In addition to performing linear classification, SVM can also efficiently perform a non-linear classification using the kernel, implicitly mapping their inputs into high-dimensional feature spaces.

Adding to the point, SVM is based on the concept of decision planes that define the boundary condition. A decision plane is one that separates between a set of objects having different class memberships. A schematic example is shown in Figure 8.20. In this example, the objects belong either to class GREEN or RED. The separating curve defines a boundary on the right side of which all objects are GREEN and to the left of which all objects are RED. Any new object falling to the right is labeled, i.e., it belongs to the classification GREEN or else it should be classified as RED and it must fall to the left of the separating line.

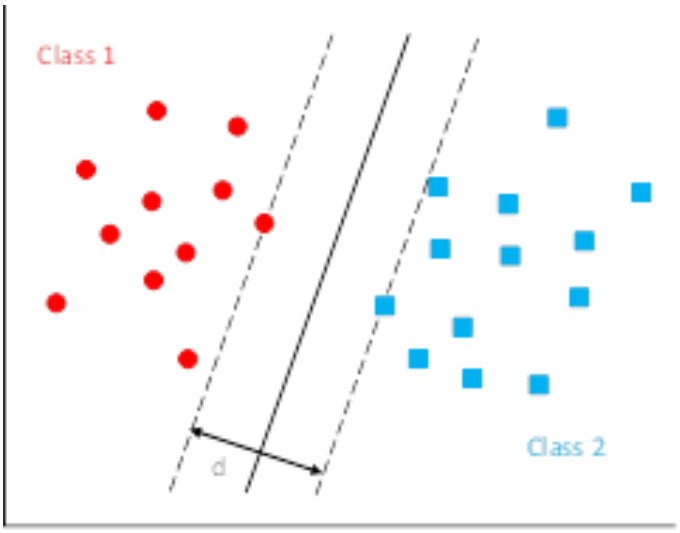

Figure 8.19 *Example of linear classification for two-class data by SVM.*

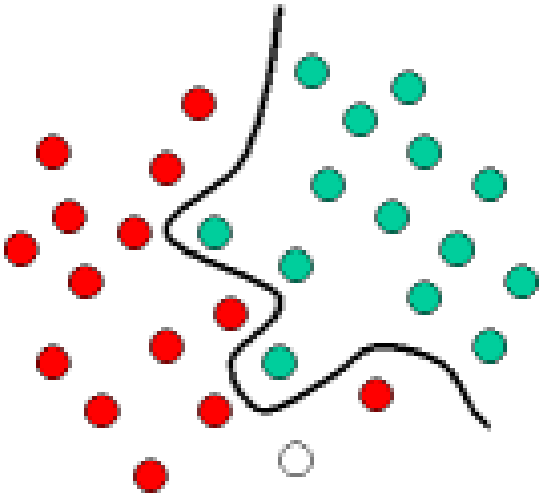

Figure 8.20 *Schematic example for SVM.*

The above is a classic example of a linear classifier, i.e., a classifier that separates a set of objects into their respective groups (GREEN and RED). Most classification tasks, however, are not simple, and often more complex structures are needed to make an optimal separation, i.e., correctly classify new objects (test cases) because of the examples that are available (train cases). This situation is depicted in the Figure 8.21 shown below. Compared to the previous schematic, a full separation of the GREEN and RED objects would require a curve

(which is more complex than a line). Classification tasks based on drawing separating lines to distinguish between objects of different class memberships are known as hyper plane classifiers. SVMs are particularly suited to handle such tasks.

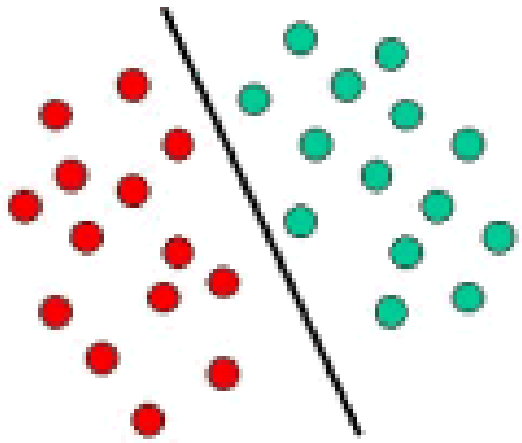

Figure 8.21 *Example for hyper plane classification.*

Figure 8.22 shows the basic idea behind SVM. Here the original objects (left side of the schematic) is mapped, i.e., rearranged, using a set of mathematical functions, known as kernels. The process of rearranging the objects is known as mapping. Note that in this new setting, the mapped objects (right side of the schematic) is linearly separable and thus, instead of constructing the complex curve (left schematic), it is better to find an optimal line that can separate the GREEN and the RED objects.

In general, SVM is mainly classified into two categories. They are hard margin and soft margin SVM. When the classes are linearly separable, then hard margin could be used for the classification. This hard margin is independent of cost parameter (C) and radial basis function, and radial basis function is commonly used kernel function in support vector gamma machine classification. The definition of the kernel involves a parameter (γ). But on the other side, when the classes are not linearly separable then soft margin is used for the

diagnosis. This soft margin is dependent of the parameters that are involved in the diagnosis. Furthermore, in the present study, soft margin is used for the diagnosis.

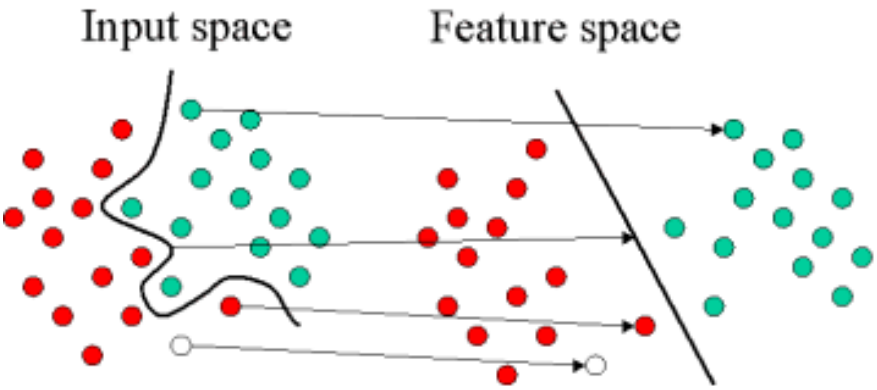

Figure 8.22 *Mapping of SVM.*

8.4.1.2 SVM Classification

SVM is primarily a classier method that performs classification tasks by constructing hyper planes in a multidimensional space that separates cases of different class labels. SVM supports both regression and classification tasks and can handle multiple continuous and categorical variables.

For categorical variables a dummy variable is created with case values as either 0 or 1. Thus, a categorical dependent variable consisting of three levels, say (A, B, C), is represented by a set of three dummy variables:

- A: {1 0 0}
- B: {0 1 0}
- C: {0 0 1}

To construct an optimal hyper plane, SVM employs an iterative training algorithm, which is used to minimize an error function. According to the form of the error function, SVM models can be classified into four distinct groups:

- Classification SVM Type 1 (also known as C-SVM classification)
- Classification SVM Type 2 (also known as nu-SVM classification)
- Regression SVM Type 1 (also known as epsilon-SVM regression)
- Regression SVM Type 2 (also known as nu-SVM regression)

In the present study, the classification SVM Type 1 is employed. Next, the classification of SVM is explained shortly. It has two main classification, i.e., classification SVM type 1 and classification SVM Type 2.

✧ **Classification SVM Type 1**

For this type of SVM, training involves the minimization of the error function:

$$\frac{1}{2} w^T w + C \sum_{i=1}^{N} \xi_i \tag{8.1}$$

In subject to the constraints:

$$y_i \left(w^T \phi(x_i) + b \right) \geq 1 - \xi_i \text{ and } \xi_i \geq 0, i = 1, \ldots, N \tag{8.2}$$

where C is the cost parameter, w is the vector of coefficients, b is a constant, and ξ_i represents parameters for handling non-separable data inputs. The index i labels the N training cases. Note that $y \in \pm 1$ represents the class labels and xi represents the independent variables. The kernel ϕ is used to transform data from the input (independent) to the feature space. It should be noted that the larger the C, the more the error is penalized. Thus, C should be chosen with care to avoid over fitting.

✧ **Classification SVM Type 2**

In contrast to Classification SVM Type 1, the Classification SVM Type 2 model minimizes the error function:

$$\frac{1}{2}w^T w - \nu\rho + \frac{1}{N}\sum_{i=1}^{N}\xi_i \tag{8.3}$$

In subject to the constraints:

$$y_i\left(w^T\phi(x_i)+b\right) \geq \rho - \xi_i, \xi_i \geq 0, i = 1,\ldots,N \text{ and } \rho \geq 0 \tag{8.4}$$

It should be noted that the larger the C, the more the error is penalized. Thus, C should be chosen with care to avoid over fitting.

8.4.1.3 Regression SVM

In a regression SVM, the task is to estimate the functional dependence of the dependent variable y on a set of independent variables x. It assumes, like other regression problems, that the relationship between the independent and dependent variables is given by a deterministic function f plus the addition of some additive noise:

$$y = f(x) + \text{noise} \tag{8.5}$$

The task is then to find a functional form for f that can correctly predict new cases that the SVM has not been presented before. This can be achieved by training the SVM model on a sample set, i.e., training set, a process that involves, like classification, the sequential optimization of an error function. Depending on the definition of this error function, two types of SVM models can be recognized:

✧ **Regression SVM Type 1**

The error function is:

$$\frac{1}{2}w^T w + C\sum_{i=1}^{N}\xi_i + C\sum_{i=1}^{N}\xi^*_i \tag{8.6}$$

The following condition can be minimized as:

$$\begin{aligned} &w^T\phi(x_i)+b-y_i \le \varepsilon+\xi_i^* \\ &y_i - w^T\phi(x_i)-b_i \le \varepsilon+\xi_i \\ &\xi_i,\xi_i^* \ge 0, i=1,\ldots,N \end{aligned} \tag{8.7}$$

✧ **Regression SVM Type 2**

The error function is given by:

$$\frac{1}{2}w^T w - C\left(\nu\varepsilon + \frac{1}{N}\sum_{i=1}^{N}\left(\xi_i+\xi_i^*\right)\right) \tag{8.8}$$

The following condition can be minimized as:

$$\begin{aligned} &\left(w^T\phi(x_i)+b\right)-y_i \le \varepsilon+\xi_i \\ &y_i-\left(w^T\phi(x_i)+b_i\right) \le \varepsilon+\xi^*_i \\ &\xi_i,\xi^*_i \ge 0, i=1,\ldots,N, \varepsilon \ge 0 \end{aligned} \tag{8.9}$$

where C is the cost parameter constant, w is the vector of coefficients, b is a constant, and ξ_i represents parameters for handling non-separable data inputs. The index i labels the N training cases. Note that $y \in \pm 1$ represents the class labels and xi represents the independent variables.

8.4.1.4 Kernel

SVM is one of the features that can improve generalization performance by choosing the kernel appropriately depending on the issue. There are number of kernels that can be used in Support Vector Machines models. These include linear, polynomial, radial basis function (RBF) and sigmoid.

The entire expression for the linear, polynomial, radial basis function and sigmoid is given as follows:

$$K(\mathbf{X}_i, \mathbf{X}_j) = \begin{Bmatrix} \mathbf{X}_i \cdot \mathbf{X}_j & \text{Linear} \\ (\gamma \mathbf{X}_i \cdot \mathbf{X}_j + C)^d & \text{Polynomial} \\ \exp(-\gamma |\mathbf{X}_i - \mathbf{X}_j|^2) & \text{RBF} \\ \tanh(\gamma \mathbf{X}_i \cdot \mathbf{X}_j + C) & \text{Sigmoid} \end{Bmatrix} \quad (8.10)$$

where $K(\mathbf{X}_i, \mathbf{X}_j) = \phi(\mathbf{X}_i) \bullet \phi(\mathbf{X}_j)$ is the kernel function that represents a dot product of input data points mapped into the higher dimensional feature space by transformation ϕ. Also, gamma is an adjustable parameter of certain kernel functions. The RBF is by far the most popular choice of kernel types used in SVM. This is mainly because of their localized and finite responses across the entire range of the real x-axis.

8.4.1.5 SVM Illustration

Consider a two-dimensional input space where training data x_i (i=1, ⋯, M) can be classified into two classes: class 1 and class 2. When a datum belongs to the class 1, take 1 for y_i. In the case of datum of the class 2, y_i is equal to -1. *i* denotes the numbers of classes.

The discriminant function is given by

$$D(x) = \sum_{i \in S} \alpha_i y_i K(x_i, x) + b \tag{8.11}$$

where $K(x_i, x)$ is called kernel and selected to suite the problem and $\alpha = (\alpha_1, \cdots \alpha_M)^T$. α_i is non-negative Lagrange multiplier and b being a constant. M is the number of data.

In a soft margin nonlinear SVM classification, it is necessary to maximize the margin parameter and generalization capability.

$$Q(\alpha) = \sum_{i=1}^{M} \alpha_i - \frac{1}{2} \sum_{i=1}^{M} \sum_{j=1}^{M} \alpha_i \alpha_j y_i y_j K(x_i, x_j) \tag{8.12}$$

Subject to

$$0 \le \alpha_i \le C \quad (i = 1, \cdots \mathrm{M}) \tag{8.13}$$

and

$$\sum_{i=1}^{M} y_i \alpha_i = 0 \quad (i = 1, \cdots \mathrm{M}) \tag{8.14}$$

where C is a cost parameter related to recognition rate and generalization capability. b is given by the following equation

$$b = y_i - \sum_{i \in S} \alpha_i y_i K(x_i, x_j) \tag{8.15}$$

Thus, the use of radial basis function kernel on two samples of ***x*** and ***x'***, represented as feature vectors in some input space,

$$K(x, x') = \exp(-\gamma \|x - x'\|^2) \tag{8.16}$$

leads to the discriminant function given by

$$D(x) = \sum_{i \in S} \alpha_i y_i \exp(-\gamma \|x_i - x'\|^2) + b \tag{8.17}$$

where γ is a parameter. The value of the kernel ranges between zero and one and decreases with distance between x and x'. Hence, in the present research work, the SVM was applied to two class models to diagnose the bearing fault on the induction motor. The definition of the kernel involves a gamma parameter γ. Smaller γ value leads to a simple decision boundary, whereas larger γ value leads to a complicated decision boundary.

Also, tuning of parameters C and γ were carried out by 8-cross-validation. Data was divided into 8 groups. Groups 1 to 7 were used as training data. Group 8 was used as evaluation data. Evaluation data is used for obtaining accuracy rate. Then, by changing the group for evaluation, 7 accuracy rates were obtained. Finally, the average accuracy rate was calculated. The above said process was repeated for different values of C and γ. Accuracy rate as functions of C and γ is shown in a two-dimensional map like Figure 8.23, which will be indicated in blue color with different grades. Deeper the color higher will be the accuracy rate. Values of C and γ with highest accuracy rate is used in the present study. Obtaining the optimum parameter values will be a tedious process, however the process that followed would be practically acceptable. The explanation about the parameters mentioned in the summary and the types of SVM are given in the Table 8.1. Above mentioned process was done in R language programming software.

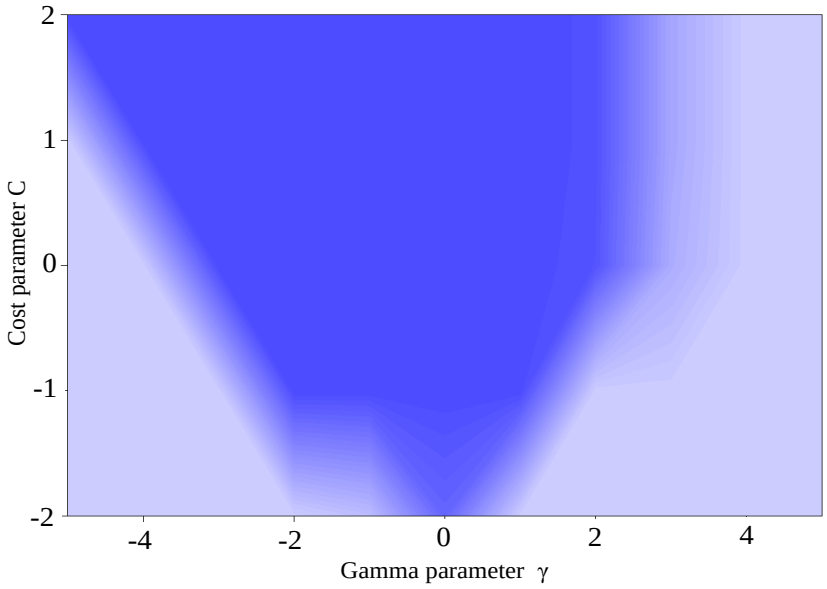

Figure 8.23 *Two-dimensional map illustrate difference between C and γ.*

Table 8.1 *Specification of SVM*

Type of SVM	**Soft Margin SVM**
Kernel	Radial Basis Function Kernel
Gamma parameter	2^{-4}
Cost parameter	2^{-1}
Number of support Vectors	8
Number of classes	2
Threshold in training	0
Threshold in prediction	0.5

The SVM-based diagnosis was carried out for hole, scratch, abrasion type scratch, using the amplitude of the 30 and 90 Hz characteristic frequency components. To match an industrial environment, the entire study of diagnosis was conducted without considering the rotating speed of the induction motor. The accuracy rate was derived as follows:

$$\text{Accuracy rate (\%)} = \frac{Number\ of\ data\ diagnosed\ properly}{Total\ number\ of\ data\ used\ for\ diagnosis} \text{X100} \qquad (8.18)$$

8.4.1.6 Diagnosis result

For easy understanding, the healthy motor, motor with hole, scratch, abrasion type scratch is indicated as H, HO, S, A, respectively. For conditions H–HO, H–S, HO-S, and H–A, 320 sets of data were used. Each dataset had amplitude of both 30 and 90 Hz frequency components. From the 320 sets, 240 were used as training data, and the remaining 80 were used as evaluation data. Four rotating speeds (1780, 1775, 1770, and 1765 min^{-1}) are combined and the diagnosis has been performed.

Table 8.2 shows the accuracy rate. 100 % accuracy rate is obtained in case of H-HO. The accuracy rates for H–S and HO–S are sufficiently high to be considered acceptable in practical applications. In the case of H–A, the accuracy rate was lower because of a significant overlapping between the healthy and faulty conditions (Figure 8.18). These significant overlaps were found between the different bearing conditions, making the diagnosis process tedious. The tests confirmed that the method can predict bearing failure in a running motor. The average accuracy rate was found to be 83.63 % and the proposed method was effective in making it suitable for variable speed application and in industrial environments.

Table 8.2 *SVM diagnosis result*

Bearing Conditions	Accuracy Rate (%)
H-HO	100
H-S	77.50
H-A	65.75
HO-S	91.25
Average	83.63

The role of gamma and cost parameters in deciding the accuracy rate is explained using HO-S bearing conditions and shown in Figure 8.24. The overlapping among features can be reduced and/or eliminated by use of the optimum gamma values. Gamma function transfers the linear

variable to higher dimension and controls the shape of the data. A small gamma value gives sharp end points, that differentiates the data from the other features. The larger value of cost parameter makes misclassification of training data, so small value of cost parameter along with small gamma value helps in increasing the accuracy rate. The three main parameters that alters the SVM accuracy rate shown in Figure 8.25. Techniques such as cross validation, re-sampling along with grid search are the straightforward ways to choose the values of cost and gamma parameters in SVM.

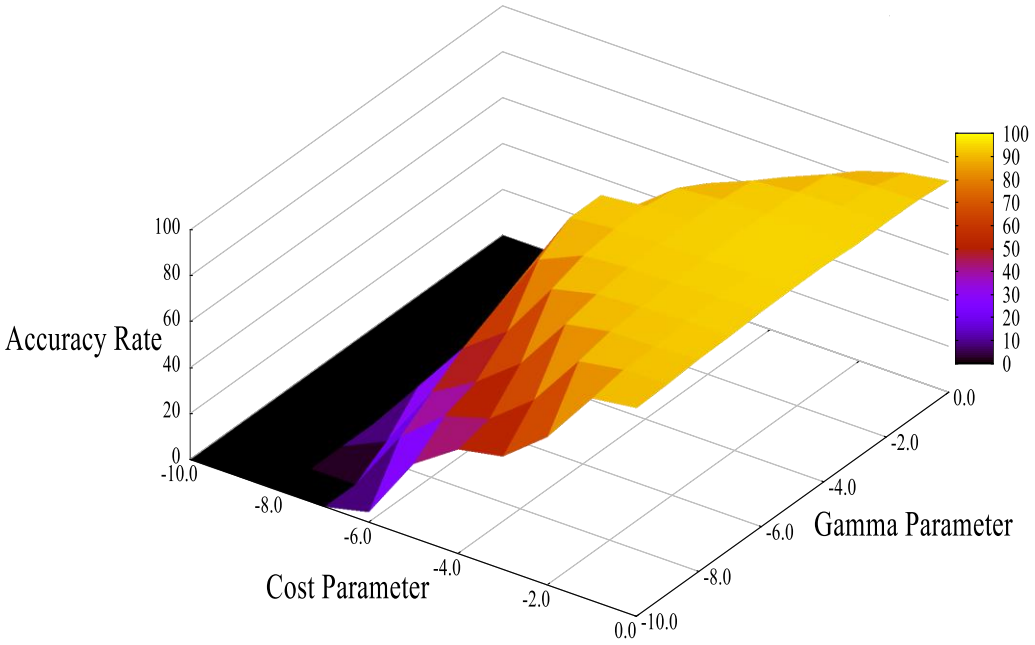

Figure 8.24 *SVM accuracy result of HO-S using cost and gamma parameter.*

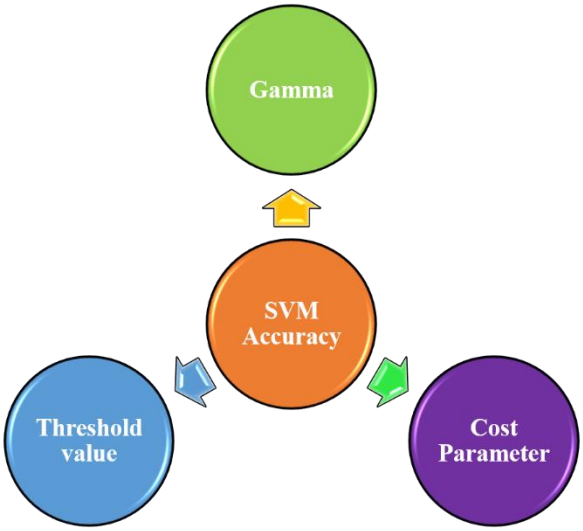

Figure 8.25 *Parameters of SVM.*

8.4.2 Naive Bayes Classifier Theorem (NBC) [4]

The amplitude of the characteristic frequency components 30 and 90 Hz show statistical variation, which get confirmed by kurtosis analysis. A statistical diagnosis method is selected for carrying the bearing failure analysis. The NBC Theorem is adopted because of its merits like multi-dimension input and suitable for continuous datasets.

8.4.2.1 Explanation of NBC Theorem

The NBC Theorem is a simple machine learning algorithm that is used to analyze the occurrence of an event based on the evidence or data. The algorithm is trained mainly for the classification problems in various domains, primarily used for the text classification issues like spam filtration of mail, predicting the health risk and their issues. Despite its simplicity, NBC is known for its quick and effective computation of unknown class from high dimensional datasets. It can perform the classification of both supervised and unsupervised data. In simple words, NBC Theorem is based on conditional probability with the

independence assumption of attributes. It is suitable for continuous, discrete, and categorical features data sets. NBC Theorem mainly classified into three types; Multinomial Naive, Bernoulli Naive, and Gaussian Naive.

- *Multinomial or Binomial NBC Theorem*

The Multinomial or Binomial Naive Bayes Network Theorem is one of the standard classic algorithm mainly used for data classification problem. The binomial model explicitly gives the count and frequency of occurred class or event based on the given data or evidence. Thus, class regulation is possible for irregular data sets and most suited for discrete data types. When classifying the data type problem, the binomial model measures the frequency of the class. Spam detection in e-mail is the practical example of Binomial Naive Bayes Network Theorem. This algorithm is unfit for continuous data types and random selection of data is not possible.

- *Bernoulli NBC Theorem*

Bernoulli NBC Theorem is a special algorithm which uses binary values (0,1) for indicating the data classifications. The method also opts for discrete data and inherently it solves the data classification problem. The Boolean function indicates the presence or absence of a class in data; 0 for absence and 1 for presence, respectively. The main principle behind the Bernoulli NBC Theorem is conditional probabilities and firmly suitable for a small group of data. The method does computational mistake for more number of classes because of its binary nature.

- *Gaussian NBC Theorem*

The Gaussian NBC Theorem is a simple algorithm among the three types and the main parameters are mean and statistic variance. In contrast to Binomial and Bernoulli NBC Theorems, Gaussian accepts input in the form of continuous datasets. It can perform the classification for both supervised and unsupervised data. Random selection is also possible

with Gaussian NBC Theorem. Additionally, a kernel function is included, which performs the mapping of large input data.

From the three models, Gaussian NBC Theorem is selected to accomplish the bearing failure diagnosis because of the statistical nature of training the data. The training is done in the unsupervised manner and each class exhibits own property of classification. The kernel function is included which may train the data in statistical way and additionally the probability function is included in the Gaussian NBC Theorem. Furthermore, the algorithm is trained by importing the data from four bearing conditions and training them properly.

8.4.2.2 Derivation of Gaussian NBC Theorem

The derivation of the algorithm is based on the NBC rules and assumptions of conditional independence. The main equation prescribes the goal of learning is P (X|Y), where X= (X_1, X_2…X_n). The Gaussian algorithm assumes that X_n is conditional independence; conditions to be specified at the time of training. The total data of X_n are allotted to Y. The value of each subset P (X|Y) is calculated according to the input X and the problem of estimating the training data is neglected.

Let us calculate the Gaussian NBC model for two input models (X=X_1, X_2). In this case, the Bayes algorithm can be derived as follows:

$$P(X|Y) = P(X_1, X_2|Y) \tag{8.19}$$

In the second step, the general property of the probability is calculated.

$$P(X|Y) = P(X_1|X_2, Y)\, P(X_2|Y) \tag{8.20}$$

The last step is to calculate the definition of conditional independence.

$$P(X|Y) = P(X_1|Y)\, P(X_2|Y) \tag{8.21}$$

Generally, the Bayes network for n attributes which satisfies the conditional independence assumption is given by,

$$P(X_1 \ldots X_n|Y) = \prod_{i=1}^{n} P(X_i|Y) \tag{8.22}$$

Both the Y and X_i are Boolean variables and assumed of conditional independence. In the current study, X takes the value of the bearing condition (X=4) and Y takes the value of the amplitude of characteristic frequency components 30 and 90 Hz.

8.4.2.3 Diagnosis procedure and the result

The entire diagnosis is performed without considering the rotating speed of the induction motor. The training data and diagnosis data are selected randomly in the ratio 70:30. Among 320 sets data of frequency components of 30 and 90 Hz, 224 data are used for training and 96 data for diagnosis. The selection condition is same for all the possible combinations of bearing. The entire diagnosis process is done using Python programming language.

The diagnosis result is shown in Table 8.3. The diagnosis is performed to four different combinations of bearing condition; (H-HO), (H-S), (H-A), and (HO-S), respectively. The average diagnosis rate is found to be 86.88 %, validating the proposed method is suitable to identify the small fault and able to identify the present condition of the bearing. Generally, it is a tedious process to diagnose the data when the overlapping occurs, but the NBC is effective in diagnosing all kinds of bearing. The statistical behavior of the NBC stands as the main reason for the high accuracy rate obtained when the diagnosis is performed without considering the rotating speed of the induction motor. The high accuracy rate is obtained even in the case of overlapping. Thus, on-line bearing failure detection is possible and suitable for industries.

Table 8.3 *NBC diagnosis result*

Bearing Conditions	Accuracy Rate (%)
H-HO	100
H-S	85.31
H-A	70.31
HO-S	91.88
Average	86.88

Generally, NBC Theorem and SVM are adopted for multi-dimensional data input, and either binary or multi-class outputs are possible. The performance of both NBC Theorem and SVM is said to vary depending upon the selection of kernel function. The output differs with the parameter selection. In the present study, NBC Theorem achieves better accuracy rate than SVM because of the formation of potential linear decision boundary. The probability function is included in case of NBC, which plays a key role in selecting and training the data sets. This can be achieved by changing the conditional dependence variable and kernel function. The NBC Theorem is also desirable because of its high speed. Though NBC shows higher accuracy rate than SVM, in case of reliability SVM takes the highest position. Because of the presence of probability function, there is considerable number of chance of missing data. However, the results of SVM depend on kernel function, cost parameter and gamma parameter and absence of probability function. The parameter optimization is also possible which reduces the missing data and gives high reliability.

8.4.3 K-nearest Neighbor Algorithm (KNN) [5]-[6]

KNN is non-parametric, versatile, and lazy learning algorithm used for both classification and regression problems. In addition, it issues a benchmark for other classifiers such as support vector machine and artificial neural network. It is lazy leaner because it memorizes the training data sets instead of learning the discriminative function. The instance-based learning helps in avoiding the errors by memorizing the training sets. In the model, non-

parametric function defines the parameters that are not fixed in advance and varies based on the data size. Its application includes economic forecasting, data compression and genetics.

KNN performs classification of testing data based on the k-nearest training samples round the test data. KNN depends on two things:

- A distance metric which is used to compute the distance between two points.
- The value of "k" defines the number of neighbors to be considered in the samples.

In case of continuous variables, Euclidean distance is used to calculate the distance between the two points (x_1, x_2, x_3,……x_n) and (y_1, y_2, y_3, ……..y_n) and is given by the following equation,

$$d = \{\sum_{i=1}^{n}(x_i - y_i)^2\}^{\frac{1}{2}} \quad (8.23)$$

The appropriate choice of parameter k makes better the accuracy and reduce errors. It makes the shape of the decision boundary. If the neighbor selection increases the k value, the boundary becomes smoother. If k decreases the boundary becomes flexible and hard. Technically, small k value gives more flexible fit with low bias and high variance. The disadvantage of the algorithm consumes large memory storage for storing all training data, prediction time is large and sensitive to the irrelevant features.

8.4.3.1 Diagnosis procedure and the result

The entire diagnosis is performed without considering the rotating speed of the induction motor i.e. amplitude data of the rotating speeds of 1780, 1775, 1770 and 1765 min^{-1} are combined. The training data and diagnosis data are selected randomly in the ratio 70:30. Among 320 sets of load current data, 224 data are used for training and 96 data for diagnosis. The selection condition is same for all the possible combinations of bearing. The entire

diagnosis process is done using Python programming language.

The diagnosis result is shown in Table 8.4. The diagnosis is performed to the following combinations; (H-HO), (H-S), (H-A), and (HO-S), respectively. The average diagnosis rate is found to be 90.55 %, validating the proposed method is suitable to identify the minor fault and able to identify the present condition of the motor. Thus, on-line bearing failure detection is possible and suitable for industries.

Table 8.4 *KNN diagnosis result*

Bearing Conditions	Accuracy Rate (%)
H-HO	100
H-S	86.25
H-A	79.65
HO-S	96.31
Average	90.55

In the present case, high accuracy rate is obtained for the k value 20. Figures 8.26 to 8.28 show the variation of accuracy rate with respect to k value. This clearly illustrates the data mining procedure of KNN algorithm.

The data boundary becomes smother with the increase in the value of k. In the present study, the k value is selected in way that it gives low bias and high variance as the result. The entire KNN algorithm depends on the k value and it reduces the depended factor and probability function when compared to NBC and SVM and stands as the advantage of KNN.

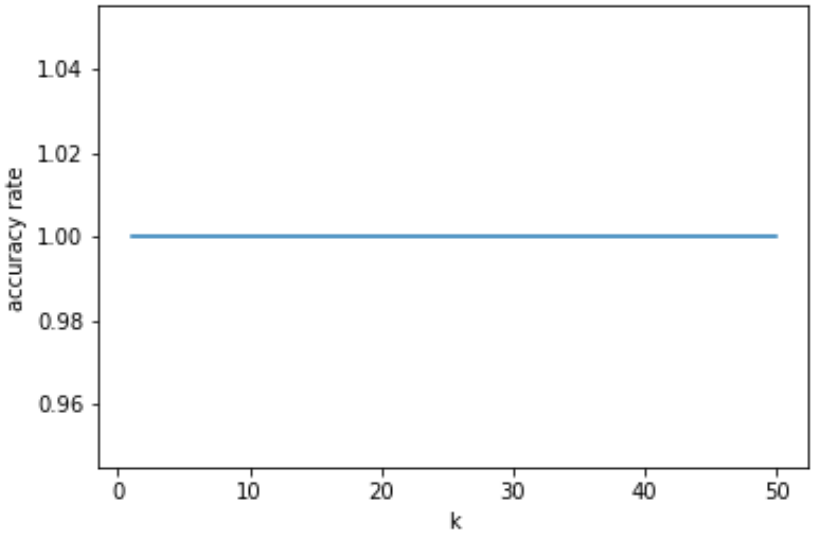

Figure 8.26 *Accuracy rate of H-HO bearing combination.*

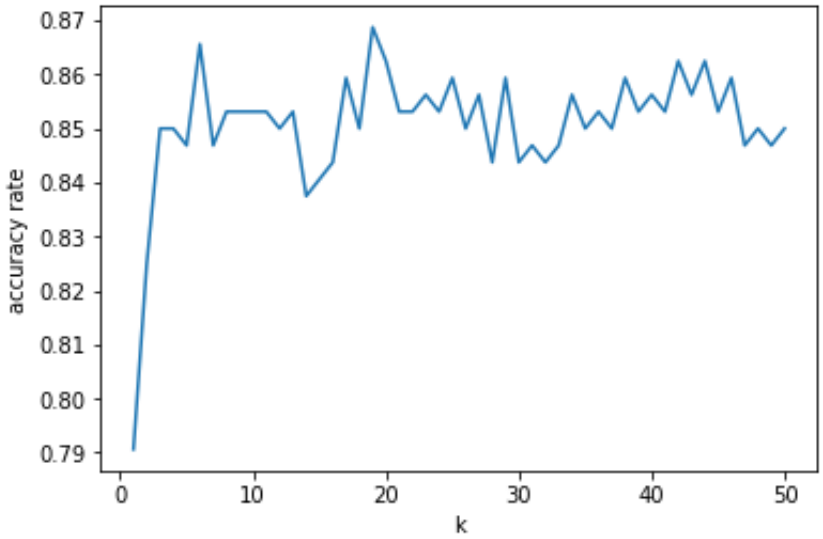

Figure 8.27 *Accuracy rate of H-S bearing combination.*

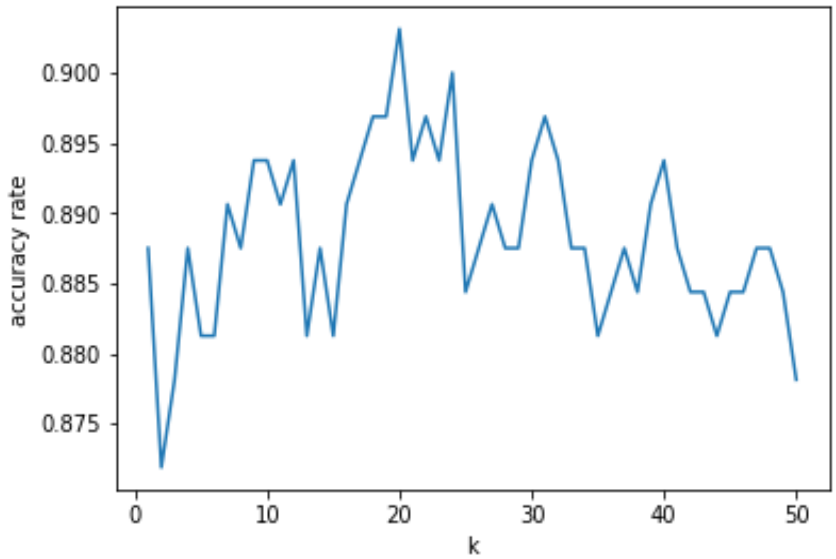

Figure 8.28 *Accuracy rate of HO-S bearing combination.*

8.4.4 Decision Tree Algorithm [7]-[8]

A decision tree is a dendritic classification model used both classification and regression problems. The classification is performed by the breakdown of data into smaller subsets and it is mainly based on the feature selection. The final structure is like a tree with branches and leaf nodes, that is the so-called decision tree. It provides a detailed framework about the consequences of the decisions. The application of decision tree is healthcare management, energy consumption of an individual, and fraudulent financial statements. In general, it can be used for all the decision-making problems.

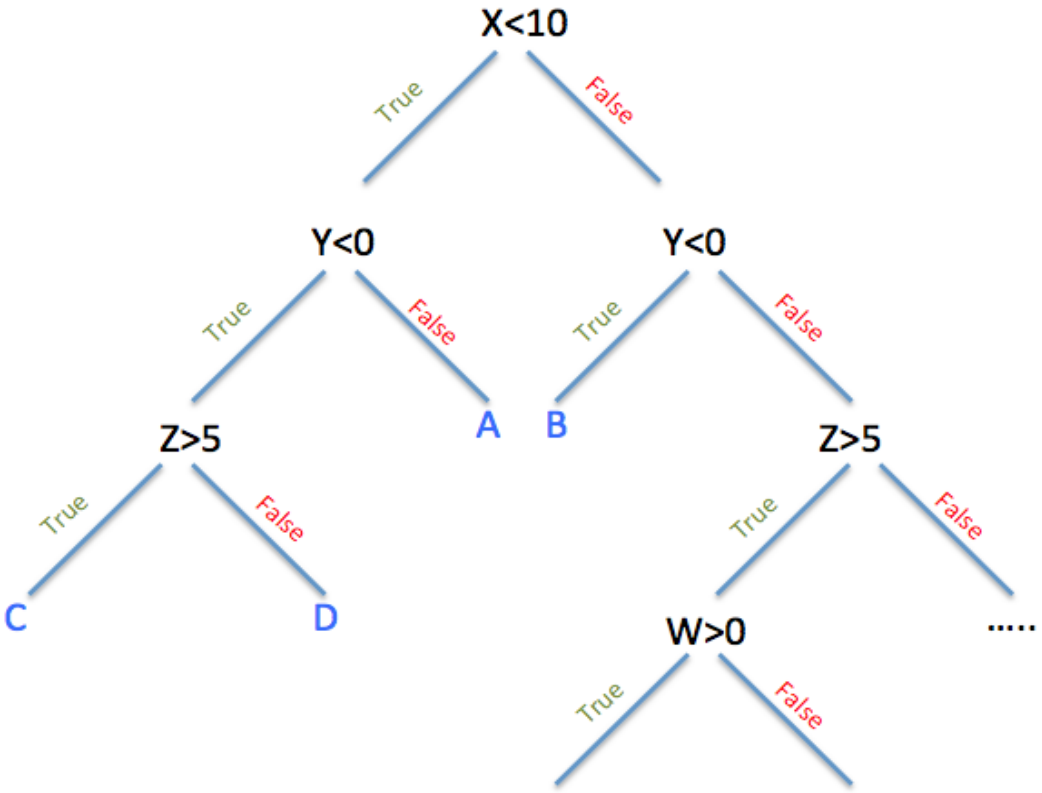

Figure 8.29 *Simple decision tree flowchart.*

A simple decision tree concept is shown in Figure 8.29. In the figure, four conditions are proposed, and they said to be X, Y, Z, and W. The flow of the decision tree goes while checking the condition at each junction. If the X condition passes through, the decision is made at that moment and the output is displayed. If the condition becomes false, it moves to the next stated condition and the process gets repeated until the output is decided. By this action, the accuracy rate can be increased as it is more like an iteration. As the iteration gets increased, the output also increases, and it is possible to get the high accuracy rate.

A decision tree is a tree where each node represents features (attributes), each branch represents decision (rule) and each leaf represents outcome (categorical or continuous value). A given set of data is divided into several sets stepwise. The model is recursively constructed

from the root node and analyzes every possible outcome of the effect of the condition.

When dividing, it is necessary to select explanatory variable so that it becomes bigger information gain. The information gain is determined by the difference between impurities before and after division. Information gain *IG* classification to X_1, X_2, ……X_n, at the node X is stated as follows,

$$IG = \mathrm{Imp}(X) - \sum_{i=1}^{n} p(X_i)\mathrm{Imp}(X_i) \tag{8.24}$$

where $\mathrm{Imp}(X)$ and $\mathrm{Imp}(X_i)$ are impurities before or after classification at node X, X_i and $p(X_i)$ is the rate of node X_i. Similarly, impurity is the index number that increases when plural classification data exist approximately the same rate in one node and given by equation of entropy. At node X, we have,

$$\mathrm{Imp}(X) = \sum_{i=1}^{c} p(i|X) \log_2 p(i|X) \tag{8.25}$$

Now, i is each classification and c is the number of all classification group.

Branch node generates a new branch node likewise, repeating until satisfying the following conditions. The constructed decision tree reaches optional depth depending on parameter n, the all of data after branches belong to the same classification, data quantity in the node is less, or can get a result only like random. The flow of the analysis using a decision tree is as follows. Input data are compared with explanatory variables at each node, and they go to the next node by the result. The total number of branches estimates the classification at the end of the final node. It is important to branch the parameter-n in the analysis. If n is small, the accuracy may be low. And if n is too large, it causes over fitting problems.

8.4.4.2 Diagnosis procedure and the result

The entire diagnosis is performed without considering the rotating speed of the induction motor i.e. amplitude data 30 and 90 Hz of the rotating speeds of 1780, 1775, 1770 and 1765 min^{-1}, are combined. The training data and diagnosis data are selected randomly in the ratio

70:30. Among 320 sets of data, 224 data are used for training and 96 data for diagnosis. The selection condition is same for all the possible combinations of bearing. The entire diagnosis process is done using Python programming language.

The diagnosis result is shown in Table 8.5. The diagnosis is performed to four different combinations of bearing condition; (H-HO), (H-S), (H-A), and (HO-S). The average diagnosis rate is found to be 86.02 %, validating the proposed method is suitable to identify the small fault and able to identify the present condition of the motor.

Table 8.5 *Decision Tree diagnosis result*

Bearing Conditions	Accuracy Rate (%)
H-HO	100
H-S	79.06
H-A	74.69
HO-S	90.31
Average	86.02

8.4.5 Random Forest [9]

The Random Forest is a classification method with majority rule using results of plural Decision Trees. First, Decision Tree is constructed by random data extracted from training data. Then the technique named tree bagging which is represented by the term B is performed for n number of times. Each Decision Tree is branched by explanatory variable that is selected from several variables and that is given as highest purity. These variables are picked randomly from the explanatory variable of training data.

More number of Decision Trees is constructed, and the class function is established. The output is concerned with majority of the voting and the final class is declared. Better accuracy rate is obtained than Decision Tree as it is the extended version. The time consumed for

diagnosis is long when compared to the Decision Tree. However, at the end, the diagnosis is performed and few over fitting is caused. The class division and the selecting/deciding the result of the majority voting are performed by the B function, which is nothing but the tree bagging. The working architecture of Random Forest is shown in Figure 8.30.

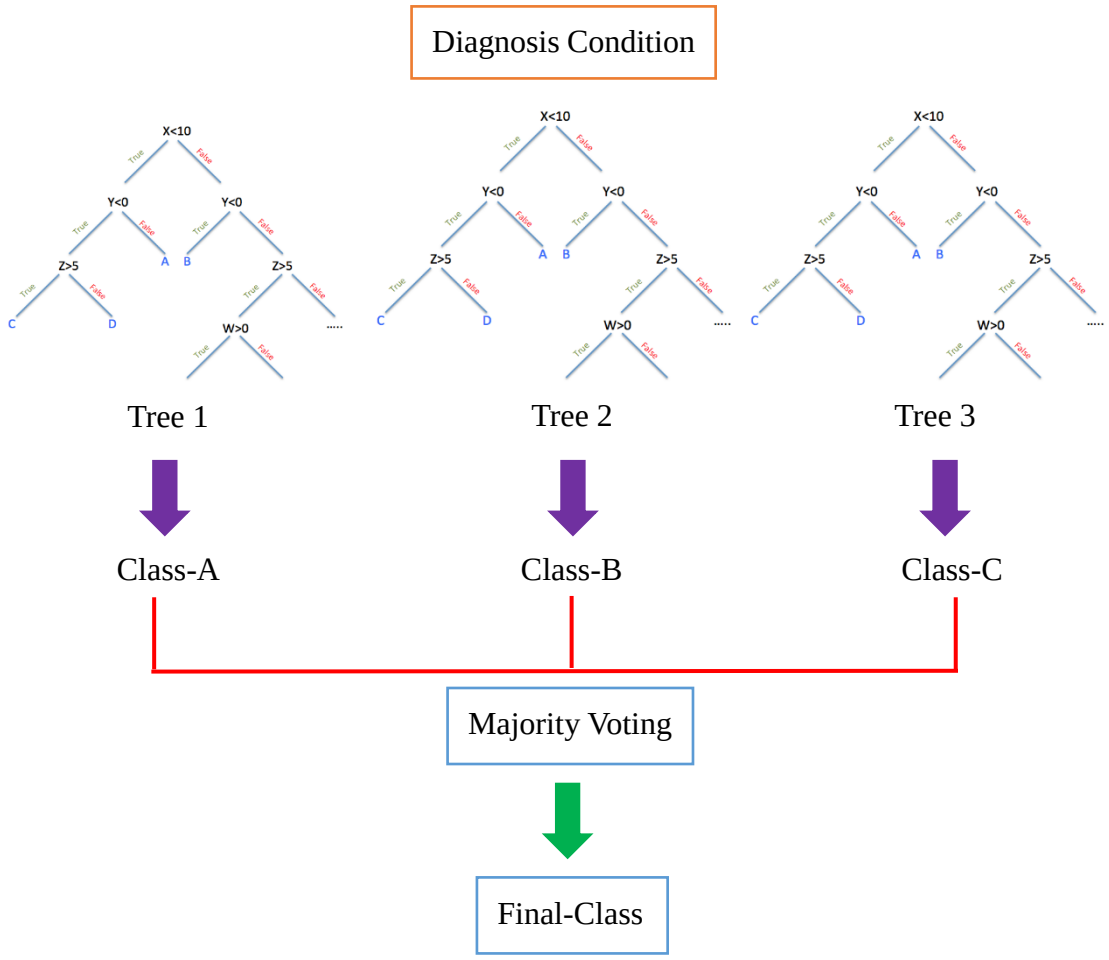

Figure 8.30 *Random Forest architecture.*

8.4.5.2 Diagnosis procedure and the result

The entire diagnosis is performed without considering the rotating speed of the induction motor (1780, 1775, 1770 and 1765 min^{-1}, are combined). Same as Decision Tree, the training data and diagnosis data are selected randomly in the ratio 70:30. Among 320 sets of data, 224 data are used for training and 96 data for diagnosis. The selection condition is same for all the possible combinations of bearing. The entire diagnosis process is done using Python programming language.

The diagnosis result is shown in Table 8.6. The diagnosis is performed to four different combinations of bearing condition; (H-HO), (H-S), (H-A), and (HO-S). The average diagnosis rate is found to be 87.80 %, validating the proposed method is suitable to identify the small fault and able to identify the present condition of the motor.

Table 8.6 *Random Forest diagnosis result*

Bearing Conditions	Accuracy Rate (%)
H-HO	100
H-S	80.94
H-A	77.36
HO-S	92.88
Average	87.80

8.5 Deep Learning Algorithm (DL Algorithm) [10]-[12]

In a pneumatic, chemical, medical, aerospace and renewable energy, the usage of neural network has been increased and in the last few decades, new techniques using the artificial neural network have developed. The artificial neural network model shows less dependence towards the process and can constantly receive the new data. The deep neural network is one of the subsets of machine neural network in Artificial Intelligence and has its application

extended to image preprocessing and medical fields. The network framed in the deep neural network can analyze both the supervised and un-supervised algorithm. Simply the deep neural network can be defined as the complicated neural network with multiple layers (more than one hidden layer). Deep neural network algorithm uses a large amount of data and information that directly obtained in the form of images, signals and text to perform the application related to the neural network.

The standard DL algorithm can be divided into three models; Denoising Auto-Encoders (DAE), Deep Belief Network (DBN) and Convolutional Neural Network (CNN). The three models are constructed with their own property of feature learning and with different base models. The DAE is used to train the un-supervised feature and DBN is used for acquiring the joint distribution between the data and the labels. The DBN belongs to the category of probabilistic generative models. CNN is widely used for training the un-supervised features and has some advantages like shift-variance, weight sharing, high accuracy rate, and data encoding.

8.5.1 Basic Concept of CNN

Among the various architecture of DL, in the present study, CNN is selected because of its various application and advantages. Typically, CNN structure consists of two layers; feature extraction layer and feature mapping layer. The neuron plays a significant role in connecting both the layers. The feature extraction layer consists of a local acceptable domain of the previous layer which is connected through the neuron. The local characteristics are extracted and forwarded to feature mapping layer, which consists of multiple feature mapping of each network. Generally, feature mapping is a plane filled with neurons of equal weight. Each convolution layer in the neural network is followed by the calculation layer that is used to perform the calculation of features.

8.5.2 Construction of CNN

The basic structure of CNN model is shown in Figure 8.31. A feed-forward network consists of input layer, hidden layer and output layer. CNN is constructed using the auto-encoder system, which suits the best for training the un-supervised algorithm.

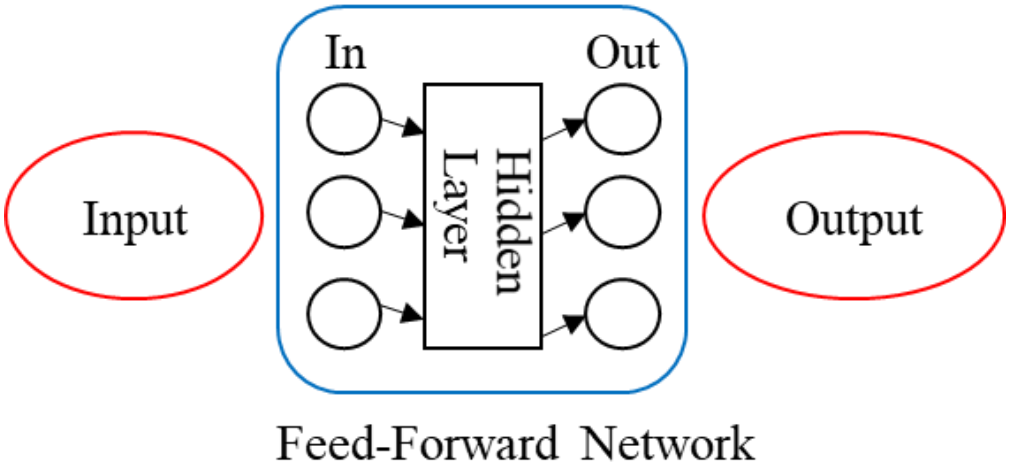

Figure 8.31 *The basic structure of CNN model.*

Additionally, the setup is comprised of one or more convolutional layers and pooling layers and they belong to the category of the feed-forward neural network. A pooling network is added to the basic structure to reduce the overlapping effects. It just performs the filtration process and also a simple discretization process. CNN with the following architecture is used for both the modelling and classification task. The layers of the neural network are fully interconnected in one direction from the input layer to the output layer including the hidden layer. The pooling layers are placed between the hidden layers to perform the data preprocessing, and data training is performed in the hidden layer. The counting or number of neurons in the hidden layer is decided based on input and output patterns that must be recognized. Additionally, auto-encoder consists of two parts; encoder and decoder. The encoder is used to extract the feature from the input data and decoder for reconstructing the sampling data from the hidden layer. The simple auto-encoder is shown in Figure 8.32, where

x represents the input layer $\{x_1, x_2 \ldots x_n\}$, h denotes the hidden layer $\{h_1, h_2 \ldots h_m\}$ and y is the outcomes of the output layer $\{y_1, y_2 \ldots y_p\}$. It is clear from Figure 8.32, the weight matrix (W_1 and W_2) filled with neurons connects the adjacent layers.

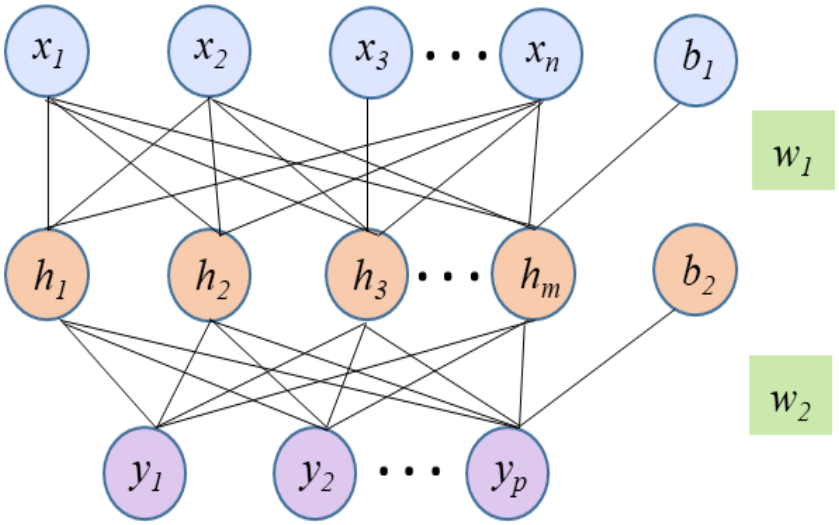

Figure 8.32 *Simple auto encoding system.*

The encoding process is defined as

$$H = F_e(W_1x+b_1) \tag{8.26}$$

where F_e is the activation function of encoder and b_1 is the encoder bias vector. Similarly, the definition of decoding is defined as

$$R = F_d(W_2h+b_2) \tag{8.27}$$

where F_d is the activation function of decoder, and b_2 is the decoder bias vector. According to the number of input, the parameters $\{W_1, W_2, b_1, b_2\}$ are adjusted. The CNN network for the present study is constructed with two pooling layers and two hidden layers and constituted by the auto-encoder system. The architecture diagram is shown in Figure 8.33.

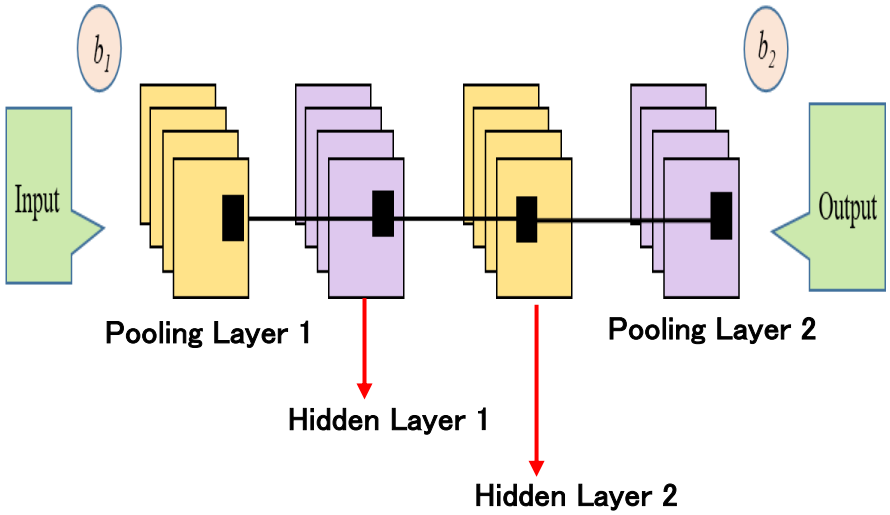

Figure 8.33 *Architecture of proposed CNN model using auto encoding system.*

8.5.3 Diagnosis Procedure

In the present study, an attempt has been made to employ the concept of the DL with CNN architecture in motor failure analysis as a diagnostic tool. Since the induction motor bearing failure diagnosis is likely to have a complex non-linear mapping problem, CNN of three-layer feed-forward neural network is selected, so that both the input and output are defined as multiple variables without clear linear relationships.

The diagnosis is performed to four different combinations of bearing condition; (H-HO), (H-S), (H-A), and (HO-S). The entire diagnosis is performed without considering the rotating speed of the induction motor i.e. amplitude data of load current of 30 and 90 Hz, four rotating speed (1780, 1775, 1770, and 1765 min^{-1}) are combined. The data sets of 30 and 90 Hz frequency components are selected randomly in the ratio 70:30. The 70% data of each bearing condition are used as the training samples and 30% are used as the diagnosis samples. A total of 336 data samples is used for training and 144 as diagnosis samples. Since DL follows stack flow method for diagnosis, healthy (H), hole (HO) and scratch (S), and abrasion type scratch (A) take stack value 0, 1, 2 and 3, respectively.

The diagnosis result is shown in Table 8.7. The average diagnosis rate is found to be 86.88 %, validating the proposed method is suitable to identify the minor fault and able to identify the present condition of the motor. The diagnosis result for the case H-S, HO-S, H-A is shown from Figures 8.34 to 8.36, respectively. The loss of the proposed CNN model is shown in Figure 8.37.

Table 8.7 *CNN diagnosis result*

Bearing Conditions	Accuracy Rate (%)
H-HO	100
H-S	80.66
H-A	79.58
HO-S	87.29
Average	86.88

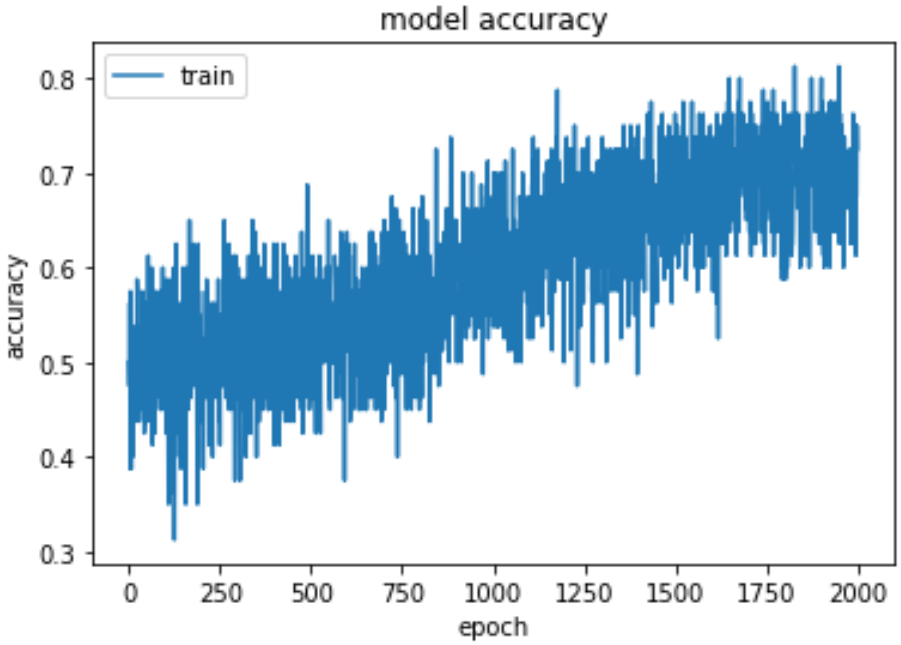

Figure 8.34 *CNN diagnosis result of H-S.*

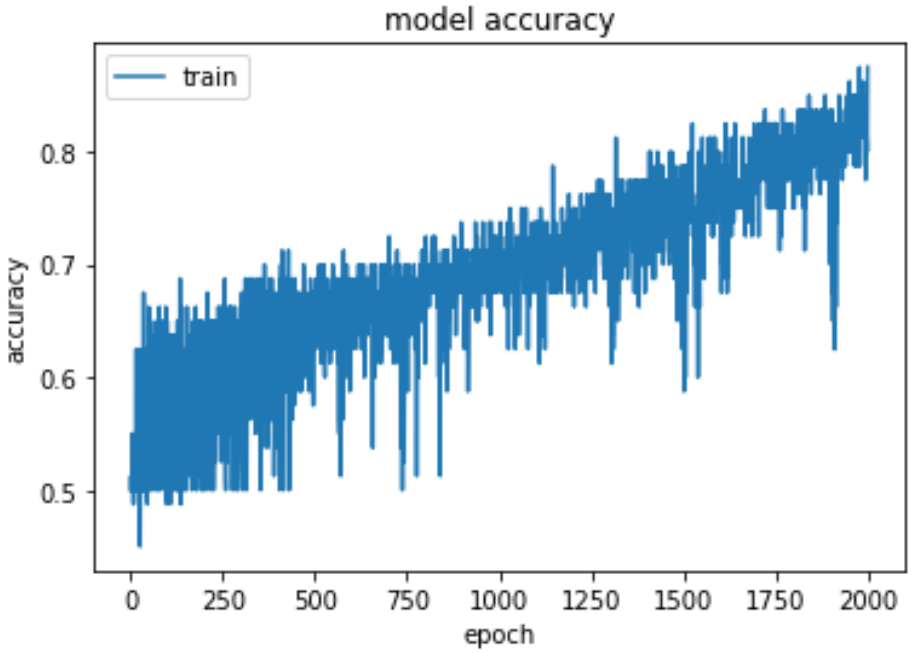

Figure 8.35 *CNN diagnosis result of HO-S.*

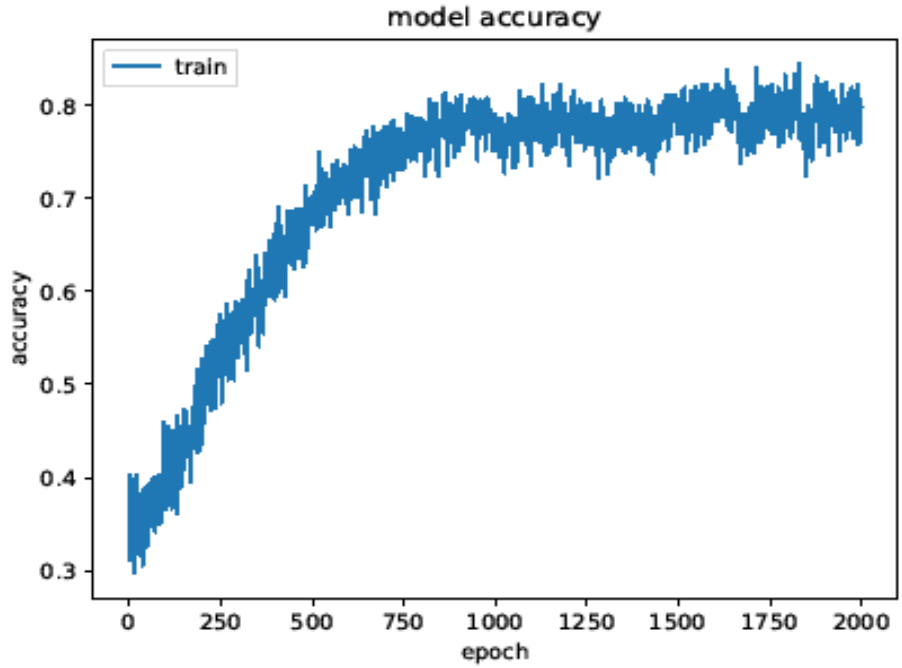

Figure 8.36 *CNN diagnosis result of H-A.*

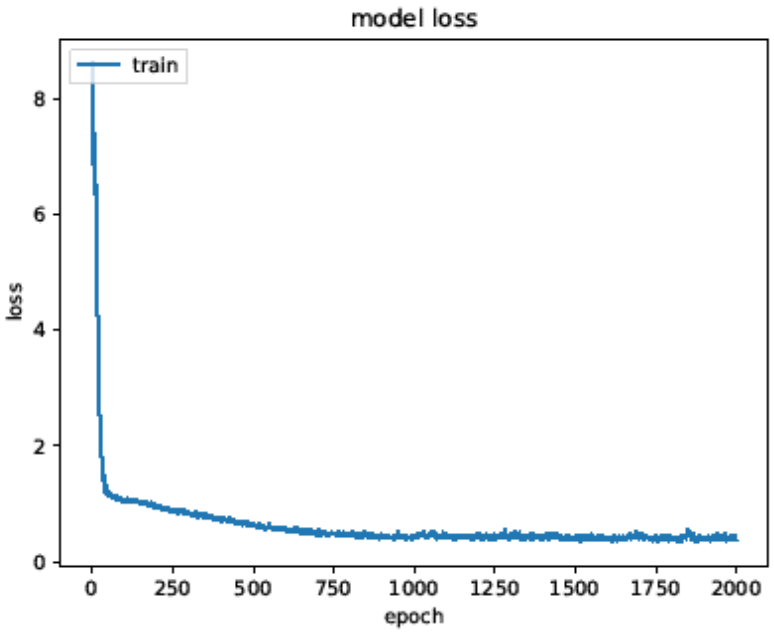

Figure 8.37 *CNN diagnosis loss.*

An epoch is a single step in training the neural network. In other words, the number of epochs is related to the number of rounds of optimization that is required to train the data. It contains one forward pass and one backward pass for all the training samples. The error on training the data can be reduced with more rounds of optimization. The error performance or loss is reduced as the number of epochs increases. But at the same time, more selection of epochs can create a critical point where the network becomes over-fit to the training data and starts to lose the performance. For that reason, selection of epochs should be given importance. A number of iteration is carried out for all the input data set based on the value of epochs. The number of iteration is decided based on the batch size; the number of training samples in one forward/backward pass. Therefore, epoch needs to be carefully selected based on the available data sets. The relation between epoch and loss is given by equation,

$$\text{Epoch} = \frac{1}{loss} \tag{8.28}$$

Thus, loss can be reduced by increasing the number of iteration or the epoch.

8.6 Summary

In this chapter, a detail study about the application of machine learning algorithms and the deep learning to bearing failure diagnosis is carried out. The hole, scratch, and the abrasion type scratch are selected for the analysis and the diagnosis is performed. To the entire diagnosis, the amplitude of the frequency 30 and 90 Hz components of load current has been used. The obtained diagnosis rate found to be acceptable in terms of both machine learning algorithm and deep learning algorithm. Thus, the proposed spectral frequencies applied to detect the motor bearing failure are appropriate.

Among the machine learning algorithm, SVM, KNN are parameters-based diagnosis function and the Decision Tree, Random Forest and NBC belong to the category of probability-based diagnosis function. The results of all machine learning algorithm belong to the same range, yet KNN takes the highest accuracy rate. From the study, the diagnosis method can be selected according to the application. For example, if the more number of bearing conditions is discussed, KNN and SVM are the best algorithm. If the number of bearing conditions are less, for example two or three classes, it is better to go with Random Forest, Decision Tree or NBC. These Random Forest, Decision Tree or NBC algorithm becomes complex in case of multiple classes, this is because of the probability-based procedure, as it takes more time for commutation and produces lower accuracy rate.

Finally, a trail to bring the deep learning algorithm to the motor fault diagnosis is achieved and the results are promising and acceptable. It has many advantage over machine learning algorithm, as it can be trained for any kind of application. The time consumption is less, and programming skill is not required to tune the parameter. The only disadvantage of CNN is the requirement of the large data count. If the number of available data is more, high diagnosis rate is obtained.

Chapter 9
Conclusions

9.1 Conclusion

This thesis presents the diagnosis method to detect the minor electrical and mechanical failure occurring in the induction motor. The Fast Fourier Transform (FFT) analysis is carried out by characterizing the magnitude of the load current spectrum at various frequencies and has been considered as the main feature. The problems in the data analysis and diagnosis due to the overlapping of features and the diagnosis rate which requires special technique or control methods to detect the fault. To enhance the accuracy of the present research work, a proper diagnosis method has been done with the help of the Machine Learning Algorithm (MLA), Clustering Techniques like Self Organizing Map (SOM) and Artificial Intelligence method (AI). The most commonly used MLA algorithm is Support Vector Machine (SVM). Among the AI, Deep Learning Algorithm (DL) has been selected for performing the induction motor fault diagnosis. The validity of the proposed method is verified by the experiments carried out in the laboratory.

Among the various electrical and mechanical faults of the induction motor, short-circuit insulation failure of stator winding fault, broken rotor bar fault and bearing failure has been selected and the diagnosis is performed.

9.1.1 Short-Circuit Insulation Failure

Till now it was found that more than two-turn short-circuit fault could be diagnosed and still one-turn short-circuit fault could not be diagnosed properly. It is well known fact, at motor running condition once the fault begins with the one-turn and if it continues to proceed further, the chance of getting the turns to count to increase. The thermal deterioration of insulating material progresses gradually and certainly increases the number of short-circuiting turns and finally the motor breakdown at some point of time. Thus, it is always better to detect the

minor fault at the early stage.

The research work is broadly classified into three distinct categories. First, frequency-spectrum analysis of the load current is performed, and characteristic frequency components are extracted by a Fast Fourier Transform (FFT). Then, the distortion ratio is derived using these components. Finally, the diagnostic method is proposed using a support vector machine (SVM), and diagnosis of one-turn stator winding fault is achieved.

9.1.2 Broken Rotor Bar Failure

Since there is no solution and research results that show the defect of identifying the slight failure in the broken rotor bar (one broken rotor bar), the present thesis work focused on diagnosing the minor fault. A three-step analysis is carried out, at first using the characteristic frequency components, the trace of investigating the existence or non-existence of the broken rotor bar is performed. Next, the analysis is performed to identify the number of the broken rotor bar(s) and continues till 4 broken bars. Finally, clustering is carried out using SOM. The problem of other diagnostic methods has been overcome and a solution of identifying the minor one broken rotor bar is achieved with high accuracy rate.

9.1.3 Bearing Failure

Accordingly, for bearing faults, many research reports are available and have explained the differences between the healthy and faulty motor. In most of the cases, the hole has been considered as the faulty factor and the dimension are large. The research report lacks in detecting the minor bearing faults and several studies, experiments are highly required to gain adequate expertise about the physical location of the fault. The challenging factors still exist, and further research is necessary.

The proposed method of scrutiny using FFT analysis and SVM diagnosis is employed to identify the bearing faults in case of scratch as the possibilities are more when considering the hole. Additionally, several analyses with respect to the hole are also performed to have a detailed study of its nature. Special compound bearing fault analysis (hole and scratch), and

abrasion scratch analysis is accomplished, and they seem to have an impact on the bearing fault as like hole and scratch. The diagnosis results confirm that not only the hole has the major factor in determining the bearing faults, but also the scratch and abrasion scratch. The minor bearing fault detection is possible and identifying the present state of the bearing is also achieved. In case of hole, minor fault detection is made possible with the hole dimension of 0.5 mm diameter and similarly for scratch, the detection is achieved till 5 mm scratch length. The role of the physical location of the fault is clearly investigated with the multiple fault analysis, orientation analysis, and localization analysis. The analysis is performed ignoring the rotating speed of the induction motor. This is one of the important criteria of the proposed system and begins the revolution to the next step of research.

9.1.4 Common and Multiple Fault Diagnosis Method

The common diagnosis method to identify the broken rotor bar fault and the bearing fault is proposed. The FFT analysis is performed and the diagnosis by SVM. The entire analysis is performed without considering the rotating speed of the induction motor. The method can identify the two different mechanical faults and identifying the present state of the motor is made possible. The SVM based diagnosis method overcomes the problem of overlapping and the high accuracy rate is obtained.

To the same motor, two kinds of mechanical faults are induced the and the diagnosis method of common fault is applied to extend the application. The acceptable diagnosis rate is obtained. The selection of the frequency components is correct, and the reliability is high, stating the proposed method is suitable for diagnosing the induction motor failure.

9.1.5 Comparison of Machine Learning Algorithm and Artificial Intelligence Method

A detail study about the application of machine learning algorithms and the deep learning to bearing failure diagnosis is carried out. To the entire diagnosis, the amplitude of the frequency 30 and 90 Hz components of load current has been used. The obtained diagnosis rate found to be acceptable in terms of both machine learning algorithm and deep learning algorithm. Among the machine learning algorithm, SVM, KNN are parameters-based diagnosis function

and the Decision Tree, Random Forest and NBC belong to the category of probability-based diagnosis function. The results of all machine learning algorithm belong to the same range, yet KNN takes the highest accuracy rate. From the study, the diagnosis method can be selected according to the application.

The deep learning algorithm is applied to the motor fault diagnosis and the results are promising. It has many advantage over machine learning algorithm, as it can be trained for any kind of application. The time consumption is less, and programming skill is not required to tune the parameter.

9.1.6 Summary

The main objective of the thesis is to propose an simple method is to detect the minor fault occurring on the induction motor at the earlier stage. With the results of pinpointing the healthy and faulty motor, and the diagnosis is performed without considering the rotating speed of the induction motor, the possibility of applying the techniques to the industries is high. Additionally, it is well-suited for speed varying application.

9.2 Future Work

Though the electrical and mechanical faults are verified experimentally, the failure analysis of the induction motor is still the challenging factor in the industrial environment. The following works are to be implemented in the future for increasing the reliability and the application of the failure diagnosis method.

- Clear and physical explanation regarding the difference observed between 30 and 90 Hz in case of motor failure. From this, it is possible to examine the applicability of the proposed method to other electric motors.

- The proposed system gives the knowledge about the presence or absence of the fault on the induction motor. But no information regarding the level of defects is available. The decision whether to continue or change the motor is not evident through the proposed study. This study is required or necessary to avoid the unnecessary cost and time caused. The results may give usefulness to the industries, because the condition monitoring and the maintenance can be achieved easily.

- Though the short-circuit fault has been diagnosed, the next step of research will be identifying the exact location and position of the raised short-circuit.

- When the data count is increased or if several cases are discussed, the proposed method fails in identifying the kinds of faults. In the future, a method to detect and state the kinds of fault will be proposed.

- To employ the method in the industrial environment, additional experiments using an inverter as a power supply to be done, as most of the motors in the factories are made to run using the inverter.

"Towards the bridge, making a way for the electrical machine"

References

Chapter 1

[1] V. Thorsen and M. Dalva, “A survey of faults on induction motors in offshore oil industry, petrochemical industry, gas terminals, and oil refineries,” *IEEE Transactions on Industrial Applications*, vol. 31, no. 5, pp. 1186–1196, 1995.

[2] D. Tobon-Mejia, K. Medjaher, N. Zerhouni, and G. Tripot, “A data-driven failure prognostics method based on mixture of Gaussians hidden markov models*,” IEEE Transactions on Reliability,* vol. 61, no. 2, pp. 491–503, Jun. 2012.

[3] Abdenour Soualhi, Hubert Razik, Guy Clerc, and Dinh Dong Doan, “Prognosis of Bearing Failures Using Hidden Markov Models and the Adaptive Neuro-Fuzzy Inference System,” *IEEE Transaction on Industrial Electronics,* vol. 61, no. 6, pp. 2864–2874, Jun. 2014.

[4] P.F. Albrecht, J.C. Appiarius, R.M. McCoy, E.L. Owen, and D.K. Sharma, "Assessment of the Reliability of Motors in Utility Applications-Updated", *IEEE Transactions on Energy Conversion,* vol. 1, no. 1, pp. 39-46, 1986.

[5] S. M. A. Cruz and A. J. M. Cardoso, “Stator winding fault diagnosis in three-phase synchronous and asynchronous motors, by the extended Park's vector approach”, *IEEE Transactions Industry Applications,* vol.37, no. 5, pp. 1227-1233, 2001.

[6] J. S. Hsu, “Monitoring of defects in induction motors through air-gap torque observation”, *IEEE Transactions Industry Applications,* vol. 31, no. 5, pp.1016-1021, 1995.

[7] O. A. Mohammed, N. Y. Abed, and S. Ganu, "Moldeling and Characterization of Induction Motor Internal Faults Using Finite-Element and Discrete Wavelet Transforms", *IEEE Transactions on Magnetics*, vol. 42, no. 10, pp. 3434-3436, 2006.

[8] J. Cusido, L. Romeral, J. A. Ortega, J. A. Rosero, and A. Garvia Espinosa, "Fault Detection in Induction Machines Using Power Spectral Density in Wavelet Decomposition", *IEEE Transactions Industry Electronics,* vol. 55, no. 2, pp. 633-643, 2008.

[9] G. C. Stone, "Condition Monitoring and Diagnostics of Motor and Stator windings – A Review", *IEEE Transactions on Dielectric and Electrical Insulation,* vol. 20, no. 6, pp. 2073-2080, 2013.

[10] Y. J. Kim, S. H. Hong, T. S. Kong and H. D. Kim, "On-Site Application of Novel Partial Discharge Monitoring Scheme for Rotating Machine", *IEEE Transactions on Dielectric and Electrical Insulation conference,* Washington, USA, pp. 85-88, 2015.

[11] G. C. Stone, C. Chan and H. G. Sedding, "Relative Ability of UHF Antenna and VHF Capacitor Method to Detect Partial Discharge in Turbine Generator Stator Winding", *IEEE Transactions on Dielectric and Electrical Insulation,* vol. 22, no. 6, pp. 3069-3078, 2015.

[12] H. Li, R. Li, B. Hu, C. Yan and Q. Guo, "Application of Guided Waves and Probability Imaging Approach for Insulation Damage Detection of Large Generator Stator Bar", *IEEE Transactions on Dielectric and Electrical Insulation,* vol. 22, no. 6, pp. 3216-3225, 2015.

[13] E. Wiedemburg, G. Frey and J. Wilson, "Early Intervention", *IEEE Industry Applications Magazine,* vol.10, no.5, pp.34-40, 2004.

[14] H. Nakamura and Y. Mizuno, “Probabilistic Diagnosis of Short-Circuit Faults and Insulation Deterioration of Stator Winding of Motor”, *IEEJ Transactions Industry Applications,* Vol. 132, no. 2, pp.258-267, 2012.

[15] F. Perisse, P. Werynski, and D. Roger, “A New Method for AC Machine Turn Insulation Diagnostic Based on High Frequency Resonances", *IEEE Transactions on Dielectric and Electrical Insulation,* vol. 14, no. 5, pp. 1308-1315, 2007.

[16] S. Savin, S. Ait-Amar and D. Roger, “Turn-to-Turn Capacitance Variations Correlated to PDIV for AC Motors Monitoring”, *IEEE Transactions on Dielectric and Electrical Insulation,* vol. 20, no. 1, pp. 34-41, 2013.

[17] S. Das, P. Purkait, C. Koley and S. Chakravorti, “Performance if a Load-Immune Classifier for Robust Identification of Minor Faults in Induction Motor Stator Winding”, *IEEE Transactions on Dielectric and Electrical Insulation,* vol. 21, no. 1, pp. 33-44, 2014.

[18] H. Nakamura, Y. Mizuno and T. Suzuki, “Diagnosis of short circuit faults in stator winding of motor based on Hidden Markov Model”, *IEEJ Transactions on Power and Energy,* vol.126, no. 9, pp. 917-925, 2006.

[19] H. Nakamura, T. Ohno, T. Abe and Y. Mizuno, “Probabilistic Diagnosis of Short Circuit Fault of Motor on the Basis of Feature Distribution”, *IEEJ Transaction on Industrial Application,* vol.130, no.9, pp.1059-1066, 2010.

[20] Y. Yagami, C. Araki, Y. Mizuno and H. Nakamura, “Turn-to-Turn Insulation Failure Diagnosis of Stator Winding of Low Voltage Induction Motor with the Aid of Support Vector Machine”, *IEEE Transactions on Dielectric and Electrical Insulation,* vol. 22, no. 6, pp. 3099-3106, 2015.

[21] X. Jin, M.H. Azarian, C. Lau, L.L. Cheng, and M. Pecht, "Physics of failure analysis of cooling fan," *PHM-Shenzhen Conference,* pp. 1-8, China, May 2011.

[22] "Report of large motor reliability survey of industrial and commercial installations, Part I," *IEEE Transaction on Industrial Application,* vol. IA-21, no.4, pp. 853-864, Jul. 1985.

[23] W. Wang and M. Pecht, "Economic analysis of canary-based prognostics and health management," *IEEE Transaction on Industrial Electronics,* vol. 58, no. 7, pp. 3077-3089, Jul. 2011.

[24] William R. Finely, "Troubleshooting Induction Motors", *Siemens Energy and Automation Report 2016,* pp. 01-04, 2016.

[25] T.J. Kang, J. Kim, S.B. Lee, and C. Yung, "Experimental Evaluation of Low-Voltage Offline Testing for Induction Motor Rotor Fault Diagnosis", *IEEE Transactions on Industrial Applications,* vol. 51, no. 2, pp. 1375–1384, 2015.

[26] I.Y. Onel, and M.E. Hachemi Banbouzid, "Induction Motor Bearing Failure Detection and Diagnosis: Park and Concordia Transform Approaches Comparative Study", *IEEE Transactions on Mechatronics,* vol. 13, no. 2, pp. 257–262, April 2008.

[27] NTN Corporation, "Healthy Monitoring of Bearing of Induction Motor", CAT. No. 3017/J.

[28] A.H. Bonnett, and G.C. Soukup, "Rotor failures in squirrel cage induction motors", *IEEE Transactions on Industry Applications,* vol. IA-22, No.6, pp.1165- 1173, 1986.

[29] G.B. Kliman, J. Stein, and R.D. Endicott, "Noninvasive Detection of Broken Rotor Bars in Operating Induction Motors", *IEEE Transaction on Energy Conversion,* vol.3, no.4, pp.873-879, 1988.

[30] B. Yazici, and G.B. Kliman, "An Adaptive Statistical Time-Frequency Method for Detection of Broken Bars and Bearing Faults in Motors Using Stator Current", *IEEE Transaction on Industrial Application,* vol. 35, no. 2, pp.442-452, 1999.

[31] O.A. Mohammed, N.Y. Abed, and S. Ganu, " Moldeling and Characterization of Induction Motor Internal Faults Using Finite-Element and Discrete Wavelet Transforms ", *IEEE Transactions on Magnetics,* vol.42, no.10, pp.3434- 3436, 2006.

[32] S.H. Kai, H. Henao, and G.A. Capolino, "Diagnosis of Broken-Bar Fault in Induction Machines Using Discrete Wavelet Transform Without Slip Estimation", *IEEE Transaction on Industrial Application,* vol. 45, no. 4, pp.1395- 1404, 2009.

[33] M.N. Uddin, W.Wang, and Z.R.Huang, " Modeling and Minimization of Speed Ripple of a Faulty Induction Motor With Broken Rotor Bars ", *IEEE Transaction on Industrial Application,* vol. 46, no. 6, pp.2243-2250, 2010.

[34] M. Riera-Guasp, J.A. Antonino-Daviu, J. Roger-Folch, and M.P.M. Palomares, "The Use of the Wavelet Approximation Signal as a Tool for the Diagnosis of Rotor Bar Failures", *IEEE Transaction on Industrial Application,* vol. 44, no. 3, pp.716-726, 2008.

[35] H. Nakamura, Y. Yagami, C. Araki, and Y. Mizuno, "Probabilistic Diagnosis of Broken Rotor Bar of Cage Induction Motor Focused on Transition Features", *IEEJ Transaction on Electronics, Information and Systems,* vol.135, no.6, pp.679-685, 2015.

[36] A. Bellini, F. Filippetti, C. Tassoni, and G.A. Capolino, "Advances in diagnostic technique for induction machines, "*IEEE Transaction on Industrial Electronics,* vol. 55, no. 12, pp. 4109-4126, Dec. 2008.

[37] S. Nandi, H.A. Toliyat and X. Li, "Condition monitoring and fault diagnosis of electrical motors-A recire," *IEEE Transaction on Energy Conversion,* vol. 20, no. 4, pp. 719-729, Dec. 2005.

[38] M. Cococcioni, B. Lazzerini, and S.L. Volpi," Robust diagnosis of rolling element bearings based on classification techniques," *IEEE Transaction on Industrial Informatics,* vol. 9, no. 4, pp. 2256-2263, Nov.2013.

[39] M.D. Prieto, G.Cirrincione, A.G. Espinosa, J. Ortega, and H. Henao, "Bearing fault detection by a novel condition-monitoring scheme based on statistical-time features and neural networks," *IEEE Transaction on Industrial Electronics,* vol. 60, no. 8, pp. 3398-3407, Aug.2013.

[40] R.B. Randall, Vibration-based condition monitoring: Industrial, Aerospace and Automotive Application. Chichester, U.K, *Wiley,* pp. 24-65, pp. 167-227, 2011.

[41] W. Zhou, B. Lu, T. Habetler, and R. Harley, "Incipient bearing fault detection via motor stator current noise cancellation using wiener filter," *IEEE Transaction on Industrial Application,* vol. 45, no. 4, pp. 1309– 1317, 2009.

[42] M. Delgado, G. Cirrincione, A. Garcia, J. Ortega, and H. Henao, "A novel condition monitoring scheme for bearing faults based on curvilinear component analysis and hierarchical neural networks," in *ICEM2012 - XXth International Conference on Electrical Machines,* pp. 2472–2478, 2012.

[43] X. Jin, M. Zhao, T. Chow, and M. Pecht, "Motor bearing fault diagnosis using trace ratio linear discriminant analysis," *IEEE Transactions on Industrial Electronics,* vol. 61, no. 5, pp. 2441–2451, May 2014.

[44] R. Schoen, B. Lin, T. Habetler, J. Schlag, and S. Farag, "An un-supervised, on-line system for induction motor fault detection using stator current monitoring," *IEEE Transactions on Industry Applications,* vol. 31, no. 6, pp. 1280–1286, Nov 1995.

[45] J. Rosero, L. Romeral, E. Rosero, and J. Urresty, "Fault detection in dynamic conditions by means of discrete wavelet decomposition for pmsm running under bearing damage," in *APEC 2009 - Twenty-Fourth Annual IEEE Applied Power Electronics Conference and Exposition,* pp. 951–956, 2009.

[46] A. Picot, Z. Obeid, J. Regnier, P. Maussion, S. Poignant, and O. Darnis, "Bearing fault detection in synchronous machine based on the statistical analysis of stator current," in IECON 2012 - *38th Annual Conference on IEEE Industrial Electronics Society,* pp. 3862–3867, October 2012.

[47] Z. Obeid, S. Poignant, J. Regnier, and P. Maussion, "Stator current based indicators for bearing fault detection in synchronous machine by statistical frequency selection," in *IECON 2011 - 37th Annual Conference on IEEE Industrial Electronics Society,* pp. 2036– 2041, 2011.

[48] J. Silva and A.J.M. Coardoso," Bearing failures diagnosis in three-phase induction motors by extended parks's vector approach." *In IECON 2005-31st Annual Conference of IEEE Industrial Electronics Society,* pp. 2591-2596, 2005.

[49] R. Obaid, T. Habetler, and J. Stack, "Stator current analysis for bearing damage detection in induction motors," in *SDEMPED 2003 - 4th IEEE International Symposium on Diagnostics for Electric Machines, Power Electronics and Drives,* pp. 182–187, 2003.

[50] F. Immovilli, M. Cocconcelli, A. Bellini, and R. Rubini, "Detection of generalized-roughness bearing fault by spectral-kurtosis energy of vibration or current signals," *IEEE Transactions on Industrial Electronics,* vol. 56, no. 11, pp. 4710–4717, 2009.

[51] A. Soualhi, G. Clerc, H. Razik, and A. Lebaroud, "Fault detection and diagnosis of induction motors based on hidden markov model," in *ICEM2012 - XXth International Conference on Electrical Machines,* pp. 1693–1699, 2012.

[52] T. W. S. Chow and H. Z. Tan, "HOS-based nonparametric and parametric methodologies for machine fault detection," *IEEE Transaction on Industrial Electronics,* vol. 47, no. 5, pp. 1051–1059, Oct. 2000.

[53] H. R. Martin and F. Honarvar, "Application of statistical moments to bearing failure detection," *Applied Acoustics,* vol. 44, no. 1, pp. 67–77, Jan. 1995.

[54] R. B. W. Heng and M. J. M. Nor, "Statistical analysis of sound and vibration signals for monitoring rolling element bearing condition," *Applied Acoustics,* vol. 53, no. 1–3, pp. 211–226, Jan. 1998.

[55] W. Zhou, T. G. Habetler, and R. G. Harley, "Bearing fault detection via stator current noise cancellation and statistical control," *IEEE Transaction on Industrial Electronics,* vol. 55, no. 12, pp. 4260–4269, Dec. 2008.

[56] L. Frosini and E. Bassi, "Stator current and motor efficiency as indicators for different types of bearings faults in induction motors," *IEEE Transaction on Industrial Electronics,* vol. 57, no. 1, pp. 244–251, Jan. 2010.

[57] A. Soualhi, G. Clerc, and H. Razik, "Detection and diagnosis of faults in induction motor using an improved artificial ant clustering technique, *"IEEE Transaction on Industrial Electronics,* vol. 60, no. 9, pp. 4053–4062, Sep. 2013.

[58] M. Blodt, P. Granjon, B. Raison, and G. Rostaing, "Models for bearing damage detection in induction motors using stator current monitoring," *IEEE Transaction on Industrial Electronics,* vol. 55, no. 4, pp. 1813–1822, Apr. 2008.

[59] W. Zhou, T. G. Habetler, and R. G. Harley, "Bearing condition monitoring methods for electric machines: A general review," in *Proceedings IEEE SDEMPED,* Krakow, Poland, pp. 3–6, 2007.

[60] E. L. Bonaldi, L. E. L. Oliveria, B. da Silva, G. Lambert-Torres, and L. E. B. da Silva, "Detecting load failures using induction motor as a transducer," in *Proceedings ICARCV,* Hanoi, Vietnam, pp. 196-199, 2008.

[61] F. Immovilli, A. Bellini, R. Rubini, and C. Tassoni, "Diagnosis of bearing faults in induction machines by vibration or current signals: A critical comparison," *IEEE Transaction on Industrial Applications,* vol. 46, no. 4, pp. 1350–1359, Jul./Aug. 2010.

[62] X. Gong and W. Qiao, "Bearing fault diagnosis for direct-drive wind turbines via current-demodulated signals," *IEEE Transaction on Industrial Electronics,* vol. 60, no. 8, pp. 3419–3428, Aug. 2013.

[63] L. Saidi, F. Fnaiech, G.-A. Capolino, and H. Henao, "Stator current bi-spectrum patterns for induction machines multiple-faults detection," in *Proceedings IEEE IECON,* Montreal, QC, Canada, pp. 5132– 5137, 2012.

[64] J. Antoni, "Fast computation of the kurtogram for the detection of transient faults," *Mechanical System Signal Processing,* vol. 21, no. 1, pp. 108–124, Jan. 2007.

[65] Valeria C.M.N. Leite, Jonas Guedes Borges da Silva, Giscard Francimeire Cintra Veloso, "Detection of Localized Bearing Faults in Induction Machines by Spectral Kurtosis and Envelope Analysis of Stator Current," *IEEE Transactions on Industrial Electronics,* vol. 62, no. 3, pp. 1855-1865, Mar. 2015.

[66] N. Sawalhi, "Rolling element bearings: Diagnostic, prognostic and fault simulations," *Ph.D. dissertation,* Faculty Engineering of Mechanical and Manufacturing Engineering, University of New South Wales, Sydney, Australia, 2007.

[67] D. Siegel, C. Ly, and J. Lee, "Methodology and framework for predicting helicopter rolling element bearing failure," *IEEE Transaction on Reliability,* vol. 61, no. 4, pp. 846–857, Dec. 2012.

[68] L. Zhen, H. Zhengjia, Z. Yanyang, and C. Xuefeng, "Bearing condition monitoring based on shock pulse method and improved redundant lifting scheme," *Mathematics and Computers in Simulation,* vol. 79, no. 3, pp. 318–338, Dec. 2008.

[69] J. K. Sinha and K. Elbhbah, "A future possibility of vibration-based condition monitoring of rotating machines," *Mechanical System and Signal Processing,* vol. 34, no. 1, pp. 231–240, Jan. 2013.

[70] F. Hemmati, W. Orfali, and M. S. Gadala, "Roller bearing acoustic signature extraction by wavelet packet transform, applications in fault detection and size estimation," *Applied Acoustics,* vol. 104, pp. 101–118, Mar. 2016.

[71] T. Yoshioka and T. Fujiwara, "A new acoustic emission source locating system for the study of rolling contact fatigue," *Wear,* vol. 81, no. 1, pp. 183–186, Sep. 1982.

[72] D. Mba and R. Rao, "Development of acoustic emission technology for condition monitoring and diagnosis of rotating machines, bearings, pumps, gearboxes, engines and rotating structures," *Shock and Vibration Digest,* vol. 38, no. 1, pp. 3–16, Mar. 2006.

[73] D. Mba, "The use of acoustic emission for estimation of bearing defect size," *Journal of Failure Analysis and Prevention,* vol. 8, no. 2, pp. 188–192, Apr. 2008.

[74] S. A. S. A. Kazzaz and G. Singh, "Experimental investigations on induction machine condition monitoring and fault diagnosis using digital signal processing techniques," *Electric Power Systems Research,* vol. 65, pp. 197–221, 2003.

[75] F. Jia, Y. G. Lei, J. Lin, X. Zhou, and N. Lu, "Deep neural networks: A promising tool for fault characteristic mining and intelligent diagnosis of rotating machinery with massive data," *Mechanical System and Signal Processing,* vol. 72–73, pp. 303–315, May 2016.

[76] M. Kang, M. R. Islam, J. Kim, J. M. Kim, and M. Pecht, "A Hybrid feature selection scheme for reducing diagnostic performance deterioration caused by outliers in data-driven diagnostics*," IEEE Transactions on Industrial Electronics,* vol. 63, no. 5, pp. 3299–3310, May 2016.

[77] T. Boukra, A. Lebaroud, and G. Clerc, "Statistical and neural-network approaches for the classification of induction machine faults using the ambiguity plane representation," *IEEE Transactions on Industrial Electronics,* vol. 60, no. 9, pp. 4034–4042, Sep. 2013.

[78] Y. G. Lei, Z. J. He, and Y. Y. Zi, "A new approach to intelligent fault diagnosis of rotating machinery," *Expert System with Application,* vol. 35, no. 4, pp. 1593– 1600, Nov. 2008.

[79] B. M. Ebrahimi, M. J. Roshtkhari, J. Faiz, and S. V. Khatami, "Advanced eccentricity fault recognition in permanent magnet synchronous motors using stator current signature analysis," *IEEE Transactions on Industrial Electronics,* vol. 61, no. 4, pp. 2041–2052, Apr. 2014.

[80] F.B. Abid, S. Zgarni, A. Braham, "Distinct Bearing Faults Detection in Induction Motor by a Hybrid Optimized SWPT and aiNet-DAG SVM," *IEEE Transaction on Energy conversion,* DOI 10.1109/TEC.2018.2839083.

[81] M. He and D. He, "Deep Learning Based Approach for Bearing Fault Diagnosis," *IEEE Transactions on Industrial Applications,* vol. 53, no. 3, pp. 3057-3065, May/June 2017.

[82] Christelle Piantsop Mbo'o, Kay Hameyer, "Fault diagnosis of bearing damage by means of the linear discriminant analysis of stator current features from the frequency selection", *IEEE Transaction on Industrial Applications,* DOI. 10.1109/TIA.2016.2581139.

[83] Jason R. Stack, Thomas G. Habetler, and Ronald G. Harley, "Fault-Signature Modeling and Detection of Inner-Race Bearing Faults", *IEEE Transaction on Industrial Applicatiosn,* vol. 42, No.1, pp. 61-67, Jan/Feb 2006.

[84] Shrinathan Esakimuthu Pandarakone, Yukio Mizuno and Hisahide Nakamura, "Frequency Spectrum Investigation and Analytical Diagnosis Method for Turn-to-Turn Short-Circuit Insulation Failure in Stator Winding of Low Voltage Induction Motor", *IEEE Transactions on Dielectrics and Electrical Insulation,* vol. 23, no. 6, pp. 3249-3255, Dec.2016.

[85] Shrinathan Esakimuthu Pandarakone, Yukio Mizuno and Hisahide Nakamura, "Online Slight Inter-Turn Short-Circuit Fault Diagnosis Using the Distortion Ratio of Load Current in a Low-Voltage Induction Motor", *IEEJ Journal of Industry Applications,* vol. 7, no. 6, pp. 1-7, 2018.

[86] Hisahide Nakamura, Shrinathan Esakimuthu Pandarakone, and Yukio Mizuno, "A Novel Approach for Detecting Broken Rotor Bar Around Rated Rotating Speed Using Frequency Component and Clustering*", IEEJ Transactions on Electrical and Electronics Engineering,* vol. 11(S2), pp. S116-S122, 2016.

[87] Shrinathan Esakimuthu Pandarakone, Yukio Mizuno and Hisahide Nakamura, "Distinct Fault Analysis of Induction Motor Bearing Using Frequency Spectrum Determination and Support Vector Machine", *IEEE Transactions on Industrial Applications,* vol. 53, no. 3, pp. 3049-3056, May/June 2017.

[88] Shrinathan Esakimuthu Pandarakone, Santhosh Gunasekaran, Yukio Mizuno and Hisahide Nakamura, "Application of Naive Bayes Classifier Theorem in Detecting Induction Motor Bearing Failure*", IEEE International Conference on Electrical Machines (ICEM),* Greece, Sep.03-06, 2018.

[89] Shrinathan Esakimuthu Pandarakone, Chika Araki, Yukio Mizuno and Hisahide Nakamura, "Diagnosis Method of Mechanical Failure in Low Voltage Induction Motor with the Aid of Support Vector Machine*", The International Conference on Electrical Engineering (ICEE),* Paper No. 90142, Okinawa, Japan, July 3-7, 2016.

[90] Shrinathan Esakimuthu Pandarakone, Makoto Masuko, Yukio Mizuno and Hisahide Nakamura, "Fault Classification of Outer-Race Bearing Damage in Low-Voltage Induction Motor with Aid of Fourier Analysis and SVM*", IEEE International Conference on Industrial Technology (ICIT),* Lyon, France, Feb.20-22, 2018.

[91] Shrinathan Esakimuthu Pandarakone, Keisuke Akahori, Toshiki Matsumura, Yukio Mizuno and Hisahide Nakamura, "Development of a Methodology for Bearing Fault Scrutiny and Diagnosis using SVM", *IEEE International Conference on Industrial Technology (ICIT),* pp. 282-287, Toronto, Canada, March 22-25, 2017.

[92] Shrinathan Esakimuthu Pandarakone, Yukio Mizuno and Hisahide Nakamura, "Evaluating the Progression and Orientation of Scratches on Outer-Raceway Bearing Using Pattern Recognition Method*", IEEE Transactions on Industrial Electronics,* vol. 66, No. 2, pp. 1307-1314, Jan. 2019.

[93] Santhosh Gunasekaran, Shrianthan Esakimuthu Pandarakone, Keisuke Asano, Yukio Mizuno and Hisahide Nakamura, "Condition Monitoring and Diagnosis of Outer Raceway Bearing Fault using Support Vector Machine*", IEEE International Conference on Condition Monitoring and Diagnosis (CMD),* Perth, Australia Sep.23-26, 2018.

[94] Shrinathan Esakimuthu Pandarakone, Makoto Masuko, Yukio Mizuno and Hisahide Nakamura, "Deep Neural Network based Bearing Fault Diagnosis of Induction Motor using Fast Fourier Transform Analysis" *IEEE Energy Conversion Congress and Exposition Conference (ECCE),* Portland, US, September 23-27, 2018.

Chapter 2

[1] P. Neti and S. Nandi, "Stator Intertun Fault Detection of Synchronous Machines Using Field Current and Rotor Search-Coil Voltage Signature Analysis", *IEEE Transactions on Industrial Applications,* vol. 45, no. 3, pp. 911–920, 2009.

[2] H. Meshgin-kelk, J. Milimonfared and H.A. Toliyat, "Interbar currents and axial fluxes in healthy and faulty induction motors*", IEEE Transactions on Industrial Applications,* vol. 40, no. 1, pp. 128–134, 2004.

[3] P. Ostojic, A. Banerjee, D.C. Patel, W. Basu and S. Ali, "Advanced Motor Monitoring and Diagnostics", *IEEE Transactions on Industrial Applications,* vol. 50, no. 5, pp. 3120–3127, 2014.

Chapter 3

[1] G. B. Kliman, J. Stein, and R. D. Endicott, "Noninvasive Detection of Broken Rotor Bars in Operating Induction Motors", *IEEE Transactions on Energy Conversion,* vol.3, no.4, pp.873-879, 1988.

[2] J. Milimondared, H. M. Kelk, S. Nandi, A. D. Minassians, and H. A. Toliyat, "A Novel Approach for Broken Rotor Bar Detection in Cage Induction Motors", *IEEE Transactions on Industry Applications,* vol.35, no.5, pp.1000-1006, 1999.

[3] T. Kohonen, "Self-Organizing Maps", *Springer-Verlag,* 1995.

[4] S. Openhaw, "Neuro-classification of spatial data", Neural Nets, Applications in Geography, *Kluwer Academic Publishers,* vol.29, pp.53-70, 1994.

[5] T. Kohonen, J. Hynninen, J. Kangas, and J. Laaksonen, "SOMPAK The Self-Organizing Map Program Package (Version 3.1)", 1995.

Chapter 4

[1] J. R. Stack, R. G. Harley, and T. G. Habetler, "Fault classification and fault signature production for rolling element bearing in electric machines," *IEEE Transaction on Industrial Applications*, vol. 40, no. 3, pp. 735–739, May/Jun 2004.

[2] W. Zhou, T. G. Habetler, and R. G. Harley, "Bearing fault detection via stator current noise cancellation and statistical control," *IEEE Transaction on Industrial Electronics*, vol. 55, no. 12, pp. 4260–4269, Dec. 2008.

[3] M. Blodt, P. Granjon, B. Raison, and G. Rostaing, "Models for bearing damage detection in induction motors using stator current monitoring," *IEEE Transaction on Industrial Electronics*, vol. 55, no. 4, pp. 1813–1822, Apr. 2008.

[4] B. Yazici and G. B. Kliman, "An adaptive statistical time–frequency method for detection of broken bars and bearing faults in motors using stator current," *IEEE Transaction on Industrial Applications*, vol. 35, no. 2, pp. 442–452, Mar./Apr. 1999.

[5] L. Eren and M. J. Devaney, "Bearing damage detection via wavelet packet decomposition of the stator current," *IEEE Transaction on Instrumentation Measurement*, vol. 53, no. 2, pp. 431–436, Apr. 2004.

[6] M. E. H. Benbouzid, M. Vieira, and C. Theys, "Induction motors' faults detection and localization using stator current advanced signal processing techniques," *IEEE Transactions on Power Electronics*, vol. 14, no. 1, pp. 14–22, Jan. 1999.

[7] M. E. H. Benbouzid, "A review of induction motors signature analysis as a medium for faults detection," *IEEE Transaction on Industrial Electronics,* vol. 47, no. 5, pp. 984–993, Oct. 2000.

[8] M. S. Ballal, Z. J. Khan, H. M. Suryawanshi, and R. L. Sonolikar, "Adaptive neural fuzzy inference system for the detection of inter-turn insulation and bearing wear faults in induction motor," *IEEE Transaction on Industrial Electronics,* vol. 54, no. 1, pp. 250–258, Jan. 2007.

[9] J. R. Stack, R. G. Harley, and T. G. Habetler, "An amplitude modulation detector for fault diagnosis in rolling element bearings," *IEEE Transaction on Industrial Electronics,* vol. 51, no. 5, pp. 1097–1102, May 2004.

[10] S. Wu and T. W. S. Chow, "Induction machine fault detection using SOM- based RBF neural networks," *IEEE Transaction on Industrial Electronics,* vol. 51, no. 1, pp. 183–194, Jan. 2004.

[11] B. Li, M. Chow, Y. Tipsuwan, and J. Hung, "Neural-network-based motor rolling bearing fault diagnosis," *IEEE Transaction on Industrial Electronics,* vol. 47, no. 5, pp. 1060–1069, Oct. 2000.

[12] R. L. Schiltz, "Forcing frequency identification of rolling element bearings," *Sound Vibration,* vol. 24, no. 5, pp. 16–19, May 1990.

[13] M. Ojaghi, V. Bahari, "Rotor Damping Effects in Dynamic Modeling of Three-Phase Synchronous Machines Under the Stator Interturn Faults－Winding Function Approach," *IEEE Transactions on Industry Application,* vol. 53, no. 3, pp. 3020-3028, May/June 2017.

[14] M. Blodt, J. Regnier and J. Faucher, “Distinguishing Load Torque Oscillations and Eccentricity Faults in Induction Motors Using Stator Current Wigner Distributions,” *IEEE Transactions on Industrial Applications,* vol. 45, no. 6, pp. 1991-2000, Nov/Dec. 2009.

Chapter 8

[1] S. Abe, “Introduction to Support Vector Machine for Pattern Recognition”, *Morikita Publishing Corporation Limited,* 2011.

[2] K. B. Liplowits and T. R. Cundari, “Applications of Support Vector Machines in Chemistry”, *Reviews in Computational Chemistry,* vol.23, chapter 6, 2007.

[3] Wikipedia, “Support vector machine”, http://en.wikipedia.org/wiki/Support vector machine.

[4] W. You, K. Qian, D. Lo, P. Bhattacharya, M. Guo, Ying Qian, “Web Service-enabled Spam Filtering with Naïve Bayes Classification,” *2015 IEEE First International Conference on Big Data Computing Service and Applications (CSDL),* pp. 99-104, CA, USA, March 2015.

[5] https://dev.classmethod.jp/machine-learning/2017ad_20171218_knn

[6] http://toukeilab.com/%EF%BD%8B%E8%BF%91%E5%82%8D%E6%B3%95

[7] https://dev.classmethod.jp/machine-learning/2017ad_20171211_dt-2/#sec4

[8] http://darden.hatenablog.com/entry/2016/12/09/221630

[9] http://drilldripper.hatenablog.com/entry/2016/10/04/211245

[10] H. D. Shao, H. K. Jiang, F. A. Wang, and H. W. Zhao, "An enhancement deep feature fusion method for rotating machinery fault diagnosis," *Knowledge Based Systems*, vol. 119, pp. 200–220, Mar. 2017.

[11] V. T. Tran, F. AlThobiani, and A. Ball, "An approach to fault diagnosis of reciprocating compressor valves using Teager-Kaiser energy operator and deep belief networks," *Expert Systems with Applications*, vol. 41, no. 9, pp. 4113–4122, Jul. 2014.

[12] O. Janssens, V. Slavkovikj, B. Vervisch, K. Stockman, M. Loccufier, and S. Verstockt, "Convolutional neural network-based fault detection for rotating machinery," *Journal of Sound and Vibrations*, vol. 377, pp. 331–345, Sep. 2016.

List of Publications

Transaction Papers:

1. Hisahide Nakamura, **Shrinathan Esakimuthu Pandarakone,** and Yukio Mizuno, "A Novel Approach for Detecting Broken Rotor Bar Around Rated Rotating Speed Using Frequency Component and Clustering", *IEEJ Transactions on Electrical and Electronics Engineering,* vol. 11 (S2), pp. S116-S122, Nov.2016.

2. **Shrinathan Esakimuthu Pandarakone,** Yukio Mizuno and Hisahide Nakamura, "Frequency Spectrum Investigation and Analytical Diagnosis Method for Turn-to-Turn Short-Circuit Insulation Failure in Stator Winding of Low Voltage Induction Motor", *IEEE Transactions on Dielectrics and Electrical Insulation,* vol. 23, no. 6, pp. 3249-3255, Dec.2016.

3. **Shrinathan Esakimuthu Pandarakone,** Yukio Mizuno and Hisahide Nakamura, "Distinct Fault Analysis of Induction Motor Bearing Using Frequency Spectrum Determination and Support Vector Machine", *IEEE Transactions on Industrial Applications,* vol. 53, no. 3, pp. 3049-3056, May/June 2017.

4. **Shrinathan Esakimuthu Pandarakone,** Yukio Mizuno and Hisahide Nakamura, "Online Slight Inter-Turn Short-Circuit Fault Diagnosis Using the Distortion Ratio of Load Current in a Low-Voltage Induction Motor", *IEEJ Transactions on Industrial Applications,* vol. 7, no. 6, pp. 1-7, Dec.2018.

5. **Shrinathan Esakimuthu Pandarakone,** Yukio Mizuno and Hisahide Nakamura, "Evaluating the Progression and Orientation of Scratches on Outer-Raceway Bearing Using Pattern Recognition Method", *IEEE Transactions on Industrial Electronics,* vol. 66, no. 2, pp. 1307-1314, Jan.2019.

International Conference Papers:

1. **Shrinathan Esakimuthu Pandarakone,** Chika Araki, Yukio Mizuno and Hisahide Nakamura, "Diagnosis Method of Mechanical Failure in Low Voltage Induction Motor with the Aid of Support Vector Machine", *The International Conference on Electrical Engineering (ICEE),* Paper No.90142, Okinawa, Japan, July 3-7, 2016.

2. **Shrinathan Esakimuthu Pandarakone,** Keisuke Akahori, Toshiki Matsumura, Yukio Mizuno and Hisahide Nakamura, "Development of a Methodology for Bearing Fault Scrutiny and Diagnosis using SVM", *18th IEEE International Conference on Industrial Technology (ICIT),* pp. 282-287, Toronto, Canada, March 22-25, 2017.

3. **Shrinathan Esakimuthu Pandarakone,** Makoto Masuko, Yukio Mizuno and Hisahide Nakamura, "Fault Classification of Outer-Race Bearing Damage in Low-Voltage Induction Motor with Aid of Fourier Analysis and SVM*", 19th IEEE International Conference on Industrial Technology (ICIT),* pp. 407-412, Lyon, France, Feb.20-22, 2018.

4. **Shrinathan Esakimuthu Pandarakone,** Santhosh Gunasekaran, Yukio Mizuno and Hisahide Nakamura, "Application of Naive Bayes Classifier Theorem in Detecting Induction Motor Bearing Failure", *23rd IEEE International Conference on Electrical Machines (ICEM),* pp. 1761-1767, Alexandroupoli, Greece, Sep.03-06, 2018.

5. Santhosh Gunasekaran, **Shrinathan Esakimuthu Pandarakone,** Keisuke Asano, Yukio Mizuno and Hisahide Nakamura, "Condition Monitoring and Diagnosis of Outer Raceway Bearing Fault using Support Vector Machine", *7th IEEE International Conference on Condition Monitoring and Diagnosis (CMD),* pp. 01-06, Perth, Australia Sep.23-26, 2018.

6. **Shrinathan Esakimuthu Pandarakone,** Makoto Masuko, Yukio Mizuno and Hisahide Nakamura, "Deep Neural Network based Bearing Fault Diagnosis of Induction Motor using Fast Fourier Transform Analysis" *10th IEEE Energy Conversion Congress and Exposition Conference (ECCE),* pp. 3214-3221, Portland, US, September 23-27, 2018.

7. **Shrinathan Esakimuthu Pandarakone,** Santhosh Gunasekaran, Keisuke Asano, Yukio Mizuno and Hisahide Nakamura, "A Novel Study on Machine Learning and Artificial Intelligence Methods in Detecting the Minor Outer-Raceway Bearing Fault", *20th IEEE International Conference on Industrial Technology (ICIT),* Melbourne, Australia, Feb.13-15, 2019 (To be presented).

National / Regional Conference Papers:

1. **Shrinathan Esakimuthu Pandarakone,** Chika Araki, Yukio Mizuno and Hisahide Nakamura, "Mechanical Failure Diagnosis of Induction Motor Based on Feature Distribution", *The 2016 Annual Meeting of the Institute of Electrical Engineers of Japan,* paper no.4-248, Sendai, March 16-18, 2016.

2. **Shrinathan Esakimuthu Pandarakone,** Toshiki. Matsumura, Keisuke Akahori, Yukio Mizuno and Hisahide Nakamura, "Role of Feature Distribution and Spectrum Analysis in Detecting the Bearing Damage of Low Voltage Induction Motor", *Tokai-Section Joint Conference on Electrical, Electronics, Information, and Related Engineers,* paper no. M1-6, Toyota, September 12-13, 2016.

3. **Shrinathan Esakimuthu Pandarakone,** Toshiki Matsumura, Keisuke Akahori, Yukio Mizuno and Hisahide Nakamura, "Investigation in Low Voltage Induction Motor for Mechanical Failure Detection and Analysis using Frequency Spectrum Component", *The 2017 Annual Meeting of the Institute of Electrical Engineers of Japan,* paper no.4-276, Toyoma, March 15-17, 2017.

4. **Shrinathan Esakimuthu Pandarakone,** Yukio Mizuno and Hisahide Nakamura, "Distinct Bearing Scratch Analysis and Diagnosis of Induction Motor with the Employ of Load Current Spectral Investigation" *Tokai-Section Joint Conference on Electrical, Electronics, Information, and Related Engineers,* paper no. K1-5, Nagoya, September 7-8, 2017.

5. **Shrinathan Esakimuthu Pandarakone,** Makoto Masuko, Santhosh Gunasekaran, Yukio Mizuno and Hisahide Nakamura, "Diagnosis of Bearing Failure in Induction Motor Based on Spectral Analysis", *The 2018 Annual Meeting of the Institute of Electrical Engineers of Japan,* paper no.4-184, Kyushu, March 14-16, 2018 (In Japanese).

6. **Shrinathan Esakimuthu Pandarakone,** Yukio Mizuno and Hisahide Nakamura, "Slight Inter-Turn Stator Insulation Failure Detection using Distortion Ratio of Load Current", *The 2018 Annual Meeting of the Institute of Electrical Engineers of Japan,* paper no.4-185, Kyushu, March 14-16, 2018 (In Japanese).

7. **Shrinathan Esakimuthu Pandarakone,** Yukio Mizuno and Hisahide Nakamura, "Diagnosis of Slight Failure in Induction Motor Using Distortion Ratio", *The 2018 IEEJ Technical Meeting on Control,* paper no. CT-18-083, Nagaoka, June 9, 2018 (In Japanese).

8. **Shrinathan Esakimuthu Pandarakone,** Santhosh Gunasekaran, Keisuke Asano, Yukio Mizuno and Hisahide Nakamura, "Detection of the Bearing Fault of Induction Motor by Spectrum Analysis and Support Vector Machine" *Tokai-Section Joint Conference on Electrical, Electronics, Information, and Related Engineers,* paper no. F3-6, Nagoya, September 3-4, 2018.